Università Politecnica delle Marche
Scuola di Dottorato di Ricerca in Scienze dell'Ingegneria
Corso di Dottorato in Ingegneria Industriale

Energy flexibility and demand management in buildings

Ph.D. Dissertation of:
Alice Mugnini

Supervisor:
Prof. Fabio Polonara

Assistant Supervisor:
Prof. Alessia Arteconi

Ph.D. Course coordinator:
Prof. G. Di Nicola

XXXIII cycle

Università Politecnica delle Marche
Dipartimento di Ingegneria Industriale e Scienze Matematiche (DIISM)
Via Brecce Bianche — 60131 - Ancona, Italy

Contents

List of Figures

List of Tables

Abstract

The exploitation of energy flexibility in buildings represents one of the most promising solutions to allow the transition to energy systems with a high penetration of renewable energy sources. Having a high flexible building means to be able to efficiently apply demand side management strategies (DSMs) which represent one of the main aspects characterizing the concept of Smart Grid. DMS is defined as the set of all those strategies aimed at influencing customer uses of electricity in ways that will produce desired changes in the utility's load shape.

Given the increasing electricity demand in the residential sector, especially for the diffusion of heating and cooling systems electrically powered (e.g., split systems and heat pumps), buildings show a predisposition to produce variations in the electrical demand, due to the different levels of thermal inertia already available in them (e.g., the thermal mass embedded in the envelope or dedicated devices as cold and/or hot water tank). Moreover, thanks to advanced control techniques, buildings could exploit different energy sources (i.e., fuels) to satisfy their thermal requirements, while reducing withdrawals from the power grid.

The work presented in this thesis fits into this context. The objective of this thesis is to provide an overview of the different aspects that characterize the energy flexibility obtainable from the management of thermal and electrical loads in residential buildings equipped with heat pumps. In particular, the analysis is gradually extended from the context of the design scenario of single buildings to the operative analysis of clusters of buildings. Firstly, a quantification methodology that allows to estimate the energy flexibility of a single building with a single indicator (the flexibility performance indicator, FPI) is presented and it is tested in different simulation-based case studies. Then, the focus is on the identification of reserves of flexibility outside the building, such as flexible energy sources (i.e. district heating and cooling networks) and the optimal management of multi energy systems (i.e. fuel switching). For the latter aspect, an analysis on the role of controls (i.e. model predictive controls) is also provided. In the final parts of the thesis, flexibility evaluations at the design level (i.e. with the FPI) are compared with operational analyses (focus on the space cooling sector) and a preliminary assessment of the energy flexibility obtainable from aggregation of buildings is realized.

All the results reported are extrapolated from a series of papers that have been published in scientific journals. In general, all the analyses and the evaluations allow to confirm the great potential of residential buildings in providing energy flexibility services. A great influence of the intrinsic features of the building (i.e., its thermal properties and the thermal inertia of its distribution system) on its design flexibility reserve has emerged. Moreover, performance differences between design and operational evaluations are observed. The assessment on cluster level highlights how the differentiation of the users involved allows to increase the number of degrees of freedom with which a demand side management event can be realized. The latter aspect can be seen as a reaffirmation of the great potential that residential buildings have to produce energy flexibility services.

Sommario

Lo sfruttamento della flessibilità energetica negli edifici rappresenta una delle soluzioni più promettenti per consentire il passaggio a sistemi energetici ad alta penetrazione di fonti rinnovabili. Disporre di un edificio energeticamente flessibile significa poter applicare in modo efficiente strategie di gestione della domanda (Demand Side Management, DSM) che rappresentano uno degli aspetti principali caratterizzanti il concetto di Smart Grid. Il DMS è definito come l'insieme di tutte quelle strategie volte ad influenzare gli usi di elettricità degli utenti in modo da produrre cambiamenti desiderati nella forma della loro curva di carico.
Data la crescente domanda elettrica del settore residenziale, soprattutto per la diffusione di impianti di riscaldamento e raffrescamento alimentati elettricamente (es. split e pompe di calore), gli edifici mostrano una predisposizione a produrre variazioni programmate della loro domanda elettrica, dovuta ai diversi livelli di inerzia termica in essi già disponibile (es. massa termica dell'involucro o dispositivi dedicati come serbatoi di acqua calda o fredda). Inoltre, grazie a tecniche di controllo avanzate, possono sfruttare diverse fonti energetiche (ad esempio combustibili) per soddisfare i propri fabbisogni termici, riducendo al contempo i prelievi dalla rete elettrica.
Il lavoro presentato in questa tesi si inserisce in questo contesto. L'obiettivo è quello di fornire un'analisi dei diversi aspetti che caratterizzano la flessibilità energetica ottenibile dalla gestione dei carichi termici ed elettrici in edifici residenziali dotati di pompe di calore. L'analisi si estende progressivamente dal contesto dello scenario progettuale dei singoli edifici a quello operativo degli aggregati (cluster di edifici). In primo luogo, è proposta una metodologia innovativa che consente di quantificare la flessibilità energetica di un singolo edificio con un unico indicatore (Flexibility Performance Indicator, FPI). Nella tesi tale metodologia è applicata per valutare diversi casi di studio. Proseguendo nell'analisi, l'attenzione è spostata verso l'identificazione e la valutazione di riserve aggiuntive di flessibilità disponibili all'esterno degli edifici, come le fonti energetiche flessibili (es. reti di teleriscaldamento e teleraffrescamento) e la gestione ottimizzata dei sistemi multienergetici (es. variazione programmata di combustibile utilizzato). Per quest'ultimo aspetto è prevista anche un'analisi sul ruolo dei controlli (es. ruolo dei controlli predittivi, Model Predictive Control). Inoltre, nelle parti finali della tesi vengono confrontate valutazioni di flessibilità a livello progettuale (con l'FPI) con analisi operative (focus sul settore del raffrescamento degli ambienti) e viene proposta

una valutazione preliminare della flessibilità energetica ottenibile dall'aggregazione degli edifici.
Tutti i risultati riportati sono estrapolati da una serie di articoli pubblicati su riviste scientifiche. In generale, tutte le analisi e le valutazioni presentate consentono di confermare le grandi potenzialità degli edifici residenziali nella fornitura di servizi di flessibilità energetica. È emersa una grande influenza delle caratteristiche intrinseche dell'edificio (cioè le sue proprietà termiche e l'inerzia termica del suo sistema di distribuzione) sulla sua riserva di flessibilità progettuale. Inoltre, si possono osservare differenze di prestazioni tra le valutazioni progettuali e quelle operative. L'analisi a livello di cluster evidenzia come la differenziazione degli utenti coinvolti consenta di aumentare il numero di gradi di libertà con cui è possibile realizzare un evento di demand side management. Quest'ultimo aspetto può essere visto come una riaffermazione del grande potenziale degli edifici residenziali nel produrre servizi di flessibilità energetica.

Chapter 1

Introduction

1.1 Background and motivation

Global energy demand is increasing rapidly in recent years, showing an average growth of 2%/year over the 2000-2018 period [1]. Facing the progressive reduction of fossil fuel reserves and the increasing amount of the greenhouse emissions, many countries developed policies to promote Renewable Energy Resources (RESs). For instance, the European Union (EU) has set the ambitious target of 32% for RES in the EU's energy mix by 2030 [2], having almost reached the share of 20 % set for 2020 (18.9% in 2018 according to Eurostat [3]).

However, in an energy system where renewable energy resources represent an important contribution to generation, problems may arise related to the casual and non-programmable nature of many of them (e.g., wind and solar energy). Indeed, the traditional way of managing the electricity grid involves the adaptation of generation to demand. This paradigm may not be effective and lead to balancing difficulties when the generation source is unpredictable.

In this scenario, to ensure the reliability and the stability of the power grid, a change of perspective will be necessary: the electricity grid of the future will have to be able to adapt the demand to the actual availability on the generation side. This concept is commonly referred to as Demand Side Management (DSM) and it is one of the main aspects characterizing the concept of Smart Grid [4]. DSM is defined as the set of all those strategies aimed at "influencing customer uses of electricity in ways that will produce desired changes in the utility's load shape" [5]. In general, it can be implemented in three different ways: (i) energy-efficient end-use devices; (ii) additional equipment, systems and controls to enable load shaping (e.g., energy storage) and (iii) communication systems between end-users and external parties, e.g., demand response (DR) [6]. Building sector appears very suitable for the implementation of these strategies. Indeed, they are responsible for a large proportion of overall energy demand. According to the European Commission [7], they are responsible for approximately 40% of EU energy consumption and 36% of the greenhouse gas emissions. Moreover, many

enabling technologies are more and more integrated into them, even thanks to their gradual refurbishment imposed by the Energy Performance of Buildings Directive (EPDB) [8]. Examples are charging stations of electric vehicles, shifting of plug-loads and management of the Heating, Ventilation and Air Conditioning (HVAC) systems [9]. This latter aspect has a great potential for easily activating demand side management services as there are both large margins of efficiency and different levels of energy storage (e.g., thermal and electrical) to be exploited. In fact, the use of heat pumps systems (HPs) is increasingly frequent in buildings. Only in EU, the number of operating heat pumps has increased by roughly 15 million between 2013 and 2019 [10] and, thanks to the transition from non-inverter to inverter technologies, their seasonal performance factor (an indicator of average annual energy performance) has incremented since 2010 to nearly 4 today for most space heating applications [11].
The interest in heat pumps is motivated by the fact that they allow to establish a direct link between the thermal and electrical demand of the building. Therefore, thanks to HPs the thermal load of the building could be managed in order to produce variations in its electricity demand. In this sense, the thermal energy storage potential of buildings can be exploited for electrical load-shifting strategies (e.g., DR) [12].
It is in this context that the analysis proposed in this thesis is inserted. Indeed, with the intention of increasing knowledge in the sector, this work wants to analyze with novel methodologies and introducing specific case studies, the different aspects that characterize the topic of the energy flexibility obtainable from the management of thermal loads in residential buildings. The analysis, by mean of both qualitative and quantitative methodologies, aims to provide an overview of the topic analyzed.

1.2 Outline

The work presented in this thesis is structured starting from the single building evaluation and then gradually enlarging the context. At first, the design operation is taken into account with the proposal of a method (i.e. calculation of a single indicator for estimating performance in terms of energy flexibility: the Flexibility Performance Indicator) to quantify the energy flexibility reserve of single buildings according to their intrinsic characteristics (i.e. thermal and geometrical properties of the building envelope and features of the heating/cooling system). Then, before moving on to the operational flexibility assessment, a focus on the possible sources of energy flexibility outside the building is presented. In particular, the flexibility derived by the fuel switching in the context of multi energy carriers is investigated. Particular attention is paid to the role of the district heating and cooling networks since they allow the exploitation of additional energy storage capabilities. Afterwards, the operational context is investigated. First of

all, the role of the control is analyzed with a focus on the effectiveness of the model-based predictive control (MPC). In this context, a case study involving the activation of the energy flexibility reserves both inside and outside the building is tested with the implementation of an operative MPC. Then, remaining in the context of a single building, a comparison between the design and operational flexibility evaluation is provided with a focus on the residential space cooling sector. Finally, the additional energy flexibility potential that can be obtained involving clusters of buildings is discussed.
To summarize the structure of the thesis, Figure 1.1 reports a schematic of the different points of view with which the energy flexibility of buildings is assessed in this thesis.

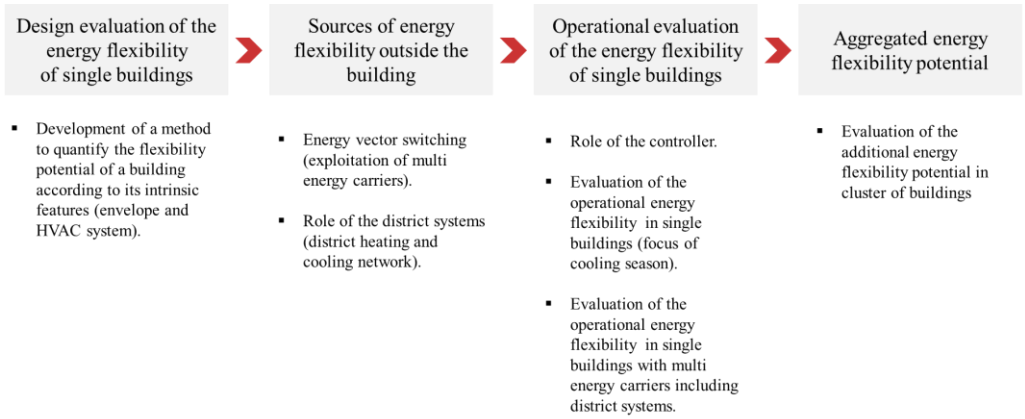

Figure 1.1: Schematic of the energy flexibility analysis.

Specifically, the thesis is divided into the following chapters:

Chapter 1 (current chapter) defines the background of the topic matter of this work and summarizes the objectives and the contents of the thesis.

Chapter 2 provides a summary of the state of art on the topic of the energy flexibility in buildings. In this chapter definitions and applications are discussed with an analysis of the scientific literature available to date.

Chapter 3 provides an evaluation of the energy flexibility of single buildings at design level. Hereby, a novel methodology to assess the potential reserve of energy flexibility of different buildings (e.g., different constrictions features, heating and cooling systems)

is introduced. It is based on the calculation of a single quantity: the Flexibility Performance Indicator (FPI). To show its effectiveness, the methodology is applied to different case studies both for heating and cooling applications.

Chapter 4 provides an overview of the potential energy reserves outside the buildings that can be exploitable for activate flexibility services. In particular, the potential of district heating and cooling systems is discussed with a focus on the cooling case. In this regard, a novel application to recover waste cold energy is introduced and its energy performance are discussed.

Chapter 5 provides an operative evaluation of the energy flexibility potential of single buildings. At first, the aspect of the controller is investigated. The performance of a Model Predictive Control (MPC) in comparison with traditional Rule Based Control (RBC) are evaluated. In particular, the role of the building model (e.g., white box, black box) in the MPC is discussed. Then, its operation to control a building with the availability of multi energy sources including district systems (i.e. district cooling) is shown.

Chapter 6 provides a comparison between a design and an operative evaluation of the energy flexibility reserve of single residential buildings. In particular, the analysis is focused on the space cooling sector.

Chapter 7 provides some points of reflections on the energy flexibility potential deriving from the aggregation of the buildings demand.

Chapter 8 summarizes the main conclusions and future developments.

1.3 Publications discussed in this work

This thesis is mainly based on the research studies and activities published in the following papers:

Paper 1. A. Mugnini; F. Polonara; A. Arteconi. Design energy flexibility for Italian residential buildings. Proceedings of 5th International High-Performance Buildings Conference, Purdue (West Lafayette, Indiana, USA), July 9-12, 2018. DOI: docs.lib.purdue.edu/ihpbc/278

Paper 2. A. Arteconi; A. Mugnini; F. Polonara. Energy flexible buildings: A methodology for rating the flexibility performance of buildings with electric heating and cooling system. Applied Energy. Volume 251, 1 October 2019, 113387. DOI: doi.org/10.1016/j.apenergy.2019.113387

Paper 3. A. Mugnini; F. Polonara; A. Arteconi. Design Optimization of Energy Flexibility for Residential Buildings. Proceedings of the 16th International Building Performance Simulation Association (IBPSA) Conference, Rome (Italy), Sept. 2-4, 2019. ISSN: 2522-2708. DOI: doi.org/10.26868/25222708.2019.210255

Paper 4. A. Mugnini; F. Polonara; A. Arteconi. Evaluation of energy flexibility from residential district cooling. Proceedings of 4th Building Simulation Applications (BSA) Conference, Bolzano (South Tyrol, Italy), June 19 – 21, 2019. ISSN: 2531-6702

Paper 5. A. Mugnini; G. Coccia; F. Polonara; A. Arteconi. Potential of District Cooling Systems: A Case Study on Recovering Cold Energy from Liquefied Natural Gas Vaporization. Energies 2019, 12(15), 3027. DOI: doi.org/10.3390/en12153027

Paper 6. A. Mugnini; G. Coccia; F. Polonara; A. Arteconi. Performance Assessment of Data-Driven and Physical-Based Models to Predict Building Energy Demand in Model Predictive Controls. Energies 2020, 13(12), 3125. DOI: doi.org/10.3390/en13123125

Paper 7. G. Coccia; A. Mugnini; F. Polonara; A. Arteconi. "Artificial-neural-network-based model predictive control to exploit energy flexibility in multi-energy systems comprising district cooling". Energy. 2021, 119958. DOI: doi.org/10.1016/j.energy.2021.119958

Paper 8. A. Mugnini; G. Coccia; F. Polonara; A. Arteconi. Energy Flexibility as Additional Energy Source in Multi-Energy Systems with District Cooling. Energies 2021, 14, 519. DOI: doi.org/10.3390/en14020519

Paper 9. G. Coccia; A. Mugnini; F. Polonara; A. Arteconi. (2020). "Artificial neural networks for building modeling in model predictive controls: Analysis of the issues related to unlocking energy flexibility". TECNICA ITALIANA-Italian Journal of Engineering Science, Vol. 64, No. 2-4, pp. 207-212. DOI: doi.org/10.18280/ti-ijes.642-412

Paper 10. A. Mugnini; F. Polonara; A. Arteconi. Quantification of energy flexibility from air conditioning of residential buildings. Proceedings of 25th IIR International

Congress of Refrigeration, Montréal (Québec, Canada). August 24-30, 2019. DOI: 10.18462/iir.icr.2019.966

Paper 11. A. Mugnini; F. Polonara; A. Arteconi. Energy flexibility in residential buildings clusters. E3S Web Conf. Volume 197, 2020 75th National ATI Congress – #7 Clean Energy for all (ATI 2020). DOI: doi.org/10.1051/e3sconf/202019703002

Chapter 2

Energy flexibility from HVAC systems in buildings: state of art

The International Energy Agency (IEA) in the program 'Energy in Buildings and Communities' (EBC) with the international Annex 67 (IEA EBC ANNEX 67) [12]) introduced the definition of energy flexibility in buildings. It is defined as the ability to manage the demand and generation of the building according to local climate conditions, user needs, and energy network requirements [9].
Focusing on the heating and cooling systems, several solutions can be identified to manage the thermal demand of a building. For instance, the thermal demand could be easily decoupled from the generation thanks to thermal energy storage systems (TESs) [13]. Different thermal energy storage systems are exploitable in buildings. For instance, with the adoption of heat pump systems, the thermal mass of the envelope can be used to accumulate thermal energy when electricity consumption is convenient or to release it when the use of electricity wants to be avoided [14]. The same role can be played by external devices in combination with the thermal distribution systems. Simple and already widespread systems are hot or cold-water tanks [15] connected to the hydronic distribution system. Interest is also growing towards the use of innovative thermal energy storage systems as phase change materials (PCM) [16] or thermo chemical materials (TCM) [17].
Another way for a building to provide energy flexibility lies in the scheduled management of thermostatically controlled loads (TCLs) [18]. Indeed, through variations in the users' set-point, the thermal demand of the building can be varied rather quickly to adapt to fluctuations in power grids.
Moreover, when multiple energy systems (MESs) are available to cover the thermal demand of a building, an additional energy flexibility source is provided by the possibility to vary the fuel used [19]. Indeed, a building may dispose of local generation systems (e.g., photovoltaic or solar panels) or it can exploit different energy networks as the power or the gas grid. Furthermore, the connection to a district heating or cooling network can be possible. In this last case, also the storage capability of the network could be used by the building as further flexibility reserve.

A very interesting interpretation of how the building demand can provide flexibility services, is given by Klein et. all [19]. For them, the impact of a building on the energy system is determined by the trajectory of the net power load (Figure 2.1). Involving the heating and/or the cooling systems of the building, this trajectory can be varied in four ways: (i) with electrical batteries, (ii) switching the fuel, (iii) with the adoption of a dedicated device as thermal energy storage and finally (iv) exploiting the thermal building mass.

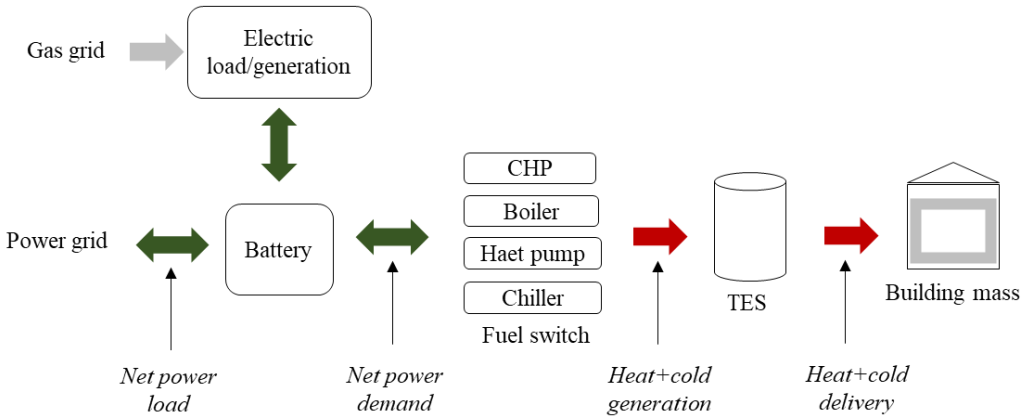

Figure 2.1. Ways of obtaining energy flexibility according to Klein et all. [19].

However, to allow the exploitation of the aforementioned sources of flexibility there is a need for an advanced logic control [20]. Both when the programmed management of demand must be done at the single building level and, even more so when aggregate strategy wants to be realized, the role of the controller is an aspect to consider when moving from the design to the operational phase.
The following subsections contain a literature review on the mains topics concerning the analysis of the energy flexibility in buildings, distinguished on the basis of the main points discussed above and also reported in Figure 1.1.

2.1 Method for quantifying the energy flexibility of buildings

As mentioned, there are some intrinsic characteristics of the building (i.e., thermal mass and thermal insulation level) and its heating and/or cooling system (i.e., the storage capability of the distribution system) which in themselves could allow the potential obtaining of greater or lesser energy flexibility services. The adoption of a common and

simple methodology to evaluate this potential can be very useful to obtain a preliminary evaluation of the load-shifting potential of single buildings. In sub-section 2.1.1, a literature analysis on the mains flexibility quantification methods are reported. The main indicators derived from this analysis are used as a starting point to formulate the Flexibility Performance Indicator (FPI) discussed in Chapter 3. Then, in sub-section 2.1.2, the state of art of the mains flexibility quantification method at aggregated level is reported.

2.1.1 Single buildings

The importance of having a method for easily quantify the energy flexibility potential of a building is highlighted by the updated EPDB [21]. Unlike the previous version [22], in which only the buildings energy labelling was required, the new one introduces the need to identify a method to calculate an indicator, the Smartness Readiness Indicator (SRI), that is able to assess the capability of a building to adapt its operation to the needs of the occupants and of the grid [8].
In this regard, many scientific works are produced in recent years [23][24]. However, according to Reynders et al. [23], regardless of the reason why the building actives its energy flexibility reserves, three general properties characterize the energy flexibility performance of the building:

- The time aspect (the time over which energy and power can be shifted or delayed).
- The capacity aspect (the amount of energy or power that can be shifted or delayed).
- The cost aspect.

This latter aspect (cost) can have different interpretations. For instance, Reynders et all. [23] refer it to the associated cost or efficiency loss at the building level that results from activating this flexibility. Jensen et al., in the position paper of the Annex 67 [12], talk about the potential cost saving or energy use associated to activating the available flexibility.
Given the dynamic nature of the problem, it seems difficult to evaluate the building response to a certain request of energy flexibility considering fixed boundary conditions. Indeed, when a building activates its energy flexibility reserve, it produces a variation of its power demand compared to its reference operation [9]. And, both the reference and the flexible operations are strongly affected by the dynamic of the system itself and on external environment (e.g., ambient temperature, solar gains…). This fact implies that, the result of a demand side management event is not univocal, but it is strongly affected by context in which the building operates (i.e. the boundary conditions) [14]. For these reasons all the quantification methods available in literature are simulation-based and requires a transient simulation tool. As mentioned, there are many works

assessing the topic of the quantification methods for evaluate the energy flexibility of single buildings. In fact, also different review papers are available [23]. However, in this literature review it is chosen to mention only some of them, as they represented the starting point for the method discussed in Chapter 3.

Mainly reference is made to the work of Reynders et al. [14]. In fact, they introduced a simulation-based method for the generic characterization of energy flexibility potential derived from the exploitation of the thermal mass of the building. The methodology is based on the calculation of three indicators (the available structural storage capacity, the storage efficiency and the power shifting capability). Also, Stinner et al. [25] introduced a quantification method based on three indicators: the temporal flexibility (forced and delayed), the power flexibility and energy flexibility. In particular, they evaluated the flexibility potential of a building heating systems by the simulation of opposite events (i.e., charge and discharge) for the storage system. Le Dréau and Heiselberg [26] characterized the behavior of the building thermal mass as storage medium during a load shifting strategy by means of the calculation of: the discharged heat (the energy use decreases compared to the reference case), the charged heat (the energy use increases compared to the reference case) and the shifting efficiency (ratio between the discharged and the charged heat). Another work that is taken into account for the formulation of the methodology presented in Papers 1 and 2 is that of Finck et al. [27]. In this work the authors also quantified the energy flexibility potential of buildings with thermal energy storage systems with the calculation of different performance indicators that sufficiently characterize flexibility in terms of energy (available storage capacity and storage efficiency), power (power shifting capability, electrical and thermal instantaneous power flexibility) and cost (the flexibility factor).

What is interesting to observe is that in all the mentioned works the application of the methodology is related to a specific case study. Contrariwise, the aim of the methodology presented in this thesis (the FPI calculation proposed in Chapter 3 referred to Papers 1 and 2) is to define a standard quantification method, the result of which depends only on the intrinsic characteristics of the building, as for the energy performance certificate (EPC).

2.1.2 Clusters of buildings

Evaluating the energy flexibility reserve of a single building is essential from a resource planning perspective. However, the energy quantities involved (except for large industrial or commercial buildings) are not interesting from a market point of view. For this reason, when planning demand response strategies, it is necessary to consider the aggregation of several buildings (i.e., a cluster of buildings). A definition of building

cluster is provided by Vigna et al. [28]: “a building cluster identifies a group of buildings interconnected to the same energy infrastructure, such that the change of behavior/energy performance of each building affects both the energy infrastructure and the other buildings of the whole cluster”. To specify in the concept, the authors highlighted that the interconnection of the building is not necessarily physical, but it can be also market related (e.g., different buildings belonging to the same owner).

In order to estimate the energy flexibility potential of different building cluster, it is necessary to identify a methodology to model the cluster. As highlighted by Goy and Finn [29], typically reference buildings (i.e., archetypes) are used. Then, buildings with similar features are grouped together with classification of clustering techniques.

Many works are available in literature in which large-scale building energy models are formulated with archetypal buildings. For instance, Mata et al. [30] presented a methodology by which national building stocks (considering buildings located in France, Germany, Spain and in the UK) may be aggregated through archetypes. In particular they differentiated the archetypes by: (i) type of buildings (e.g., residential or not residential), (ii) construction year, (iii) climate region and (iv) the main fuel source for heating purposes. Also Famuyibo et al. [31] introduced a methodology for the development of archetypes based on information from literature and a sample of detailed energy-related housing data. To differentiate the archetypes, they used characteristics that are significant in establishing how house energy use might change according to the building regulations (e.g., wall U-value, roof U-value, window U-values, floor U-value, air change rate, floor area, heating system efficiency, dwelling type and domestic hot water cylinder insulation thickness) and characteristics of construction detail or construction type (e.g., wall construction types, roof insulation types, floor construction types and window insulation types). Hence, through cluster analysis, they identified 13 archetypes representing 65% of the population of the existing Irish housing stock.

Another interesting work available in literature is presented by Hu and Xiao [32]. They adopted clustering techniques starting from archetypal buildings to model the energy dynamics of the cluster. In particular, the authors introduced two aspects, which are partly connected to each other, that cannot be neglected when the analysis of the load shifting potential of a cluster of buildings wants to be evaluated: the uncertainty in quantification of the energy flexibility and the role of the occupancy profile of the users. Indeed, they observed how the evaluation of the building cluster’s energy flexibility is more reliable than that of a single building (aggregated energy flexibility exponentially decreased from 19.12% for 8 households to 0.74% for 5120 households).

In this latter work, the energy flexibility is evaluated by calculating the load shedding compared to a baseline. In particular, the energy-flexible case is modelled raising the set point temperature during on-peak hours.

This can be one of the indicators for evaluating the peak reduction capacity of a cluster. However, as also the authors highlight in [32], most existing studies focused on the energy flexibility of individual buildings rather than building clusters. Indeed, all the indicators proposed by Vigna et al. [28] derived by works in which the single building is investigated.
Although therefore there are few studies that aim to provide methods of quantifying flexibility at the cluster level, what should not be overlooked is cluster modeling approach. In fact, all the studies cited above show the importance of the archetypal buildings and occupancy patterns definition.

2.2 Flexibility sources outside the building

A building can provide flexibility sources to obtain different levels of performance improvement (e.g., to reduce polluting emissions, to maximize self-consumption of certain energy sources as RES or minimize energy bill). The medium with which the energy flexibility is activated can be inside the building (i.e., with the exploitation of storage systems or with the management of thermostatically controlled loads) or outside the building. This latter is possible when multi energy sources to cover the thermal demand of the building are available. Indeed, in this context the energy flexibility provided by the fuel switching is exploitable (Figure 2.1).
When different energy sources are integrated into a building, they are commonly named as hybrid or multi-energy systems (MESs). A MES is where electricity, heating, fuels, and other type of energy vectors optimally interact with each other at various levels [33]. Focusing on residential buildings, natural gas and electricity can be the energy sources to different generators such as boilers, electric heat pumps (HPs), chillers and combined heat and power (CHP) systems, which can be used to produce electricity, heating and cooling [33]. Furthermore, MESs can integrate RESs and use energy sources recovered from optimized system management (e.g., energy harvesting from natural gas distribution networks [34]). Also, the interaction of buildings at district level (e.g., heating or cooling energy in district heating or cooling networks) can be exploited and building loads can be easily shifted thanks to the different energy storage systems that can be integrated in MESs [35].
As highlighted by Zong et al. [36] there are several configurations of multi-energy systems applied to buildings analyzed in literature. Among all possible, the energy sources that can be available for the satisfaction of the building thermal demand, attention must be paid to the integration of district heating and cooling system in an

efficient multi energy system. In the next sub-section, a dedicated focus on the importance of district heating and cooling systems in an energy flexibility context is provided.

2.2.1 District systems

According to IEA [37], district heating and cooling systems are expected to play a key role in the energy grid and supply, particularly when heat pumps are connected to the system. Indeed, they offer important advantage to the whole energy systems.
As summarized by Guelpa and Verda [37] with their literature review, the adoption of district heating and cooling systems provide many advantages, thanks to the possibility of combining [38][39]:

- Renewable energy sources.
- Heat pumps systems.
- Waste heat recovered by industrial plants or energy plants.
- Cogeneration plants for the combined production of electricity and heat.
- Conventional plants (i.e., boiler system).
- Heat produced by the prosumers connected to the network.

Moreover, as highlighted by Vandermeulen et al. [35], thanks to the different levels of thermal inertia that can be exploited in thermal networks, district heating and cooling systems show great potential also in providing flexibility services. Indeed, they distinguished three different contributions to accumulate energy, located in different point of the network: (i) the heat or cold carrier fluid, (ii) the possible addition of a thermal storage device and (iii) the thermal inertia of the buildings to which heat or cold is supplied.
Given all these advantages highlighted, it is clear how to set up a flexibility analysis that also involves the contribution of shared energy sources such as district heating and cooling networks can be fundamental to broaden the context of the assessment from an individual point of view to an aggregate one (i.e., from the single building to clusters).

2.3 Control logics to activate flexibility services

Advanced control methods for energy management in buildings are required if the goal is obtaining an optimized operational performance [20]. In general, the controls of the HVAC of a building can be distinguished in two main categories: traditional control

strategies and advanced control strategies [40]. The first one can be in turn classified in rule-based control (e.g., on-off control) and process control (e.g., PID control) [40]. As well, three classifications for advanced control strategies can be identified: (i) soft-computing control strategies (e.g., reinforcement learning, deep learning based on artificial neural network, fuzzy logic controls and agent-based controls), (ii) hard-computing control strategies (e.g., auto-tuning PID control, gain- scheduling control, self- tuning control, supervisory/optimal control, model predictive control and robust control) and (iii) hybrid control strategies, which is a combination of soft and hard control strategies [40].

Among all, model predictive control (i.e., hard-computing control strategies) represents one of the most investigated controls in academic literature [41][42], given its ability to easily merge the principles of feedback control and numerical optimization [43]. In the last decade, MPC has become a dominant control strategy in research on intelligent building operation [44]. Indeed, as highlighted by Drgôna et al. [44], the main benefit of model predictive controls in buildings is a systematic thermal comfort improvement with simultaneous energy savings [45][46], as well as grid flexibility services via price-responsiveness and active demand response capabilities [47].

The basic concept of the MPC is to use a dynamic model to forecast a system behavior and to optimize the actuations in order to operate under the best sequence of decisions [48]. A key feature of MPCs consists in selecting future control actions, taking into account both predictions of future disturbances and system constraints [43], while the goal is pursued. Therefore, in order to be effective, the MPC should be provided with an accurate model that is able to forecast the actual building energy demand [49]. Analyzing the scientific literature, three categories of building energy modeling are widespread for short-term predictions: physical-based, data-driven, and hybrid models [50].

Physical-based systems are white box models [51] that need a detailed description of the building's physical and thermal properties in order to describe the building's dynamics with mathematical equations. Typically, they solve energy conservation equations based on heat transfer phenomena. No training data are required, and the parameters of the model are usually obtained from design plans, manufacture catalogues, or on-site measurements [50]. Most of the popular software, such as Energy Plus, TRNSYS, DOE-2, or ESP-r, is based on a physical-based approach [52]. On the other hand, data-driven (or black box) models do not require a physical knowledge of the system, but they need a large amount of training data to be collected over an exhaustive period [50], i.e., both the data and the considered period should be statistically representative of the system operation. Statistical models have been directly applied in order to capture the correlation between building energy consumption and available measurement data [51]. The most common black box models are support vector machines, statistical regression (e.g., linear auto regressive models with exogenous inputs, ARX) and artificial neural

networks (ANNs) [53]. Unlike white box models, in which all the model parameters have a physical meaning, the parameters involved in a black box model cannot be interpreted in such terms. A compromise between the two approaches is represented by hybrid (or grey box) models. Grey box models are a combination of physical-based and data-driven prediction models; thereby, some internal parameters and equations are physically interpretable, while others are estimated with a data-driven approach. Grey box models are widespread in building energy modeling [54], although they require both the system structure and training data.

Different works are available in literature assessing the adoption of model predictive control to manage the HVAC of a building. They are mainly focused on evaluating the best model configuration to be adopted in an MPC (e.g., parameters identification, selection of inputs and outputs) or on the energy benefits that can be obtained through the adoption of such controls in specific buildings. For instance, Ferracuti et al. [55] compared the performance of three different data-driven models for short-term thermal prediction in a real building: a lumped element grey box model, an ARX, and a nonlinear ARX. They demonstrated that all the data-driven models investigated can be used to predict the short-term flexibility of the building for DR applications. In fact, for a prediction horizon of one hour, all the models showed a maximum root mean square error, *RMSE* (Root Mean Square Error), less than 0.5 °C in the tested period (among the grey box models, the third order one showed the best performance). Touretzky and Patil [56] developed an ARX model to forecast the building power demand, also adopting physics-based modeling approaches for building energy management. They investigated different configurations of options for inputs and outputs in relation to the available measurements, highlighting the importance of an appropriate selection of exogenous inputs in order to capture the effect of common demand management practices.

On the other hand, there are many examples of studies that focus on the energy performance improvement that is obtained when a predictive control is used in a building with respect to a classic ruled-based control. For instance, Drgôna et al. [57], obtained an energy use savings equal to 53.5% and a thermal comfort improvement of 36.9% for an office building in Belgium when a white box MPC based on first-principle physical equations is adopted. Ferreira et al. [58] found similar energy savings (greater than 50%) when an MPC is adopted in the building sector. In this case, they proposed a discrete MPC that used radial-basis-function ANNs as predictive models and demonstrated the feasibility of the model with experimental results obtained in a building of the University of Algarve. Also, Joe and Karava [59] introduced a smart operation strategy based on an MPC in order to optimize the performance of hydronic radiant floor systems in office buildings. They obtained a 34% cost saving compared to the baseline feedback control during the cooling season and a 16% energy use reduction during the heating season.

It is important to note that the works mentioned represent only a small part of all the scientific production available in the literature on the use of model predictive controls in buildings. For this reason, they are chosen as controls to be used for the activation of energy flexibility in buildings in the analysis proposed in this thesis. In particular, an aspect that is not always considered when applying the MPCs in buildings for flexibility analysis, is the ability of the model contained in the control to predict not only the energy demand of the building but also its ability to vary its needs when flexibility due to TCLs is activated. This aspect is treated in this thesis also comparing differing model techniques (i.e., white and black box approaches).

Chapter 3

Quantification of the design energy flexibility in single building

In this chapter, the methodology for buildings energy flexibility labelling introduced in Paper 2 is presented. The method is based on a standard procedure that allows the assessment of the flexibility performance of buildings equipped with electrically driven heating and cooling systems. In particular, the methodology allows to calculate a single indicator: the Flexibility Performance Indicator (FPI) that summarizes the energy flexibility performance of a building and its HVAC system. The objective is to broaden the energy characterization of the building also considering the aspect of the potential reserve of flexibility contained in it. Indeed, as for the energy efficiency labelling already defined in the energy performance certificate, the FPI allows the identification of flexibility classes to label buildings according to their energy flexibility potential derived by their intrinsic features (e.g., level of thermal insulation, thermal mass, characteristics of the emission system). Details about the methodology formulation are provided in Section 3.1, while in Section 3.2 its application to different case studies id discussed.

3.1 Flexibility performance indicator

The flexibility performance indicator depends on the most relevant parameters for energy flexibility (i.e., time, power and capability) as suggested in literature [14]. As the methodology is designed to evaluate the flexibility that can be provided to the electricity grid, only the electricity demand is taken into account.
As mentioned, since the energy flexibility evaluation requires a dynamic analysis, a transient simulation tool must be used. However, before introducing the calculation method (sub-section 3.1.2), in order to introduce a univocal quantification method standard boundary conditions has to be defined (sub-section 3.1.1).

3.1.1 Standard boundary conditions

The boundary conditions which affect the energy flexibility assessment are: (i) the weather data, (ii) the demand response (DR) event and (iii) the thermal comfort constraints.
To represent the dynamic of the external environment (i), a climatic file representing a typical meteorological year must be considered for each location. First of all, a representative day in which the DR event occurs must be selected. It is assumed to be, the most representative day of summer and winter season referring to available standard data. For instance, for the Italian case the reference standard UNI 10349-1 [60] reports the climatic data to assess the buildings energy performance. In particular, for the most representative Italian cities with a weather station, the standard identifies an average daily temperature for each month. This method proposes to select from the climatic file as representative day that one whose average daily temperature matches better with the values obtained from the standard (the lowest average daily temperature indicated by the standard in winter and the highest average daily temperature in summer are taken in order to capture the most extreme cases).
Once the day is identified, it is also necessary to set the starting time of the demand response event. First of all, the selected DR event (ii) is a peak shaving strategy. It consists in interrupting power supply to the heating/cooling system at the electric grid peak power demand time until the internal comfort conditions reach a desired lower bound. This is the first phase called “response period”. Then the heating/cooling system is switched on to restore the initial internal comfort conditions (“recovery period”). From the building point of view the DR event is realized with a rule-based control that varies the comfort temperature set points to reduce the demand during peak periods.
To evaluate the peak time, it is suggested to consider the peak electricity demand times for the country where the building is located. For example, for the Italian case, from the daily balancing data available on Terna website [61], it can be noted that the Italian electricity demand has always two peaks, one in the first part of the day and the other in the second part (Figure 3.1). In winter the first peak occurs between 10.00 am and 12.00 pm, and the second one between 6.00 pm and 7.00 pm. In summer, instead, the first peak occurs between 12.00 pm and 1.00 pm and the second one between 5.00 and 6.00 pm. Therefore, considering the most severe cases, the Italian starting time for the demand response event to be used is 7.00 pm for the heating case and 12.00 pm for the cooling case.

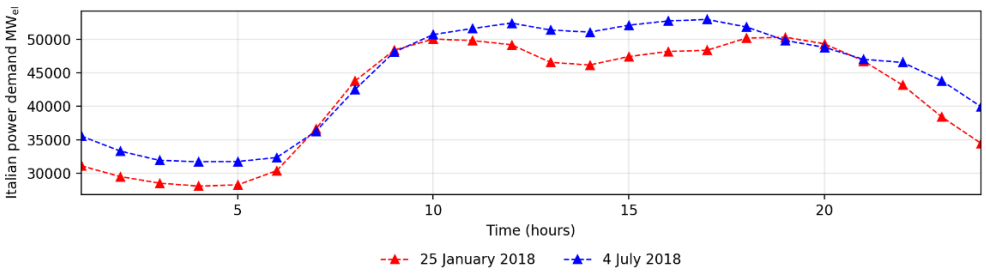

Figure 3.1. Two Italian daily electric power demand curves: 25 January 2018 and 4 July 2018.

As concern the comfort bounds (iii), according to Fanger [62], the following comfort temperature ranges are selected:

- For the heating season between 20 °C and 22 °C.
- For the cooling season between 24 °C and 26 °C.

Moreover, in the cooling season, when also a punctual humidity control is allowed by the HVAC system, a comfort range between 60% and 70% is selected for the indoor relative humidity (RH).

During the demand response event the flexibility provided by the management of the thermostatically controlled load is activated is this way: for the heating case a 2 °C decrease is allowed starting from a setpoint temperature of 22 °C, while for the cooling case the temperature can increase 2 °C from a temperature setpoint of 24 °C and, if it can be controlled, a 10% RH increase is allowed.

In Figure 3.2 is showed a representation of a demand response event in heating season with a distinction between the two phases: the response and the recovery periods.

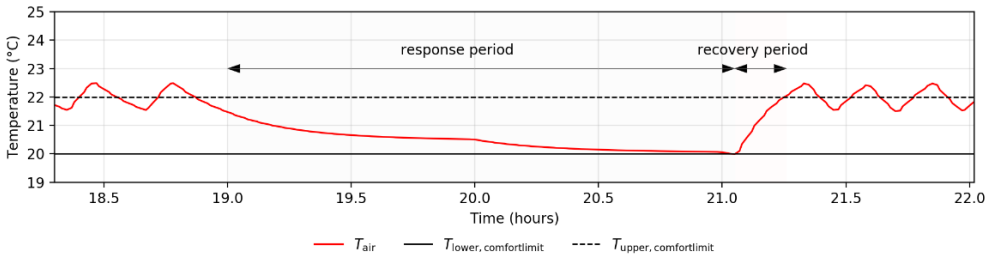

Figure 3.2. Indoor temperature during the demand response event in heating case: distinction between response and recovery periods.

3.1.2 Labelling method

The methodology to quantify and label the buildings energy flexibility is formulated according to the method of Reynders et al. [14] and it is introduced in its definitive formulation in Paper 2. As mentioned, the quantification method allows the calculation of a single indicator (the Flexibility Performance Indicator, FPI) which includes the aspect of both the time, the power and the capability.
In general, the FPI depends on four flexibility parameters:

- The response time (t_{res}) that represents the time necessary to the internal temperature to reach the lower or upper comfort temperature bound respectively in winter and summer. This parameter quantifies how much time the heating/cooling generator can remain off while the building can maintain its comfort conditions.
- The committed power ($\dot{P}_{res}$) that represents the effect of the demand response event in terms of electrical power engaged. It is defined as the integral of the difference between the heat pump reference power demand (i.e., without DR) and the heat pump power demand during the demand response event divided by the duration of the response phase (i.e., t_{res}).

$$\dot{P}_{res} = \frac{1}{t_{res}} \int_0^{t_{res}} \left(\dot{P}_{REF} - \dot{P}_{DR}\right) dt \qquad \text{Eq. (1)}$$

  $\dot{P}_{REF}$ refers to normal operation of the system, when no event is in place, and it represents the heat pump electric power demand for heating/cooling during the same period in the representative day as for the demand response event.
- The recovery time (t_{rec}) that represents the time necessary to the restore the starting comfort conditions.
- The actual energy variation (E_{DR}) that is defined as the difference in energy use between the reference condition and the demand response event during the whole demand response event (i.e., t_{DR}).

$$E_{DR} = \int_0^{t_{DR}} \left(\dot{P}_{REF} - \dot{P}_{DR}\right) dt \qquad \text{Eq. (2)}$$

The first two parameters are more interesting for the electric grid side. Indeed, they refer to the response period when the heating/cooling systems are switched off and then the network load is reduced. The other two parameters, on the other hand, are of greater interest for the user side, because they consider how fast the initial comfort is restored after a demand response event and the actual impact of the event on energy use.

The flexibility performance indicator is defined in a dimensionless form as weighted average of four contributions, as shown in Equation (3):

$$\mathrm{FPI} = \frac{1}{4}\left(p_1 \cdot t^*_{res} + p_2 \cdot \dot{P}^*_{res} - p_3 \cdot t^*_{rec} + p_4 \cdot \eta_{DR}\right) \quad \text{Eq. (3)}$$

With:

$$t^*_{res} = \frac{t_{res}}{24} \quad \text{Eq. (4)}$$

$$\dot{P}^*_{res} = \frac{\left|\dot{P}_{res}\right|}{\dot{P}_{rated}} \quad \text{Eq. (5)}$$

$$t^*_{rec} = \frac{t_{rec}}{24} \quad \text{Eq. (6)}$$

$$\eta_{DR} = \begin{cases} \dfrac{E_{DR}}{\int_0^{t_{DR}} \dot{P}_{REF}\, dt} \\ 0 \text{ if } E_{DR} < 0 \text{ in peak shaving} \end{cases} \quad \text{Eq. (7)}$$

The first term in Equation (4) is the response time referred to 24 h, with a weight of 60% (p_1 equal to 60). The second is the committed power normalized to the installed rated power ($\dot{P}_{rated}$) with a weight of 20% (p_2 equal to 20). The third is the recovery time normalized on 24 h with a weight of 10% (p_3 equal to 10) and the last one is a sort of demand response energy efficiency, since it is calculated as the ratio between the actual energy variation achieved during the event and the building electricity use in reference operation (i.e., without DR) during the duration of the event (i.e., t_{DR}). It has a weight of 10% (p_4 equal to 10). As highlighted, in Equation (7), the demand response efficiency is zero if the peak shaving strategy does not produce any energy saving.

The weights distribution is determined with an empirical approach by observing simulation data representing the behavior of a large amount of buildings configurations during a demand response event. Different configurations of buildings are tested and most of them are discussed in the next section (Section 3.2). The trend of the different parameters composing the FPI is analyzed and, keeping in mind their effect on the available flexibility, they received a weight that could provide reasonable overall FPI values with a trial and error approach. In particular, on the basis of the expected flexibility performance, different combinations of weights are tried and, the one that seemed to best represent the differences between the cases studied is chosen. Furthermore, the criterion that is used also provides that the numerical values of the weights are assigned to emphasize the impact of the demand response event on the

electricity grid. Therefore, a greater weight is given to those parameters which denote the interaction with the grid side (i.e., p_1 and p_2), especially to the response time that represents the time that the heating system is independent from the grid. Whereas it is assumed the same weight for the two parameters representing the user's side (p_3 and p_4). It is important to note that the numerical values of the weights reported in this formulation represents a first hypothesis to calculate the FPI that is based on the observed case studies. However, the results could be different if the weighting factors of the FPI are differently selected. Though, the chosen set of values represents the configuration that seems to best represent the different performance of buildings in terms of energy flexibility.

Once the FPI is calculated, through the definition of limit thresholds, it is possible to rate a building in a specific flexibility class. The same approach as the energy labelling is supposed. Indeed, to calibrate the actual building flexibility and reduce the influence of the building location (i.e., weather data) ideal reference conditions are assumed.

In the ideal reference conditions a building with the same thermal resistance of the building under evaluation is considered, but its thermal mass (both for the envelope and heating/cooling distribution system) is neglected. It is assumed that the building is subject to the same demand response event when the outside ambient temperature is constant at the design value used to size the heating and cooling systems, respectively in winter and summer. An FPI_{limit} value in steady state conditions is calculated with the following assumptions:

- Thermal losses evaluated considering an average indoor condition 21 °C in winter and 25 °C and 60% of relative humidity in summer.
- Solar gains and internal gains are considered only in summer and they include both sensible and latent contributions if the plant can control the relative humidity.
- The heating/cooling system without the demand response event works at fixed conditions equal to design values.
- In case without the demand response event the heating/cooling system works for the whole period at nominal power.
- In case with the demand response event the heating/cooling system works during the recovery period at nominal power.

Consequently, the flexibility parameters are calculated in the following way:

- The response time is calculated as the energy necessary to produce a 2 °C variation of the indoor air divided by the net value of thermal losses and gains.
- The committed power is equal to nominal power.
- The recovery time is calculated as the energy necessary to produce a 2 °C variation of the indoor air divided by the heating/cooling system nominal capacity.
- The actual energy variation is calculated as showed in Equation (2).

The FPI_{limit} refers to an extreme case where the inertia of the building is neglected, and the heating/cooling system load is always at its design value.
The reference condition represents a configuration with limited flexibility due to thermal mass but with a fast responsiveness of the heating/cooling system (i.e., it works always at nominal conditions), then it is assumed to be a medium flexibility level and it is set in class B.
The flexibility class for the considered building is determined on the basis of the ratio between FPI and FPI_{limit} as represented in Figure 3.3, where the subdivision in classes is showed. However, more details about the methodology formulation and the flexibility classes partition can be founded in Paper 2, where the methodology is presented.

	Class A3	**$\geq 3.6\ FPI_{limit}$**
$2.4\ FPI_{limit} \leq$	**Class A2**	**$< 3.6\ FPI_{limit}$**
$1.5\ FPI_{limit} \leq$	**Class A1**	**$< 2.4\ FPI_{limit}$**
$0.9\ FPI_{limit} \leq$	**Class B**	**$< 1.5\ FPI_{limit}$**
$0.6\ FPI_{limit} \leq$	**Class C**	**$< 0.9\ FPI_{limit}$**
	Class D	**$< 0.6\ FPI_{limit}$**

Figure 3.3. Energy flexibility classes for buildings labelling.

3.2 FPI application

In order to evaluate the reliability of the methodology, the FPI is calculated for different buildings both in heating and in cooling season. Buildings are differentiated according to location (e.g., different weather data are considered), thermal and geometrical features (e.g., wall stratigraphy, thermal losses and heaviness of the envelope) and HVAC system (e.g., radiant distribution systems, fan coils units, radiators and split systems).
The presented case studies are evaluated in Papers 1, 2 and 3. All of them are representative for the Italian scenario and TRNSYS [63] is used as dynamic energy simulation tool to implement the methodology. It is important to notice that, the mentioned works are aimed to evaluate the effectiveness of the methodology in showing variations in the flexibility performance indicators when buildings with different features are tested. In particular, in the sub-section 3.2.1 the construction age of the buildings is taken into account. In sub-section 3.2.2 the analysis is focused on the role of the heaviness and the composition of the building envelope in different locations. And, finally, in sub-section 3.2.3 is presented a case study in which the FPI is used to

evaluate the effect of the most widespread renovation strategies on the energy flexibility performance.

3.2.1 Role of the construction age

The effectiveness of the methodology in evaluating the different energy flexibility performance of buildings with different construction ages is evaluated in Paper 1. In this case a preliminary version of the methodology is used. In particular, a tighter comfort limit is used (from 19 °C to 20 °C for the heating season and from 23 °C to 25 °C in the cooling season), the weights of the four parameters composing the FPI (Equation (3)) are different (p_1 equal to 50 %, p_2 equal to 20%, p_3 equal to 15 % and p_4 equal to 15 %) and the FPI_{limit} calculation is not intended. Thus, the flexibility classes are defined only according to the value of the FPI: when the FPI is greater than 10 the building is labelled in class A+, for values between 8 and 10 the class is A, for FPI between 5.5 and 8 the class becomes B, for values between 4 and 5.5 the class is C and, finally, for FPI lower than 4 the D is the flexibility class.
To test the methodology, a set of representative buildings are selected. Their main characteristics are extrapolated from TABULA project [64]. Since only heating and cooling systems provided with heat pump must be considered for the flexibility evaluation, not all the construction classes that are included in the TABULA are considered, but only those built from 1961 to the present. However, Table 3.1 contains values of the thermal transmittances of the selected age classes.

Table 3.1. U-value (W m^{-2} K^{-1}) implemented in Paper 1.

Age class	External walls	Floor	Roof	Windows
1961-1975 (Class 5)	1.57	1.09	1.30	5.83
1976-1990 (Class 6)	0.90	0.99	0.74	5.68
1991-2005 (Class 7)	0.60	0.69	0.53	2.83
2006-today (Class 8)	0.29	0.29	0.28	1.40

All the dwellings are composed of single climatic zone with a living area of 100 m^2 as apartments in multi-family houses (i.e. each apartment is are considered on a raised floor, with a wall and the floor adjacent to another apartment and on the top floor of the building). For each wall, 10% of percentage of windowed area is assumed and an air changes per hour (ACH) are equal to 0.5 h^{-1} is considered.
As concerning the HVAC systems, compatibly with the age class, four configurations for the heating system and two configurations for the cooling system are modelled. Starting from the heating systems, for the most recent classes (classes 7 and 8 in Table 3.1) a radiant distribution system coupled with air to water heat pump is modelled. In

this case the heat pump, whose performance are derived from a manufacturer catalogue [65], is sized to cover 70% of the building design power (calculated as the maximum thermal load of the buildings at reference conditions for the external environment [66]). For these two age classes (7 and 8) also a split system is modelled for the thermal distribution. In this case the refrigerant exchanges heat at the condenser/evaporator directly with the indoor air.

For the age class 7, imagining a small variation of the typical heating systems of buildings of this age (i.e. methane gas boiler and radiators), also an air source heat pump coupled with radiators is modelled as heating system. In a retrofit scenario, the air source heat pump replaces the boiler. In this case the system is equipped with a small thermal storage (a hot water tank of 60 liters) to limit the on-off cycles of the heat pump.

For the older buildings (classes 5 and 6 in Table 3.1), assuming a possible renovation, a hybrid heating system is present. An heat pump is added to a classic 25 kW boiler, used both for heating and domestic hot water. An alternative-parallel configuration is considered in which the heat pump is sized for an external temperature of 5 °C [67]. Also, in this case the system is equipped with a small thermal storage to limit the on-off cycles of the heat pump (80 liters for class 6 and 100 liters for class 5).

As far as the cooling system is concerned, a typical configuration with direct expansion air source heat pump (i.e., split system) is applied to all the age classes. For the most recent classes (7 and 8 in Table 3.1) also a radiant distribution system coupled with an internal air dehumidifier is modelled. In this latter configuration the same heat pump used in the heating case reverses its operation and sends chilled water to the distribution system. Summing up the case studies analyzed for the heating season are:

(i) Age class 8 (2006-today) with an air to water heat pump coupled with radiant floor as distribution system.
(ii) Age class 7 (1991-2005) with an air to water heat pump coupled with radiant floor as distribution system.
(iii) Age class 8 (2006-today) with a direct expansion air source heat pump (split system).
(iv) Age class 7 (1991-2005) with a direct expansion air source heat pump (split system).
(v) Age class 7 (1991-2005) with an air to water heat pump with radiators as distribution system.
(vi) Age class 6 (1976-1990) with an hybrid system (air to water heat pump and traditional boiler) with radiators as distribution system.
(vii) Age class 5 (1961-1975) with an hybrid system (air to water heat pump and traditional boiler) with radiators as distribution system.

For the cooling season, instead, the modelled case studies are:

(i) Age class 8 (2006-today) with a direct expansion air source heat pump (split system.
(ii) Age class 8 (2006-today) with an air to water heat pump and dehumidifier with radiant distribution system.
(iii) Age class 7 (1991-2005) with an air to water heat pump and dehumidifier with radiant distribution system.
(iv) Age class 7 (1991-2005) with a direct expansion air source heat pump (split system).
(v) Age class 6 (1976-1990) with a direct expansion air source heat pump (split system).
(vi) Age class 5 (1961-1975) with a direct expansion air source heat pump (split system).

More details about the case studies are reported in Paper 1, where also the description of the different HVAC systems sizing procedure is presented.

In this evaluation, all the models are located in the city of Ancona (43°35′39″ N, 13°30′12″ E) in central Italy. The representative winter day is January 18 (the average daily temperature obtained from the climate file is 6 °C when the average monthly temperature for the month of January for the city of Ancona indicated in the norm is 6.3°C [66]). In the summer case, the representative day considered is July 11. In this day the average daily temperature is 24.5°C when the standard indicates to consider a temperature of 24.4°C [66].

Figure 3.4 shows the results for the application of the methodology to the heating case (Figure 3.4(a)) and to the cooling case (Figure 3.4(b)). It is important to notice that the results presented, in accordance with Paper 1, are obtained starting the DR event in heating season at 11.00 am (first peak power, Figure 3.1) while, for the cooling case the 12.00 pm is maintained.

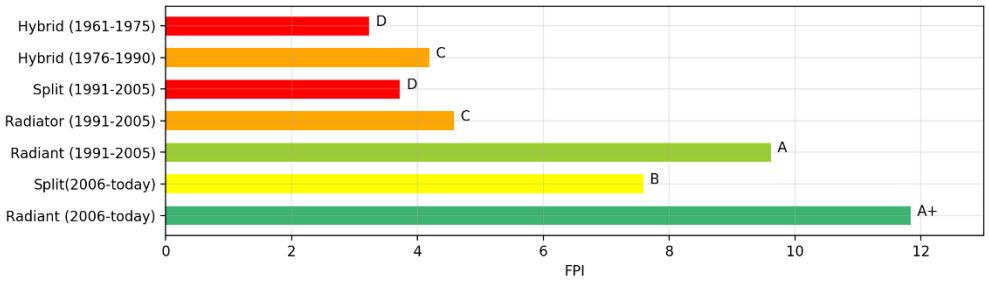

(a)

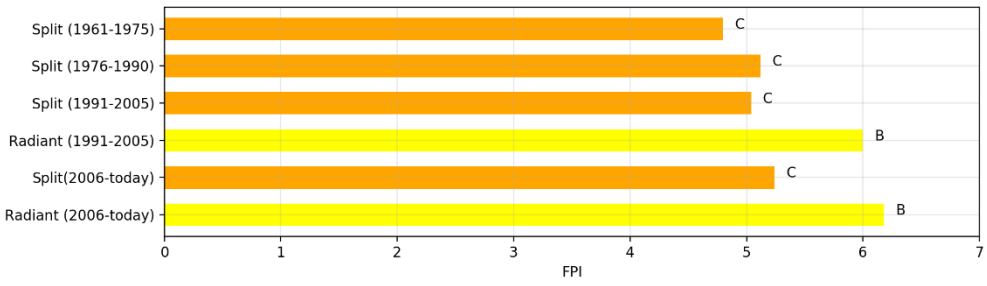

(b)

Figure 3.4. Buildings flexibility label for the case studies considered in Paper 1: (a) FPI for buildings in heating season and (b) FPI for buildings in cooling season.

Starting from the evaluation in the building season, as expected, the methodology label in the higher flexibility class (A+) the building with a more recent age class, therefore with an excellent level of thermal insulation and equipped with a radiant floor as distribution system (Figure 3.4(a)). On the other hand, the model with the worst performance (flexibility class C) is the older one equipped with radiators. Table 3.2 shows the values of the flexibility indicators in their dimensionless form.

Table 3.2. Flexibility parameters and labelling in heating case for case studies considered in Paper 1.

Heating system	Age class	t^*_{res}	$\dot{P}^*_{res}$	t^*_{rec}	η_{DR}
Radiant floor	2006-today	0.67	0.31	0.37	0.13
Split system	2006-today	0.19	0.38	0.01	0.88
Radiant floor	1990-2005	0.42	0.37	0.55	0.11
Radiator	1990-2005	0.03	0.40	0.01	0.59
Split system	1990-2005	0.02	0.39	0.01	0.41
Hybrid	1976-1990	0.01	0.29	0.01	0.68
Hybrid	1961-1975	0.01	0.28	0.01	0.44

Looking at the results, the methodology allows to appreciate both the influence of the isolation level and the thermal inertia of the distribution system. Indeed, comparing the two building of age class 8 (2006-today) and 7 (1990-2005) equipped with the radiant floor as heating system, different values of t^*_{res} and t^*_{rec} are obtained. The higher level of thermal insulation of the building in class 8 (2006-today) allows to obtain a greater inertia in the thermal response. Then it is translated into the building ability to maintain the conditions within the comfort zone for a longer period (t^*_{res}). Also, the t^*_{rec} differs slightly between the two models as a consequent of the higher thermal loss in the building in class 7 (1990-2005). However, with this heating system, relatively low values

of η_{DR} (13% for building in class 8 and 11% for building in class 7 (1990-2005), Table 3.4) are obtained. This is due to the great energy consumption in the recovery phase that makes the actual energy saving lower.
Passing at the observation of the results for the other models, an overall decrease of t^*_{res} is observed compared to the two cases discussed so far. It mainly depends on the almost total absence of thermal inertia introduced by the other distribution systems. With the same construction class, for example class 8 (2006-today), t^*_{res} decreases by 72% if the building is equipped with a direct expansion heating system rather than with a radiant floor system and a very consistent variation is obtained for class 7 (1990-2005) too.
Another observation can be made by looking at the results obtained for the models in class 7 (1990-2005) equipped respectively with radiant floor, radiators and split system. Looking at Figure 3.5, another difference in the application of the method in Paper 1 resect the above discussed methodology can be notice. Indeed, the demand response event starts at 11.00 am for the test in heating season. However, a different in the evolution of the event due to the thermal inertia of the distribution system can be observed. Although small, in fact, radiators have a thermal inertia greater than splits, this allows to take a longer time in reaching the comfort limit condition. These types of distribution systems (radiators and splits) however, show lower performance compared to the radiant floor, even if their demand response efficiency is higher (Table 3.2).

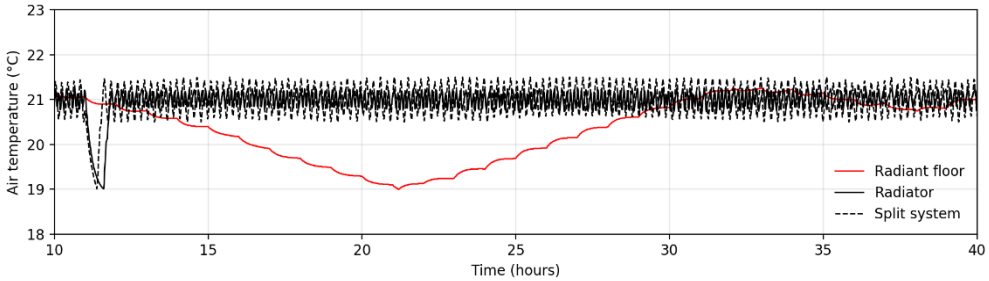

Figure 3.5. Air temperature during the demand response event in heating season for building of class 7 (1990-2005) with different heating systems: radiant floor, radiator and split system.

Regarding the models of older age classes (i.e., 6 and 5, respectively buildings build between 1976 and 1990 and between 1961 and 1975), the flexibility time indices are greatly influenced by the low thermal inertia of the system. Consequently, relatively low values of flexibility indices are obtained.
Passing to the cooling season analysis, Table 3.3 shows the flexibility indicators obtained for the cooling case. From a first observation of the results (Table 3.3 and Figure 3.4(b)), the methodology evaluates the best performance in term of energy

flexibility for the radiant system coupled with the air dehumidifier (applied only to the most recent construction classes: 7 and 8, respectively buildings build between 1990 and 2005 and from 2006 onwards).

Table 3.3. Flexibility parameters and labelling in cooling case for case studies considered in Paper 1.

Cooling system	Age class	t^*_{res}	$\dot{P}^*_{res}$	t^*_{rec}	η_{DR}
Radiant and dehumidifier	2006-today	0.07	0.59	0.02	0.60
Split system	2006-today	0.02	0.68	0.02	0.41
Radiant and dehumidifier	1990-2005	0.06	0.61	0.02	0.55
Split system	1990-2005	0.02	0.60	0.01	0.45
Split system	1976-1990	0.02	0.71	0.01	0.35
Split system	1961-1975	0.02	0.57	0.01	0.44

In these models, since it is possible to control the humidity of the indoor air too, the t^*_{res} indicator is so evaluated with the comfort limit condition reached earlier, between temperature and humidity. In the specific case, the boundary condition for humidity is reached faster, limiting the duration of the response phase and therefore the exploitation of the thermal inertia of the distribution system.
As far as the other cooling system is concerned (all the dwellings are modelled with a split system), considering all the modelled age classes, from 5 to 8, the demand response events have a duration ranging between 0.73 hours and 0.89 hours and also the efficiency of the event the has similar values among the various cases (from 35 % to 45 %). This behavior makes possible to conclude that, according to the model formulation, for the modelled dwellings in summer period there is a lower overall capacity to provide energy flexibility than the heating season. Furthermore, there is a small influence of the structural composition of the building in case of reduced thermal inertia of the distribution system.
However, albeit in a preliminary formulation, the calculation of the FPI has shown itself capable of representing the variation in the intrinsic features of the buildings (i.e. level of thermal insulation and thermal inertia of the HVAC system) both in heating and cooling season.

3.2.2 Role of the envelope composition

In order to assess the reliability of the methodology, in this section the FPI is calculated for buildings differentiated in base of locations (i.e., the weather data) and of the building envelope characteristics. This analysis is contained in Paper 2, where the final version of the methodology is also presented.

Two extreme climatic zones are assumed as building locations in the Italian scenario: Messina (climatic zone B, 38° 11′ N, 15° 32′ E) and Turin (climatic zone E, 45° 7′ N, 7° 43′ E) respectively in the south and in the north of Italy. Then, different building specifications are modelled (i.e., variation of the wall stratigraphy and heaviness of the building envelope). To extend the analysis, two HVAC systems are introduced for each building: an air to water heat pump coupled with a radiant distribution system and with fan coils units.
As reference conditions for the thermal features of the buildings, the Italian regulation D.M. 11 March 2008 [68] is assumed since it is representative of a consistent share of the building stock where the heat pump technology can be integrated. Table 3.4 shows the prescribed thermal transmittances (U-values) of the building envelope for the two different climatic zones modelled.

Table 3.4. U-values (W m^{-2} K^{-1}) implemented in Paper 2.

Location	External walls	Floor	Roof	Windows
Climatic zone B	0.48	0.49	0.38	3.00
Climatic zone E	0.34	0.33	0.30	2.20

All the buildings are modelled with the same value of thermal transmittance for each location but, to evaluate the effect of the envelope thermal inertia, the external walls (i.e., vertical walls, roof and floor) are considered with different compositions and thermal properties of the construction materials. In particular, the wall stratigraphy is varied by changing the position of the thermal insulation. Three position of the thermal insulation (thermal conductivity 0.04 W $m^{-1}K^{-1}$) are tested: external insulation, cavity wall insulation and internal insulation. Then, for each insulation position, two different heaviness for the walls, which differ in the load-bearing layers, are distinguished.
A heavy structure is modelled with solid bricks (density 1800 kg m^{-3}, thermal conductivity 0.72 W $m^{-1}K^{-1}$ and specific heat 1000 J $kg^{-1}K^{-1}$) and a more light structure with hollow bricks (density 1000 kg m^{-3}, thermal conductivity 0.34 W $m^{-1}K^{-1}$ and specific heat 1000 J $kg^{-1}K^{-1}$). More details about the characteristics of the building models are reported in Paper 2, where also the thermal properties of each layer of the building envelope are provided.
Going to the HVAC systems, as mentioned, two different heating and cooling systems are introduced in order to distinguish a low and a high thermal inertia contribution. The first one has a high/medium thermal inertia level as it is composed of an air to water heat pump coupled with a radiant distribution system, underfloor for the heating case and chilled ceiling for the cooling case. The cooling system includes also an air dehumidifier to control the internal humidity.

In heating season, the heat pump is sized to cover 70% of the building peak demand (calculated on the basis of the maximum thermal load of the buildings in stationary conditions, considering the outdoor temperature equal to the minimum winter temperature for the chosen locations, as suggested by UNI ENI 10349-2 [66]), as typically assumed in presence of high thermal inertia distribution systems [15]. In this case, the system is not equipped with a storage tank, since the thermal inertia introduced by the floor is sufficient to limit the on-off cycles of the heat pump [15].
In cooling mode, instead, the heat pump is sized to cover only the amount of sensible heat while the treatment of latent heat is entrusted to an internal air dehumidifier (the cooling system is sized by means of the Carrier-Pizzetti technical dynamic method [69]). In particular, the chilled ceiling is composed of pipes set on panels in the first internal layer of the roof, for this reason it is considered a medium thermal inertia system if compared with underfloor systems (high thermal inertia system).
The low thermal inertia HVAC system is composed of an air to water heat pump coupled with fan coil units used both for heating and cooling season. In this case the heat pump is sized to cover the whole heating/cooling thermal load and a small water tank is introduced in to limit its on-off cycles. In this case, even if a management of the latent contribution is possible in cooling case, a relative humidity punctual control is not possible.
Summing up, for each location the following building models are tested:

(i) Internal thermal insulation position with light envelope and fan coil units.
(ii) Internal thermal insulation position with light envelope and radiant system.
(iii) Cavity wall thermal insulation position with light envelope and fan coil units.
(iv) Cavity wall insulation position with light envelope and radiant system.
(v) External thermal insulation position with light envelope and fan coil units.
(vi) External thermal insulation position with light envelope and radiant system.
(vii) Internal thermal insulation position with heavy envelope and fan coil units.
(viii) Internal thermal insulation position with heavy envelope and radiant system.
(ix) Cavity wall thermal insulation position with heavy envelope and fan coil units.
(x) Cavity wall insulation position with heavy envelope and radiant system.
(xi) External thermal insulation position with heavy envelope and fan coil units.
(xii) External thermal insulation position with heavy envelope and radiant system.

The value of the FPI_{lim} for the considered cases are reported in Tables 3.5 and 3.6 respectively for buildings located in Messina and in Turin.

Table 3.5. FPI_{lim} for buildings located in Messina (Paper 2).

Location	Season	HVAC	FPI_{lim}
Messina	Heating	Fan coil units	6.36
Messina	Heating	Radiant system	6.14
Messina	Cooling	Fan coil units	6.39
Messina	Cooling	Radiant system	5.62

Table 3.6. FPI_{lim} for buildings located in Turin (Paper 2).

Location	Season	HVAC	FPI_{lim}
Turin	Heating	Fan coil units	6.29
Turin	Heating	Radiant system	6.03
Turin	Cooling	Fan coil units	6.39
Turin	Cooling	Radiant system	5.66

According to the boundary conditions specifications described in sub-section 3.1.1, the representative winter day for Messina is February 6 and for Turin January 11, while the representative summer day for Messina is July 2 and for Turin July 8.
In Figures 3.6 and 3.7 are presented the results of the methodology for the modelled case studies. In particular, the FPI calculated for all the heating and cooling cases are showed together with their flexibility label. Moreover, in Tables 3.7, 3.8, 3.9 and 3.10 the flexibility parameters calculated for each building are reported.

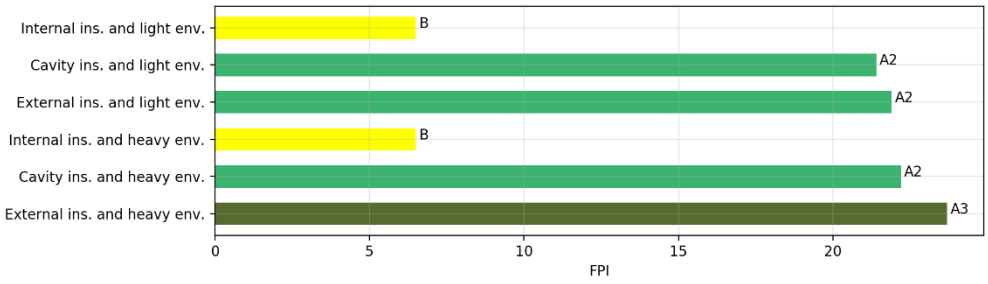

(a)

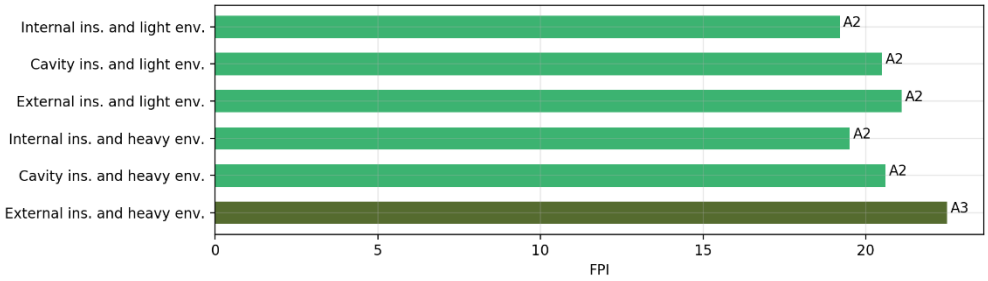

(b)

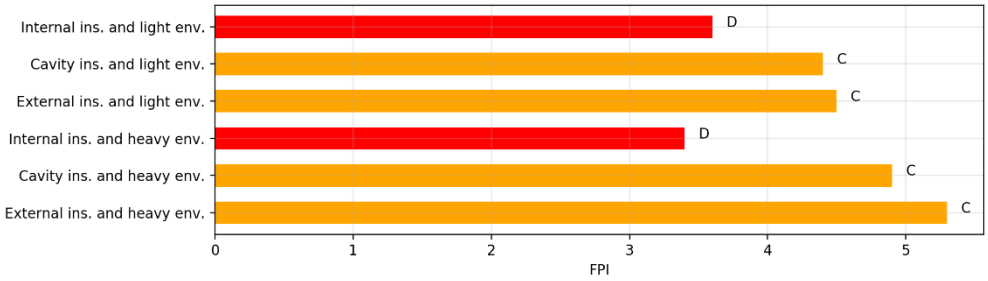

(c)

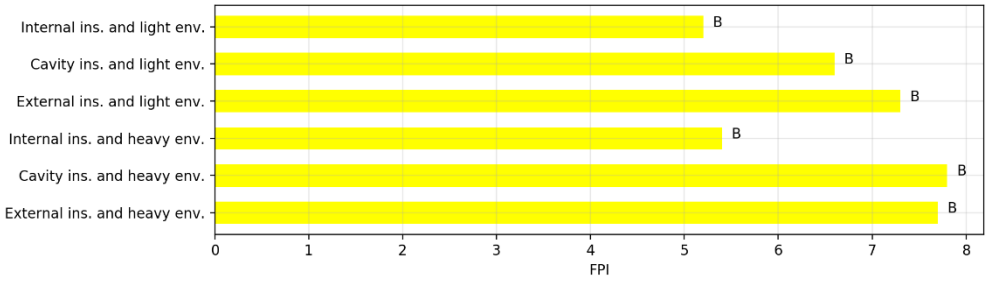

(d)

Figure 3.6. Buildings flexibility labels for the case studies considered in Paper 2 (located in Messina): (a) FPI for buildings in heating season and equipped with fan coil units, (b) FPI for buildings in heating season and equipped with radiant system, (c) FPI for buildings in cooling season equipped with fan coil units and (d) FPI for buildings in cooling season equipped with radiant system.

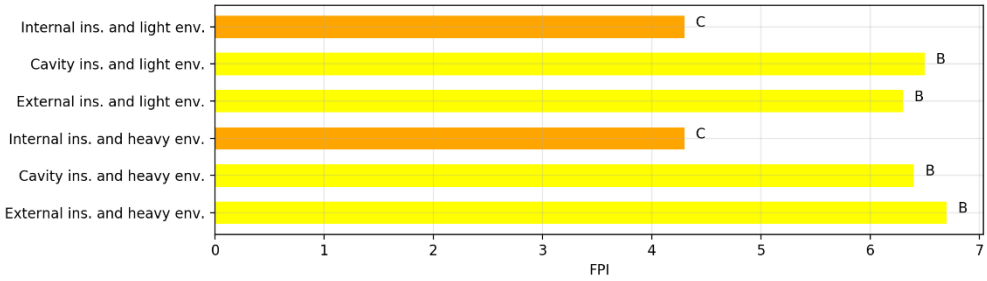
Internal ins. and light env.
Cavity ins. and light env.
External ins. and light env.
Internal ins. and heavy env.
Cavity ins. and heavy env.
External ins. and heavy env.
C
B
B
C
B
B
0
1
2
3
4
5
6
7
FPI

(a)

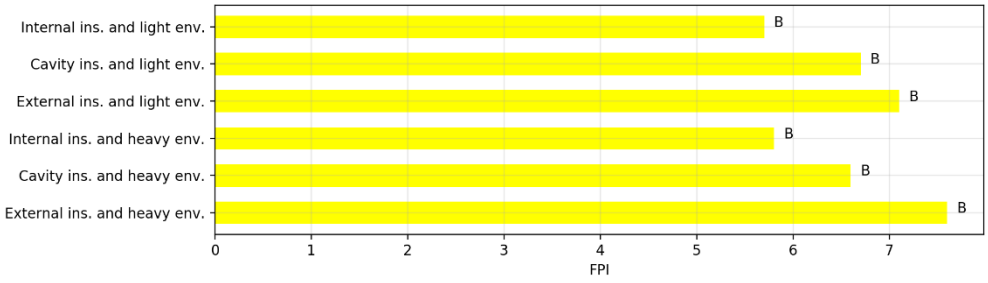
Internal ins. and light env.
Cavity ins. and light env.
External ins. and light env.
Internal ins. and heavy env.
Cavity ins. and heavy env.
External ins. and heavy env.
B
B
B
B
B
B
0
1
2
3
4
5
6
7
FPI

(b)

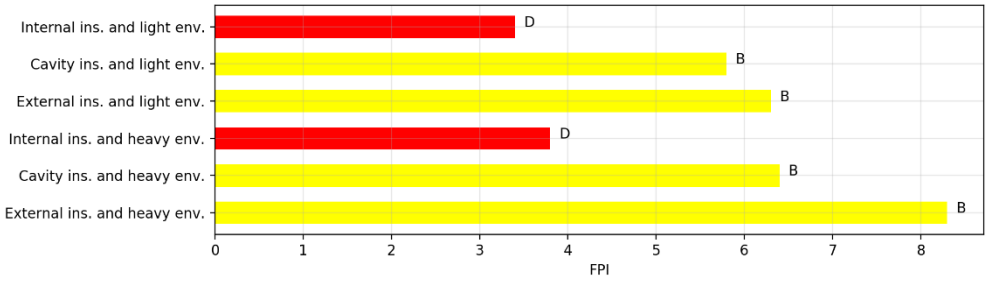
Internal ins. and light env.
Cavity ins. and light env.
External ins. and light env.
Internal ins. and heavy env.
Cavity ins. and heavy env.
External ins. and heavy env.
D
B
B
D
B
B
0
1
2
3
4
5
6
7
8
FPI

(c)

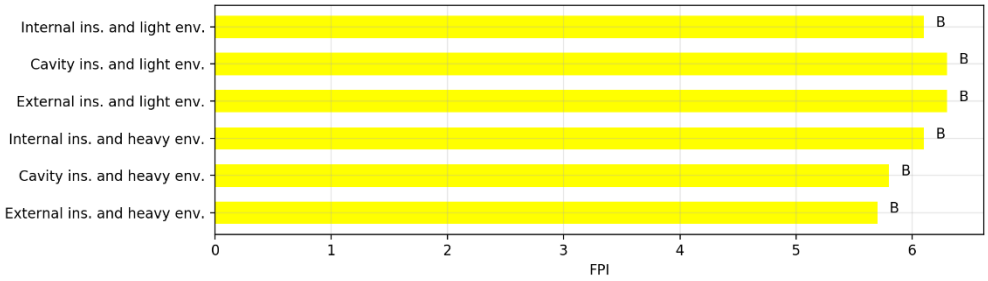

(d)

Figure 3.7. Buildings flexibility labels for the case studies considered in Paper 2 (located in Turin). (a) FPI for buildings in heating season and equipped with fan coil units, (b) FPI for buildings in heating season and equipped with radiant system, (c) FPI for buildings in cooling season equipped with fan coil units and (d) FPI for buildings in cooling season equipped with radiant system.

Table 3.7. Flexibility parameters in heating season for case studies considered in Paper 2 (located in Messina).

Heaviness of the envelope	**Insulation position**	**HVAC**	$\mathbf{t^*_{res}}$	$\mathbf{\dot{P}^*_{res}}$	$\mathbf{t^*_{rec}}$	$\boldsymbol{\eta_{DR}}$
Heavy	External	Fan coil units	1.37	0.17	0.02	0.95
Heavy	Internal	Fan coil units	0.25	0.17	0.02	0.76
Heavy	Cavity	Fan coil units	1.27	0.17	0.02	0.93
Light	External	Fan coil units	1.25	0.17	0.02	0.94
Light	Internal	Fan coil units	0.24	0.18	0.02	0.83
Light	Cavity	Fan coil units	1.22	0.18	0.02	0.92
Light	External	Fan coil units	1.34	0.40	0.39	0.55
Heavy	External	Radiant system	1.21	0.32	0.50	0.39
Heavy	Internal	Radiant system	1.25	0.37	0.47	0.47
Heavy	Cavity	Radiant system	1.28	0.36	0.44	0.48
Light	External	Radiant system	1.19	0.34	0.52	0.38
Light	Internal	Radiant system	1.25	0.35	0.47	0.45
Light	Cavity	Radiant system	1.37	0.17	0.02	0.95
Light	External	Radiant system	0.25	0.17	0.02	0.76

Table 3.8. Flexibility parameters in cooling season for case studies considered in Paper 2 (located in Messina).

Heaviness of the envelope	Insulation position	HVAC	t^*_{res}	$\dot{P}^*_{res}$	t^*_{rec}	η_{DR}
Heavy	External	Fan coil units	0.10	0.34	0.01	0.83
Heavy	Internal	Fan coil units	0.02	0.43	0.01	0.38
Heavy	Cavity	Fan coil units	0.09	0.34	0.01	0.80
Light	External	Fan coil units	0.06	0.35	0.01	0.75
Light	Internal	Fan coil units	0.02	0.46	0.01	0.42
Light	Cavity	Fan coil units	0.05	0.36	0.01	0.73
Light	External	Fan coil units	0.17	0.78	0.08	0.60
Heavy	External	Radiant system	0.09	0.74	0.13	0.29
Heavy	Internal	Radiant system	0.18	0.81	0.12	0.56
Heavy	Cavity	Radiant system	0.17	0.77	0.11	0.50
Light	External	Radiant system	0.09	0.67	0.12	0.31
Light	Internal	Radiant system	0.14	0.71	0.11	0.46
Light	Cavity	Radiant system	0.10	0.34	0.01	0.83
Light	External	Radiant system	0.02	0.43	0.01	0.38

Table 3.9. Flexibility parameters in heating season for case studies considered in Paper 2 (located in Turin).

Heaviness of the envelope	Insulation position	HVAC	t^*_{res}	$\dot{P}^*_{res}$	t^*_{rec}	η_{DR}
Heavy	External	Fan coil units	0.22	0.18	0.01	0.99
Heavy	Internal	Fan coil units	0.09	0.18	0.01	0.86
Heavy	Cavity	Fan coil units	0.21	0.19	0.01	0.93
Light	External	Fan coil units	0.21	0.19	0.01	0.87
Light	Internal	Fan coil units	0.07	0.18	0.01	0.96
Light	Cavity	Fan coil units	0.21	0.19	0.01	0.99
Light	External	Fan coil units	0.33	0.64	0.48	0.26
Heavy	External	Radiant system	0.31	0.39	0.47	0.16
Heavy	Internal	Radiant system	0.32	0.54	0.51	0.17
Heavy	Cavity	Radiant system	0.34	0.53	0.46	0.22
Light	External	Radiant system	0.30	0.41	0.49	0.14
Light	Internal	Radiant system	0.34	0.49	0.50	0.16
Light	Cavity	Radiant system	0.22	0.18	0.01	0.99
Light	External	Radiant system	0.09	0.18	0.01	0.86

Table 3.10. Flexibility parameters in cooling season for case studies considered in Paper 2 (located in Turin).

Heaviness of the envelope	Insulation position	HVAC	t^*_{res}	$\dot{P}^*_{res}$	t^*_{rec}	η_{DR}
Heavy	External	Fan coil units	0.30	0.32	0.01	0.91
Heavy	Internal	Fan coil units	0.03	0.37	0.01	0.59
Heavy	Cavity	Fan coil units	0.18	0.32	0.01	0.88
Light	External	Fan coil units	0.17	0.33	0.01	0.88
Light	Internal	Fan coil units	0.03	0.33	0.01	0.53
Light	Cavity	Fan coil units	0.13	0.34	0.01	0.86
Light	External	Fan coil units	0.10	0.58	0.04	0.53
Heavy	External	Radiant system	0.14	0.68	0.13	0.39
Heavy	Internal	Radiant system	0.11	0.57	0.04	0.58
Heavy	Cavity	Radiant system	0.12	0.60	0.03	0.62
Light	External	Radiant system	0.14	0.66	0.12	0.38
Light	Internal	Radiant system	0.12	0.61	0.04	0.63
Light	Cavity	Radiant system	0.30	0.32	0.01	0.91
Light	External	Radiant system	0.03	0.37	0.01	0.59

Looking at the results show in Figures 3.6 and 3.7 and the flexibility parameters reported in Tables 3.7, 3.8, 3.9 and 3.10, it can be noted that the weather data have a great impact on the achievable flexibility performance according to the presented methodology. Indeed, comparing corresponding cases in terms of building and HVAC technical specification (i.e. Figure 3.6(a) vs Figure 3.7(a) and Figure 3.6(b) vs Figure 3.7(b)), a great difference in the FPI values, especially in the heating season is highlighted between buildings located in Messina and in Turin. As the FPI is calculated in operating conditions during a limited period of time (one or two days according to the duration of the response and the recovery period), the influence of weather data is more relevant than for the average annual energy demand used in energy performance labelling. This behavior allows to observe that the energy efficiency minimum requirements may not be enough to identify buildings able to provide also good level of energy flexibility.
Looking at Tables 3.7 and 3.9 for the heating season, it is possible to see that the difference between the FPI values is ascribable mainly to the length of the response period. Indeed, the buildings located in Messina can maintain their internal temperature within the comfort band for a time about four times greater than that of the building located in Turin. For the summer case similar considerations can be made. The warmer weather in Messina negatively affects the duration of the response period in contrast with the milder summer in Turin (Table 3.8 vs Table 3.10). However, in term of flexibility classes (Figure 3.6(c) vs Figure 3.7(c) and Figure 3.6(d) vs Figure 3.7(d)) the behaviors are rather mitigated in relation to the values assumed by others flexibility parameters.

Considering the evaluation of the influence of the building thermal mass and the thermal insulation position on FPI calculation, a single representative case is discussed: building with fan coil units located in Turin for the heating season (Figure 3.7(a) and flexibility parameters contained in Table 3.9) and in Messina for cooling season (Figure 3.6(b) and flexibility parameters contained in Table 3.8). The choice is made not to involve the effect of the thermal inertia of the heating system and the location. Indeed, the more severe weather conditions in winter and in summer are considered. However, the same consideration can be extended to the other case studies modelled.
Starting from the heating season evaluation, it can be noted that when the building thermal mass increases, the FPI value increases too. Considering buildings with the same heaviness, the external insulation and the cavity walls insulation allow to obtain a better flexibility performance than the internal insulation according to the presented methodology. This is mainly represented by duration of the response period as shown also in Figure 3.8. In particular, in buildings with external walls it is more than two times greater than that with internal insulation. The same behavior can be observed both for heavy and light envelope (Table 3.9). Consequently, the actual energy variation is lower in case of internal insulation, even if the efficiency maintains always similar values in all cases.

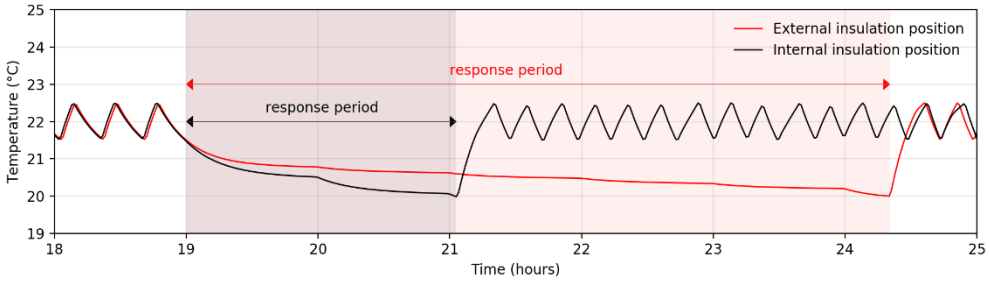

Figure 3.8. Comparison between inside temperature in presence of external and internal insulation in heating mode for a building with heavy walls and fan coil units located in Turin.

Results allow to conclude that the insulation position has a great influence on the energy flexibility performance of the buildings and the FPI can represent this trend (moving the thermal insulation position from the inside to the outside of the wall, the flexibility class increases from C to B in Turin (Figure 3.6(a)) and in Messina (Figure 3.7(a)) from B to A3). On the other hand, the heaviness of the walls does not seem to have the same impact on the FPI. Indeed, its increase with the heaviness of the envelope is not relevant and the flexibility class remains the same for the same stratigraphy.

Also, in cooling season, moving the insulation towards the external side of the wall increases the FPI value (Figure 3.6(b)). However, for the same building, the flexibility performance is generally lower than in heating case and the differences are more mitigated. The introduced building models allow to confirm the role of the thermal inertia of the distribution system, in particular when the building thermal mass is low (i.e. in case of internal insulation). As regards the heating case, for both locations, a great difference in response period duration can be observed between the radiant system and the fan coil units (Figures 3.7, 3.8, 3.9 and 3.10). However, such greater inertia also affects the recovery phase. Indeed, with the radiant system, the initial comfort condition restoration takes more time than for the case with fan coil units, which instead is very rapid. Furthermore, considering the last indicator η_{DR} in Tables 3.7 and 3.9 a great difference in the two distribution systems can be highlighted. If the radiant system allows the achievement of higher response durations, the efficiencies of the demand response event (η_{DR}) have an opposite trend. This is due to the great energy use during the recovery phase, which makes the total saving small compared to the energy use in reference conditions.

Regarding the cooling case, the radiant distribution system coupled with the dehumidifier achieves a better flexibility performance than fan coil units (see Tables 3.8 and 3.10). In these cases, as already mentioned, it is possible to control also the humidity of the indoor air and response duration is evaluated based on the comfort limit condition, between temperature and humidity, reached earlier.

From the simulations results, a strong connection between internal temperature and humidity trends and building envelope thermal inertia emerges. When the building thermal mass increases, the internal temperature tends to rise more slowly. The increase in internal temperature, however, counteracts the rise in relative humidity. Therefore, when the internal temperature decreases at a low rate, the relative humidity increases fast. This aspect affects the limit condition that is reached first: as shown in Figure 3.9, in Turin where buildings have a better level of thermal insulation, the relative humidity reaches the comfort limit condition first than the temperature for heavy and externally insulated walls.

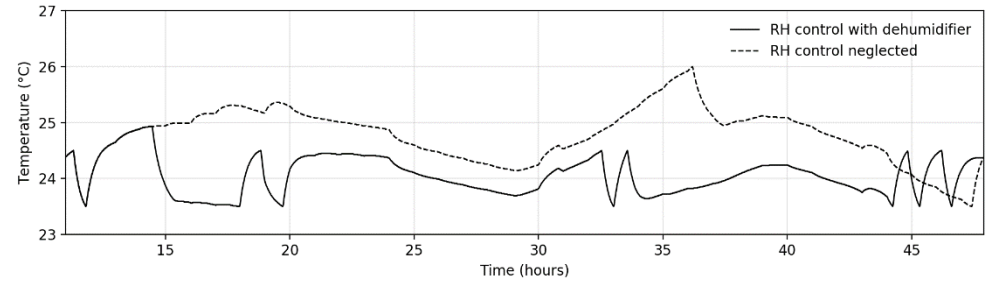

(a)

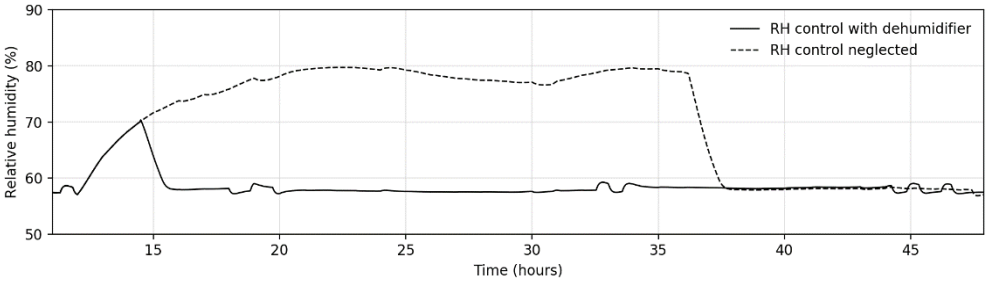

(b)

Figure 3.9. Temperature (a) and relative humidity (b) during demand response event in cooling case for a building located in Turin with heavy walls materials and external insulation position. Chilled ceiling distribution system with and without air dehumidifier.

However in these latter cases, the two flexibility indicators that represent the flexibility behavior of the building in term of power and energy ($\dot{P}^{*}_{res}$ and η_{DR}) account for both the heat pump and the dehumidifier energy demand. Since the thermal inertia introduced by the chilled ceiling is lower than that of the underfloor heating system, the response period as well as the recovery one, although longer than that with fan coil units, are significantly reduced compared to the winter radiant system. However, the energy saving, and the not-engaged-electric-power have improved values. The FPI label for buildings equipped with fan coil units is generally in a lower class than that of buildings with chilled ceiling. Furthermore, the FPI shows typically a lower overall capacity to provide energy flexibility in cooling mode.

3.2.3 Optimization of energy flexibility in buildings under renovation

In this last section, starting from a low energy performance reference building, the energy flexibility performance obtainable with different energy efficiency interventions is assessed with the FPI calculation. In addition, to show the effectiveness of the proposed quantification methodology, the aim of this analysis (presented in Paper 3), is to provide guidelines to improve the energy flexibility of buildings in phase of refurbishment.

With reference to Paper 3, a single-family house belonging to class 5 (1960-1975) of Tabula project [64] is selected as starting reference building. The building is located in Milan (45°25' N, 9°16' E, climatic zone E) and it has an area of 100 m^2 and 10% of window surface area.

Starting from this reference building model, different renovation strategies are considered by adding insulation to the external walls, roof and floor respectively and by changing the windows. Thermal insulation (1 cm increments) is added to all the opaque structures. The final most energy performing configuration considered is in accordance with values from the Italian regulation for buildings undergone to energy requalification from 2021 [70]. It is obtained with an external wall insulation thickness of 11 cm, a roof insulation thickness of 14 cm, 11 cm for the insulation layer in floor and argon gas double glazing windows. Table 3.11 shows the U-values both for the starting reference building, which does not contain thermal insulation in the walls ,and for the most energy performing configuration.

Table 3.11. U-value (W m^{-2} K^{-1}) implemented in Paper 3.

Building	External walls	Floor	Roof	Windows
Starting reference	1.26	2.00	2.20	5.83
Most energy performing	0.24	0.28	0.29	1.40

For the flexibility evaluation only the heating season is considered. In particular, an air to water heat pump [71] is used and low temperature radiators are adopted as thermal distribution system. A small water tank (from 60 liters to 200 liters) is also introduced in the heating system to limit the on-off cycles of the heat pump. However, it is important to notice that, as the thickness of the thermal insulation layer increases the design peak load of the building decreases. Indeed, five different commercial heat pump sizes are chosen for all the possible renovation configurations (and consequently the size of the tank). They are:

(i) Level 1: from a maximum of 13.2 kW to a minimum heat load of 11.2 kW (design capacity of the heat pump of 12.2 kW).

(ii) Level 2: from a maximum of 11.2 kW to a minimum heat load of 9.2 kW (design capacity of the heat pump of 10.2 kW).
(iii) Level 3: from a maximum of 9.2 kW to a minimum heat load of 7.2 kW (design capacity of the heat pump of 8.2 kW).
(iv) Level 4: from a maximum of 7.2 kW to a minimum heat load of 5.2 kW (design capacity of the heat pump of 6.2 kW).
(v) Level 5: from a maximum of 5.2 kW to a minimum heat load of 3.2 kW (design capacity of the heat pump of 4.2 kW).

In order to evaluate a large number of building renovation configurations, TRNSYS is combined to GenOpt [72], a generic optimization tool. The algorithm *Mesh* is used as it allows to span a multi-dimensional grid in the space of the independent parameters so to evaluate the objective function (i.e., FPI) at each grid point (more details about the optimization problem are reported in Paper 3).

According to the boundary conditions specifications described in the previous section, the representative winter day for Milan is January 27 (average daily temperature 3.6 °C [60]). However, as for the case tested in sub-section 3.2.1, also in this case the flexibility classes are defined only with the values of the FPI (FPI_{limit} is not calculated). However, the same formulation introduced in sub-section 3.1.2 is adopted (Equation (3)). In particular, a building is labelled in class A3 if its FPI is greater than 20, if the FPI is between 10 and 20 the class is A2, if the FPI is between 8 and 10 the class is A1, if the FPI is between 5.5 and 8 the class is B, if the FPI is between 4 and 5.5 the class is C and finally, when the FPI is lower than 4 the class is D. With these assumptions the results can be evaluated.

The FPI for the starting building shows very poor flexibility performance. In fact, without thermal insulation, the comfort limit condition is reached very quickly (t_{res} is equal to 0.05 hours) and the building is labelled in flexibility class D with a FPI of 2.5. Insulating only a singular part of the envelope (external walls, roof or floor) the flexibility performance does not increase significantly. Even with 11 cm of thermal insulation added to one surface at a time, the flexibility class remain D. Similar considerations can be made if only the windows are replaced. This is due to the fact that, with these single renovation strategies, the heat losses of the other not insulated surfaces are still significant and the comfort limit condition is early reached.

No improvements are observed even if two portions of the structure are thermally insulated or if one of them is combined with windows replacement.

The flexibility class remains D, if thermal insulation is added to the external walls and roof, while if also the windows are replaced, a slow improvement begins to be observed for high levels of insulation. In particular, the building flexibility class becomes C with

an FPI of 4.2 with windows replacement, 11 cm of insulation for the external wall and 14 cm for the roof.
Introducing a minimum level of thermal insulation (1 cm) in the floor stratigraphy increases sensibly the FPI values. Referring to Figure 3.10, this behavior can be observed. The building reaches flexibility class B (FPI equal to 6) with 12 cm of thermal insulation in the roof and 8 cm in the external walls. The response period is about 2.37 hours, the recovery 0.25 hours and the actual energy variation (E_{DR}) is about 2.83 kWh.

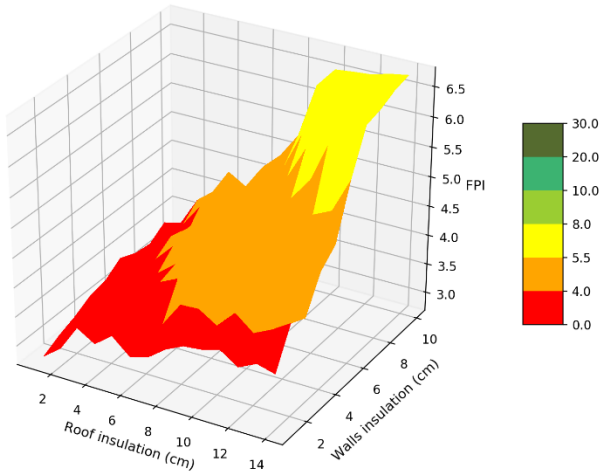

Figure 3.10. Flexibility performance indicator by varying the insulation thickness in the roof and external walls with windows replacement and a minimum floor insulation (1 cm, fixed).

A great improvement can be observed only if each part of the envelope is well thermally insulated and windows are replaced. Figure 3.11 shows the building flexibility performance by varying the thickness insulation in the external walls and in the roof, assuming a high level of thermal insulation in the floor (11 cm) and new windows. The thermal loss reduction derived from the whole envelope insulation, in addition to the effect of more energy efficient windows, allows the increase of building thermal inertia, which can be activated during the demand response event so to maintain for long time the internal comfort conditions. It is possible to see that the high level of thermal insulation in the floor allows to obtain a strongly increasing trend of the FPI with the increase of the insulation thickness of the other walls of the building. The maximum FPI achievable is 10.8 (class A2) and the building can maintain for about 9.4 hours the comfort conditions (t_{res}).

Important FPI improvements are anyway observed for high values of thermal insulation (from 8 cm upwards for external walls and roof). Medium insulation thickness (from 5 to 7 cm) allows to obtain FPI values between 4.5 and 7, so buildings are generally classified in flexibility class C or, at maximum, B.

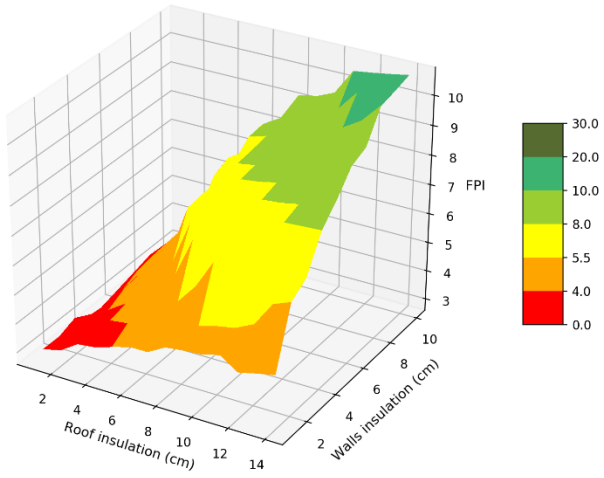

Figure 3.11. Flexibility performance indicator by varying the insulation thickness in the roof and external walls with windows replaced and 11 cm floor insulation (fixed).

From the analysis of the presented results, it is possible to observe that although a consistent reduction of thermal energy demand can be obtained by increasing the insulation level of the building envelope, the same behavior seem to not be verified for the energy flexibility evaluation.
If the energy flexibility is quantified with the proposed methodology (i.e., with the FPI), the positive effect on flexibility due to building thermal mass is evident only if the thermal insulation is applied at the same time in the external walls, floor and roof.
If there is even only one surface with high heat losses, the building is not able to maintain in an acceptable band the internal comfort and the flexibility performance is low.

Chapter 4

Evaluation of district cooling solutions

As mentioned in Section 2.1, solutions for district air conditioning (i.e., district heating and cooling systems) show great potential to increase the performance of the energy supply process. In this thesis greater attention is placed on district cooling (DC) networks as they are often less analyzed than the heating application (i.e., district heating).
The identification of flexible and efficient solutions to cover the building cooling requirements is an increasingly urgent need given the growth of the cooling demand [73] and the higher difficulty in its prediction [74]. Indeed, the cooling demand depends on different factors that can change quickly, such as solar radiation, internal heat gains, and the urban heat island [75].
In general, the building cooling demand can be met using individual solutions (air-conditioning split systems, or more efficient solutions such as absorption cycles and electric chillers), or using one solution for the whole building or cluster of buildings [76]. In this last case, DC systems can have a paramount role. According to EU Energy Efficiency Directive [77], district cooling networks are one of the most important pillars for achieving the energy efficiency target of reducing primary energy consumption by 20%. Furthermore, the Strategic Energy Technologies Information System (SETIS) [78] has recognized district cooling systems as Best Available Technology (BAT) for the cooling market in the European Union.
To provide a definition, district cooling systems are networks able to distribute thermal energy, usually as chilled water, from a central source to industrial, commercial, and residential consumers, to be used for space cooling/dehumidification. A typical district cooling system includes the following elements: a central generation unit, a distribution network, customers and a heat rejection system. Given its cost-effectiveness, chilled water is often used as heat transfer fluid.
In the following subsections an analysis about the energy potential of exploiting district cooling systems to cover the cooling demand of residential buildings is provided. In particular, in sub-section 4.1, a preliminary qualitative analysis of the energy flexibility that can be obtained from a small residential district cooling network is presented in reference to Paper 4, while in sub-section 4.2, an innovative case study in which a district cooling network is powered with wasted cold energy is presented (Paper 5).

4.1 Preliminary energy evaluation

As mentioned above, there are several studies in the literature that prove the energy benefits of district heating networks, but not much can be found on district cooling systems. With this sub-section, that retraces the work presented in Paper 4, a preliminary qualitative analysis of the energy flexibility that can be obtained from a small residential district cooling network is provided. In particular, the effect of the different thermal inertia levels (i.e., the pipes of the network, the buildings envelope thermal mass and the contribution of a dedicated device) available in the DC systems is investigated in an attempt to maximize the use of the available cooling energy, while maintaining indoor thermal conditions of the users. The evaluation is realized by means of daily energy simulations of a hypothetical residential district realized in TRNSYS [63].

In general, the specific thermal inertia contribution is activated when there is a cooling demand but there is no more cooling availability on the supply side. Each thermal inertia contribution is activated as explained in the following:

- For the network contribution, that is represented by the thermal energy carried by the fluid in the pipes, the fluid can warm up until a limit condition occurs (i.e., thermal balance with the ground temperature).
- For the building inertia, it is activated with a control strategy on the users' temperature setpoints. In this case, the building thermal mass is used as passive thermal storage with a precooling of the living areas with programmed lowering of the users' indoor temperature.
- For the addition of a dedicated device, a sensible thermal energy storage (i.e., a cold-water tank) is added to the district cooling circuit.

A hypothetical daily profile of available cooling thermal power (Figure 4.1) is provided to the district as a cold flow rate available at a given supply temperature. It is assumed that the cooling power profile can satisfy the average daily cold energy demand and the peak cooling power demand of the district but with a random time displacement between demand and supply curves.

To evaluate the effectiveness of the different thermal inertia levels, two qualitative indicators are calculated: (i) the wasted cold energy (defined as the percentage of daily energy actually used compared to the given supply cooling energy availability) and (ii) the overheating time (defined as the hours per day in which the user comfort, set at 26 °C, cannot be maintained).

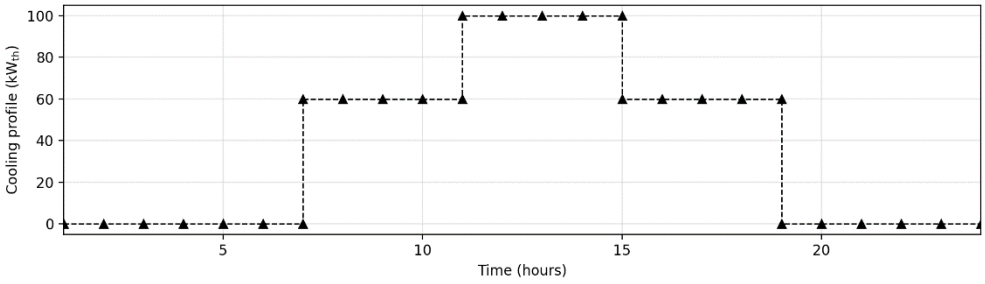

Figure 4.1. Cooling power profile available in the district cooling network modelled in Paper 4.

The modelled case study is composed of a small residential district (14 buildings) located in Rome (41° 55' N, 12° 31' E). Each user is modelled in a simplified way (i.e., single thermal zone with a simple lumped capacitance structure) with Type 88 in TRNSYS. Its thermal and geometrical characteristics are derived by Tabula Project [64].
Each building is modelled as modern single-family houses built after 2006 (Table 4.1). More details about the building model are contained in Paper 4, where also the stratigraphy of the building envelope is reported.

Table 4.1. U-value (W m^{-2} K^{-1}) implemented in Paper 4.

External walls	Floor	Roof	Windows
0.34	0.33	0.28	2.20

The cooling emission system of each user is realized by fan coil units (Type 996). The design peak cooling demand is about 6.3 kW (comfort conditions are set to 26 °C and 50% of relative humidity) with a latent contribution of about 2 kW.
Figure 4.2 represents the link between the cooling system of each user and the district cooling network. In particular, the heat exchange between the water circuit of the fan coil units and the district cooling network is realized by means of a simple constant effectiveness heat exchanger. A mixture of water and glycol is used as heat transfer fluid [79] and, in design conditions, it is delivered at a temperature of -10 °C (with a design temperature difference between supply and return of 5 °C). On the other hand, the cold water in the fan coil circuit is supplied at a design temperature of 7 °C, with a temperature difference between delivery of 5 °C.
The pipes of the district cooling network are modelled as underground pipes (ground temperature of 14 °C) with Type 31 that models the thermal behavior of a fluid flow in a pipe using variable size segments of fluid.

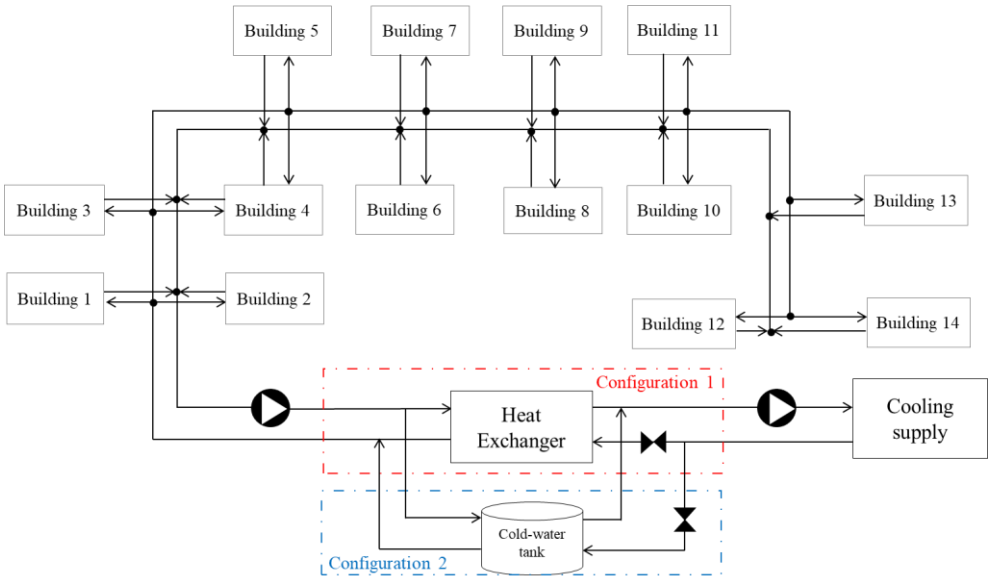

Figure 4.2. District cooling network plant scheme. Configuration 1: heat exchange between demand and supply realized with a heat exchanger. Configuration 2: heat exchange between cooling demand and supply realized with a cold-water tank.

As showed in Figure 4.2, two plant configurations, which differ on the interaction between the supply side and the demand side, are modelled. In the first one (configuration 1) the heat exchange between the cooling demand and the supply is realized with a simple heat exchanger. It is used to investigate the flexibility potential of the network and of the building envelope. The second configuration (configuration 2), by comparison, includes a cold-water tank on the demand side. In this case, the heat exchanger is not included and, when there is cooling power availability, the heat transfer fluid enters directly into the cold side of the tank (when the temperature difference between the inlet and outlet tank flow rates is below 2 °C the tank is considered discharged).

The results of the analysis are presented for the day in which the daily users cold demand is closer to the average cooling supply (820 kWh). In this way, the wasted cold energy is mainly due to a not effective use of the energy flexibility rather than to a difference between energy demand and supply.

Starting from the investigation of the flexibility contribution provided by the pipes of the network, Figure 4.3 reports the daily energy demand, supply and total heat exchanged by the heat exchanger on the supply side when the cooling power availability is directly combined with the cooling demand of the users (configuration 1 in Figure 4.2).

As can be noticed in Figure 4.3, the network flexibility contribution is low. At 7.00 pm, when there is no more cooling power availability, but users continue to ask for cooling, the network thermal inertia allows the demand to be satisfied for a very short time (about 25 minutes). The wasted cold energy is about 468 kWh (57 % of the total) with more than 4 hours of overheating.

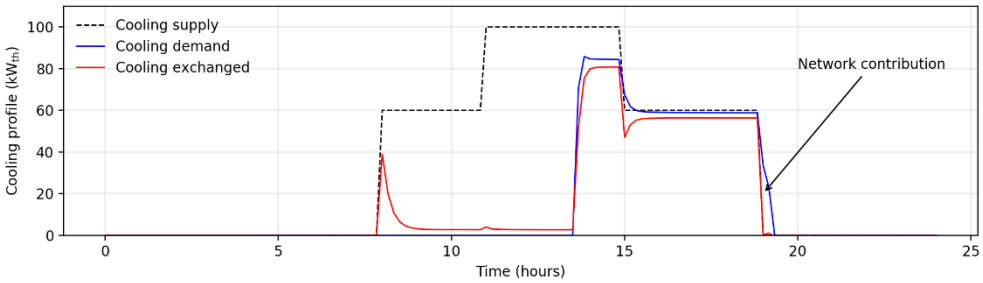

Figure 4.3. Daily cooling power demand, supply and heat exchanged in the case of district cooling system configuration 1 (Figure 4.2).

As far as the inertia of the envelope of the buildings is concerned, a good flexibility performance can be observed. Figure 4.4 shows the case in which the thermal inertia of the building is activated for 1 hour (precooling the buildings by lowering the internal temperature set-points by 1 °C) before the daily cooling demand occurs. In this case no overheating is measured and the wasted cold energy decreases to 337 kWh (41 %). Furthermore, different precooling strategies to activate the buildings thermal mass are tested. The most interesting case can be noticed when the internal temperature set point is lowest during the early hours of the day (for 3 hours, from 8.00 am to 11.00 am) by all the users simultaneously. Indeed, during this period, there is no cooling demand, but cold supply energy is available. The wasted cold energy becomes 13 % without overheating. However, it is important to underline that this solution needs predictive control and more sophisticated management systems to be implemented.

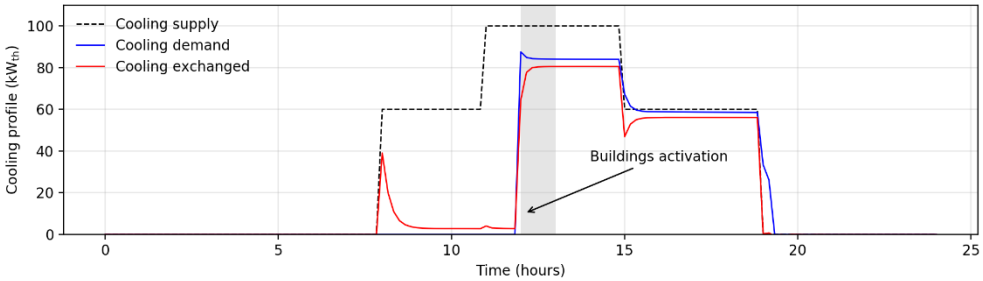

Figure 4.4. Daily cooling power demand, supply and heat exchanged in case of district cooling system configuration 1. Building envelope thermal inertia activation for 1 hour.

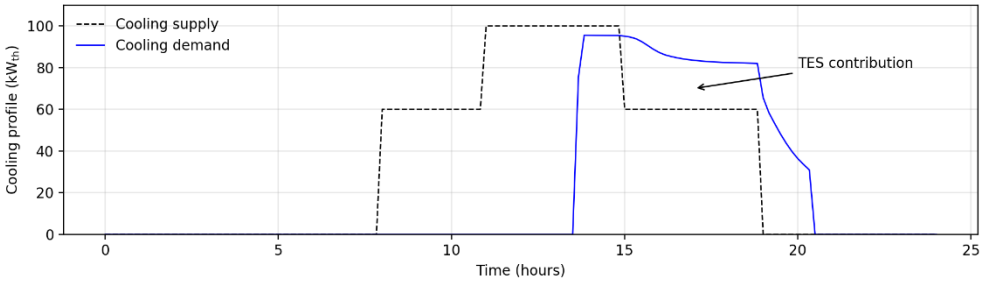

Figure 4.5. Daily cooling power demand and supply in the case of district cooling system configuration 2 with a 4500 liters TES.

Coming to the flexibility contribution provided by the addition of a dedicated thermal energy storage system (i.e., a cold-water tank), it is clear from the results that it is the means that allows a simpler and better decoupling in real-time of demand and supply. In Figure 4.5, the cooling demand and the supply availability, when a 4500 liters cold water tank (1 hour of autonomy) is added to the demand side, is shown. The thermal comfort can be maintained (overheating < 1%) with 36% of wasted cooling energy.
Increasing the size of the tank, the energy flexibility performance increases as shown in Table 4.2, where performance indicators are summarized for all the tested cases. Practically, without overheating (consistently less than 20 minutes), the wasted cold energy decreases, arriving at the minimum value when a 26000 liters TES (6 hours of autonomy) is used.
However, comparing the flexibility obtainable from the tank with the building thermal mass flexibility (Table 4.2), it is interesting to notice that, assuming it is possible to control the inside temperature set points with appropriate predictive control strategies, the activation of the thermal inertia of the buildings can also guarantee good results.

Indeed, the building precooling for 1 hour allows a similar flexibility as a 4500 liters tank, while a building precooling for 3 hour offers the same flexibility as a 26000 liters TES (6 hours). It can therefore be concluded, even if a higher management complexity is required, a great flexibility potential is contained in the building envelope thermal mass. This result highlights how promoting the diffusion of smart buildings, whose energy demand could be managed by a district energy manager, can be a useful solution to optimize the energy sustainability and flexibility of the space cooling sector.

Table 4.2. Qualitative indicators for the flexibility contributions analyzed. Wasted cold energy assessed as percentage of the average daily cold energy supply (820 kWh). Overheating hours as percentage of 24 hours (ref. to Paper 4).

Flexibility contribution	Wasted cold energy (%)	Overheating time (%)
Network	57 %	18 %
Buildings (activation 1 hour)	41 %	0 %
Buildings (activation 3 hour)	13 %	0 %
Tank of 4500 liters (autonomy 1 hour)	36 %	<1 %
Tank of 9000 liters (autonomy 2 hours)	17 %	<1 %
Tank of 13000 liters (autonomy 3 hours)	19 %	<1 %
Tank of 26000 liters (autonomy 6 hours)	7 %	<1 %

4.2 Evaluation of a case study on recovering cold energy from liquefied natural gas vaporization

As highlighted by Werner [80], district cooling networks have strong potentials to be viable cold supply options in a future world, because they can deliver higher security of supply, lower costs, and lower carbon dioxide emissions. Indeed, district cooling systems can carry cooling energy obtained in multiple ways. Waste cold energy from the industry, commercial, and transport sectors can be usefully recovered as cold source of DC network.

A suitable source for district cooling systems seems to be liquefied natural gas (LNG). LNG is widely used to transport natural gas, especially when the distance between the production site and the market is longer than 2000 km [81]. It is obtained by cooling natural gas to -162 °C at the atmospheric pressure. One cubic meter of LNG contains around 600 m^3 of natural gas, making the energy density of LNG significantly higher [82]. Before being sent to the customers, LNG is re-gasified and a large quantity of cold energy can be released. A typical liquefaction process requires around 2900 kJ kg^{-1} of energy. Of this amount, 2070 kJ kg^{-1} are dissipated as heat, while 830 kJ kg^{-1} are stored in LNG as cold [83].

Liquefied natural gas can also be used as vehicle fuel in its liquid form or re-gasified as compressed natural gas (CNG). In the latter case, the Liquid to Compressed Natural Gas (L-CNG) refuelling station has higher efficiency than traditional CNG refuelling stations [84]. In these peculiar fuel stations, natural gas is stored in its liquid form and the CNG to refuel vehicles is obtained from LNG vaporization. The LNG is typically stored in a low-pressure cryogenic tank and then pumped with a cryogenic pump to increase the pressure of LNG up to the CNG pressure. Then, a high-pressure atmospheric vaporizer converts LNG into CNG, stored in pressurized cylinders [85].
L–CNG refuelling plants present several advantages:

- The possibility to distribute CNG when no grid is available nearby.
- A higher fuel purity, since LNG is already purified at the liquefaction stage.
- A reduced operational cost compared to a standard compressor solution, thanks to the power saving from the LNG pumping.
- The possibility to supply also directly LNG to vehicles using it as fuel.

Nowadays in Italy there are 85 LNG and CNG refuelling stations powered by LNG [86] and their diffusion throughout the territory is increasing. Since the cooling potential of vaporized L–CNG represents a free cooling source, its efficient exploitation may greatly reduce the electric demand of the air-conditioning sector. Indeed, the application that will be discussed in this section, and presented for the first time in Paper 5, aims to evaluate the impact of the recovery of the waste cold energy derived from a typical L–CNG refuelling stations to cover the cooling demand of a residential neighbouring.
In order to analyze the potential of district cooling network as a technologic solution to improve the sustainability and the efficiency of the air-conditioning sector, a simulation-based case study is presented (Figure 4.6).
To estimate the potential daily availability of recoverable cold energy from a L-CNG plant in a fuel station, data of CNG end-uses (available for 2015) in Italy are manipulated. Franci [87] reports that the CNG consumption for the automotive sector and derived by L-CNG plants was about 5400 t $year^{-1}$. Assuming a quantity of energy of about 830 kJ kg^{-1} of LNG wasted during the LNG regasification process, about 380 kWh day^{-1} of cold energy can be recovered if the fuel station is in operation every day of the year; excluding the weekends the amount could result in about 550 kWh day^{-1}.

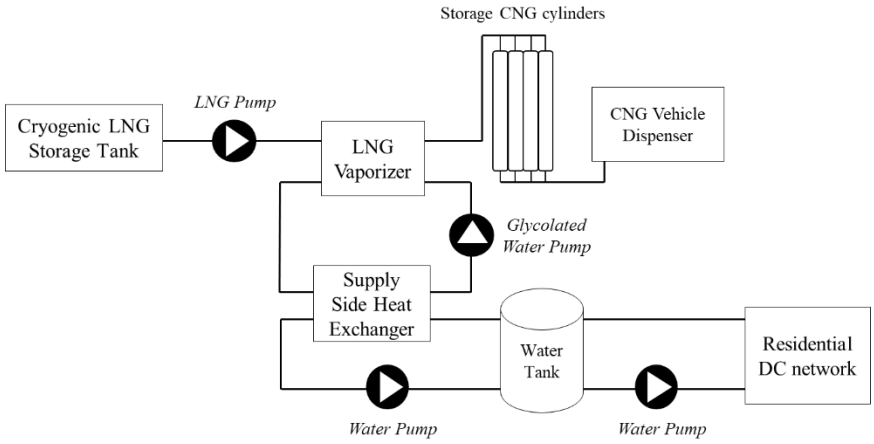

Figure 4.6. Plant scheme: cooling energy recovery from L-CNG vaporizer to fulfil a residential district cooling network (focus on the cooling supply side).

In order to evaluate the capability of the district cooling network to adapt its demand to the supply, the available cold energy is provided to the network by means of three different daily cooling power profiles (Figure 4.7). In the first case (Figure 4.7(a), profile P1), the cooling power is constant and available 10 hours a day, for every day of the year. This situation describes the typical opening and closing times of the Italian fuel stations, which are assumed to be from 7.00 am to 7.00 pm and represents the best possible condition for the DC plant. However, this condition is unlikely to occur. In Italy, many CNG fuel stations are closed during the central hours of the day and the weekends; thus, a more realistic cooling power profile is considered in Figure 4.7(b) (profile P2). The last case, shown in Figure 4.7(c) (profile P3), introduces a peak power availability, too. In fact, as Farzaneh-Gord et al. [88] highlighted in their analysis by monitoring the number of refueling CNG vehicles in a day, a peak is generally observed between 6.00 and 7.00 pm. This last scenario is therefore introduced to consider a cooling power availability variable during the day.

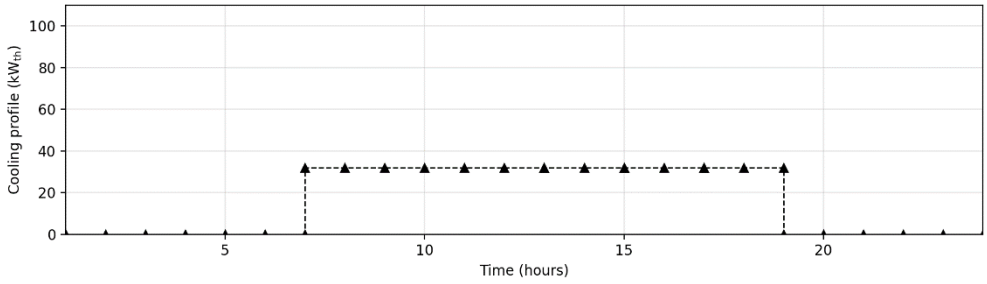

(a)

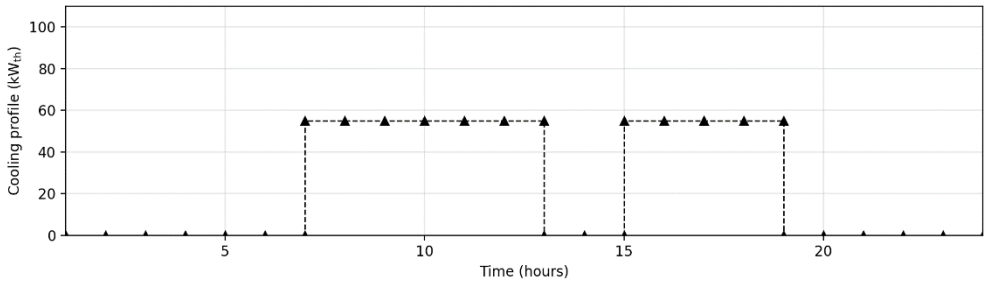

(b)

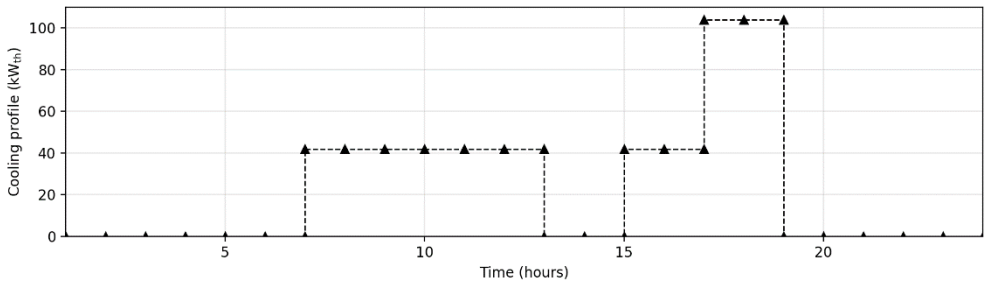

(c)

Figure 4.7. Daily cooling power recovery from a L–CNG fuel station: (a) constant profile for a station working every day of the year (P1), (b) constant profile for a station not working during weekends and stopping during lunch time (P2) and (c) variable profile for a station not working during weekends and stopping during lunch time (P3).

The cooling power is supplied to the DC network by means of a heat exchanger ("supply side heat exchanger" in Figure 4.6). The free cooling, released by the LNG vaporizer, is transported by a heat transfer fluid (water glycol mixture) supposed available at a

temperature of -10 °C and used to maintain the supply water temperature in the district cooling at 5 °C.
To model the cooling demand in the DC system, a hypothetical residential neighborhood composed of 14 users with the same thermal and geometrical features, located in Rome, Italy (41° 55' N, 12°31' E), is modelled in TRNSYS. As for the building presented in the previous section (sub-section 4.1), the single user is modelled in a simplified way with Type 88. Also in this case the main features of the envelope are extrapolated from TABULA Project [64] and a single-family house building with the most recent construction year class (from 2006 onwards) is chosen. Therefore, the description of the building model in the same reported in sub-section 4.1 (Table 4.1). However, for more details, Papers 4 and 5 can be consulted.
As concern the cooling distribution system of the single user, it comprises fan coil units, whose water circuit is supplied at a temperature of about 10 °C, with a design temperature difference between delivery and return of 5 °C. To cover higher energy demands or to cool buildings on days when there is no free cooling availability, every user is equipped with a backup system. The latter includes an air-to-water heat pump connected to the fan coils water circuit. Since there may be days in which there is no cold availability from the network (e.g., weekends), the heat pumps are sized to cover the entire design sensible load (see sub-section 4.1). Figure 4.8 represents the schematic of the model from the DC network point of view.

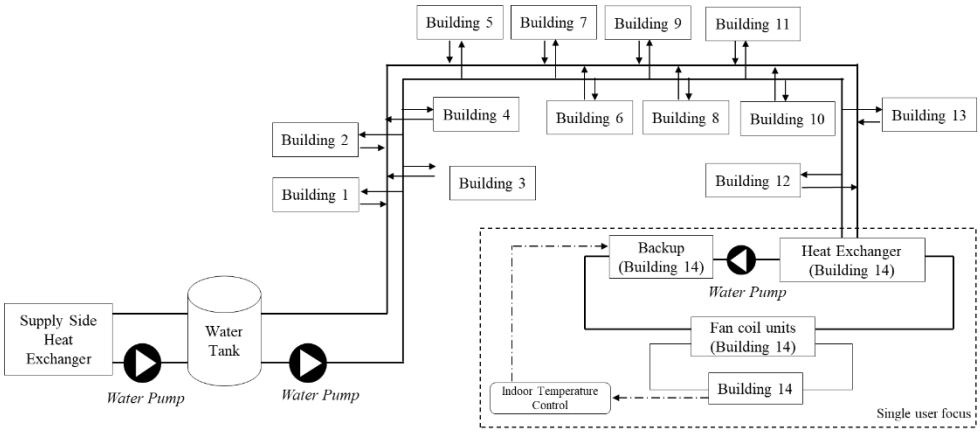

Figure 4.8. Residential district cooling network scheme (see Figure 4.6 for the details of the supply side). Focus on a single user configuration.

Looking at Figure 4.8 it can be noted that, the connection between the water fan coil units circuit and the district cooling is realized with a heat exchanger (Type 91 in

TRNSYS). To uncouple the cooling demand from the supply, a sensible thermal energy storage is also introduced (modelled through Type 4 as a stratified cold-water tank).
In the district cooling network, water is selected as heat transfer fluid. It is delivered from the tank at a temperature of 5 °C, with a design temperature difference between supply and return of 3 °C.
To evaluate the energy performance of the application, a reference case is introduced. It is represented by the same residential district in case of separate cooling systems: fan coil units powered by the same heat pump used for the backup. From the energy simulation for the summer warmer months (July and August), a total cold energy requirement of about 47 MWh and an electrical consumption of about 17 MWh are obtained.
The first analysis evaluates the capability of the district cooling to adapt its cooling demand to the free cooling power availability. A preliminary case, in which the district cooling network is directly connected to the supply side heat exchanger (without the thermal energy storage), is evaluated and the three profiles of free cooling power reported in Figure 4.7 are applied to the supply side.
In general, results show that the case study has a great energy recovery potential. Figure 4.9 represents how the cooling energy requirements of the users are satisfied during the warmer summer months in case of different free cooling power profiles. In all cases the coverage of the buildings cooling demand exceeds 49%. However, although in a slight way, the shape of the free cooling profile seems to influence the district energy behavior. If the DC is supplied with a constant cooling power profile (P1, Figure 4.7(a)) every day, 50 % of the user cooling demand is covered by the DC itself and the electricity consumption is reduced by 52 % compared to the reference case. With the increasing of the free cooling power capability (profile P2, Figure 4.7(b)) during weekdays, a better exploitation of the cold energy provided by the DC is obtained and the electricity saving becomes 58 %. Introducing a most variable cooling power profile (P3, Figure 4.7(c)) this improvement seems to be mitigated. Due to the daily mismatch between the cooling demand and supply, the P3 higher cooling peak power cannot be well exploited. Therefore, it is evident that to minimize the electricity used for backup systems, a sufficiently high and continuous free cooling power is beneficial (i.e., P2).

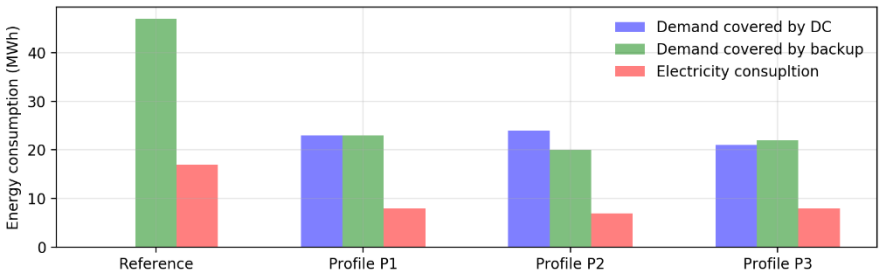

Figure 4.9. Total district electric consumption and users' cold energy demand divided into the share provided by DC and by the backup systems (i.e., heat pump) with different free cooling power profile (months of July and August).

The effect of the introduction of a certain level of thermal inertia at the demand side is investigated in order to evaluate if it helps to decouple the cooling demand and the supply both in terms of time and of peak power potential. The installation of a tank of 60 m^3, which in design conditions can provide the users' peak power demand (about 88 kW) for 2 hours with a temperature difference of 3 °C, is considered. Figure 4.10 shows how the users' cooling energy requirements are satisfied during the warmer summer months in case of different free cooling power profiles when the thermal energy storage is introduced at the demand side. Comparing them to the data shown in Figure 4.9, a good increase in the district cooling energy performance can be noticed in case of P3 profile: the seasonal demand covered by the district cooling goes up to 59% with an electricity consumption reduction of about 60 % compared to the reference case. For the other two cases (P1 and P2), the storage has practically no contribution, being their trend much more regular. Figure 4.11 shows how the thermal energy stored in the tank allows a better daily balance of energy demand and supply, avoiding the switching on of the backup systems to maintain the users' temperature set points.

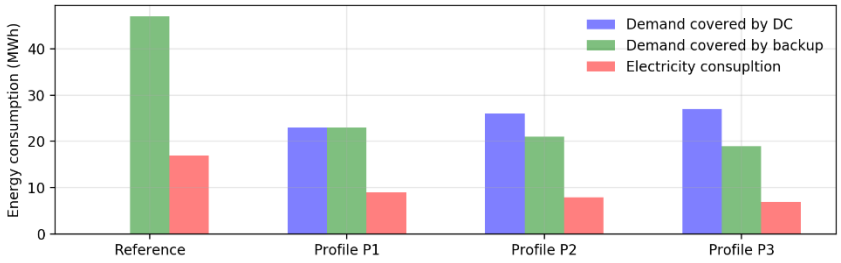

Figure 4.10. Total district electric consumption and cold energy demand of the users divided into the share provided by DC and by the backup systems (i.e., heat pump) with different free cooling power profile (months of July and August) in presence of a cold-water tank of 60 m^3.

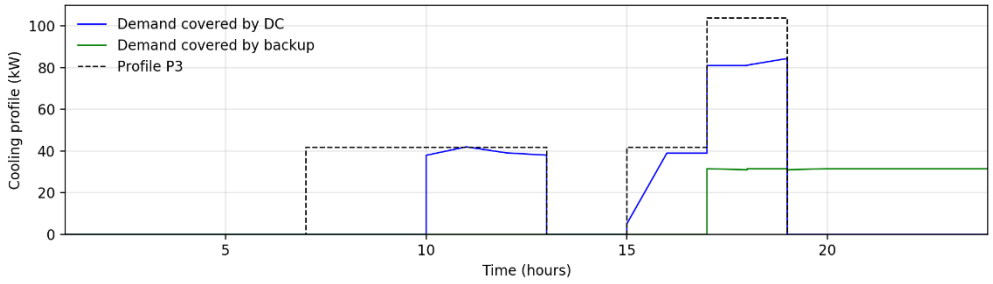

(a)

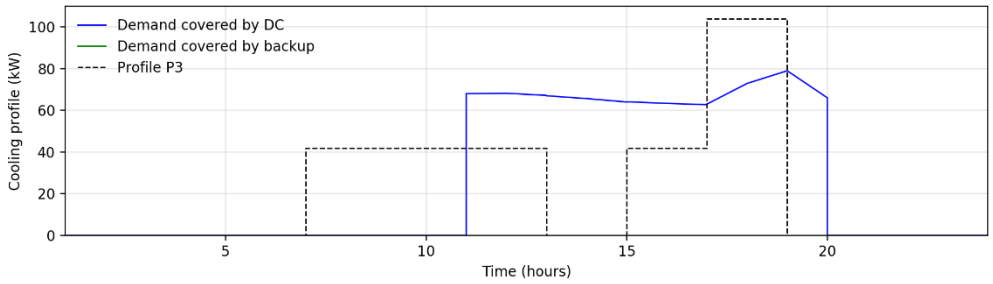

(b)

Figure 4.11. Daily cooling demand breakdown into the DC and backup (i.e., heat pump) in case of cooling supply profile P3: (a) without the tank, (b) in presence of a cold-water tank of 60 m^3.

Even though in the analyzed case the use of a thermal storage allows a higher level of energy recovery with higher electricity saving, in the district cooling plant sizing special attention must be paid to the choice of the tank volume. Tanks too small or too large, in fact, could cause performance degradation. Figure 4.12 reports the cold energy recovery from the L-CNG vaporizer compared to the global district cooling demand and the percentage of electricity saving for different volumes of the tank (profile P3). The best energy performance is obtained for tanks with a size between 30 m^3 and 90 m^3. Lower values do not provide enough level of thermal inertia, while higher values seem to slow down the dynamics of the system too much. In fact, if the tank is empty and the cooling power demand is at its peak, the large thermal inertia introduced by the tank prevents from satisfying the demand because the tank has to be first recharged; therefore, backup systems need to be switched on. Moreover, increasing the size of the tank enlarges the heat losses towards the environment, thus resulting in an energy efficiency penalization of the system.

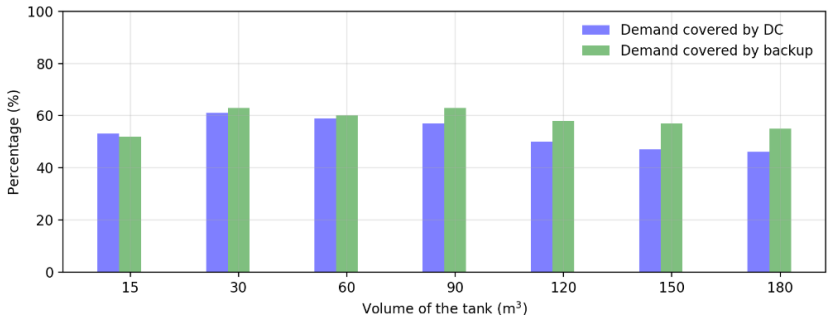

Figure 4.12. Percentage share of cooling from DC to meet the total users' demand and electricity saving for different cold tank sizes.

To conclude, although a simplified case study is analyzed, the evaluations presented in this section (deducted from Paper 5) allow to highlight that cold energy recovery from liquified natural gas vaporization in refueling stations can be effectively used to supply a residential district cooling network. Furthermore, since both the transport and the residential sector are included into the urban environment, the potential benefits of this integrated system are evident.

4.3 Criticalities of the analysis

The results presented in the previous subsections confirm the potential of district cooling systems combined with waste energy sources to increase both the flexibility (subsection 4.1) and efficiency (subsection 4.2) of the residential space cooling sector. However, it is important to highlight that the extent of the benefits obtained appears to be very dependent on the configurations of the system.

Two fundamental points emerged from the simulation of the scenarios presented. First of all, the design choice. This is understood as the selection of some fundamental parameters such as the configuration of the network (e.g., topographical structure) or the number and the type of users to connect to it. Connecting a small number of users can lead to the non-exploitation of a quota of energy available in the network. On the other hand, a high number of connected users can lead to a high use of additional cooling systems (i.e. backup systems). This choice is not obvious even in the face of the second criticality that has emerged. This concerns the dependence of performance on the energy availability curve of the network. Which in turn depends on the heat/cold generation or on the recovery profile. In many cases the estimation of the latter is not simple since, as in the case analyzed in sub-section 4.2, it depends on some random factors such as the stop of cars in a refueling station.

It is clear that, this criticality can compromise the estimation of efficiency and flexibility performances. In addition, system design can also be challenging. Therefore, due to the daily variability of the thermal power availability curve, the performance and operation of the network could vary considerably from one day to the next. In the results presented in sub-section 4.2 only a variation between holidays and weekdays is modeled. However, the results obtained for the cooling season (months of June and July) showed a different operation of the system between this latter variation and the approximation of an average (constant) daily availability profile.

A possible solution that has emerged from both the analyzes presented could be the decoupling of demand from generation, for instance, through the installation of an additional thermal inertia device (a sensible thermal energy storage). Moreover, the adoption of predictive controls or algorithms capable of training itself with experience can also represent an important operational solution. However, they would not allow us to overcome the initial problem of network sizing. The results shown therefore suggested the need for further studies to identify a unique evaluation method. This involves the need for a focus on estimating energy availability and on quantifying the dependence of flexibility and efficiency performance on it.

Chapter 5

Operational energy flexibility evaluation: role of the control

Considering the operational scenario rather than the design characterization, it is important to assess the role of the control in the activation of the energy flexibility of buildings. Indeed, as mentioned in Chapter 2 (sub-section 2.3), in order to obtain optimized operational energy performance, advanced control methods are required and, among them, model predictive control (MPCs) are the most promising.
In this Chapter, an analysis on the application of model predictive controls to unlock the energy flexibility in buildings is provided. The performances of the MPC are compared to a traditional Rule Based Control (RBC) realized with a simple thermostat.
Before providing an operative evaluation, a focus on the role of the building model techniques adopted in the MPC to manage the flexibility of the building derived by thermostatically controlled loads (TCLs) is provided (Section 5.1). Then, an operative comparison between the two extreme building modeling approaches (i.e., white and black box models) in a MPC formulized to control a building with multi energy sources (including district cooling) availabilities is shown (Section 5.2). At the end of the Chapter, based on the results obtained, the Section 5.3 is dedicated to summarizing all the considerations and the issues obtained regarding the comparison between the two modelling approaches in an operative MPC.

5.1 Model predictive controls

The basic concept of MPC is to use a dynamic model to forecast the system behavior (i.e., the building energy requirements and the temperature trends) and to optimize the actuations in order to operate under the best sequence of decisions [89]. In other words, the model predictive controls select future control actions, taking into account both predictions of future disturbances and system constraints [43], while the goal is pursued.
A typical structure of a MPC adopted in a building is showed in Figure 5.1. As can be noted it is mainly composed of two parts: the building predictive model and the

optimizer. The building predictive model should be able to dynamically forecast the building's energy response in a certain period (prediction horizon, *PH*), while its inputs can vary both in a controlled (manipulated variables) and in an uncontrolled (disturbances) way.

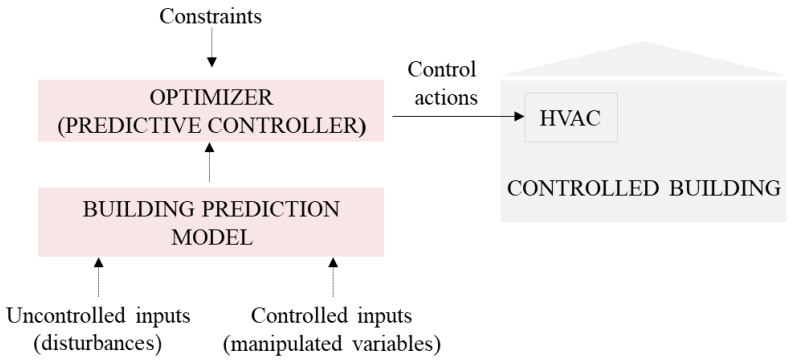

Figure 5.1. Architecture of a typical model predictive control (MPC) applied to a building.

To solve the optimization problem, it is important to define a proper objective function (OF) and to respect the system constraints; in this way, the optimizer has the possibility to select the best control actions to maximize the performance. Following a "receding horizon" logic (Figure 5.2), the model predictive control updates the best control actions at each timestep, moving the prediction horizon forward and repeating the optimization [89].

In buildings, model predictive controls can be applied for many purposes: to exploit the energy storage capability in high-massive buildings, to maximize the use of renewable energy sources, or to implement demand side management strategies. However, in order to be effective, an MPC must be based on a reliable model of the system under study [49]. In the following sub-section (5.1) a focus on the role of the different building modelling approach in an operative MPC is evaluated retracing the analysis proposed in Papers 6 and 7.

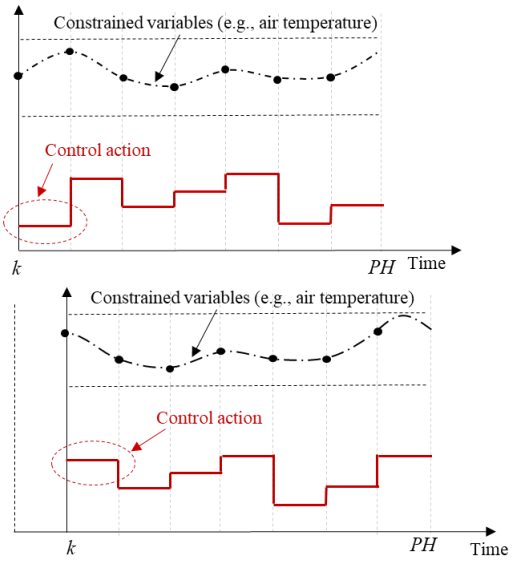

Figure 5.2. Model predictive control receding horizon scheme.

5.1.1 Focus on the building model

A building is a complex systems consisting of smaller systems which interact with the occupants [90]. Its dynamic evolution depends on several factors: the environment, the envelope, the HVAC system, the occupancy patters and the indoor environmental quality [91]. In general, for short-time predictions, three categories of building energy modelling are available: white, black, and grey box models [50].

White bock or physical-based models need a detailed description of the physical and thermal properties of the building in order to describe its dynamics with mathematical equations [51]. Typically, white box models solve energy conservation equations based on heat transfer phenomena. The parameters of the model are usually obtained from design plans, manufacture catalogues, or on-site measurements [50]. Therefore, no training data are required. Most of the popular software, such as Energy Plus, TRNSYS, DOE-2, or ESP-r, is based on a physical-based approach [52].

On the other hand, black box or data-driven models do not require a physical knowledge of the system, but they need to collect a large amount of training data [50]. The most common black box models are [53] support vector machines [92], statistical regression (e.g., linear auto regressive models with exogenous inputs [93]), and artificial neural

networks (ANNs) [94]. However, unlike white box models, the parameters involved in a black box model have no physical meaning.

A compromise between the two approaches is represented by grey box (or hybrid) models. They are a combination of physical-based and data-driven prediction models; thereby, some internal parameters and equations are physically interpretable, while others are estimated with a data-driven approach. Grey box models are widespread in building energy modeling [54], although they require both the system structure and training data.

As mentioned in sub-section 2.3, many works are available in the literature concerning the performance evaluation of the different hybrid and data-driven building models to be used in an building MPC [95][55][96]. However, most of the works focus on evaluating the best model configuration to be adopted in a model predictive control (e.g., parameters identification, selection of inputs and outputs) with little reference to operational assessments. Instead, the evaluation presented in this thesis and introduced in Paper 6, is aimed at operatively comparing the two extremes modelling approaches (i.e., the physical based and the data driven approach) when also the energy flexibility provided by the thermostatically controlled load is unlocked. The comparison is realized by evaluating: the capability of the models to reproduce the building energy behavior of a reference case and the practical implementation of a simple model predictive control designed to minimize the energy supply cost. In this sub-section the description of the two modelling approaches are reported, while their comparison is discussed in the next sub-section (5.1.2).

Starting from the white box model, a lumped-parameter model based on the thermal–electrical analogy is chosen. The building thermal dynamic is represented by an equivalent circuit of thermal resistances and capacitances (i.e., RC network) [97]. A third order model is selected since it represented a good compromise between network complexity and capability of predicting the short-term dynamic of the building [98]. Each node is described by a temperature (T) and a thermal capacitance (C). Then, four thermal resistances (R) are used to model the heat transfer between the nodes. Figure 5.3 report the RC-network.

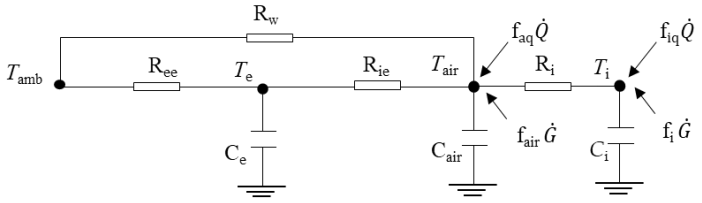

Figure 5.3. RC-network network for building model (white box approach).

All the numerical values of the parameters (R and C) are deducted by the knowledge of the thermal and geometrical building features. Specifically, the first node (T_e, C_e) represents the external building thermal mass, the second node (T_{air}, C_{air}) is the indoor air node, while the last node (T_i, C_i) is the internal building thermal mass. The numerical value of the envelope capacitances (C_e and C_i) are calculated by summing the heat capacitances of all the building elements (up to the thermal insulation) in direct thermal contact with the internal air zone [99]. As concerns the thermal resistance, R_w is the thermal resistance from the indoor air node temperature to the ambient air temperature (T_{amb}), due to air changes and windows. R_{ee} and R_{ie} are the thermal resistances between the external building thermal mass node and T_{amb} and T_{air}, respectively. They are calculated as equivalent thermal resistances due to the conductive heat transfer of all the building envelope layers, from outdoor to the thermal insulation for R_{ee}, and from thermal insulation to indoor for R_{ie}. These thermal resistances also take into account the convective heat transfer phenomena between the external surface and ambient temperature (R_{ee}) and between the internal building envelope surface and indoor air temperature (R_{ie}). In the same fashion, R_i considers the thermal resistance between the indoor air node and the internal thermal mass T_i. The heat fluxes, directly applied to the internal thermal nodes T_{air} and T_i, are the heating or the cooling power derived by the HVAC system ($\dot{Q}$) and the total heat gains ($\dot{G}$). The latter includes both solar and internal contributions, which are provided with a scalar factor (f) for both the internal air (f_{air}) and the internal mass node (f_i).
The dynamics of the resistance–capacitance model can be represented by the following equations:

$$C_{air}\frac{dT_{air}}{dt} = \frac{(T_e - T_{air})}{R_{ie}} + \frac{(T_{amb} - T_{air})}{R_w} + \frac{(T_i - T_{air})}{R_i} + f_{air}\dot{G} + \dot{Q} \qquad \text{Eq. (8)}$$

$$C_e\frac{dT_e}{dt} = \frac{(T_{amb} - T_e)}{R_{ee}} + \frac{(T_{air} - T_e)}{R_{ie}} \qquad \text{Eq. (9)}$$

$$C_i\frac{dT_i}{dt} = \frac{(T_{air} - T_i)}{R_i} + f_i\dot{G} \qquad \text{Eq. (10)}$$

Using these relations, a discrete time invariant State Space Model (SSM) formulation can be set up:

$$\boldsymbol{X}(k+1) = \mathbf{A}\cdot\boldsymbol{X}(k) + \mathbf{B}\cdot\boldsymbol{U}(k) \qquad \text{Eq. (11)}$$

where $\boldsymbol{X}$ represents the system state at each simulation step k, $\boldsymbol{U}$ is the vector of the inputs, and $\mathbf{A}$ and $\mathbf{B}$ are coefficient matrices.
As concern the black box model, a data-driven system based on an artificial neural network (ANN) is adopted. In an ANN, the inputs (x) have the same role of biological dendrites, while the outputs (y) can be regarded as biological axons [100]. The processing of the data takes place in the neurons, which in an ANN apply a nonlinear activation function, g, on the input data. Being a pure mathematical model without physical meaning, an ANN needs to be trained with existing data. The purpose of the training, which can be carried out with different error minimization techniques, is to determine the coefficient weights and biases of the network (i.e., the parameters that fully describe an ANN). Taking into account a feedforward ANN consisting of only one layer of neurons (also called hidden layer, because its activation values are not directly accessible from outside the network) and a linear activation function in the output layer (with just one output), the mapping carried out by the ANN on the input can be expressed as follows:

$$y = \sum_{j=1}^{\mathrm{m}} \left(\widehat{w}_j \mathrm{g} \left(\sum_{i=1}^{\mathrm{d}} \mathrm{w}_{ji} x_i + \mathrm{b} \right) + \hat{\mathrm{b}} \right) \qquad \text{Eq. (12)}$$

where d is the number of inputs, w_{ji} is the weights matrix of the inputs, b is the bias vector of the inputs, m is the number of neurons in the hidden layer, $\widehat{w}_j$ is the weights matrix of the hidden layer, and $\hat{\mathrm{b}}$ is the bias vector of the hidden layer.
Generally, training data are divided into inputs and targets, and a well-trained ANN is expected to determine its outputs with a low deviation in respect to the provided targets. The available data of the system under study need to be studied carefully, in order to train the ANN only with the inputs that mostly influence the objective targets. If the physics of the system under study is complex, a method to individuate the most effective inputs involves the use of statistical approaches such as factor analysis. Instead, if the physics of the system is not entirely unknown, the operator can try to select the input variables that mostly influence the desired target. In the present work, since the thermal behavior of a building is known, these four input variables are selected: (i) outdoor temperature, (ii) solar gains, (iii) internal gains and (iv) indoor temperature.
ANNs are available in different architectures, based on the physical-mathematical problem being studied. In the present work, since the goal is to estimate the thermal power required by a building, a fitting ANN is chosen. In MATLAB (which corresponds to the environment in which it is developed the MPC, see sub-section 5.1.2), fitting ANNs have a feedforward architecture and are trained according to a Levenberg-Marquardt backpropagation algorithm, which uses regression analysis and *RMSE* to

evaluate the performance. One hidden layer with 5 neurons is used (it is well-know that even one layer of neurons is sufficient to represent complex, nonlinear problems [100]). The neurons use a hyperbolic tangent sigmoid as activation function. The ANN has therefore the architecture represented in Figure 5.4.

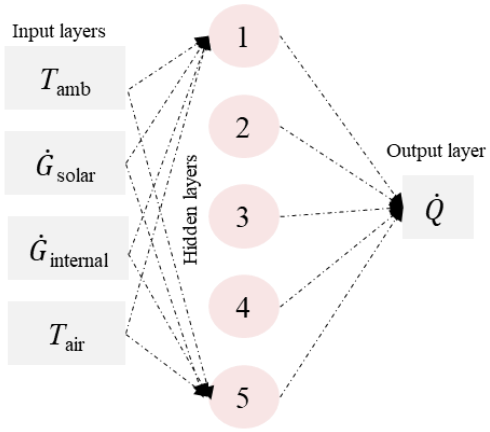

Figure 5.4. ANN architecture of building prediction model.

5.1.2 Preliminary operative evaluation

In this sub-section, the two extreme modelling approaches (i.e., the physical based approach based on the RC-network and the data driven model implemented with an artificial neural network) for the building prediction model (sub-section 5.1.1) are applied to an operative model predictive control. The MPC routine is written in MATLAB [101], and for each timestep (t in Figure 5.2) the controlled building starts the MATLAB engine to run the controller. The uncontrolled inputs of the models are weather conditions (T_{amb}) and heat gains ($\dot{G}$), while the manipulated variable is the hourly building energy demand ($\dot{Q}$).
In this preliminary evaluation, for both the approaches, an ideal HVAC system is considered in the building and in particular the cooling season is evaluated. Therefore, the cooling demand ($\dot{Q}$) is directly treated as a control action (Figure 5.1).
The optimizer solves the optimization problem in the prediction horizon, *PH*, to minimize the total energy cost with constraints on the internal comfort conditions:

$$\text{minimize}\left(\sum p(k)\dot{Q}(k)\right) \qquad \text{Eq. (13)}$$

$$\forall\, k \quad \mathrm{T_{min}} \leq T_{\mathrm{air}}(k) \leq \mathrm{T_{max}} \qquad \text{Eq. (14)}$$

$$\forall\, k \qquad 0 \leq \dot{Q}(k) \leq \dot{\mathrm{Q}}_{\mathrm{max}} \qquad \text{Eq. (15)}$$

Where $\mathrm{T_{min}}$ and $\mathrm{T_{max}}$ are the comfort constraints allowed for the internal comfort and $\dot{\mathrm{Q}}_{\mathrm{max}}$ is the maximum capability of the HACV system.
Looking at Equation (13), it can be noted the presence of a factor *p.* Indeed, as incentive for the exploitation of the energy flexibility, a dynamic energy cost tariff is considered [102]. Therefore, to amplify the cost variations, a penalty signal (*p*) is used in the MPC optimizer (Equation (13)). It is obtained with a statistical method based on mean and standard deviation:

$$p(t) = \frac{c(t) - \mu_c}{\sigma_c} \qquad \text{Eq. (16)}$$

where *c* is the energy cost, while μ_c and σ_c are the cost signal mean value and standard deviation, respectively. Figure 5.5 represents the original energy cost profile (Figure 5.5(a)) and its corresponding penalty signal (Figure 5.5(b)) in a representative summer week. As can be noted, the use of the penalty signal, instead of the actual energy cost, allows to amplify the costs variation and, thus, to incentivize the unlocking of the building energy flexibility.

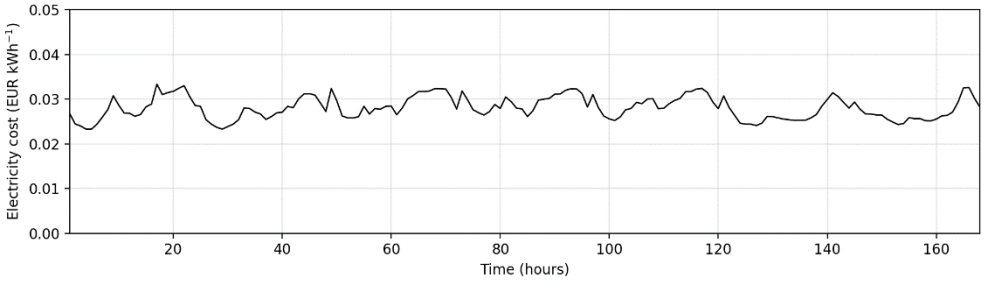

(a)

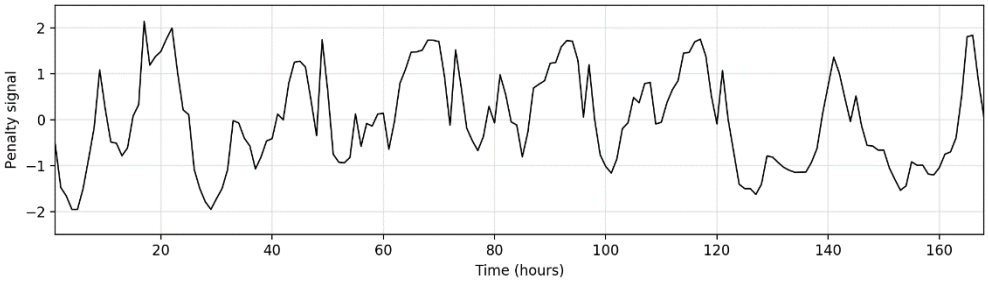

(b)

Figure 5.5. Electricity cost signal for the selected summer week: (a) hourly energy cost and (b) penalty signal.

To evaluate the performance of the two modelling approaches, the Root Mean Square Error (*RSME*) and the Root Square Error (*RSE*) are calculated in reference to available data:

$$RMSE = \sqrt{\frac{1}{n}\sum_{j=1}^{n}\left(T_{\text{model,j}} - T_{\text{data,j}}\right)^2} \qquad \text{Eq. (17)}$$

$$RSE_j = \left|T_{\text{model,j}} - T_{\text{data,j}}\right| \qquad \text{Eq. (18)}$$

where n is the number of points considered.
Data relating to the controlled building (Figure 5.1) are obtained from a detailed building model implemented in TRNSYS using Type 56. The model is composed of a single thermal zone and the envelope characteristics are the same reported in Table 4.1.
In this analysis (also reported in Paper 6), as mentioned, the cooling season is selected for the MPC test and no specific HVAC system is modelled. Instead, an ideal cooling system is used in Type 56 to extrapolate the training data. Therefore, the control actions calculated by the control are applied as convective heat gains to the air nodes (negative for cooling). An indoor air temperature range of 25-27 °C is chosen as comfort condition (i.e., T_{min} and T_{max} in Equation (14)) and a maximum cooling load power of 7 kW is fixed (i.e., $\dot{Q}_{max}$ in Equation (15)). Since the cooling power is directly applied to the air zone, the ideal HVAC can be compared to a traditional heat pump split system. Assuming an average $\overline{COP}$ of 2.5, the thermal energy requirement can be converted in electricity consumption, and the penalty signal obtained consequently (Equation (16)).
By means of energy simulations on the controlled building, different scenarios of data are obtained:

- data to compare the effectiveness of the MPC in comparison to a traditional RBC (a thermostat that maintains a fixed setpoint of 26 °C).
- data to train the data-driven building model and to evaluate the performance of the two buildings modelling approaches (Equations (17) and (18)).

In particular, to train the ANN, 168 hourly-based input/target data referred to a typical week are used (the same shows in Figure 5.5). These data are not obtained with a fixed setpoint condition. In this case, in fact, the ANN performance would have been insignificant, as there would have been no correlation between the output and the controlled variable (i.e., the indoor temperature). Indeed, the control unlocks the energy flexibility of the building and allows indoor temperature variations in a given comfort range. Therefore, to improve the ANN prediction capability, the building simulation environment is allowed to work with multiple indoor setpoint temperatures, varying in a reasonable comfort range. To avoid overfitting of the data, (i.e., an exaggerated interpolating behavior of the ANN), only a fraction of the dataset is actually used to train the network (more details about the training and validation process od the ANN are reported in Paper 6).

Comparing the two building models, it is important to notice that, for the ANN the indoor temperature is a controlled input (Figure 5.4) while for the RC-network it is obtained as a component of the state vector (i.e., which coincides in this case with an output). Also, for the ANN the objective function of the optimization algorithm can be written as in Equation (13), subject to the constraints defined in Equations (14) and (15). Therefore, if the optimization problem for the RC network (linear programming optimization) is linear, that of the ANN is not. For this latter the optimization algorithm chosen is a programming solver based on the gradient method, that uses an initial value for the indoor temperature as first attempt of solution.

Passing at the performance analysis, the ANN training data are selected as comparison terms to test the two building models. Figures 5.6 and 5.7 show the results in the entire 168-point dataset for the ANN-based model and for the RC-network, respectively. Since the output of the models is different in the two approaches, for the ANN the hourly cooling power forecasting is evaluated (Figure 5.6(a)), while for the RC-network the internal air node temperature is considered (Figure 5.7(a)). As can be seen, both the prediction models are able to reply the dynamic variation of the training data. In the first case, the *RMSE* is 0.26 kW, while the value found for the RC-network is 0.34 °C. As highlighted by the *RSE* profile in Figure 5.6(b), for the ANN the deviation is mainly due to the inability of the network to simulate the cases with reduced or zero cooling demand. For the physical-based model, instead (Figure 5.7(b)), there seems to be a regular prediction error rather than specific peaks. It is worth noting that the *RSE* assumes a maximum value of 0.9 °C in the RC-network, and a value of 0.8 kW in ANN model.

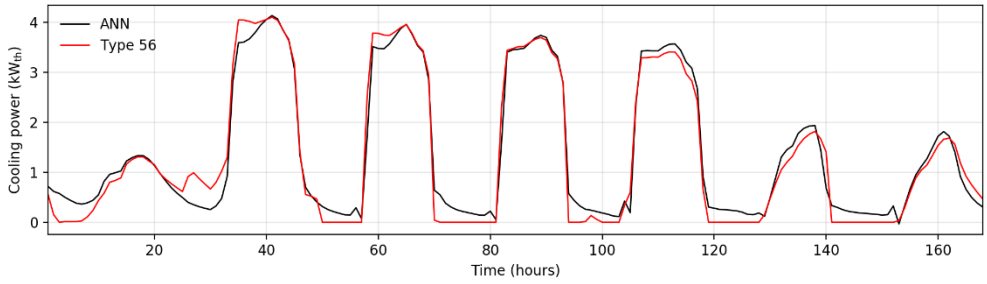

(a)

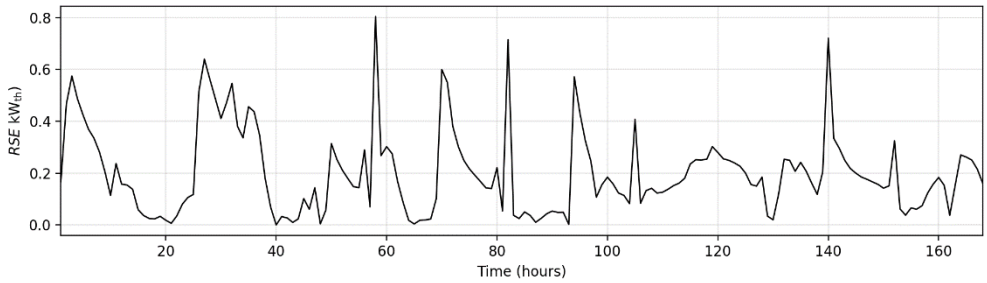

(b)

Figure 5.6. ANN model prediction results compared to training data: (a) cooling power demand and (b) *RSE*.

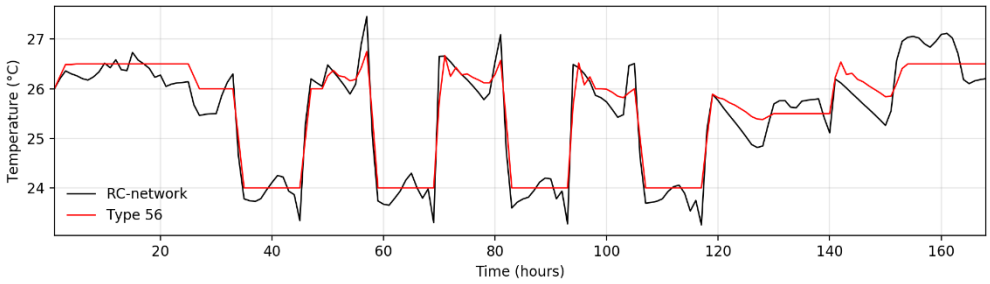

(a)

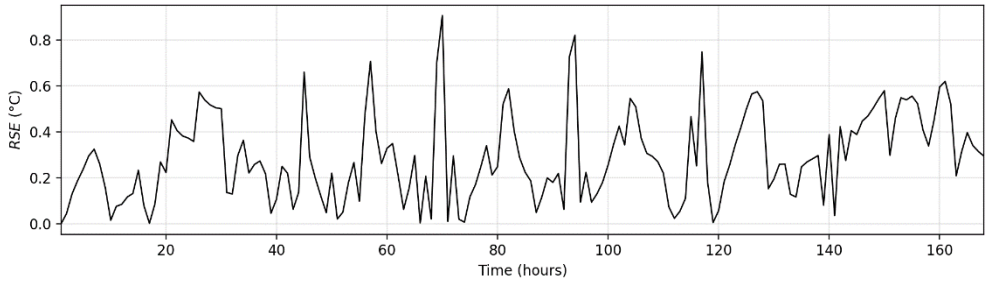

(b)

Figure 5.7. RC-network model prediction results compared to training data: (a) indoor air temperature and (b) *RSE*.

On the other side, Figures 5.8 and 5.9 show the MPC results for both the prediction models. The results are presented with a prediction horizon, *PH*, of 6 hours. Specifically, Figures 5.8(a) and 5.9(a) show the comparison between the building actual internal air temperature (i.e., Type 56 as controlled building) and the MPC predicted value for the same time step (*t*). Instead, in Figures 5.8(b) and 5.9(b), the control actions selected by the controller at each time step (*t*) are represented. Looking at the black curves in Figures 5.8(a) and 5.9(a), it is possible to note that both the prediction models are able to activate the building energy flexibility exploiting the whole comfort temperature range. Low temperature values are preferred when the energy cost is low and subsequent increases are expected. Conversely, the temperature is maintained close to the higher comfort range when high energy costs are detected.

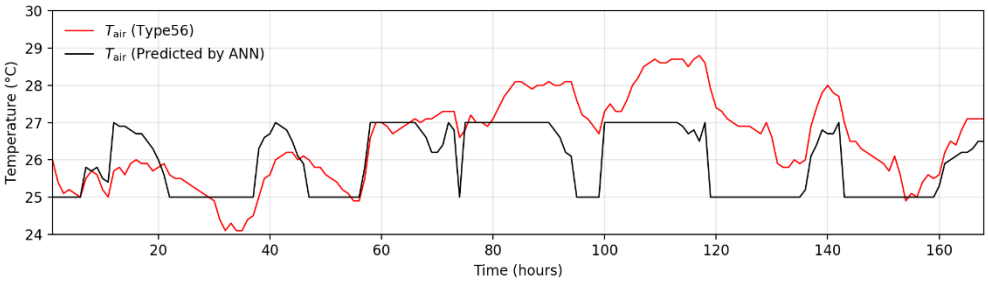

(a)

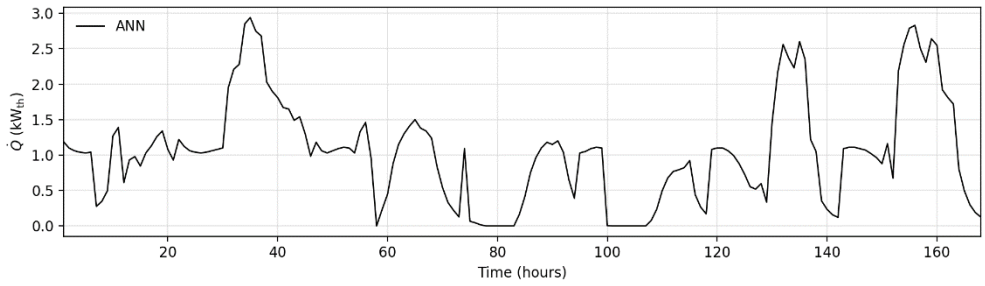

(b)

Figure 5.8. MPC with ANN as building prediction model: (a) internal air temperature, comparison between the actual Type 56 air zone temperature and ANN prediction at each timestep and (b) cooling power profile (control action sequences).

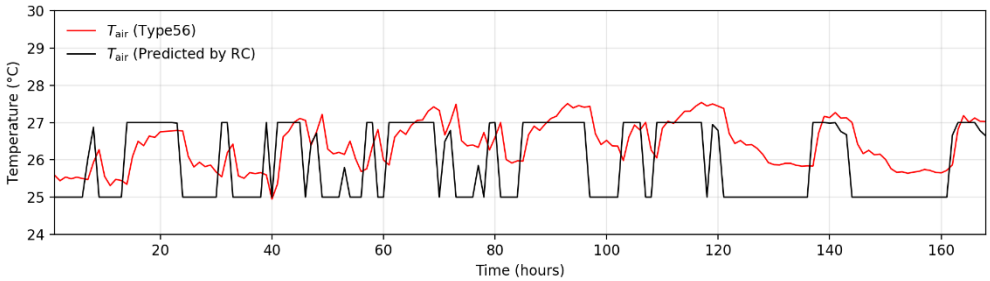

(a)

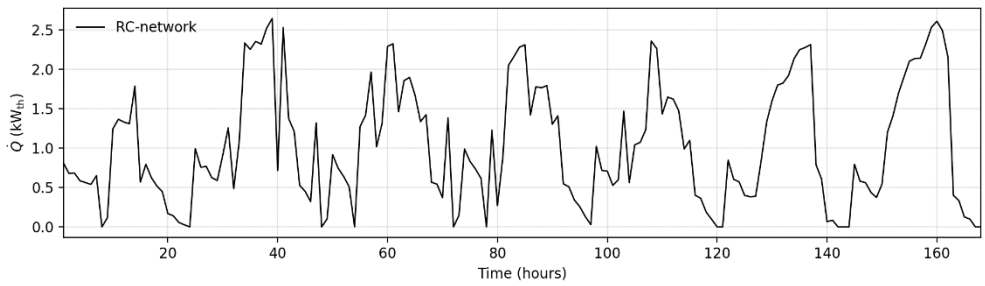

(b)

Figure 5.9. MPC with RC as building prediction model: (a) internal air temperature, comparison between the actual Type 56 air zone temperature and RC-network prediction at each timestep and (b) cooling power profile (control action sequences).

The application of the MPC with both the prediction models produces a total cost reduction of about 16 % if compared to the reference building with a fixed setpoint of 26 °C (i.e., RBC). The *RMSE* between the actual air temperature and that predicted by the MPC at each time step also shows similar error values for the two models: 1.1 °C for the controller with the ANN, and 0.99 °C for the RC model. However, comparing these values with the *RMSE*s found in first part of the analysis, a degradation in the prediction performance can be noted for both the approaches. This is due to the fact that the building operates in variable dynamic conditions when the energy flexibility is activated. Thus, the prediction depends on constantly updated factors (such as the starting temperature conditions, the charge and discharge level of thermal inertia, etc.) which clearly amplify the prediction error.

Although the models seem to have similar performances, different on-time trends for the two models can be expected if the actual building air temperature is observed (the red curves in Figures 5.8(a) and 5.9(a)). In particular, the MPC with the RC-network seems to follow the system dynamics more accurately than the controller with the ANN. Indeed, when the ANN is operatively used in the controller, it appears to perform worse than the RC-network. In both cases, in the second half of the tested period, the prediction error starts to grow but, in case of ANN, the actual air zone temperature exceeds more than one degree the upper comfort limit (28.8 °C is the maximum value reached with the ANN in the controller, against 27.5 °C in case of the RC-network). The behavior is also confirmed by the duration curves reported in Figure 5.10. In the building regulated by the ANN-based MPC, the indoor temperature is found to be above the upper control limit for the 36 % of the simulation time. This percentage drops to 24% when the RC-network is used. This behavior is due to the difficulty of the control to maintain the comfort when the temperature is too close to the upper comfort boundary: also, a small error in prediction can cause temperature violations.

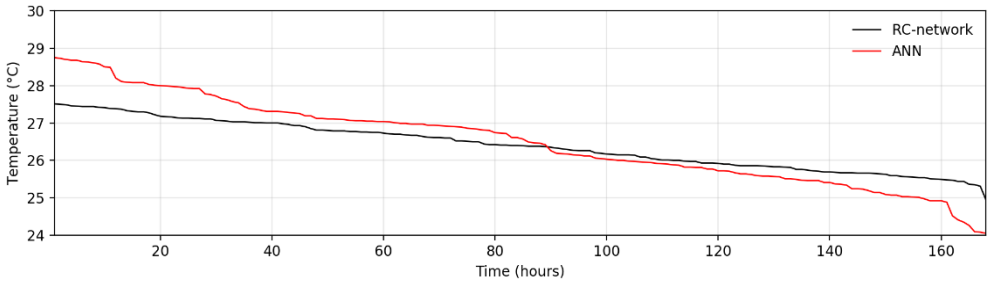

Figure 5.10. Indoor air temperature duration curves.

Therefore, according to the presented results, both the controllers show good ability to replicate the reference case behavior at equal inputs, but in case of real implementation some differences can be noted. Indeed, for the ANN-based MPC the comfort constraint violations can occur more frequently with a higher difficulty of the control to follow the real-time variations of the system. About this, as will be discussed more fully in the sub-section 5.3 after the examination of the two modelling approaches in a MES building (sub-section 5.2), the use of a data-driven model poses an issue on the training dataset operatively representing the energy flexibility contribution in buildings. On the other hand, the physical-based model seems to better reproduce the system dynamics but, it must always be considered that an accurate knowledge of the building, which is not always possible, is required.

5.2 Effectiveness of the model predictive control to manage multi energy system (MES) in buildings

In this section a simulation-based case study in which a MES building is managed with a MPC is assessed with two different modelling approaches (i.e., with a data-driven and a physical based building model) in comparison to a typical RBC.
The case study consists of a residential building modelled in TRNSYS (i.e., controlled building in Figure 5.1) whose cooling power demand can be satisfied with different energy sources: electricity form the power grid, photovoltaic modules (both used to feed a variable load heat pump) and the connection to a district cooling network. Additionally, a certain degree of energy flexibility is provided by a wider variation of the indoor air temperature comfort conditions allowed (i.e., flexibility derived by TCLs). The variation of the cooling demand according to the setpoint can be exploited by the control as additional virtual energy source.
As for the MPC formulized in Section 5.1, the MPC is used to control the HVAC of the building. In this case however, the control actions should lead to an optimal exploitation of each energy source available in the MES, according to the goal to be reached. Therefore, the optimizer should determine whether each source has to be used by the HVAC, while the energy requirement of the building is being satisfied. Thus, the predictions of the energy sources availability profile must be also provided as inputs to the optimizer. In Figure 5.11, a scheme of the proposed MPC is presented.

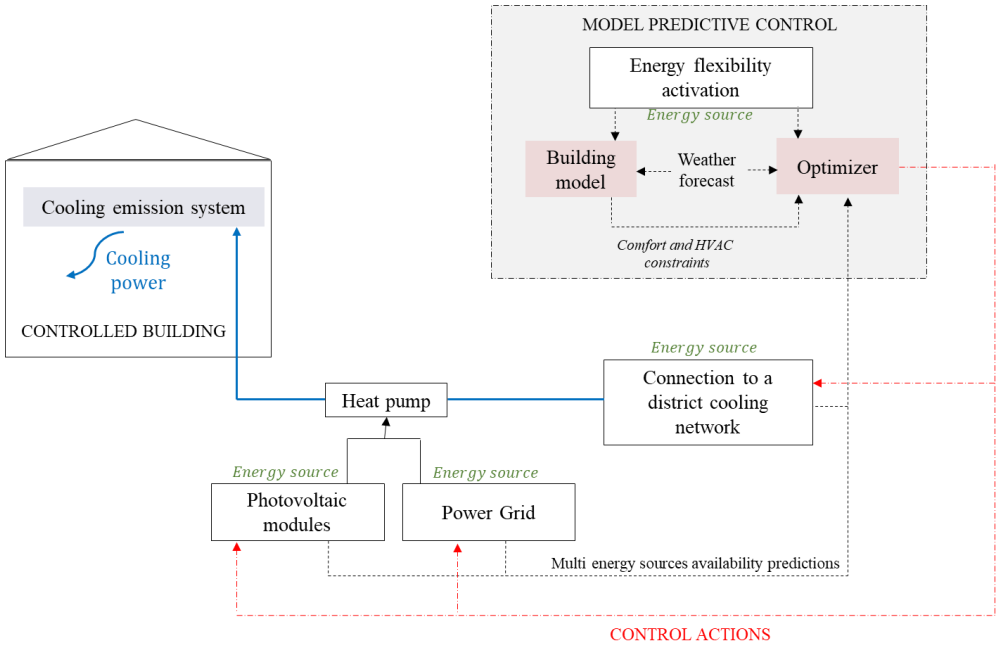

Figure 5.11. Schematic of the MPC to control the MES building case study.

In the following sections the two different modelling approaches discussed in Section 5.1 (i.e., the data driven and the physical based building models) are compared in the MPC showed in Figure 5.11. Although, they are referred to the same case study, there is a difference in the RBC setting of the cooling system between the two approaches. In the analysis introduced in Paper 7, the cooling demand of the building is satisfied with a ON/OFF control logic. Therefore, the combination of the energy sources provides to the building always the nominal power. On the other hand, the RBC adopted in Paper 8 is realized with a compensation curve (the heat pump can modulate the load). However, the in the following sub-sections (5.2.1 and 5.2.2) mode details are provided.

Before showing the results of the two analyses, more details about the case study has to be provided. Starting from the controlled building, it is composed of a single thermal zone. Also in this case the thermal and geometrical features of the building are extrapolated by Tabula Project [64] for a detached house (single family house) recently built (Table 4.1). Moreover, the floor is directly placed on ground and an ACH equal to 0.2 hr^{-1} is selected for natural ventilation. As concerns the internal gains, they are supplied by artificial lighting and occupancy. An artificial light density of 5 W m^{-2} is considered when the total horizontal radiation is less than 120 W m^{-2}, while an occupancy of four people is

hypothesized (heat gain of 120 W per person) [103]. Also in this case, the controlled building is located in Rome, Italy (41°55' N, 12°31' E), and a typical meteorological year [104] is adopted to derive the outdoor temperature and the solar radiation contribution. In this way, the weather forecasts are obtained (Figure 5.11).
The cooling power is provided with of fan coil units (FCUs) working as an air-to-water heat exchanger, in which the internal air is cooled by cold water acting as heat transfer fluid. As mentioned, the water circuit can be cooled by different energy sources (Figure 5.11): (i) cooling power coming from a district cooling network (DC) or from a variable-load air-to-water heat pump (HP), which is supplied by electricity that can be produced by either (ii) on-site photovoltaic (PV) modules or (iii) drawn from the grid.
Starting from the DC source, the connection of the user to the network is made through a heat exchanger in which the cold side uses glycolate water [79] as heat transfer fluid ($\dot{m}_{dc}$), while the hot fluid flowing in the FCU is water ($\dot{m}_{water}$).
The cooling power availability profile is assumed in relation to the possible cold energy recovery application presented in Section 4.2, in which a DC network can be used to dispose of cold energy coming from a liquid-to-compressed natural gas (L-CNG) refueling plant vaporizer. Figure 5.12 reports the daily availability profile of the source.

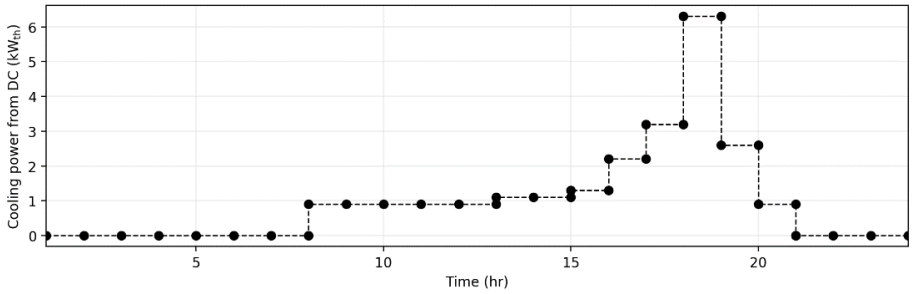

Figure 5.12. Daily cooling power profile from DC (for the single building).

The peak cooling power (6.3 kW from 6.00 pm to 7.00 pm) is comparable to the design peak cooling load of the building (6.7 kW), obtained applying the Carrier-Pizzetti technical dynamic method [69]. Therefore, the water flowrate ($\dot{m}_{water}$) is calculated to guarantee a difference between supply and delivery temperature of 5 °C. In this condition, a design water supply temperature of 7 °C is assumed. As far the glycolate water side is concerned, a constant flow rate ($\dot{m}_{dc}$) is assumed and the cooling power availability profile (Figure 5.12) determines its inlet temperature into the heat exchanger. In particular, the numerical value of $\dot{m}_{dc}$ is calculated considering a temperature difference of 7 °C at the peak cooling power, with a minimum supply temperature of -5 °C.

The variable-load air-to-water heat pump (HP) is connected in series to the heat exchanger. It is modelled interpolating the manufacturer's data of a commercial unit (VITOCAL 200-S) [65], according to EN 14825 [105]. The model 201.D04 [65] is selected (the performance in cooling mode, according to EN 14511 [106].
The heat pump can be powered either by the electricity from the grid (G) or produced by photovoltaic (PV) modules installed on-site. The PV plant is modelled in TRNSYS with Type 194 and it is composed of 3 arrays. Each array includes 4 polycrystalline-silicon panels connected in series with a nominal peak power of 250 W. The characteristics of the single panel are derived from a commercial datasheet [107]. The expected electricity availability from the panels is obtained by simulating the hourly electricity generation of the PV plant for the whole cooling season (from June to September).
To evaluate the performance of the MPC in the optimal exploitation of the energy sources, a classic rule-based control (RBC) is modelled as reference operation. It acts as a simple thermostatic control: cooling power is required when the indoor zone temperature exceeds a maximum setpoint temperature (25.5 °C), with a tolerance of 0.5 °C (from 25 °C to 26 °C). The cooling control is then turned off when the measured temperature falls below the setpoint reduced by the tolerance (25 °C). The RBC acts on the fan coil units, and the energy sources exploitation occurs sequentially according to the order provided in Figure 5.11. Cold thermal energy provided by the DC is consumed at first then, if it is insufficient to cover the demand, the HP is activated. Unable to follow an optimized control logic, the HP uses the electricity produced by the PV modules only if it is available at the considered time step, otherwise the HP withdraws energy from the power grid.

5.2.1 Application of a data-driven building model in MPC

As discussed in the previous section (sub-section 5.1.2), when a ANN is used in an MPC to predict the cooling demand of a building, it can be trained with a large amount of data, deriving from either experimental measures or numerical evaluations. Before training, however, it is important choosing the best architecture of the ANN that represents the system in exam under a logical-mathematical point of view.
The application of the ANN-based MPC to the MES building described above is introduced for the first time in Paper 7. As mentioned, the performance of the predictive controller is evaluated in comparison to a reference scenario. This latter is a simple a rule-based control in which the cooling demand of the building is satisfied with a heat pump managed by a ON/OFF control logic. In this case, the heat pump works always near the design nominal capacity, equal to 6.7 kW. In other words, the modelling of the

cooling demand basically consists in determining when the building needs to be cooled, and this can be regarded as a Boolean problem. The most appropriate ANN to choose in this case is therefore an architecture dedicated to classification problems. In MATLAB, the ANNs used to solve classification problems are referred to as pattern recognition networks. Pattern recognition networks are feedforward networks that can be trained to classify inputs according to the target classes.

To reduce the classification errors of the network, it is important to train the ANN with a proper dataset. The main variables influencing the cooling demand are therefore investigated: (i) indoor setpoint temperature, (ii) outdoor temperature, and (iii) building thermal gains. Among these variables, the most relevant input is the indoor setpoint temperature, which strongly influences the thermal behaviour of the building. For the reasons mentioned in Section 5.1.2 (i.e., to allow to the ANN to represent the flexibility of TCLs), also in this case, a random daily setpoints profile is used to obtain training data (for more refer to Paper 7).

Once the ANN is obtained, it is able to predict the cooling demand ($\dot{Q}$) of the building as a function of the imposed setpoint T_{sp} (T_{sp} and T_{air} in Figure 5.4 coincide in this configuration of ANN that solves classification problem). At this point, the MPC should be allowed to know the free energy sources available in the system in a certain *PH*: the waste cold thermal energy provided by the DC ($\dot{Q}_{\mathrm{DC}}$) and the electricity producible by the PV plant ($\dot{P}_{\mathrm{PV}}$), as well as the coefficient of performance (*COP*) of the heat pump used in the building. If all these quantities are known, the MPC can process an energy minimization algorithm and determine an optimal indoor setpoint temperature (T_{sp}) according to the energy flexibility availability of the building. The optimization variable T_{sp} is not allowed to assume any possible value, but its domain is limited in the set of constraints from 24.5 °C to 27.5 °C with 1°C increases.

The goal of the MPC discussed in this study (Paper 7) is to reduce the electricity taken from the grid. Given the nature of the multi-energy system under study, the MPC is not limited to just calculating an optimal setpoint temperature. In fact, based on the availability of the free sources in the chosen *PH*, the MPC should also evaluate for each time step if either the DC or the HP are allowed to work. In summary, the supervisory MPC should provide the local control unit with three data for each time step: an optimal indoor setpoint temperature (T_{sp}), a Boolean control for the heat exchange with the DC ($CTRL_{\mathrm{DC}}$), and a Boolean control for the functioning of the HP ($CTRL_{\mathrm{HP}}$). While T_{sp} is the result of an energy minimization carried out for the whole prediction time, the selection of the two Boolean controls also depends on the actual availability of the free energy sources in the current time (t) step under evaluation. In fact, there could be occurrences where there is no availability of the free sources in the current time step, even if they will become available in the following hours. In such a case, the Boolean

controls determined by the MPC for the current time step should be $CTRL_{\mathrm{DC}}$ equal to $CTRL_{\mathrm{HP}}$ equal to 0. This trivial example highlights that the MPC cannot be based only on an energy balance referred to the chosen prediction horizon, but it is also necessary to carefully evaluate what happens in the first hour of the evaluation period.
Based on the aforementioned considerations, there is no possibility to write a standalone objective function based on an energy balance equation and it is therefore necessary to subdivide the energy problem in cases.
Let $\dot{Q}$ be the cooling demand of the building for all the admissible values of T_{sp} and PH be the chosen prediction horizon for the current time step *t*. The MPC should evaluate the cases provided in Table 5.1. As will be noted, some of these cases result in trivial mathematical problems to be solved, where it is sufficient to select the highest admissible T_{sp} (i.e., 27.5 °C). Most of the cases, however, requires the definition of a proper energy objective function, E_{G}, that must be minimized by the MPC optimization algorithm.

Table 5.1. Cases managed by the MPC routine with ANN (hourly resolution).

Case	Equations	Comments
0	$\dot{Q}[1,PH]=0$ $T_{\mathrm{sp}}[1,PH]=\mathrm{T}_{\max}$ $CTRL_{\mathrm{HP}}=0$ $CTRL_{\mathrm{DC}}=0$ $E_{\mathrm{G}}(t)=0$	There is no cooling demand in the current time step and in the whole prediction horizon, for all the admissible setpoint values
1	$\dot{Q}_{\mathrm{DC}}(t)=0$ $\dot{P}_{\mathrm{PV}}(t)=0$ $\dot{Q}(t)=0$ $T_{\mathrm{sp}}[1,PH]=\mathrm{T}_{\max}$ $CTRL_{\mathrm{HP}}=0$ $CTRL_{\mathrm{DC}}=0$ $E_{\mathrm{G}}(t)=0$	At the current time step, there is no cooling demand and no free energy source available
2	$\dot{Q}_{\mathrm{DC}}(t)=0$ $\dot{P}_{\mathrm{PV}}(t)\neq 0$ $\dot{Q}(t)=0$ find $T_{\mathrm{sp}}[1,PH]$ so that $E_G[1,PH]=\min\left(E_G[1,PH]\right)$ $T_{\mathrm{sp}}[1,PH]=\mathrm{T}_{\mathrm{sp,minimization}}$ $CTRL_{\mathrm{HP}}=0$ $CTRL_{\mathrm{DC}}=0$	At the current time step, there is no cooling demand, but the photovoltaic source is available. The optimal value of T_{sp} is chosen based on the minimization of the energy objective function
3	$\dot{Q}_{\mathrm{DC}}(t)\neq 0$ $\dot{P}_{\mathrm{PV}}(t)=0$ $\dot{Q}(t)=0$ find $T_{\mathrm{sp}}[1,PH]$ so that $E_G[1,PH]=\min\left(E_G[1,PH]\right)$	At the current time step, there is no cooling demand, but the waste cold thermal energy provided by the DC is available. The optimal value of T_{sp} is chosen based on the

	$T_{\mathrm{sp}}[1, PH] = T_{\mathrm{sp,minimization}}$ $CTRL_{\mathrm{HP}} = 0$ $CTRL_{\mathrm{DC}} = 1$	minimization of the energy objective function
4	$\dot{Q}_{\mathrm{DC}}(t) \neq 0$ $\dot{P}_{\mathrm{PV}}(t) \neq 0$ $\dot{Q}(t) = 0$ find $T_{\mathrm{sp}}[1, PH]$ so that $E_G[1, PH] = \min(E_G[1, PH])$ $T_{\mathrm{sp}}[1, PH] = T_{\mathrm{sp,minimization}}$ $CTRL_{\mathrm{HP}} = 1$ $CTRL_{\mathrm{DC}} = 1$	At the current time step, there is no cooling demand, but both the free energy sources are available. The optimal value of T_{sp} is chosen based on the minimization of the energy objective function
5	$\dot{Q}_{\mathrm{DC}}(t) = 0$ $\dot{P}_{\mathrm{PV}}(t) = 0$ $\dot{Q}(t) \neq 0$ find $T_{\mathrm{sp}}[1, PH]$ so that $E_{\mathrm{G}}[1, PH] = \min(E_{\mathrm{G}}[1, PH])$ $T_{\mathrm{sp}}[1, PH] = \mathrm{T_{max}}$ $CTRL_{\mathrm{HP}} = 1$ $CTRL_{\mathrm{DC}} = 0$	At the current time step, there is cooling demand for at least one value of T_{sp}, but both the free energy sources are not available
7	$\dot{Q}_{\mathrm{DC}}(t) \neq 0$ $\dot{P}_{\mathrm{PV}}(t) = 0$ $\dot{Q}(t) \neq 0$ find $T_{\mathrm{sp}}[1, PH]$ so that $E_G[1, PH] = \min(E_G[1, PH])$ $T_{\mathrm{sp}}[1, PH] = T_{\mathrm{sp,minimization}}$ $CTRL_{\mathrm{HP}} = 1$ $CTRL_{\mathrm{DC}} = 1$	At the current time step, there is cooling demand for at least one value of T_{sp}, and the waste cold thermal energy provided by the DC is available. The optimal value of T_{sp} is chosen based on the minimization of the energy objective function
8	$\dot{Q}_{\mathrm{DC}}(t) \neq 0$ $\dot{P}_{\mathrm{PV}}(t) \neq 0$ $\dot{Q}(t) \neq 0$ find $T_{\mathrm{sp}}[1, PH]$ so that $E_G[1, PH] = \min(E_G[1, PH])$ $T_{\mathrm{sp}}[1, PH] = T_{\mathrm{sp,minimization}}$ $CTRL_{\mathrm{HP}} = 1$ $CTRL_{\mathrm{DC}} = 1$	At the current time step, there is cooling demand for at least one value of T_{sp}, and both the free energy sources are available. The optimal value of T_{sp} is chosen based on the minimization of the energy objective function

The objective function that the MPC optimization algorithm must minimize is based on a general energy balance of the building, evaluated for the whole prediction horizon chosen. It can be written as:

$$E_{\mathrm{G}} = \sum_{k}^{PH} \dot{P}_{\mathrm{G}}(k)\, \Delta k \qquad \text{Eq. (19)}$$

where Δk is the timestep and for each *k* in *PH* (hourly resolution) and:

$$\text{if } (\dot{Q}(k) - \dot{Q}_{\mathrm{DC}}(k))/COP(k) - \dot{P}_{\mathrm{PV}} > 0$$
$$\dot{P}_{\mathrm{G}}(k) = (\dot{Q}(k) - \dot{Q}_{\mathrm{DC}}(k))/COP(k) - \dot{P}_{\mathrm{PV}}(k) \quad \text{Eq. (20)}$$

$$\text{if } (\dot{Q}(k) - \dot{Q}_{\mathrm{DC}}(k))/COP(k) - \dot{P}_{\mathrm{PV}} \leq 0$$
$$\dot{P}_{\mathrm{G}}(k) = 0 \quad \text{Eq. (21)}$$

Through Equation (19), for each time step *t* of the simulation, the MPC can estimate the overall electrical energy that the system will collect from the grid from *t* to the end of the prediction horizon (*PH*). The minimization algorithm of the MPC must therefore find for which indoor setpoint temperature, T_{sp}, the overall electricity absorbed from the grid is minimum. With a mathematical formulation, this can be written as:

$$\text{find } T_{\mathrm{sp}}[1, PH] | E_{\mathrm{G}}[1, PH] = \min (E_{\mathrm{G}}[1, PH]) \quad \text{Eq. (22)}$$

The optimization problem described by Equation (22) belongs to the paradigm of constraint programming [108] . Referring to a general constraint satisfaction problem [109], this can be defined by a triplet (*X*, *D*, *C*) where:

- $X = T_{\mathrm{sp}}$ is the variable of the problem.
- $D = \mathbb{Q}_{+}$ is the mathematical domain of the variable, in this case the field of positive rational numbers.
- *C* = {24.5, 25.5, 26.5, 27.5} °C is the set of constraints, that in the present case are hard equality constraints defined in a finite domain.

When a constraint satisfaction problem is associated to an objective function, constraint optimization problems are used [108].

As can be noted from Equation (22) and the problem cases reported above (Table 5.1), the T_{sp} value found by the MPC minimization algorithm for each time step *t* is referred to the whole evaluation time *PH*, and not to the current time step. In other words, the setpoint temperature found by the MPC is a single, optimal average value that minimizes E_{G} in the whole evaluation time. This simplification of the optimization process is necessary in order to guarantee acceptable calculation times for the MPC. In fact, being it based on a pattern recognition ANN, the $\dot{Q}$ function that appears in the objective function described by Equation (19) is a complicated nonlinear mapping of the building cooling demand, that extends the optimization process significantly. The simplification, however, does not worsen the optimization results excessively, as they are anyway bounded in the set of constraints reported in Equation (22). In summary, the optimization problem under study is defined under a limited set of equality constraints and the objective function depends on one variable only. In this case, a substitution method can

be used, i.e. Equation (22) can be solved for the four allowable values of T_{sp}, and then the MPC can select the actual value of T_{sp} that minimizes E_{G}.
Analyzing the behavior in different *PH*s, it seems that the choice of the prediction time horizon has a role in the performance of the MPC. Taking into account the typical meteorological conditions for Rome (41°55' N, 12°31' E), during the cooling season (from June to September), Figure 5.13 shows how the MPC performs respect to the RBC (i.e., simple thermostat control) for typical values of the prediction horizon (6, 12, 18, 24 hours). As can be seen, the use of the MPC allows to reduce the electricity collected from the grid regardless of the extent of the prediction horizon. However, it is found that the prediction horizon value that minimizes E_{G} is 18 hours. In this case, the MPC is able to reduce the energy absorbed from the grid by -71%. This trend highlight how the best prediction horizon is usually a tradeoff between a short prediction time, more precise but more limited in the prediction capability, and a long prediction time, which provides more information to the control, but whose reliability could be inferior.

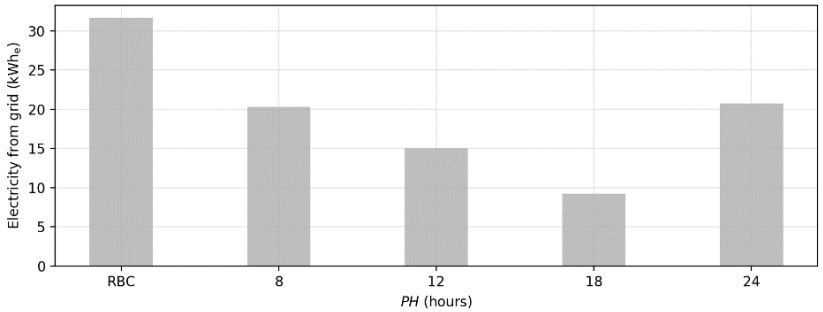

Figure 5.13. Electricity absorbed from the grid for different values of the prediction time horizon. The energy deviations are referred to the baseline (i.e., RBC).

Focusing on the results obtained for a prediction horizon of 18 hours, Figure 5.14 reports the mix of energy sources used by the building, subdivided for the months considered in the cooling season. In each month, the MPC prioritizes the use of the waste cold thermal energy provided by the DC. In the periods with higher availability of solar radiation (mainly July and August), the MPC also tries to use the electricity produced by the PV plant, if available. If there is no possibility to meet the cooling demand of the building with the free energy sources, the MPC allows the heat pump to collect the remaining fraction of energy from the electrical grid. This fraction, however, is limited during the cooling season. In fact, the MPC has the possibility to unlock the energy flexibility of the building by adjusting the variable indoor setpoint temperature, thus allowing a pre-cooling of the building several hours before the actual request of cooling demand.

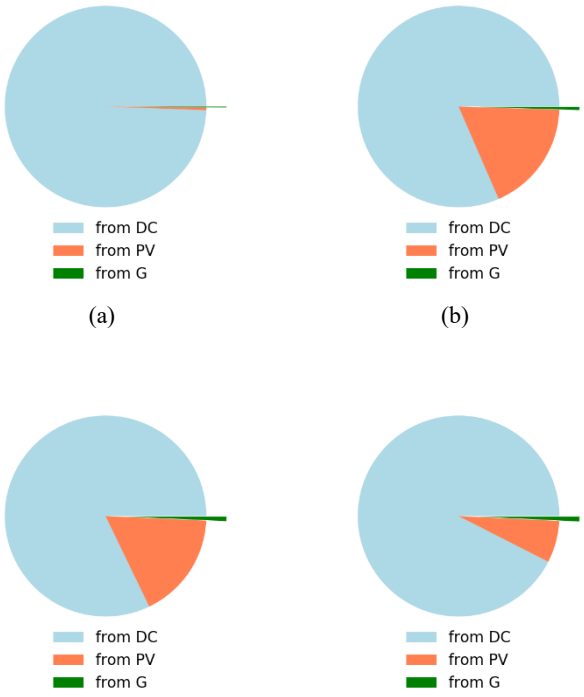

Figure 5.14. Use of the energy sources by the building with the MPC working at a prediction horizon of 18 hours: (a) month of June, (b) month of July, (c) month of August and (d) month of September.

To investigate in detail how the MPC operates, it is necessary to analyze the trend of the variable indoor setpoint temperature, as well as the availability and use of the free energy sources. Starting from the former, Figure 5.15 shows how indoor temperature changes for the building during a typical week. Referring to the RBC, it can be seen that the setpoint temperature is fixed at 25.5 °C, and the corresponding indoor temperature fluctuates in a narrow band (± 0.5 °C). In the same Figure, it is possible to note that, for a prediction horizon of 18 hours, the MPC allows the setpoint temperature to vary in the range 24.5-27.5 °C. For each hour, the indoor setpoint temperature used in the local thermostat control of the building comes from the energy optimization carried out by the supervisory MPC, which tries to unlock the energy flexibility of the building. As a consequence of flexibility, there is a wider fluctuation of the actual indoor temperature.

By predicting a cooling demand in the hottest hours of the day, the MPC takes advantage of the availability of waste cold thermal energy from the DC in the morning hours and lowers the setpoint temperature to obtain a pre-cooling of the building.

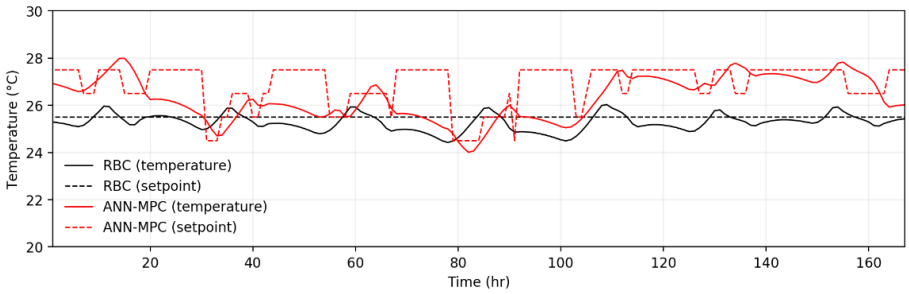

Figure 5.15. Indoor and setpoint temperatures during a typical week for the baseline (i.e., RBC) and the MPC working at a prediction horizon of 18 hours.

Even without the MPC, the system is able to use the free energy sources available, as depicted for example in Figure 5.16 for the cold thermal energy drawn from the DC. However, this is only possible when there is a temporal match between the availability of the source and the cooling demand, because in the RBC there is no possibility to use the energy flexibility of the building. Without the MPC, the RBC is not able to operate a pre-cooling of the building, thus there are periods where the operation of the heat pump cannot be avoided (as visible in the central four days of Figure 5.17). In this case, the only way to avoid electricity absorption from the grid relies on the availability of the solar source. When there is a match between electricity demand and production from the PV plant, there is no absorption from the grid even in the RBC. In some days, however, this condition is not met, and the multi-energy system is forced to draw electrical energy from the grid, as shown in two days of Figure 5.18. In these situations, the operation of the multi-energy system and the interaction between its subsystems are not optimized, leading to an inadequate exploitation of the free energy sources available. The reduction of electrical energy consumption is therefore limited, even in presence of a DC fed with waste cold thermal energy and a PV plant.

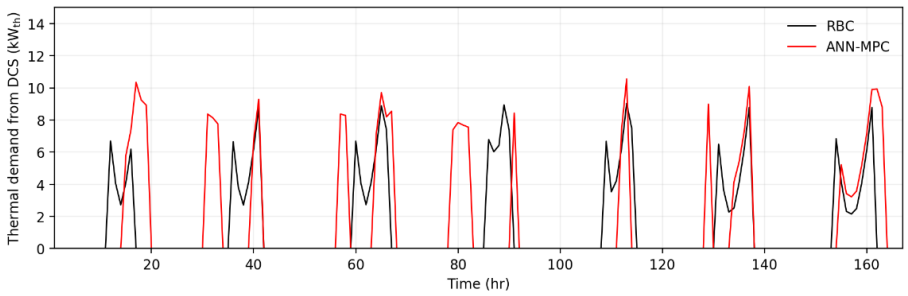

Figure 5.16. Cooling demand covered by the DC during a typical week for the baseline (i.e., RBC) and the MPC working at a prediction horizon of 18 hours.

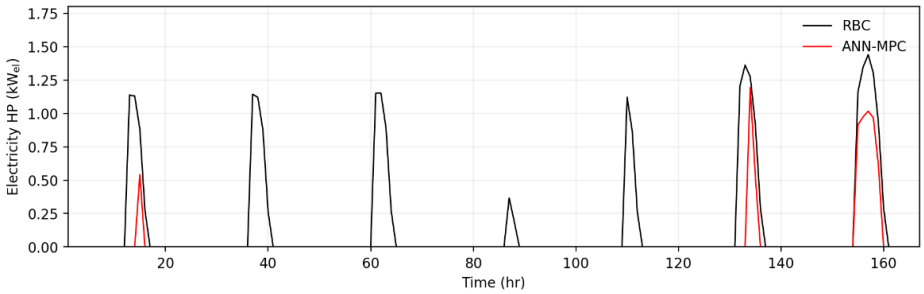

Figure 5.17. Electrical power used by the HP to meet the cooling demand of the building during a typical week. The curves refer to the baseline (i.e., RBC) and the MPC working at a prediction horizon of 18 hours.

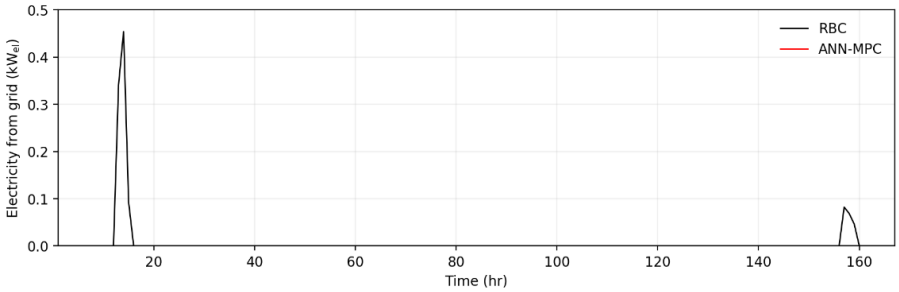

Figure 5.18. The curves refer to the baseline (i.e., RBC) and the MPC working at a prediction horizon of 18 hours.

Attempting to generalize the results, the development and use of a dedicated supervisory ANN-MPC, able to predict both the sources and the demand in a proper prediction horizon, can help the management of the energy systems. Through the prediction, the MPC is able to unlock the energy flexibility provided by the building and thus to minimize the temporal mismatches between the free energy sources and the demand. However, it should be also noted that MPCs based on black box models such as ANNs require an articulated formulation of the control along with a series of training data that are not easy to have (i.e., the behavior of the building with a random set point profiles). Anyhow the black box models have the possibility to be trained again when new data are available, thus they can continuously improve the model they represent. This remarkable advantage, however, is counterbalanced by other issues, in particular a greater difficulty in training an ANN capable of managing energy flexibility properly. It is possible to deal with this issue by using, for the training of the ANN, an adequate dataset able to account for the effects of flexibility in the parameters considered; otherwise, the trained ANN would show poor performance in this regard, worsening the general performance of the ANN-based MPC.

5.2.2 Application of a physical based building model in MPC

The application of the MPC with a physical based model (i.e., RC-network with a white box approach to identify the parameters) to the MES building is presented in Paper 8. In particular, as for the analysis presented in the previous sub-section, the objective of this mentioned work is to highlight the effectiveness of exploiting building energy flexibility provided by thermostatically controlled loads (TCLs) to manage a multi-energy system (MES) through a model predictive control (MPC) formulated with a RC-network building model.
Starting from the model of the building, a RC-network similar to Figure 5.3 is introduced. Also, in this case (as discussed in Section 5.1.1), the performances of the model are compared to the results of a detailed model in TRNSYS (i.e., Type 56) with the evaluation of the *RMSE* (Equation (17)).
Despite of the ANN-based MPC, the application of a RC-network-based involves the real-time resolution of a linear optimization problem, whose objective function and equality or inequality constraints are linear. As explained, when the MPC is adopted to control a MES building, forecasts of the energy sources availability have to be included in the optimizer inputs (Figure 5.11). In case of linear optimization problem, however a further distinction should be made between the energy sources that depend on the actual system state and those that do not. Indeed, as described in Section 5.1.1, in case of physical based model, the system state is represented by the nodes temperatures (T_{air},

T_{i} and T_{e}), which are strongly linked to the thermal demand of the building ($\dot{Q}$). Therefore, $\dot{Q}$ acts as a controlled input for the building model and, hence, as a continuous decision variable for the optimization problem. In this context, the exploitation of an energy source can take place according to two different logics. When the source availability is defined by a given profile (uncontrollable input), the system adapts its state to use the source in the right measure. On the contrary, if the availability of the source is potentially limitless and its employment is strongly linked to the actual energy request of the building, such source has to be considered as a manipulated variable in the optimization problem (i.e., to maintain the linearity of the problem). The latter category is represented by the energy sources that are taken from the grid (e.g., natural gas or electricity drawn from the grid).

To formulize the control in general terms, this distinction among energy sources needs. Let ES be the number of usable energy sources acting as uncontrolled inputs (index e) and Δk the control timestep, $\dot{E}_e(k)$ is the availability profile for each e at each *k* while $\dot{E}_{\mathrm{G}}(k)$ is the energy source drawn from the grid (G). Associating a penalty factor (PF_e, PF_{G}) to each energy source ($\dot{E}_e$ and $\dot{E}_{\mathrm{G}}$), the optimization problem can be formulated in general terms (Equations (23) and (24)).

By varying PF, the utilization of some sources rather than others can be penalized or encouraged according to the intended purpose of the optimization problem (e.g., minimizing the total costs or the primary energy consumption).

$$\mathrm{OF}(\dot{Q}, UF) = \sum_{1}^{PH} \Delta k \left[PF_{\mathrm{G}}(k) \left(\frac{\dot{Q}(k)}{CF_{\mathrm{G}}(k)} - \sum_{e=1}^{\mathrm{ES}} \frac{CF_e(k)\dot{E}_e(k)UF_e(k)}{CF_{\mathrm{G}}(k)} \right) + \sum_{1}^{\mathrm{ES}} PF_e(k)\dot{E}_e(k)UF_e(k) \right] \quad \text{Eq.(23)}$$

$$\text{minimize } \mathrm{OF}(\dot{Q}, UF) \quad \text{Eq.(24)}$$

In Equation (23), CF_e and CF_{G} are the conversion factors of $\dot{E}_e$ and $\dot{E}_{\mathrm{G}}$ into thermal energy. Therefore, $CF_e\dot{E}_e$ and $CF_{\mathrm{G}}\dot{E}_{\mathrm{G}}$ represent the building thermal demand that can be covered by each *e* or drawn by the grid G. Since *e* is referred to an uncontrollable input, its actual use is decided by an utilization factor (UF_e), acting as continuous decision variable, which can assume values between 0 and 1.

The objective function defined in Equation (24) must be minimized by respecting some system constraints. Firstly, the internal comfort of the occupants has to be satisfied for each *k*. This condition is represented by Equation (14). Furthermore, the optimization constraints related to the HVAC system must be defined. They concern the maximum

capability ($\dot{Q}_{max}$) of the system involved (Equation (15)) and, if a withdrawal from the grid is envisaged, the constraint expressed by Equation (25) has to be added in order to avoid unacceptable solutions when the availability of the energy sources is too high (i.e. negative values of electricity drawn for the grid).

$$\forall\, k \qquad \dot{E}_{G}(k) \geq 0 \qquad \text{Eq. (25)}$$

With this formulation, the objective function, the decision variables and the constraints are all linear functions. Therefore, the optimization problem can be treated as a typical linear programming. However, it is important to notice that, to ensure the linearity of the optimization problem, the presented formulation allows the involvement of a single energy source drawn from the grid. In fact, the latter is interpreted by the controller as a supplementary energy source to be used when the availability of other energy sources is not enough.

As described at the start of Section 5.2, three energy sources can be used to cover the cooling demand of the building in the specific case study: (i) cold thermal energy from the DC network, (ii) electricity produced by on-site PV modules to power the HP and (iii) withdrawal of electricity from the power grid. The first two sources act as uncontrollable inputs for the optimizer (ES equal to 2, according to Equation (23)). To refer to the individual energy sources, each element *e* is identified with the specific subscript DC and PV, therefore they coincide with $\dot{Q}_{DC}$ and $\dot{P}_{PV}$. Since $\dot{Q}_{DC}$ represents a thermal power, its conversion factor (CF_{DC}) is set equal to 1 for each *k* while, for $\dot{P}_{PV}$ and $\dot{P}_{G}$, the conversion factor is represented by the heat pump expected coefficient of performance (COP_{exp}):

$$CF_{PV}(k) = CF_{G}(k) = COP_{exp}(k) \qquad \text{Eq. (26)}$$

In order to maintain the linearity of the optimization problem, an approximation is made for the assessment of the *COP* in the MPC optimizer. In fact, since the heat pump is modelled as a variable-load air-to-water unit, its performance varies according to the outdoor air temperature, the water supply temperature and the capacity ratio. However, the two latter quantities are closely related to the actual energy demand $\dot{Q}$, which is a decision variable of the optimization problem. The inclusion of these expressions in the constraints of the optimization problem would make it nonlinear. Therefore, as suggested by [111], the *COP* is considered, with an acceptable error, as a function of the expected value of the water supply temperature (assumed equal to 9.5 °C). To avoid an overestimation of heat pump performance in the control, a capacity ratio of 1 is considered. In this way, the expected coefficient of performance COP_{exp} could be

calculated a priori as only function of the outdoor air temperature, which is an input of the MPC.
Assigning different values to the penalty factors (*PF*), the different ways to exploit the available energy resources by the MPC can be evaluated. Three objective functions are used for the purpose to test the effectiveness of the MPC. They concern the minimization within *PH* of: (i) the electricity taken from the grid, (ii) the energy cost and (iii) the total primary energy consumption.
As far as the first objective function is concerned, Equation (23) can be written for the case study assigning the value 0 to PF_{DC} and PF_{PV}, and 1 to PF_{G}:

$$\mathrm{OF_G}(\dot{Q}, UF) = \sum_k^{PH} \Delta k \left[\frac{\dot{Q}(k)}{COP_{\mathrm{exp}}(k)} - \frac{\dot{Q}_{\mathrm{DC}}(k) UF_{\mathrm{DC}}(k)}{COP_{\mathrm{exp}}(k)} - \dot{P}_{\mathrm{PV}}(k) UF_{\mathrm{PV}}(k) \right] \quad \text{Eq. (27)}$$

Instead, if the total energy cost has to be minimized, the penalty factors represent the costs per unit of energy consumption. In particular, PF_{DC} is the cost per energy unit of the cold thermal energy absorbed by the DC network ($\mathrm{c_{th,DC}}$), while PF_{PV} and PF_{G} are, respectively, the costs per energy unit of the electricity produced by PV $\left(\mathrm{c_{el,PV}}\right)$ and supplied from the grid $(\mathrm{c_{el,G}})$. Their numerical values are: 0.20 EUR kWh^{-1} for $\mathrm{c_{el,G}}$ [112], 0 EUR kWh^{-1} for $\mathrm{c_{el,PV}}$ (on-site generation) and 0.035 EUR kWh^{-1} for $\mathrm{c_{th,DC}}$. With regard to $\mathrm{c_{th,DC}}$, in absence of real data, the following hypothesis is made: the cost of 1 kWh from DC is 30% lower than the production of the same amount of energy with a traditional heat pump (a rated $\overline{COP}$ of 4 is considered). With these assumptions, the objective function can be written as:

$$\mathrm{OF_C}(\dot{Q}, UF) = \sum_k^{PH} \Delta k \left[\mathrm{c_{el,G}} \left(\frac{\dot{Q}(k)}{COP_{\mathrm{exp}}(k)} - \frac{\dot{Q}_{\mathrm{DC}}(k) UF_{\mathrm{DC}}(k)}{COP_{\mathrm{exp},k}} - \dot{P}_{\mathrm{PV}}(k) UF_{\mathrm{PV}}(k) \right) + \mathrm{c_{th,DC}} \dot{Q}_{\mathrm{DC}}(k) UF_{\mathrm{DC}}(k) \right] \quad \text{Eq.(28)}$$

Finally, Equation (29) represents the third objective function: the minimization of the overall primary energy consumption. In this case, *PF* stands for the primary energy factor (pf) to convert each energy source into primary energy. The corresponding numerical values are extrapolated from [70] and are: 2.42 ($\mathrm{pf_G}$) for the electricity taken

from the grid, 1 ($\mathrm{pf_{PV}}$) for the PV generation, and 0.5 ($\mathrm{pf_{DC}}$) for the cold thermal energy from DC.

$$\mathrm{OF_P}(\dot{Q}, UF) = \sum_k^{PH} \Delta k \left[\mathrm{pf_G} \left(\frac{\dot{Q}(k)}{COP_{\mathrm{exp}}(k)} - \frac{\dot{Q}_{\mathrm{DC}}(k) UF_{\mathrm{DC}}(k)}{COP_{\mathrm{exp}}(k)} - \dot{P}_{\mathrm{PV}}(k) UF_{\mathrm{PV}}(k) \right) + \mathrm{pf_{DC}} \dot{Q}_{\mathrm{DC}}(k) UF_{\mathrm{DC}}(k) + \mathrm{pf_{PV}} \dot{P}_{\mathrm{PV}}(k) UF_{\mathrm{PV}}(k) \right] \quad \text{Eq.(29)}$$

As described, the constraints of the optimization problem concern the internal comfort (with $\mathrm{T_{max}}$ and $\mathrm{T_{min}}$ equal to 24 °C and 27 °C in Equation (14)), the maximum capability of the cooling system ($\dot{\mathrm{Q}}_{\mathrm{max}}$ assumed equal to the design peak power in Equation (15)) and the condition on the withdrawal from the grid expressed by Equation (25). For the case under study, the latter can be expressed as:

$$\forall k: \quad \left(\frac{\dot{Q}(k)}{COP_{\mathrm{exp}}(k)} - \frac{\dot{Q}_{\mathrm{DC}}(k) UF_{\mathrm{DC}}(k)}{COP_{\mathrm{exp}}(k)} - \dot{P}_{\mathrm{PV}}(k) UF_{\mathrm{PV}}(k) \right) \geq 0 \quad \text{Eq.(30)}$$

Also in this case, the optimization problem is solved with a MATLAB, where the whole MPC routine is written. At each time step *t*, the measurement of the internal air temperature at the previous ($T_{\mathrm{air}}(t-1)$) is passed to the controller as starting condition for the MPC building model. Once the optimization problem is solved, the controller determines the control actions for the cooling system within *PH*. They are: (i) the control signal for the DC pump ($CTRL_{\mathrm{DC}}(t)$), (ii) the circuit flowrate ($\dot{\mathrm{m}}_{\mathrm{dc}}(t)$) modulated in relation to the UF_{DC}, (iii) the control signal for the heat pump ($CTRL_{\mathrm{HP}}(t)$) and (iv) the heat pump water supply temperature ($T_{\mathrm{sup}}(t)$). $CTRL_{\mathrm{DC}}$ and $CTRL_{\mathrm{HP}}$ are Boolean variables (the value 1 indicates a switch on, while 0 a switch off) related to the decision variables UF_{DC} and UF_{PV}, while the water supply temperature, instead, is derived from the energy demand prediction $\dot{Q}(k)$. More details about the MPC formulation are reported in Paper 8, where also parts of the algorithm in provided.

Passing to analysis of the results, all the cooling season is taken into account (from June to September) as for the case analyzed in the previous sub-section. Table 5.2 reports the seasonal energy performance and cost when the rule-based control is used to cover the building cooling demand managing the multi energy systems. Since the control involves the sequential use of the MES (first DC, then PV and finally G, Figure 5.11), a good use of the available resources (DC and PV) can be noted observing the values shown in

Table 5.2. In fact, 46% of the total cooling demand is covered by the DC, while the remaining 54% is provided by the HP. In particular, 64% of the HP electricity demand is satisfied by PV generation, while the rest supplied by the power grid (G).

Table 5.2. Energy and cost performance with the RBC for the whole cooling season.

Quantity	Value
Total cooling demand (kWh)	4263
Cooling demand covered by DC (kWh)	1944
Cooling demand covered by HP (kWh)	2319
Total electricity demand (kWh)	665
Electricity demand covered by PV (kWh)	426
Electricity demand covered by G (kWh)	239
Total energy cost (EUR)	116
Total primary energy consumption (kWh)	1977

However, in this case (i.e., RBC) the choice of a specific energy source to cover the thermal demand of the building depends exclusively on the instantaneous demand and on the cooling system configuration. Moreover, no exploitation of the energy flexibility of the building is allowed, since a simple thermostat is used as control system (i.e., the RBC). Instead, when the MPC is implemented, the control logic acts to manage the MES to maximize the energy performance of the building based on an objective function, regardless of the position of each source in the cooling system and exploiting the energy flexibility provided by the TCLs as additional resource.

In particular, when the MPC involves the minimization of the electricity withdrawal from the grid (OF_G in Equation (27)), a penalty factor is applied only to the source G ($PF_G = 1$) while the remaining are not penalized ($PF_{DC} = PF_{PV} = 0$). In this way, the logic of the control has no preference in privileging the source DC rather PV. Thus, the same result in term of objective function (i.e., electricity supplied by the grid consumption) could be obtained with different ways of exploitation of the two free sources at times when the two availabilities far exceed the demand.

Focusing on a representative summer week, Figures 5.19 and 5.20 show the uncontrolled energy sources exploitation (DC and PV) in meeting the energy demand of the building both in case of RBC (Figure 5.19) and MPC operation with a *PH* of 18 hours (Figure 5.20). Apparently, there does not seem to be a sensitive difference between the two ways of exploitation of the DC and PV sources. In particular, it can be noted that a greater exploitation of the DC is obtained with the RBC (80% of the total weekly cold energy availability in relation to the 71% in case of the MPC, Figure 5.19(a) and Figure 5.20(a)), while the opposite behavior is achieved for the PV use (Figure 5.19(b) and Figure

5.20(b)): 52% of the total weekly electricity production is consumed by the heat pump in case of MPC operation, while 41% with the RBC.

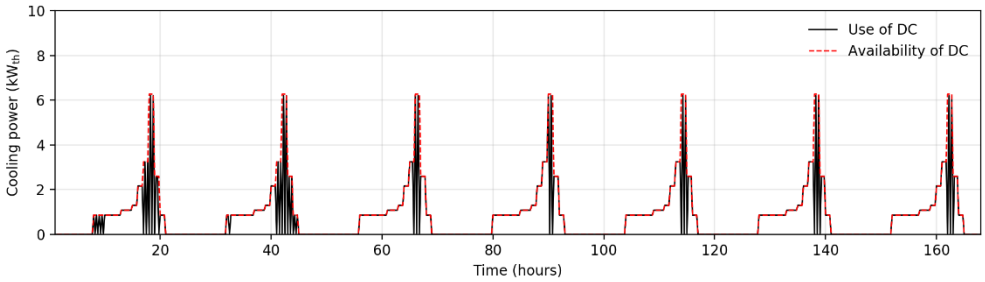

(a)

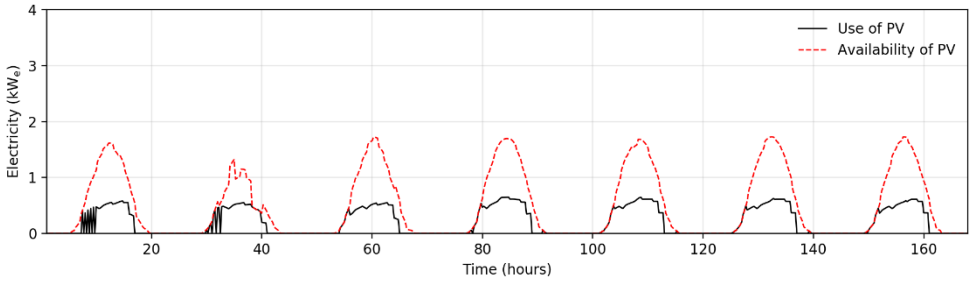

(b)

Figure 5.19. Energy sources used to cover the weekly cooling demand of the building compared to the availability profiles with RBC: (a) DC and (b) PV.

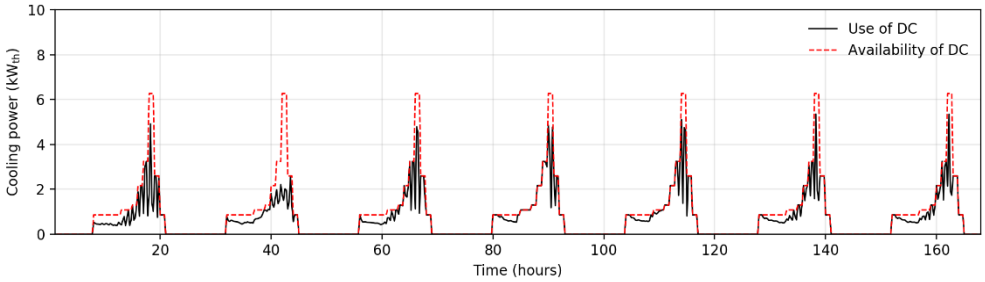

(a)

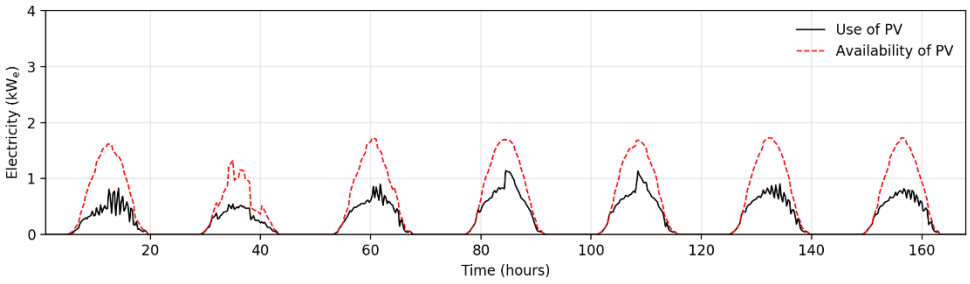

(b)

Figure 5.20. Energy sources used to cover the weekly cooling demand of the building compared to the availability profiles with MPC (OF_G, *PH* of 18 hours): (a) DC and (b) PV.

However, looking at the electricity taken from the power grid, the effectiveness of the MPC can be observed. Figure 5.21 compares, in the same week, the use of G source in case of RBC and MPC with OF_G. The area highlighted represents the time when the other energy sources (DC and PV) are available. Thanks to the activation of the energy flexibility of TCLs, the MPC acts both reducing the electricity consumption in the period in which no other sources are available, by lowering the total cooling demand (and maintaining the maximum allowed setpoint, Figure 5.22), and removing the electricity peaks that occur during periods of sources availability (Figure 5.21). In the representative week, in fact, the electricity consumption passes from 26.4 kWh in case of RBC to 10 kWh in case of MPC (reduction of 62%). In particular, to confirm the effectiveness of the control, the electricity use in case of DC and PV availability presence is reduced by 76% in case of MPC operation (from 7.7 kWh with RBC to 1.9 kWh with MPC).

Looking at Figure 5.22, a good performance of the control in predicting the real-time internal air temperature value can also be noted. Comparing the actual value of T_{air} with its prediction in the same timestep, an *RMSE* of 0.43 °C is calculated for the representative week with a maximum overheating temperature of 27.4 °C.

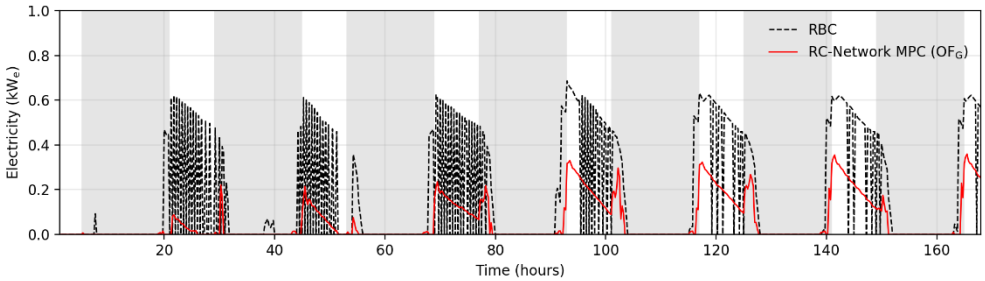

Figure 5.21. Electricity from the power grid (G) used to cover the weekly cooling demand of the building. Comparison between RBC and MPC (OF$_G$, *PH* of 18 hours).

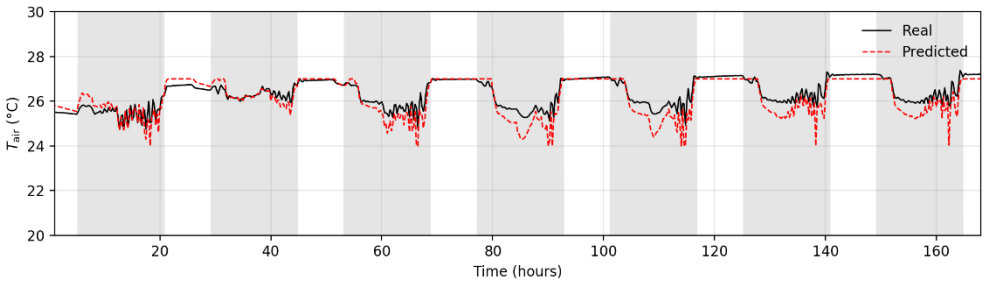

Figure 5.22. Comparison between actual indoor air temperature (T_{air}) and its prediction in the MPC. MPC with OF$_G$ and *PH* of 18 hours.

Generalizing the considerations made to the entire cooling season, a reduction of 53% of the consumption of the electricity from the grid (G) is obtained compared to the RBC. In particular, the electricity withdrawal in presence of DC and PV availability is reduced by 77% (from 68.7 kWh to 16 kWh). An *RMSE* of 0.33 °C is obtained, with a maximum indoor air temperature of 27.4 °C.

On the other hand, when the MPC is formulized with OF$_C$, the total energy costs are minimized. In this case, a penalty is also assigned to the DC ($PF_{DC} = c_{th,DC}$, $PF_G = c_{el,G}$, $PF_{PV} = 0$) and the use of the heat pump with electricity from PV is encouraged, as shown in Figure 5.23. The DC use becomes 22% of the total energy availability, while 78% of the electricity produced by the PV is consumed by the HP. To avoid the use of other energy sources (DC and G), the virtual energy sources represented by the building energy flexibility is involved. Indeed, the MPC acts to maintain the highest comfort band when there is not PV availability, and to lower temperature only when there is PV availability (Figure 5.24, where the highlighted areas represent the periods of PV

generation). In this way, the total cooling demand is reduced by 20% compared to the RBC operation. The operative *RMSE* in the week depicted in Figure 5.24 becomes 0.38 °C, with a maximum temperature reached of 27.6 °C.

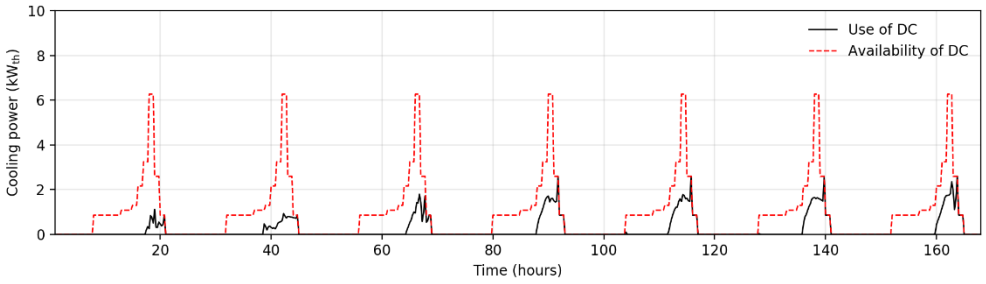

(a)

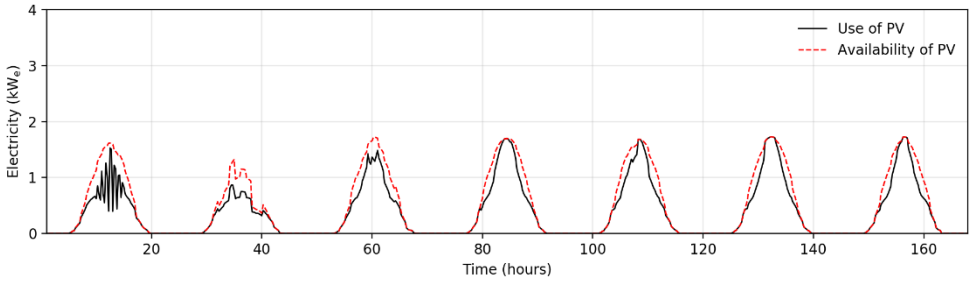

(b)

Figure 5.23. Energy sources use to cover the weekly cooling demand of the building compared to the availability profiles with MPC (OF_C, *PH* of 18 hours): (a) DC and (b) PV.

Referring to the use of the sources to meet the weekly cooling demand, the PV exploitation increases by 107 % respect to the RBC, while the DC and G sources use decreases, respectively, by 66 % and 46 %. The total weekly energy cost is reduced by 61%. The behavior of the control is confirmed also in case of seasonal evaluation. In fact, a cost reduction of 64 % is obtained in reference to the RBC operation with an increase of PV use of 102 % (from 426 kWh to 862 kWh). The *RMSE* lowers to 0.33 °C with a maximum overheating temperature of 27.6 °C (Figure 5.24).

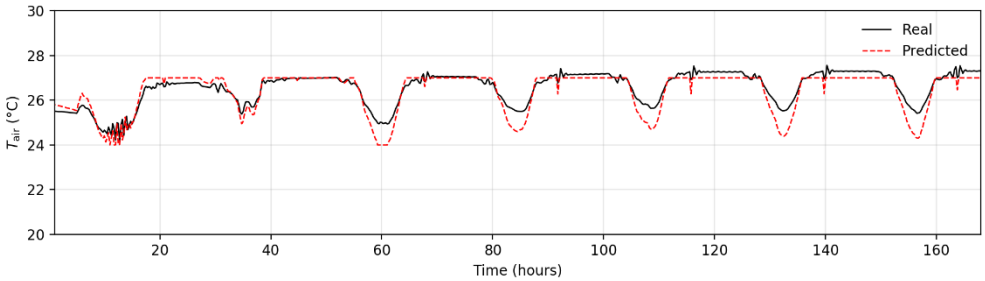

Figure 5.24. Comparison between actual indoor air temperature (T_{air}) and its prediction in the MPC. MPC with OF_C and *PH* of 18 hours.

Finally, if the MPC acts to minimize the total primary energy consumption, no free sources ($PF = 0$) are available and a penalty factor is assigned to all the energy sources ($PF_{DC} = pf_{DC}$, $PF_G = pf_G$, $PF_{PV} = pf_{PV}$). Figure 5.25 and Figure 5.26 represents the sources exploitation (Figure 5.25(a) for the DC and Figure 5.25(b) for PV) and the internal temperature T_{air} in case of MPC operation with OF_P, in a representative week. Looking at Figure 5.26, it can be noted that in this case the control tends to minimize the overall energy demand keeping the indoor air temperature close to the upper temperature limit imposed to the optimization problem. The total demand is reduced by 28% compared to the baseline, and an operatively *RMSE* of 0.30 °C is calculated. In this case, the maximum temperature reached is 27.7 °C.

A weekly primary energy consumption reduction of about 34% is obtained compared to the RBC and a reduction of the same order of magnitude also occurs in case of seasonal evaluation (30%, from 1977 kWh in case of RBC to 1386 kWh in case of MPC with OF_P and a *PH* of 18 hours). The *RMSE b*ecomes 0.25 °C and a maximum temperature of 27.8 °C is reached.

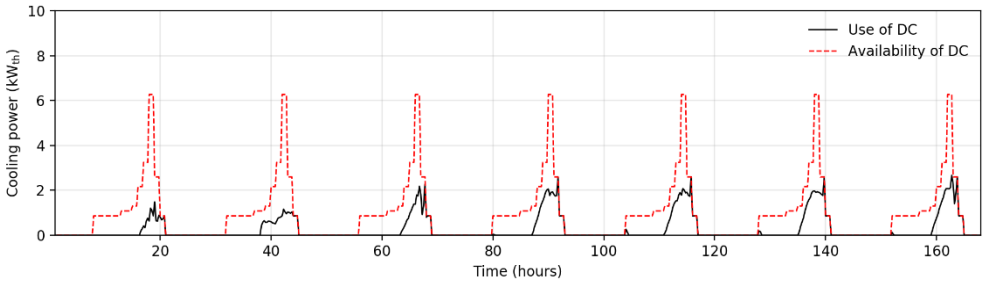

(a)

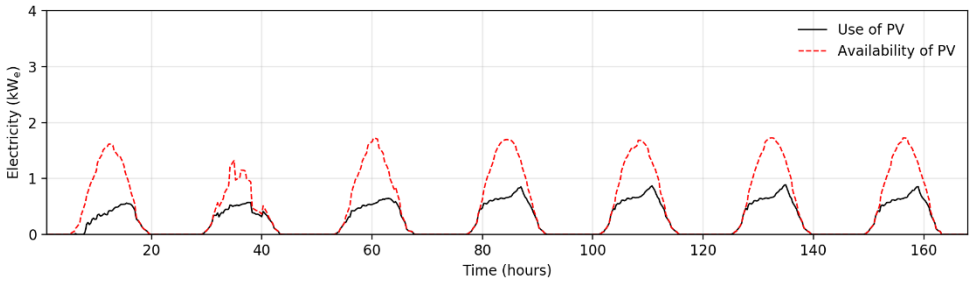

(b)

Figure 5.25. Energy sources used to cover the weekly cooling demand of the building compared to the availability profiles with MPC (OF_P, *PH* of 18 hours): (a) DC and (b) PV.

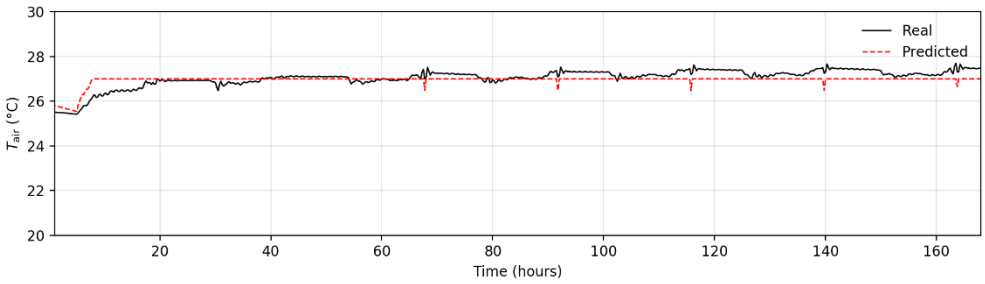

Figure 5.26. Comparison between actual indoor air temperature (T_{air}) and its prediction in the MPC. MPC with OF_P and *PH* of 18 hours.

Comparing all the discussed cases in the whole cooling season, the different use of the available energy sources by the MPC, according to the tested objective functions (OF_G, OF_C and OF_P), can be evaluated. In Figure 5.27, the shares of sources exploitation to meet the total seasonal demand are provided in comparison with the RBC operation (Figure 5.27(a)). The seasonal simulations confirm the trends observed during the reference week for the various controls.

As expected, in fact, due to the system configuration (Figure 5.11), the highest consumption of cooling from DC is realized by the RBC (46% of the cooling demand). A small reduction of 8 % in the DC use is obtained with the MPC operating with OF_G (42% of the cooling demand, Figure 5.27(b)), while in case of OF_C and OF_P the total demand share covered falls by 75% and 60% (Figures 5.27(c) and (d)). As concerns the use of HP with PV, in all the tested controls there is an increase in the exploitation of the resource. In particular, the highest use is obtained with OF_C (the share of total demand

covered by the PV increases from 35 % to 78 %, with an increase of 122 %; Figures 5.27(a) and (c)), while increases of smaller amplitudes are obtained with OF_G (increase of 41 % respect to RBC, Figure 27(b)) and OF_P (increase of 81% respect to RBC, Figure 5.27(d)). To confirm the effectiveness of the control, the lowest share of demand covered by the grid is realized with OF_G: the demand share decreases by 54 % respect to RBC, while in case of OF_C and OF_P the reduction become 43 % and 4 % respectively.

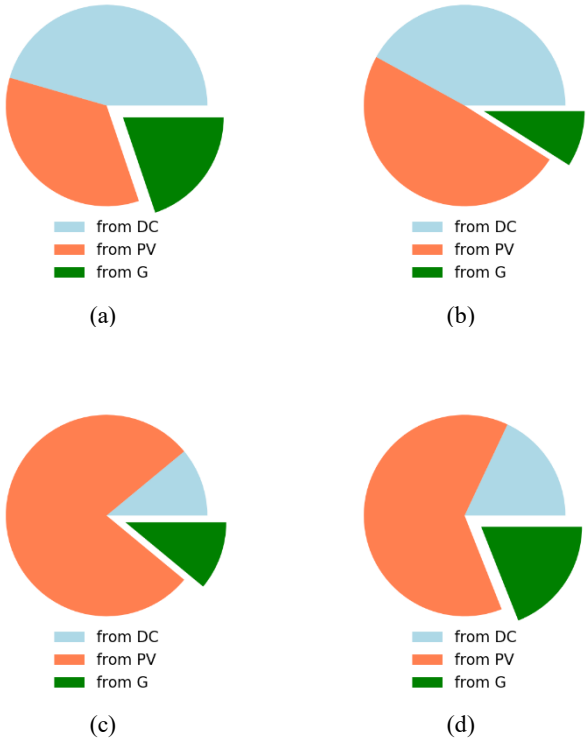

Figure 5.27. Seasonal thermal demand satisfaction divided by energy sources: (a) RBC, (b) MPC with OF_G, (c) MPC with OF_C and (d) MPC with OF_P. Results obtained with a *PH* of 18 hours.

In all the tested MPCs (i.e., OF_G, OF_C and OF_P), results show a large exploitation of the energy flexibility provided by the TCLs. In particular, for OF_C and OF_P, the minimization of the cooling demand (maintaining the temperature as high as possible) is evaluated by the control as the better strategy to achieve the objective. Instead, in case of OF_G, the dynamic variation of the indoor temperature is realized by the control

lowering the setpoint in moments with high availability of free sources (DC and PV) and minimizing the demand at other times. Figure 5.28 summarizes the results discussed so far, allowing a faster comparison between the ways to exploit the available energy sources (Figure 5.28(a)) when the different objective functions are pursued. Compared to the RBC operation, where there is no logic able to choose the use of one source rather than another, the MPC formulated to manage the MES shows good operational performance in terms of optimized management of resources, according to the OFs. Results show that the highest percentage reduction in the desired optimized quantities is obtained with each specific OF implementation, confirming the successful management of the available energy sources (Figure 5.28(b)).

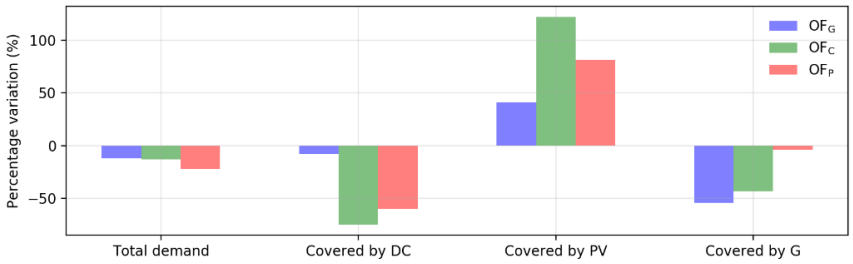

(a)

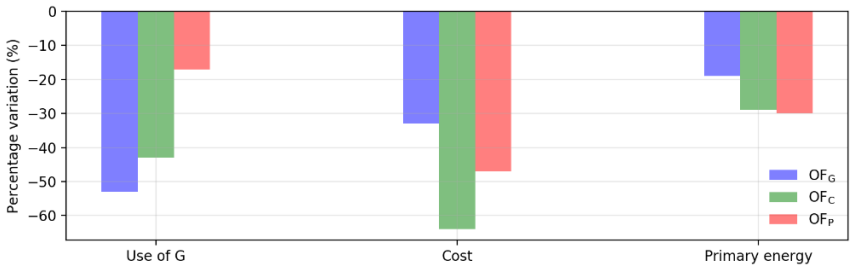

(b)

Figure 5.28. Comparison between OF_G, OF_C and OF_P in the MPC for the whole cooling season (*PH* of 18 hours) in terms of percentage variation, compared to RBC, of: (a) thermal demand composition and (b) seasonal values of the three optimized quantities percentage reduction.

To conclude, as showed by the results, the predictive control formulized with the RC-network building model allow to manage the exploitation of the energy sources according to the formulated objective function in the optimization problem: the control acts to maximize the use of free and of energy flexibility to avoid the use of penalized

sources. Moreover, results show good operational performance of the control in terms of seasonal optimized quantities, according to the defined OFs and the exploitation of the energy flexibility of TCLs is fundamental to allow the controller to apply the optimal control actions.

5.3 Comparison between data-driven and physical based approaches in an operative MPC

Assuming that both control formations (ANN-MPC and RC-network-MPC) show they are able to exploit TCLs flexibility as an additional energy source, a reversal of performance between the two models can be found when the evaluation is carried out for the application in a realistic MPC controller. Indeed, while the ANN has showed grater performances in replicating training data than the RC-network, in the operative scenario the behaviors appear the opposite. The main reason is related to the difficulty in selecting the proper dataset for the ANN training. In fact, the model must not only be able to replicate the response of the building in the same input conditions (and this is done well in the present studies), but must also predict the system response in different scenarios, taking into account the contribution given by energy flexibility derived by thermostatically controlled loads. When the latter is introduced, it becomes difficult to identify a dataset that can train the black box model adequately, since the problem becomes dynamically affected by the operation of the system. Therefore, as also summarized in Paper 9, specifically three different issues can be found for an ANN dedicated to the aforementioned purpose:

(i) Difficulty in the training of the ANN.
(ii) Errors in the prediction of the thermal demand.
(iii) Difficulty in managing energy flexibility with the MPC used in the real buildings.

When referring to point (ii), it is not meant that there is a certain deviation between the results of the ANN and the training dataset. This deviation, in fact, could be opportunely reduced by modifying the architecture of the ANN or by changing the training parameters. Instead, it is mean that the prediction capability of the ANN could result in amplified deviations when new situations (combinations of outdoor and indoor variables for the building) are provided to the network. This issue cannot be solved easily and requires a careful evaluation of the performance of the MPC when integrated in the real building. In extreme cases, the ANN should be trained again (perhaps with a reinforcement learning approach) with new data that consider behaviors of the building that the network fails to predict correctly. The same considerations can be applied also for the third issues (iii), i.e. the difficulty in managing energy flexibility with the MPC

used in the real buildings. In fact, the possibility given to the optimizer to work in a larger comfort band could result in an MPC that tends to operate often near the boundaries of the defined comfort band. As a consequence, the thermal comfort quality in the building could be significantly worsened respect to the reference case, and in some scenarios this could not be acceptable. In the same fashion of the second issue (i.e., errors in the prediction of the thermal demand) there is no simple solution for this problem, which is likely dependent on the fact that a black box model, having no information on the thermo-physics of the building as well as no details on the behavior of the occupants, struggles to simulate energy flexibility properly. As indicated, reinforcement learning could represent a valid technique to bypass the problem.

Passing to the white box approach, the flexibility contribution seems to be better represented by model based on the RC network. When using a white box model however, a relevant amount of detailed data relating to the design and construction characteristics of the building should be known in order to implement an accurate model. Moreover, it is not always obvious choosing the best network structure to use in the physical-based approach. For very complex buildings, it may be exceedingly difficult to identify an appropriate model and the corresponding parameters, even if a detailed knowledge of the building is available. Another aspect that should be considered when using a purely physical-based model is that some dynamics (e.g., occupancy) cannot be considered in any way, unless dedicated models are not added. When, instead, measured data are used for the model training, such information may be intrinsically provided to the model. For these reasons, it could be convenient monitoring data and using hybrid models.

To conclude, Table 5.3 reports a comparison summary between the two building model approaches, subdivided into the main steps of configuration and implementation in an MPC.

Table 5.3. Comparison summary between a physical-based and a data-driven approach in an operative MPC (in Paper 6).

Step	Physical-based approach	Data-driven approach
Preparation of the building model	▪ No measured data are required. ▪ An accurate knowledge of the geometrical and thermal characteristics of the building is needed.	▪ Measured data are required. ▪ The knowledge of the geometrical and thermal characteristics of the building is not needed.
Identification of the model configuration	▪ Difficulty in selecting the proper RC network and the numerical values of the parameters for complex buildings. ▪ Necessity to provide an accurate occupancy model if this aspect needs to be considered.	▪ There is no systematic procedure to choose the best network architecture, and the optimal number of neurons is the result of a trial-and-error process. ▪ Difficulty in selecting proper input and output quantities when representing energy flexibility.
Model development	Linear model that can be represented with a state-space formulation	Nonlinear model, one hidden layer of neurons is generally sufficient
Comparison with the reference building	Good ability to replicate the reference case behavior at the same inputs	Good ability to replicate the reference case behavior at the same inputs
Implementation in an MPC	▪ Improved performance in terms of objective functions compared to the reference operation. ▪ Good ability to represent flexibility and follow thermal dynamics, with occasional comfort constraint violations ▪ An amplification of the prediction error however occurs when real implementation is tested	▪ Improved performance in terms of objective functions compared to the reference operation. ▪ Relevant errors in demand prediction when energy flexibility is managed. ▪ Comfort constraint violations can occur during real implementation. ▪ An amplification of the prediction error occurs when real implementation is tested.

Chapter 6

Operational energy flexibility evaluation: focus on the residential space cooling sector

In this Chapter a comparison between the design and the operative energy flexibility evaluation is provided with a focus on the space cooling (SC) sector. The attention on the space cooling is motivated by the fact that it is one of the sectors whose energy demand is constantly growing. Indeed, the IEA in a recent report estimates that space cooling is the fastest growing end energy use in buildings, having increased by 3.3% a year since 2010 [113]. In this context, the investigation of the energy flexibility performance that can be obtained by the demand management of the residential cooling systems, can have a paramount role to limit grid instability and reduce overall demand. About that, the objective of this Chapter is to evaluate the role of the different residential space cooling technologies in obtaining different level of flexibility resources. A preliminary evaluation is presented in Paper 10 where the methodology to quantify the energy flexibility performance (i.e., FPI) discussed in Chapter 3 is applied to a building with different cooling systems (sub-section 6.1). Moreover, in the sub-section 6.2, the flexibility evaluation of the different residential space cooling technologies is moved on operative scenario.

6.1 Case studies and design flexibility evaluation

In order to make the analysis independent of the thermal characteristics of the building envelope, the same building model is used to test different space cooling technologies. In particular, the building is modelled in TRNSYS with thermal properties derived from the Italian regulation D.M. 26 June 2015 [70], since it is representative of a consistent share of the building stock where modern cooling systems can be integrated. A single building with four apartments of 100 m^2 of living area is modelled (i.e., four thermal zones, schematic of the planimetry with the different cooling system in Figure 6.1). In particular, Table 6.1 reports the value of the building envelope surfaces facing outwards, in accordance with [70].

Table 6.1. U-value (W m^{-2} K^{-1}) implemented in Paper 10.

External walls	Floor	Roof	Windows
0.36	0.36	0.28	2.10

As concern the space cooling technologies, four different systems, whose distribution systems have different thermal inertia levels, are taken into account. They are sized on the basis of the peak cooling demand [69] of the building. In Rome, Italy (41°55' N, 12°31' E) where the building is located, the cooling peak load, with the outside design condition suggested by Italian standard UNI 10349-2 [66] (0 °C) and an internal temperature of 25°C with 60% RH is about 5.7 kW, of which 4.5 kW sensible and 1.2 kW latent. In particular, the modelled cooling systems are:

(i) Split system (S). It is composed of an air source heat pump with direct expansion split system. In this system, the indoor air cooling is realized by direct contact with the evaporator in which the refrigerant flows. The split system allows only a punctual control of the indoor temperature. Moreover, it is the system with lower thermal inertia. However, it is introduced for its large diffusion due to its inexpensiveness and installation easiness (Figure 6.1).

(ii) Fan coil units (FCU). It is composed of an air to water heat pump with fan coil units as emission system. As for the split system, only the indoor temperature is controlled, and a punctual control of the relative humidity is not possible. Although characterized by a low thermal inertia as split systems, the presence of a water loop allows the addition of a thermal energy storage (i.e., a cold-water tank), with consequent increase in thermal inertia. In this case a 200 liters cold water tank is added in order to model a medium thermal inertia cooling system (Figure 6.1).

(iii) Radiant ceiling panels system (CP). It is composed of an air source heat pump coupled with ceiling panels. In this case also an air dehumidifier (DH) is added to the system to treat the latent contribution. Therefore, both the internal temperature and relative humidity can be controlled. The chilled ceiling is composed of pipes set on panels in the first internal layer of the roof, for this reason it is considered a medium thermal inertia system if compared with radiant cooling concrete ceiling (Figure 6.1).

(iv) Radiant cooling concrete ceiling (CC). It is composed of an air source heat pump with radiant cooling concrete ceiling. It is modelled as a massive layer in the ceiling stratigraphy. Even in this case the treatment of latent heat is entrusted to an internal air dehumidifier (DH). This emission system has the highest thermal inertia, since the pipes are embedded in a concrete layer of 0.1 m (Figure 6.1).

A separate discussion must be made on generation systems. Indeed, in case of the analysis showed in Paper 10, all the cooling systems are modelled in TRNSYS with

Type 954 for the air source heat pump and Type 941 for the air to water heat pump. Both the Types have a ON/OFF regulation. In the operative evaluation, discussed in the following sub-section (sub-section 6.2), this approximation is outdated by modelling all the systems in Python [114]. In this environment a commercial variable load heat pump is modelled [65] for fan coil units, ceiling panels system and radiant cooling concrete ceiling, while for the split ON/OFF system has always been modeled .

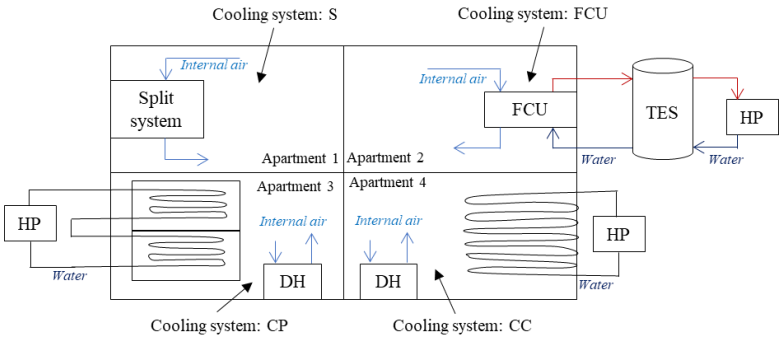

Figure 6.1 Schematics of the cooling systems in the considered building.

According to the methodology illustrated in Chapter 3, the FPI (Equation (3)) is calculated for the presented cooling systems. Since the models are located in Rome, the demand response representative summer day is August 18 and the DR starting time is 12.00 pm, when frequently the Italian electric demand has a peak in summer weekdays (sub-section 3.1.1). Table 6.2 summarizes the flexibility parameters and the FPI calculation for all the cooling systems. As for the case studies discussed in sub-sections 3.2.1 and 3.2.3, also in this case, the flexibility classification of the buildings is realized with the only FPI (the FPI_{lim} is not formulized, see sub-section 3.2.3).

Table 6.2. Flexibility parameters and labelling in cooling season for case studies considered in Paper 10.

Space cooling system	t^*_{res}	$\dot{P}^*_{res}$	t^*_{rec}	η_{DR}
Split system	0.07	0.42	0.01	0.76
Fan coil units with TES	0.08	0.18	0.01	0.78
Ceiling panels system with dehumidifier	0.07	0.91	0.23	0.19
Concrete ceiling with dehumidifier	0.05	0.89	0.13	0.18

As showed in Figure 6.2, all of them have low design energy flexibility since the FPI remains always between 4.1 and 5.5 (Class C or B).

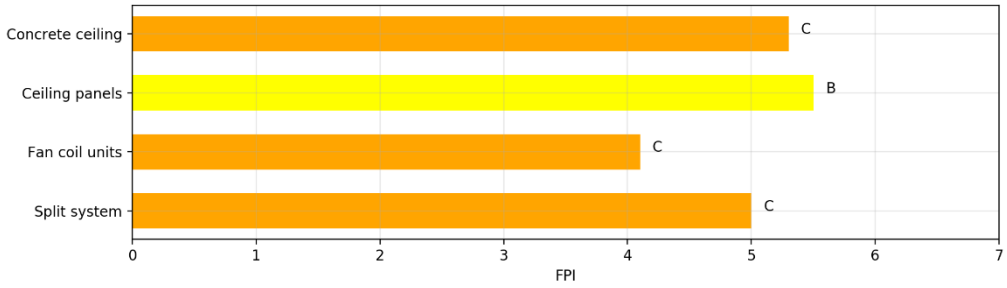

Figure 6.2. Buildings flexibility label for the case studies considered in Paper 10.

Focusing on the split and fan coil unit systems, a very similar behavior can be observed between them. The cold-water tank coupled with the fan coil circuit allows to obtain a response time 22 minutes longer than the split system. As Figure 6.3 shows, due to the cold-water tank discharge, from time 12 hours to 12.7 hours, when the heat pump is off, the indoor temperature continues to comply with the initial set-point. However, from the electricity consumption point of view, the adoption of a fan coil units with a cold-water tank produces less savings in committed power and actual energy use, which negatively affect the FPI calculation.

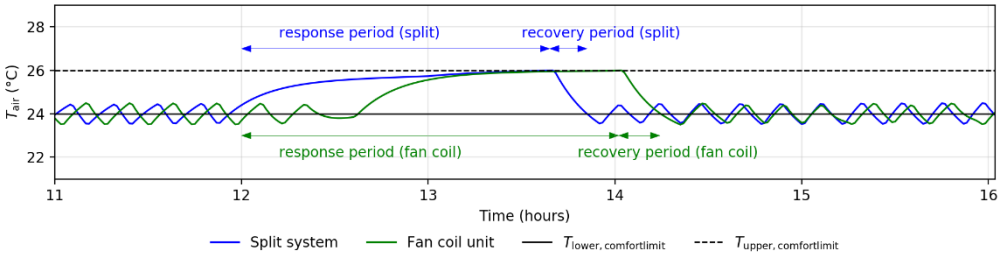

Figure 6.3. Inside temperature, comparison between split system and fan coil units with cold-water tank.

As said before, these space cooling systems do not allow a punctual control of the relative humidity, so the phases of the demand response event are determined by the indoor temperature only (Figure 6.3). Instead, in CP and CC systems, where an air dehumidifier is installed, the response and the recovery period are ruled by both. It can be immediately noted that, even if a distribution system with a higher thermal inertial (i.e., CP or CC) is adopted, the response time remains rather low (Table 6.1), since the relative humidity conditions affect a lot the building behavior. Moreover, the thermal

inertia has an impact on the speed with which the relative humidity increases, and so on the comfort limit condition that is reached first. When there is more thermal inertia, indeed, the internal temperature tends to rise more slowly, and the relative humidity increases faster, as it can be seen in Figure 6.4(b). The CC system provides a higher inertia than CP and the relative humidity reaches firstly the limit conditions (i.e., t_{res} is 30% lower for CC than CP, determining a lower E_{DR} value). However, when the response period ends, the indoor temperature in CP system reaches 25.7 °C, while for CC about 25 °C. This fact affects the recovery period, which for CP is 2 hours and 12 minutes higher than for CC.

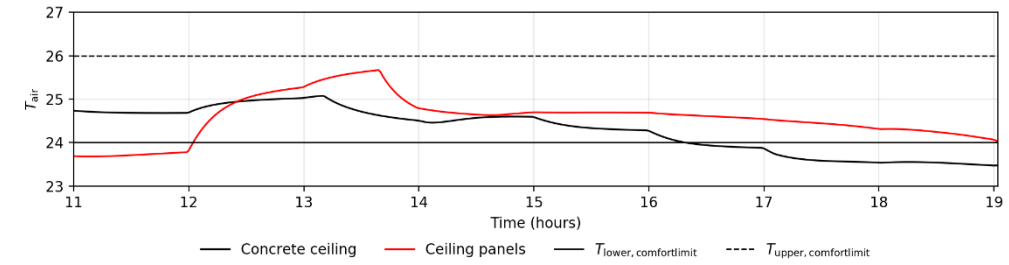

(a)

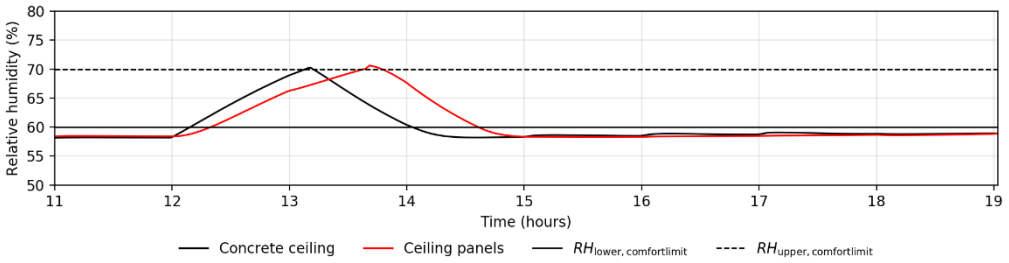

(b)

Figure 6.4. Comparison between ceiling panels and concrete ceiling cooling systems: (a) inside temperature and (b) inside relative humidity.

This analysis makes possible to conclude that, for the modelled dwellings in summer period there is a low overall design energy flexibility performance. The thermal inertia seems to affect positively the response duration only if the control system is just temperature-based. If a more accurate control of the comfort condition is possible (both

temperature and relative humidity), its influence on the response period is mitigated. However, this last case allows to obtain a little improvement in flexibility performance.

6.2 Operative flexibility evaluation

The evaluation provided in sub-section 6.1 is mainly focused on the design phase. Indeed, the flexibility performance indicator (sub-section 3.1) is calculated under standard boundary conditions (sub-section 3.1.2). On the contrary in this sub-section an operative evaluation is presented. In particular, the same case studies presented in above are modelled in Python with white box RC-network models.
A building with the same thermal properties (Table 6.1) is modelled as single-family houses (all the envelope surfaces are facing outward) for all the investigated space cooling technologies. The detailed RC-network is represented in Figure 6.5. It is composed of 10 thermal resistances and 7 thermal capacitances [115].

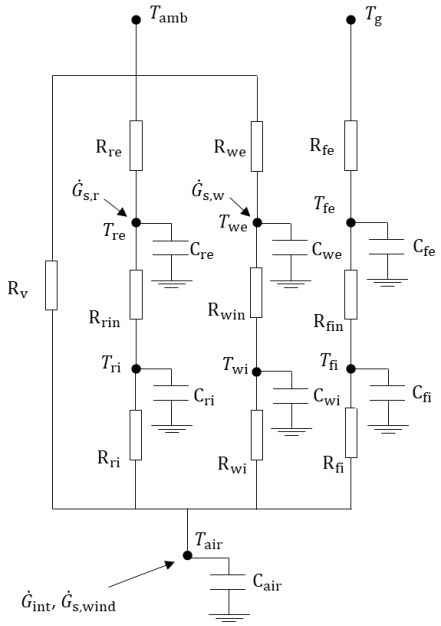

Figure 6.5. 10R7C network building model.

Looking at Figures 6.5 it can be noted that each opaque surface of the building envelope is modelled with two capacitances (thermal nodes) and three thermal resistances [116].

In particular, the two thermal capacities represent all the layers of the surface in the positions preceding and following the thermal insulation. Consequently, the two temperatures are the surface temperatures of the insulation layer.
Assuming one-dimensional heat transfer, the system dynamics can be described as a classic linear state-space model (Equation (11)). As can be noted in Figure 6.5, the contribution of the cooling system ($\dot{Q}_{\mathrm{SC}}$) is not shown since the way it is supplied depends on the specific space cooling technology. Indeed, when the cooling system is composed of an air distribution system (e.g. split systems and fan coil units), $\dot{Q}_{\mathrm{SC}}$ is directly removed from the internal air node temperature (T_{air}). Instead, in case of addition of a thermal energy storage to the fan coil circuit, the thermal power that is supplied to the internal air thermal node ($\dot{Q}_{\mathrm{building}}$) is decoupled from that produced by the cooling system ($\dot{Q}_{\mathrm{SC}}$). Their link is formalized in the thermal energy storage (TES) model:

$$\mathrm{C_{TES}} \cdot \frac{\mathrm{d}T_{\mathrm{TES}}}{\mathrm{dt}} = \dot{Q}_{\mathrm{SC}} + \dot{Q}_{\mathrm{building}} + \mathrm{K_l}(T_{\mathrm{env}} - T_{\mathrm{TES}}) \qquad \text{Eq. (31)}$$

Where the TES is assumed to be a perfectly mixed water tank. Its storage capability is modelled with a thermal capacitance ($\mathrm{C_{TES}}$) and with a node temperature (T_{TES}). The thermal losses with the environment temperature (T_{env}) are modelled with a loss coefficient factor ($\mathrm{K_l}$).
In case of ceiling cooling systems (ceiling panels and cooling concrete ceiling), $\dot{Q}_{\mathrm{SC}}$ is removed from the inner roof thermal node. For high massive system (CC) this node coincides with the node T_{ri} in Figure 6.5, while for the ceiling panels (CP) system a further thermal node for the ceiling is distinguished ($T_{\mathrm{ri,cp}}$, which stands for the position immediately after the internal plaster). As described in sub-section 6.1, in these last two space cooling systems, also the humidity control is enabled. With reference to the effective capacitance humidity model [63], the moisture balance is carried out in parallel with the sensible energy balance calculation. For the air node it is expressed as:

$$\mathrm{M_{air}} \frac{\mathrm{d}x_{\mathrm{air}}}{\mathrm{dt}} = \dot{\mathrm{m}}_{\mathrm{vent}}(x_{\mathrm{amb}} - x_{\mathrm{air}}) + \frac{\dot{Q}_{\mathrm{DH}}}{\mathrm{h_v}} \qquad \text{Eq. (32)}$$

where $\mathrm{M_{air}}$ and x_{air} are the mass and the absolute humidity of the internal air, $\dot{\mathrm{m}}_{\mathrm{vent}}$ and x_{amb} are the natural ventilation flowrate and its absolute humidity, $\dot{Q}_{\mathrm{DH}}$ is the latent contribution of the dehumidifier systems and $\mathrm{h_v}$ is the heat of evaporation of water (by approximation assumed constant in the balance).

To provide an operative flexibility evaluation, the capability of a space cooling system to respond to a programmed load variation is evaluated by simulating different demand response (DR) events and comparing them with a reference case (baseline, BL). The baseline represents the demand curve of each cooling system to maintain the comfort conditions. It is computed as the solution of a optimization problem that has the objective of minimizing the thermal requirement of the building:

$$\text{minimize}\left(\sum_{\mathrm{k_{start}}}^{\mathrm{k_{end}}} \dot{Q}_{\mathrm{SC}}(k)\cdot \Delta \mathrm{k}\right) \qquad \text{Eq. (33)}$$

Here, the thermal power of the cooling system ($\dot{Q}_{\mathrm{SC}}$) is the decision variable of the optimization problem and it is limited at each timestep (Δk) by the maximum power of the generating system. However, a distinction has to be made between the optimization problem solved for the split system (i.e., ON/OFF regulation) and the other cooling systems (i.e., FCU, CP and CC equipped with a variable load heat pump). Instead, if for the FCU, CP and CC systems a typical linear programming (LP) optimization problem is formulized, for the split a MILP (mixed-integer linear programming) is introduced to reproduce the ON/OFF regulation. In this case, the optimization problem formulized in Equation (33) can be rewritten as:

$$\text{minimize}\left(\sum_{\mathrm{k_{start}}}^{\mathrm{k_{end}}} \dot{\mathrm{Q}}_{\mathrm{max}}\cdot CTRL_{\mathrm{S}}(k)\cdot \Delta \mathrm{k}\right) \qquad \text{Eq. (34)}$$

where $CTRL_{\mathrm{S}}$ is the Boolean decision variable for the split system.
For all the SC systems, the comfort constraints on the air temperature node must be satisfied. They are modelled with a setpoint temperature (T_{sp}) and an allowed comfort band defined with a $\Delta \mathrm{T_{max}}$ and a $\Delta \mathrm{T_{min}}$:

$$\forall\, k \qquad \left(T_{\mathrm{sp}} - \Delta \mathrm{T_{min}}\right) \leq T_{\mathrm{air}}(k) \leq \left(T_{\mathrm{sp}} + \Delta \mathrm{T_{max}}\right) \qquad \text{Eq. (35)}$$

Moreover, if the cooling system is able to control also the internal humidity, the same condition expressed in Equation (35), can be written for the relative humidity (RH):

$$\forall\, k \quad \left(RH_{\mathrm{sp}} - \Delta \mathrm{RH_{min}}\right) \leq\ RH(k) \leq \left(RH_{\mathrm{sp}} + \Delta \mathrm{RH_{max}}\right) \qquad \text{Eq. (36)}$$

The constraint formulated in Equation (36), is actually mathematically expressed in terms of absolute humidity (x). Therefore, the effective constraint is:

$$\forall\, k \quad \mathrm{x_{min}} \leq x_{\mathrm{air}}(k) \leq \mathrm{x_{max}} \qquad \text{Eq. (37)}$$

With $\mathrm{x_{min}}$ and $\mathrm{x_{max}}$ calculated as the absolute humidity at allowed upper comfort limit for the temperature $(T_{\mathrm{sp}} + \Delta \mathrm{T_{max}})$ and respectively the lower $(RH_{\mathrm{sp}} - \Delta \mathrm{RH_{min}})$ and the upper $(RH_{\mathrm{sp}} + \Delta \mathrm{RH_{max}})$ comfort limit for the relative humidity.
When the cooling power is not directly provided to the internal air node (T_{air}) (e.g., for fan coil units coupled with TES, ceiling panels or cooling concrete ceiling systems), a constraint on the temperature of the thermal mass (TMD) of the specific distribution system node is required:

$$\forall\, k \qquad \mathrm{T_{TMD,min}} \leq T_{\mathrm{TMD}}(k) \leq \mathrm{T_{TMD,max}} \qquad \text{Eq. (38)}$$

In particular, T_{TMD} coincides with T_{TES} for the cooling system composed of fan coil units and TES, $T_{\mathrm{ri,cp}}$ for radiant ceiling panels and T_{ri} for radiant cooling concrete ceiling system.
A demand response event based on a peak shaving strategy is defined. It is modeled by imposing at a certain time $\mathrm{k_{start,DR}}$ and for a period $\Delta \mathrm{k_{DR}}$ a variation of the electrical power peak of the baseline, according to a reduction factor ($\mathrm{f_{PSS}}$).

$$\text{For } \mathrm{k_{start,DR}} \leq k \leq \mathrm{k_{end,DR}} \qquad \dot{P}_{\mathrm{DR}} = \mathrm{f_{PSS}} \cdot \dot{P}_{\mathrm{max,BL}} \qquad \text{Eq. (39)}$$

With: $\mathrm{k_{end,DR}} = \mathrm{k_{start,DR}} + \Delta \mathrm{k_{DR}}$
In order to provide an operative evaluation, the effect of different demand response events is tested by varying the characteristics of the event (i.e., $\mathrm{f_{PSS}}$ or $\Delta \mathrm{k_{DR}}$) and observing the response of the analyzed cooling systems.
This condition is modelled as an additional constraint for the optimization problem:

$$\forall\, k \quad \dot{P}_{\mathrm{SC}}(k) \leq \dot{P}_{\mathrm{DR}}(k) \qquad \text{Eq. (40)}$$

where $\dot{P}_{\mathrm{SC}}$ is the electrical absorption of the individual cooling systems.
To ensure a certain level of flexibility to all the space cooling technologies, the exploitation of the energy flexibility provided by thermostatic controlled loads (TCLs) is used when the demand response event is applied. It is activated by allowing the air node temperature (T_{air}) to drop down to a higher $\Delta \mathrm{T_{min}}$ or to rise to a higher $\Delta \mathrm{T_{max}}$.

The exploitation of the temperature range $[T_{sp} - \Delta T_{min}; T_{sp}]$ is always granted, while the upper interval (T_{sp}; $[T_{sp} + \Delta T_{max}]$) is allowed only during the event (Δk_{DR}). If also the humidity can be controlled by the cooling system, a ΔRH_{max} and a ΔRH_{min} are introduced with the same logic.
To quantify the ability of each system to be energy flexible, different quantities are used:

- The energy shifted during the demand response event:

$$E_{shift} = E_{BL} - E_{DR} = \int_{k_{start,DR}}^{k_{end,DR}} (\dot{P}_{BL} - \dot{P}_{DR}) dk \qquad \text{Eq. (41)}$$

  This is a characteristic of the modeled event as it depends on the duration of the event (Δk_{DR}) and peak shaving reduction factor (f_{PSS}).
- The use of the energy flexibility of the thermal mass of the distribution system (TMD):

$$Flex_{TMD} = \frac{T_{TMD,DR} - T_{TMD,BL}}{T_{TMD,BL}} \qquad \text{Eq. (42)}$$

  This quantity can be calculated only in cases in which the cooling power produced by the generation system is removed to a thermal node (T_{TMD}) different from the internal air node (T_{air}). The strategy that can be implemented is the pre-cooling of this thermal mass in the hours preceding the event. To estimate this exploitation, the quantity $Flex_{TMD}$ (in percentage) is calculated. It represents the temporal variation between the demand response and the baseline scenario of the distribution system temperature mass (T_{TMD}), referred to the baseline.
- The use of the energy flexibility of thermostatically controlled loads:

$$Flex_{TCL} = \frac{T_{air,DR} - T_{air,BL}}{T_{air,BL}} \qquad \text{Eq. (43)}$$

  Again, the strategies that can be implemented are the pre-cooling of the internal air in the hours preceding the event and the raising of the temperature during the event (Δk_{DR}). To estimate this exploitation, the quantity $Flex_{TCL}$ (in percentage) is calculated. It represents the temporal variation between the demand response and the baseline scenario of the temperature of the internal air thermal node (T_{air}), referred to the air temperature of the baseline.
  If a humidity control is possible for the cooling system, the same quantity can be calculated for the relative humidity (*RH*):

$$Flex_{\mathrm{RH}} = \frac{RH_{\mathrm{DR}} - RH_{\mathrm{BL}}}{RH_{\mathrm{DR}}} \qquad \text{Eq. (44)}$$

Furthermore, the pre-cooling time interval ($\Delta \mathrm{k}_{\mathrm{prc}}$) is calculated as the time (before the DR event) in which the air temperature in demand response scenario is lower than in the baseline.

- The payback loads in the electricity power curve. This effect can derive both from the use of flexibility from thermostatically controlled loads (TCLs) and from the exploitation of the thermal inertia of the system. It can be detected by the observation of the $\dot{P}^{*}_{\mathrm{shift}}$ curve ($\dot{\mathrm{P}}_{\mathrm{rated}}$ represents the rated electricity power of the specific space cooling technology):

$$\dot{P}^{*}_{\mathrm{shift}} = \frac{\dot{P}_{\mathrm{DR}} - \dot{P}_{\mathrm{BL}}}{\dot{\mathrm{P}}_{\mathrm{rated}}} \qquad \text{Eq. (45)}$$

and quantified by means of the energy consumption variation (in percentage terms) in the time before and after the demand response event:

$$\mathrm{E}_{\mathrm{shift,bDR}} = \frac{\mathrm{E}_{\mathrm{DR}} - \mathrm{E}_{\mathrm{BL}}}{\mathrm{E}_{\mathrm{BL}}} = \frac{\int_{\mathrm{k}_{\mathrm{strat}}}^{\mathrm{k}_{\mathrm{strat,DR}}} (\dot{P}_{\mathrm{DR}} - \dot{P}_{\mathrm{BL}}) \mathrm{dk}}{\int_{\mathrm{k}_{\mathrm{strat}}}^{\mathrm{k}_{\mathrm{strat,DR}}} \dot{P}_{\mathrm{BL}}\, \mathrm{dk}} \qquad \text{Eq. (46)}$$

$$\mathrm{E}_{\mathrm{shift,aDR}} = \frac{\mathrm{E}_{\mathrm{DR}} - \mathrm{E}_{\mathrm{BL}}}{\mathrm{E}_{\mathrm{BL}}} = \frac{\int_{\mathrm{k}_{\mathrm{end,DR}}}^{\mathrm{k}_{\mathrm{end}}} (\dot{P}_{\mathrm{DR}} - \dot{P}_{\mathrm{BL}}) \mathrm{dk}}{\int_{\mathrm{k}_{\mathrm{end.DR}}}^{\mathrm{k}_{\mathrm{end}}} \dot{P}_{\mathrm{BL}}\, \mathrm{dk}} \qquad \text{Eq. (47)}$$

As mentioned, to model the cooling generation systems, a commercial variable load heat pump (HP) is selected (Vitocal B04/A04) [71] for the FCU, CC and CP models. For fan coil model, the performances are evaluated with a supply temperature of 7 °C while for the radiant distribution systems (CC and CP) it is fixed to 18 °C. For the split system, instead, an ON/OFF air-to-air heat pump is used and in particular, the full load performance of [71] with a flow temperature of 7 ° C. As concern the air dehumidifier (DH) equipped with CP and CC systems, its characteristics are selected with references to commercial dehumidified to be combined with radiant systems [117]. In particular, the IN+300 model is chosen. It has a dehumidification capacity of 20.8 l day^{-1} with an electricity absorption of 320 W.

Passing to the results, a summer representative day is selected to analyze the systems operation. It is chosen as in accordance with the data reported in the standard UNI 10349-1: 2016 [118]. In particular the day in which the average daily outdoor air temperature is closer to the value reported in the standard is taken (21 July).
As mentioned, different demand response events are tested for each cooling system to obtain an as complete as possible characterization of the load-shifting capability of the technology, the parameters that characterize DR event ($k_{start,DR}$, Δk_{DR}, f_{PSS}, ΔT_{min}, ΔT_{max}, ΔRH_{min} and ΔRH_{max}) are varied in the analysis.
Starting from the split system, it can be noted that, with an ON/OFF regulation, the temperature of the air node (T_{air}) cannot be maintained at the constant value of the set-point (T_{sp} equal to 26 °C) but it oscillates within the band allowed by the thermostat (Figure 6.6(a)). In Figure 6.6(b) is showed the thermal and electric power consumption of the heat pump in case of baseline operation.

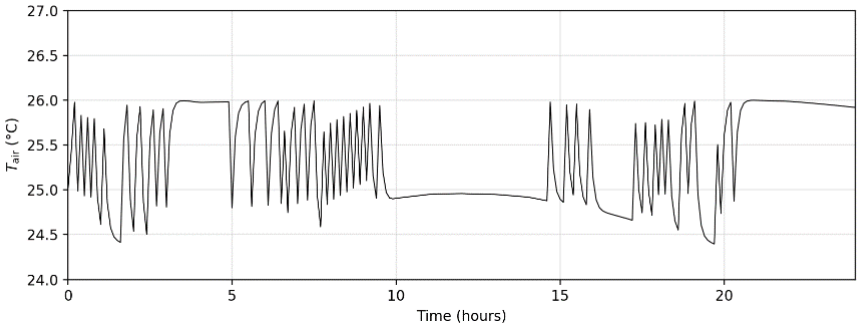

(a)

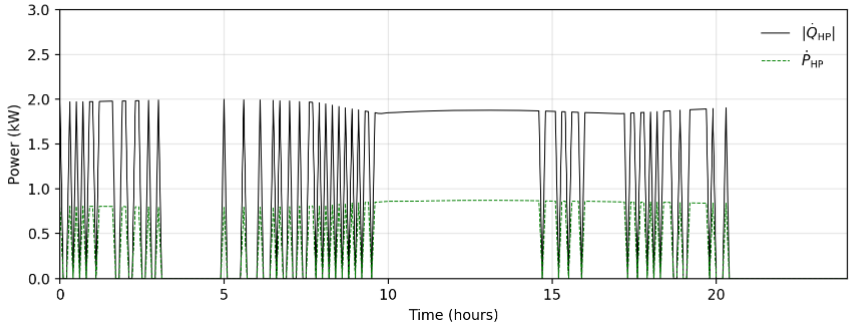

(b)

Figure 6.6. Daily (21 July) baseline operation for split system with ON/OFF regulation: (a) internal air node temperature and (b) thermal and electrical heat pump power.

Since no modulation of the heat pump can be exploited, only a demand response event with a reduction factor (f_{PSS}) equal to zero can be tested. It is not possible the realization of demand response events located at the peak ($k_{start,DR}$ equal to $k_{peak,BL}$) and lasting longer than a timestep (Δk_{DR} of 6 minutes) with ΔT_{max} equal to 0 °C. Accordingly, a higher comfort limit must be guaranteed during the event. In Figure 6.7 it is represented the behavior of the split system in term of air temperature (Figure 6.7(a)) and thermal and electrical power (Figure 6.7(b)) when an event of 1 hour is tested with a ΔT_{max} of 0.5 °C.

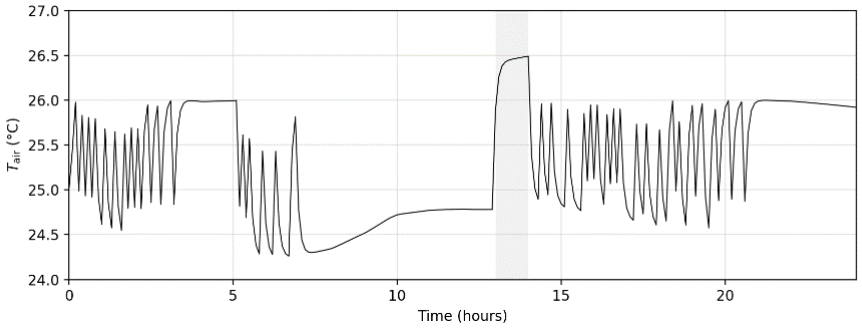

(a)

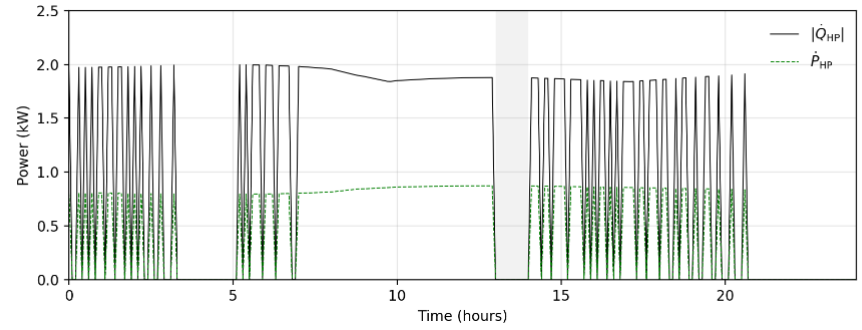

(b)

Figure 6.7. Daily (21 July) DR (f_{PSS} equal to 0, ΔT_{min} equal to 2 °C, ΔT_{max} equal to 0.5 °C and $k_{start,DR}$ equal to $k_{peak,BL}$) operation for split system with ON/OFF regulation: (a) internal air node temperature e (b) thermal and electrical heat pump power.

As can be seen by comparing Figure 6.6(a) with Figure 6.7(a), the realization of the event requires a large activation of the energy flexibility from thermostatically controlled loads. Indeed, the calculated pre-cooling time interval (Δk_{prc}) is about 8.7 hours and for all the duration of the event (area highlighted in gray in Figure 6.7(a)) all the upper

comfort band (ΔT_{max}) is exploited. Given the cycling of the system, it is difficult to graphically appreciate the presence of payback loads [119] by the observation of the power curve (Figure 6.7(b) and Figure 6.6(b)). However, a + 27% of $E_{shift,bDR}$ is calculated.

The DR parameters that can be varied in case of split system are ΔT_{min}, ΔT_{max}, Δk_{DR} and $k_{start,DR}$. Table 6.3 reports the flexibility evaluation quantities for different demand response events and in Figure 6.8 the curves of $Flex_{TCL}$ and $\dot{P}^{*}_{shift}$ are showed. As can be noted, results are reported for a fixed value of ΔT_{min} (equal to 2 °C) as lower values are not feasible in the optimization problem. The split system appears rather inflexible in producing load variations. Even by activating the energy flexibility from TCLs, the peak cannot be zero neither for an hour nor for less (Table 6.3) with a ΔT_{max} equal to 0 °C. On the contrary, allowing ΔT_{max} higher than 0 °C, the DR event can be realized with rather long times of pre-cooling of the air temperature. However, looking at the Figure 6.8, the advance planning of an action strategy by a potential supervisor (aggregator) would appear rather difficult.

Table 6.3. Flexibility evaluation quantities as the DR parameters varies (fixed f_{PSS} equal to 0, $\Delta T_{sp,min}$ equal to 2 °C and $k_{start,DR}$ equal to $k_{peak,BL}$). Split system with ON/OFF regulation.

Δk_{DR} (hours)	$\Delta T_{sp,max}$ (°C)	Optimization	E_{shift} (Wh)	Δk_{prc} (hours)	$E_{shift,bDR}$ (%)	$E_{shift,aDR}$ (%)
1.0	0.0	*infeasible*	-	-	-	-
1.0	0.5	*feasible*	871	8.7	+ 27.2	-15.2
1.0	1.0	*feasible*	871	3.5	+1.6	+19.4
0.3	0.0	*infeasible*	-	-	-	-
0.3	0.5	*feasible*	261	7.7	+16.0	-
0.3	1.0	*feasible*	261	2.7	+ 1.5	-

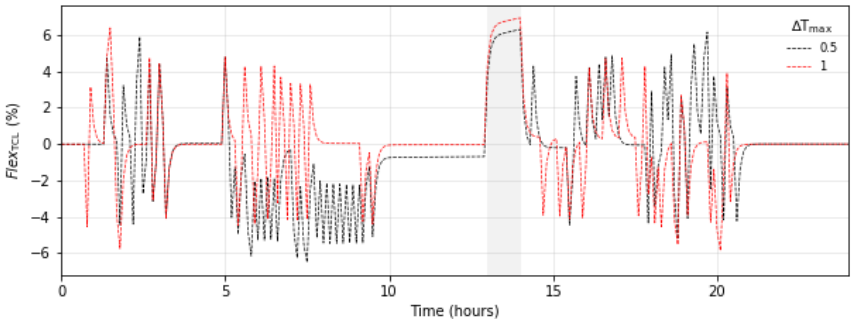

(a)

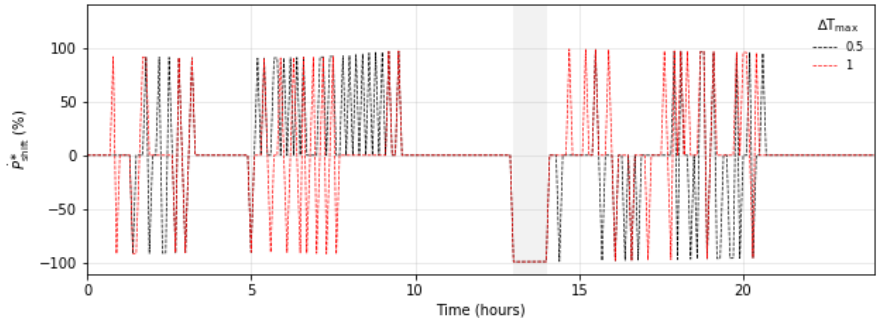

(b)

Figure 6.8. Flexibility evaluation curves for split system with ON/OFF regulation (f_{PSS} equal to 0, Δk_{DR} equal to 1 hour, $k_{start,DR}$ equal to $k_{peak,BL}$ and ΔT_{min} equal to 2 °C): (a) $Flex_{TCL}$ and (b) $\dot{P}^{*}_{shift}$.

Introducing a fan coil unit system coupled with a variable-load heat pump, different electricity peak reduction can be obtained allowing a certain margin of flexibility to the indoor air temperature (T_{air}). In Figure 6.9(a) a DR event in which a halving of the electricity peak (f_{PSS} equal to 0.5) is applied for 1 hour (Δk_{DR}) is shown in comparison with the baseline. Looking at dotted black curve in Figure 6.9(a) in comparison to Figure 6.6(a), it can be noted a different behavior in terms of T_{air} during the baseline. The adoption of a variable load heat pump allows to provide to the building the minimum cooling power to maintain the comfort setpoint temperature of 26 °C.
In in Figure 6.9(a) the flexibility range allows a ΔT_{min} of 1 °C and a ΔT_{max} of 0.5 °C. In absence of thermal inertia, the flexibility provided by thermostatically controlled loads is realized by means of a precooling of about 3.3 hours and of a temperature rising of 0.5 °C during the event. Clearly, the extent of this exploitation of flexibility depends on the possible setpoint band granted. If indeed it is admitted a ΔT_{max} equal to 1 °C, no precooling is required while if ΔT_{min} is 2 °C with a ΔT_{max} of 0.5 °C the precooling becomes only 1.5 hours long.

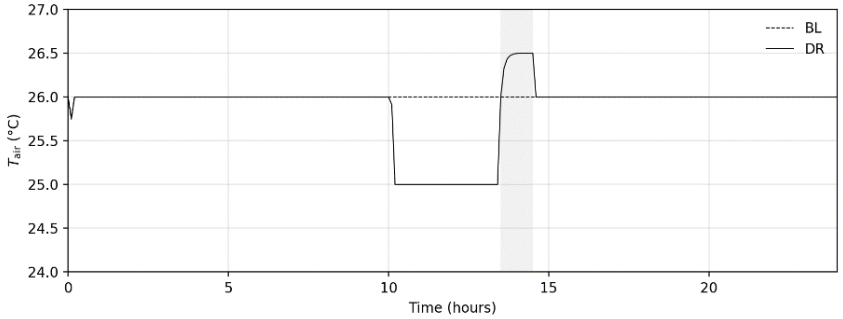

(a)

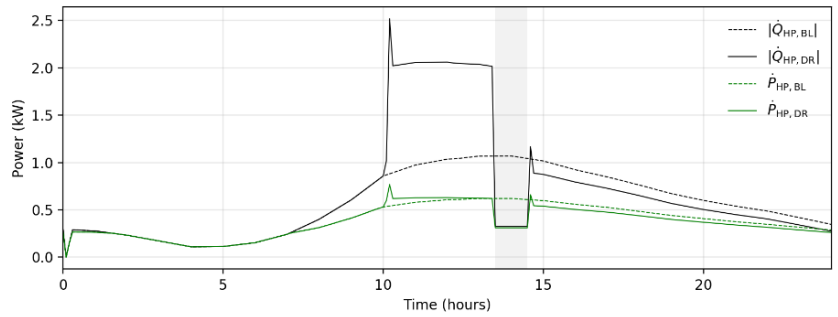

(b)

Figure 6.9. Daily (21 July) comparison between BL and DR event (f_{PSS} equal to 0.5, Δk_{DR} equal to 1 hour, ΔT_{max} equal to 0.5 °C and $k_{start,DR}$ equal to $k_{peak,BL}$) for fan coil unit system: (a) internal air node temperature and (b) thermal and electrical heat pump power.

However, it is important to note that when there is no thermal inertia, the possible variation in demand, produced by exploiting the thermostatically load controls, is limited. Indeed, the demand response event shown in Figure 6.9 is not possible (not feasible optimization problem) with a ΔT_{max} of 0 °C. On the contrary, if the TES (i.e., cold water tank) is added to the water circuit of the fan coil, its thermal inertia allows to realize different types of demand response events even without setpoint temperature modifications. In Figure 6.10 it is shown the same peak reduction of Figure 6.9 realized in the fan coil system when a cold-water tank of 200 liters (as for the case discussed in sub-section 6.1) is added (ΔT_{max} of 0 °C). In this case the air node temperature is maintained at the constant value of 26 °C and the cooling power stored in the TES is used during the DR event, leaving unaltered the amount of heat removed into the environment (black line in Figure 6.10(b)). However, with a such a relatively small tank (i.e., 200 liters) an anticipated peak power occurs (blue curve in Figure 6.10(b)) to cool the water in the tank. Introducing a larger tank, for example of 750 liters, as suggested

by commercial catalogue [120], the behavior is corrected and no payback loads emerge (Figure 6.11).

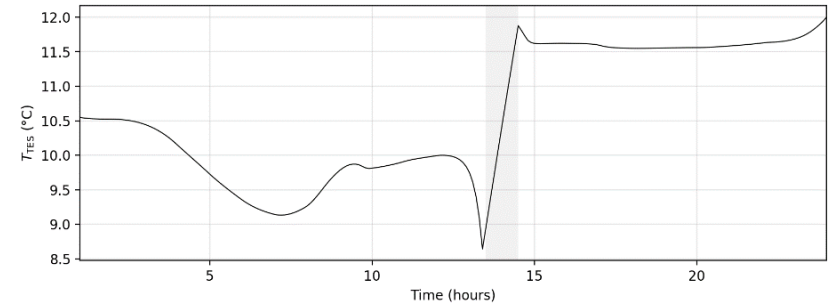

(a)

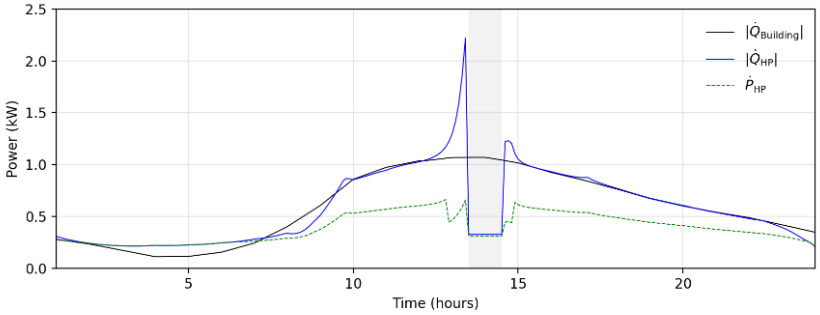

(b)

Figure 6.10. Daily (21 July) comparison between BL and DR event event (f_{PSS} equal to 0.5, Δk_{DR} equal to 1 hour, ΔT_{max} equal to 0 °C and $k_{start,DR}$ equal to $k_{peak,BL}$) for fan coil unit system with a cold-water tank of 200 liters (i.e., TES): (a) TES thermal node and (b) thermal and electrical heat pump power.

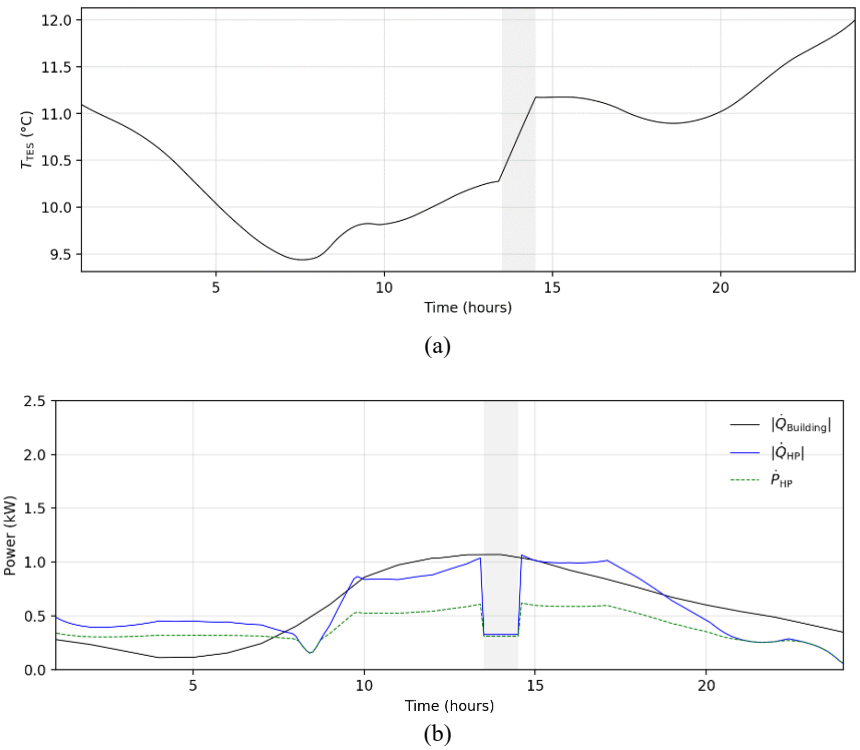

Figure 6.11. Daily (21 July) comparison between BL and DR event (f_{PSS} equal to 0.5, Δk_{DR} equal to 1 hour, ΔT_{max} equal to 0 °C and $k_{start,DR}$ equal to $k_{peak,BL}$) for fan coil unit system with a cold-water tank of 750 liters (i.e., TES): (a) TES thermal node and (b) thermal and electrical heat pump power.

However, unlike the split system, the fan coil (without the addition of a TES) allows the realization of a larger number of peak reductions. Starting from the analysis of an event at $k_{peak,BL}$ and lasting 1 hour (Δk_{DR}), Table 6.4 summarizes the calculation of the flexibility quantities for different reduction factors (f_{PSS}), ΔT_{max} and ΔT_{min}. Since the distribution system does not have any thermal storage capacity, the events can only be realized thanks to the flexibility of thermostatically controlled loads. As mentioned, the peak annulment (f_{PSS} equal to 0) can not be obtained with ΔT_{max} equal to 0 °C. However, the value of ΔT_{min} plays an important role in the success of the event. Indeed, if it is equal to 1 °C, not even variation with a f_{PSS} of 0.25 and 0.50 can be produced. While in case of ΔT_{min} of 2 °C, even if the optimization is not feasible with Δk_{DR} equal to 1 hour, the maximum time in which the peak can be annulled is 0.98 hours. With a ΔT_{min} of 1 °C and ΔT_{max} equal to 0 °C, only the case of f_{PSS} equal to 0.75 can

be realized with a pre-cooling time of 7.6 hours. In all the other peak reductions, the flexibility allowed by the management of TCLs allows the realization of the event with different pre-cooling times. In particular, the adoption of higher ΔT_{max} (1 °C instead of 0.5 °C) allows to satisfy the peak constrain in Δk_{DR} without any involvements of the air temperature in the hours before the event (Table 6.4). On the other hand, a ΔT_{max} of 0.5 °C enables all the events but, the use of higher ΔT_{min} (2 °C instead of 1 °C) allows in all cases at least to halve the precooling time (Δk_{prc}). On the contrary, exception made for f_{PSS} equal to 0, a ΔT_{min} of 2 °C, involves a stronger payback loads in the power curve ($E_{shift,bDR}$). As example, Figure 6.12 compares in term of $Flex_{TCL}$ and $\dot{P}^*_{shift}$ curves a DR event (f_{PSS} of 0.25) with ΔT_{max} equal to 0.5 and a ΔT_{min} of 1 and 2 °C.

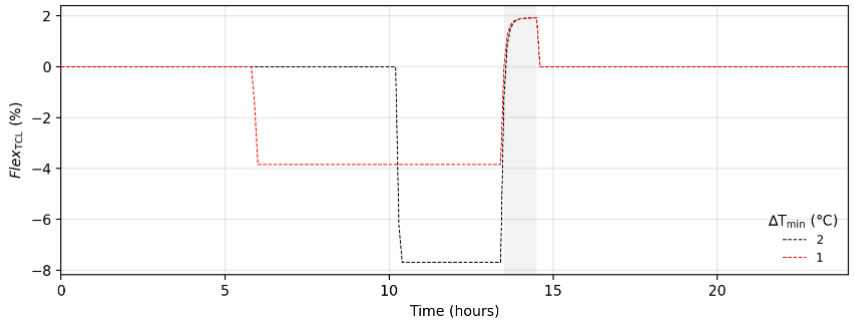

(a)

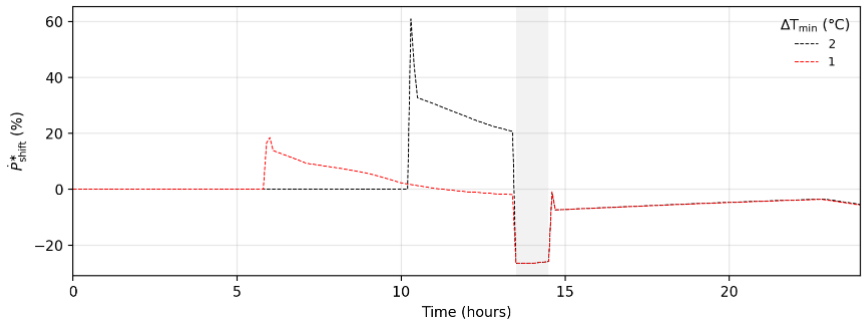

(b)

Figure 6.12. Flexibility evaluation curves for fan coil unit system without TES (f_{PSS} equal to 0.25, Δk_{DR} equal to 1 hour, ΔT_{max} equal to 0.5 °C and $k_{start,DR}$ equal to $k_{peak,BL}$): (a) $Flex_{TCL}$ and (b) $\dot{P}^*_{shift}$.

Table 6.4. Flexibility evaluation quantities as the DR parameters varies (fixed Δk_{DR} equal to 1 hour and $k_{start,DR}$ equal to $k_{peakt,DR}$) for fan coil unit system.

f_{PSS}	ΔT_{max} (°C)	ΔT_{min} (°C)	Optimization	E_{shift} (Wh)	Δk_{prc} (hours)	$E_{shift,bDR}$ (%)	$E_{shift,aDR}$ (%)
0.00	0.0	1.0	*infeasible*	-	-	-	-
0.00	0.0	2.0	*infeasible*	-	-	-	-
0.00	0.5	1.0	*feasible*	618	13.0	+ 57.1	-34.5
0.00	0.5	2.0	*feasible*	618	4.9	+ 44.7	-33.5
0.00	1.0	1.0	*feasible*	618	0	0	+3.9
0.00	1.0	2.0	*feasible*	618	0	0	+3.9
0.25	0.0	1.0	*infeasible*	-	-	-	-
0.25	0.0	2.0	*feasible*	463	10.6	+ 69.3	-87.3
0.25	0.5	1.0	*feasible*	463	7.5	+ 13.5	-20.9
0.25	0.5	2.0	*feasible*	463	3.1	+ 35.2	-20.6
0.25	1.0	1.0	*feasible*	463	0	0	+3.3
0.25	1.0	2.0	*feasible*	463	0	0	+3.3
0.50	0.0	1.0	*infeasible*	-	-	-	-
0.50	0.0	2.0	*feasible*	308	7.7	+ 53.3	-62.9
0.50	0.5	1.0	*feasible*	308	3.3	+ 2.9	-9.2
0.50	0.5	2.0	*feasible*	308	1.5	+ 19.5	-9.1
0.50	1.0	1.0	*feasible*	308	0	0	+2.6
0.50	1.0	2.0	*feasible*	308	0	0	+ 2.6
0.75	0.0	1.0	*feasible*	153	7.6	+ 13.7	- 24.1
0.75	0.0	2.0	*feasible*	153	3.2	+ 35.0	- 23.7
0.75	0.5	1.0	*feasible*	153	0	0	+ 1.1
0.75	0.5	2.0	*feasible*	153	0	0	+ 1.0
0.75	1.0	1.0	*feasible*	153	0	0	+ 1.0
0.75	1.0	1.0	*feasible*	153	0	0	+ 1.0

If the TES is added to the FCU distribution system, its thermal mass contribution (the temperature T_{TES} represents the temperature of the TMD) allows to realize all the peaks reduction so far discussed without any involvement of the air node set-point temperature. In fact, considering in the most extreme case treated (Δk_{DR} of 1 hour, $k_{start,DR}$ equal to $k_{peak,BL}$, ΔT_{max} equal to 0 °C and ΔT_{min} equal to 1 °C), a $Flex_{TCL}$ of 0 % is calculated throughout the day. However, to charge the TES in the hours before the event

(Figure 6.13(a)), an average increase of 18.5 % in the electricity consumption is obtained ($E_{shift,bDR}$is 19.8 % in case of f_{PSS} equal to 0, 19.2 % for f_{PSS} equal to 0.25, 18.6 % f_{PSS} equal to 0.50 and 16.7% f_{PSS} equal to 0.75). The increase in the electricity consumption can be observed also in Figure 6.13(b) where the $\dot{P}^*_{shift}$ is represented.

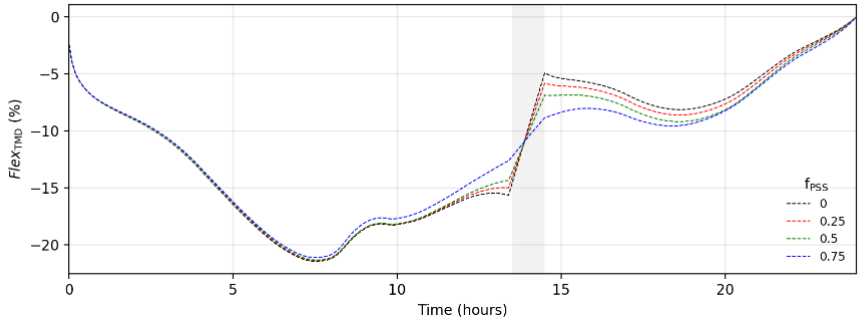

(a)

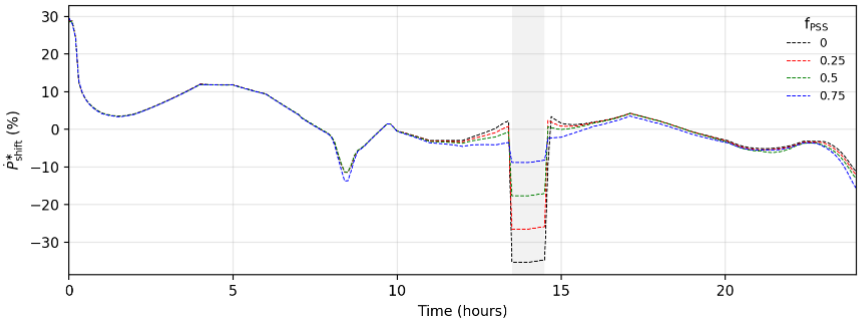

(b)

Figure 6.13. Flexibility evaluation curves for FCU with cold water tank of 750 liters (i.e., TES) (Δk_{DR} equal to 1 hour, ΔT_{max} equal to 0 °C, ΔT_{min} equal to 1°C and $k_{start,DR}$ equal to $k_{peak,BL}$): (a) $Flex_{TMD}$ and (b) $\dot{P}^*_{shift}$.

Passing to the high massive systems, i.e. ceiling panels (CP) and concrete ceiling (CC) coupled with air dehumidifier (DH), a different behavior can be observed in an operative scenario. Staring from the system with the lower thermal inertia level (CP), Figure 6.14 represents the realization of a demand response event with f_{PSS} equal to 0.5 for Δk_{DR} of 1 hour and with ΔT_{max} of 0 °C. Thanks to the decoupling between the air node and the node to witch the cooling power is applied, a minimum level of thermal inertia can be derived by the envelope mass and the system is able to realize the peak reduction of

Figure 6.9 with ΔT_{max} of 0 °C. Actually, with this kind of cooling system even an event that produces a f_{PSS} of 0 for 1 hour (Δk_{DR}) can be realized with a ΔT_{max} of 0 °C. Focusing on a 50 % peak reduction (f_{PSS} of 0.5), the comparison between the demand response event and the baseline in term of sensible loads is shown in Figure 6.14(b). Thanks to the thermal mass of the roof layer, the CP system allows a lower exploitation of thermostatically controlled loads than the case of the FCU system without the TES (Figure 6.9(a) in comparison with Figure 6.14(a)). The precooling is about 2.2 hours long if a ΔT_{max} of 0 °C is imposed while it becomes 1.8 hours if ΔT_{max} of 0.5 °C is allowed. However, to cool down the roof node temperature instead of T_{air}, the anticipated overconsumption of the heat pump is significantly higher (Figure 6.14(b)). The thermal and electrical energy consumption before the DR event vary by +102 % and +86% respectively in relation to the consumption in baseline.

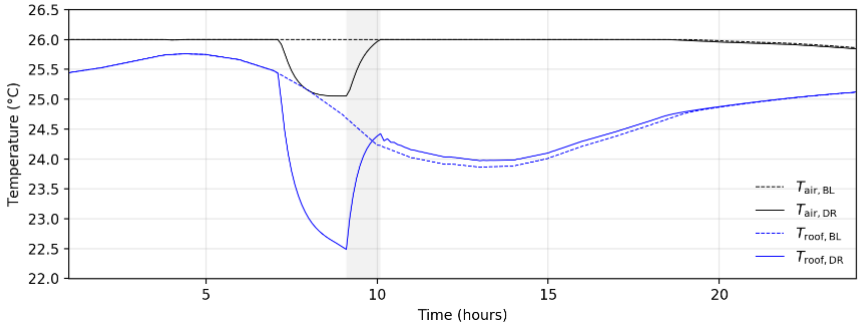

(a)

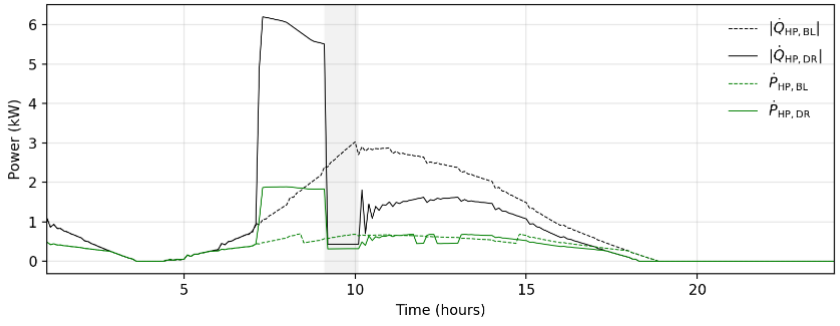

(b)

Figure 6.14. Daily (21 July) comparison between BL and DR event (f_{PSS} equal to 0.50, Δk_{DR} equal to 1 hour, ΔT_{max} equal to 0 °C, ΔT_{min} equal to 1 °C and $k_{start,DR}$ equal to $k_{peak,BL}$) for ceiling panels with dehumidifier: (a) air and roof node temperatures and (b) thermal and electrical heat pump power.

In this case, since the cooling system is also equipped with a dehumidifier (DH) for control of the indoor relative humidity, the electricity peak time is estimated on the total electricity consumption curve (DH and HP).
In particular, in Figure 6.15(a) it is shown the comparison between the relative humidity (*RH*) curves in case of baseline and DR event (Figure 6.15(a)) and the thermal (latent) and electricity consumption of the dehumidifier (DH) (Figure 6.15(c)). Looking at Figure 6.15(a), it can be noted that during the demand response event, the relative humidity is higher than 50 % albeit the $\Delta \mathrm{RH}_{\max}$ is equal to 0 %. This is due to the way its constraint is formulated. Indeed, the maximum value of $x_{\max}$ in the optimization problem is calculated with an air temperature and a relative humidity equal to the upper comfort limits (respectively $[\mathrm{T}_{\mathrm{sp}} + \Delta \mathrm{T}_{\max}]$ and $[\mathrm{RH}_{\mathrm{sp}}+\Delta \mathrm{RH}_{\max}]$). However, when the energy flexibility is used to precool the internal air (T_{air}), the final value of relative humidity is calculated with a lower temperature value.
Therefore, the radiant ceiling panels allow the realization of peak shaving event with the exploitation of both the thermal mass of the system and the thermostatically controlled loads. For this reason, there are not configurations in which the optimization problem is infeasible. As the storage capacity of the distribution system is used, the variation of the comfort limits (e.g., $\Delta \mathrm{T}_{\max}$, $\Delta \mathrm{T}_{\min}$, $\Delta \mathrm{RH}_{\max}$ and $\Delta \mathrm{RH}_{\min}$) has less influence on the realization of the event. With reference to Table 6.5, the only parameter that seems to improve the performance of the demand response event is $\Delta \mathrm{T}_{\max}$. Regardless of the values assumed by other quantities ($\Delta \mathrm{T}_{\min}$ and $\Delta \mathrm{RH}_{\max}$), a 18% decrease in the pre-cooling duration ($\Delta \mathrm{k}_{\mathrm{prc}}$) can be achieved if at least a $\Delta \mathrm{T}_{\max}$ of 0.5 °C is allowed with also a consequent decrease of $\mathrm{E}_{\mathrm{shift,bDR}}$.

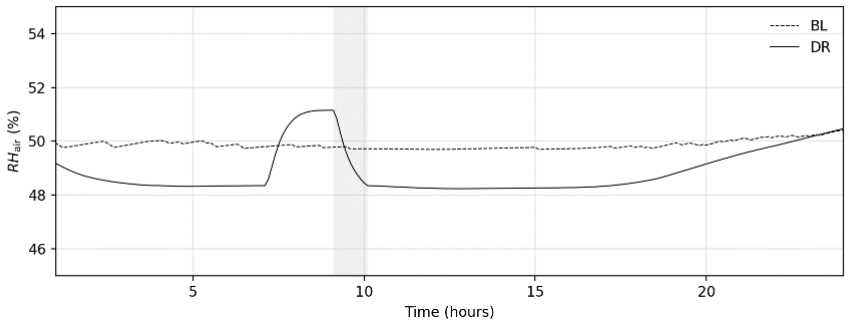

(a)

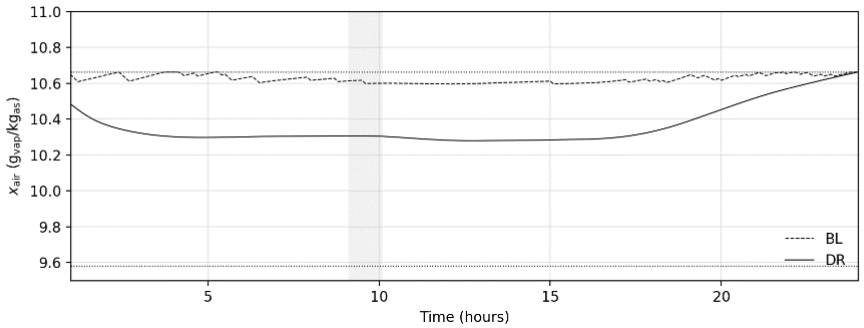

(b)

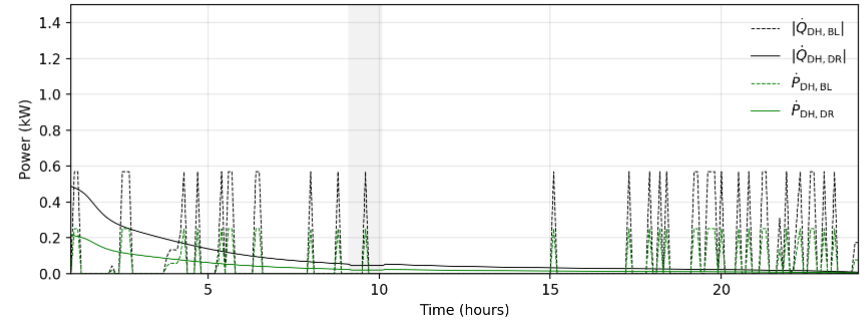

(c)

Figure 6.15. Daily (21 July) comparison between BL and DR event (f_{PSS} equal to 0.50, Δk_{DR} equal to 1 hour, ΔRH_{max} equal to 0 %, ΔRH_{min} equal to 5 % and $k_{start,DR}$ equal to $k_{peak,BL}$) for ceiling panels and dehumidifier in term of: (a) relative humidity, (b) absolute humidity and (c) thermal and electrical power of the dehumidifier.

In Figure 6.16 is showed the comparison, in terms of flexibility performances, between the case in which the peak reduction is produced with ΔT_{max} equal to 0 °C and 0.5 °C. Due to the storage capability of the ceiling panels and its slower speed in following precise variations in the internal temperature (heat is not removed directly from T_{air}), even with a ΔT_{max} of 0.5 °C, only in the last moments of the event the setpoint temperature exceeds T_{sp} (Figure 6.16(a)). For this reason, the same behavior is evaluated with higher ΔT_{max}. Looking at Figure 6.16(b), a variation of $Flex_{RH}$ can be appreciated. However, it is only a consequence of the sensitive cooling of the internal air in the precooling (Δk_{prc}). In Figure 6.16(c) instead, is represented the utilization of the thermal mass of the distribution system ($Flex_{TMD}$). Because of the low thermal

inertia of the $T_{\mathrm{ri,cp}}$ node, the latter has the same trend of $Flex_{\mathrm{TCL}}$ ($\Delta k_{\mathrm{prc,TMD}}$ and Δk_{prc} have the same order of magnitude: 2.2 hours and 2.3 hours in for ΔT_{max} equal to 0 °C and 1.8 °C and 2.0 °C for ΔT_{max} equal to 0.5 °C, Table 6.5). However, $Flex_{\mathrm{TMD}}$ reaches almost the value of - 10%, when $Flex_{\mathrm{TCL}}$ is - 4 %. This is the reason why high overconsumption are evaluated (Figure 6.16(d)).

Table 6.5. Flexibility evaluation quantities as the DR parameters varies (f_{PSS} equal to 0, Δk_{DR} equal to 1 hour, ΔRH_{min} equal to 5 % and $k_{start,DR}$ equal to $k_{peak,BL}$) for ceiling panels with dehumidifier.

ΔRH_{max} (%)	ΔT_{max} (°C)	ΔT_{min} (°C)	Optimization	E_{shift} (Wh)	Δk_{prc} (hours)	$\Delta k_{prc,TMD}$ (hours)	$E_{shift,bDR}$ (%)	$E_{shift,aDR}$ (%)
0	0.0	1.0	*feasible*	467	2.2	2.3	+92.8	-17.7
0	0.0	2.0	*feasible*	467	2.1	2.3	+97.8	-17.2
0	0.5	1.0	*feasible*	467	1.8	2.0	+86.8	-15.9
0	0.5	2.0	*feasible*	467	1.8	2.0	+86.7	-15.8
0	1.0	1.0	*feasible*	468	1.8	2.0	+89.1	-17.5
0	1.0	2.0	*feasible*	467	1.8	2.0	+87.4	-16.3
5	0.0	1.0	*feasible*	467	2.2	2.3	+92.6	-17.5
5	0.0	2.0	*feasible*	467	2.1	2.2	+97.3	-16.9
5	0.5	1.0	*feasible*	467	1.8	2.0	+84.3	-14.3
5	0.5	2.0	*feasible*	467	1.8	2.0	+86.7	-15.8
5	1.0	1.0	*feasible*	468	1.8	2.0	+89.1	-17.3
5	1.0	2.0	*feasible*	467	1.8	2.1	+87.3	-16.3

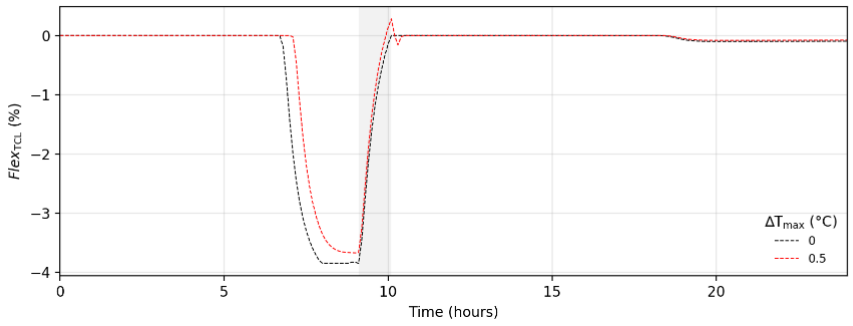

(a)

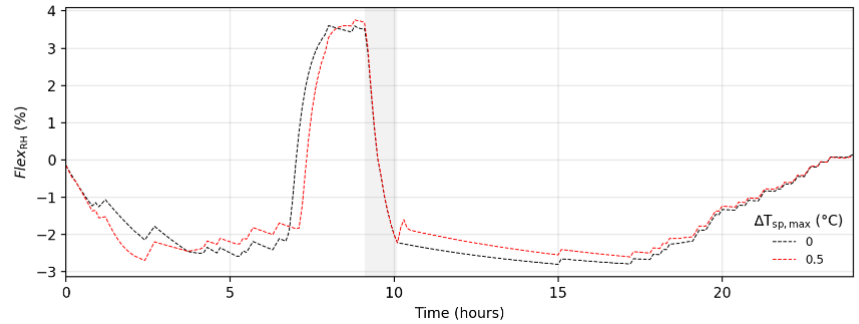

(b)

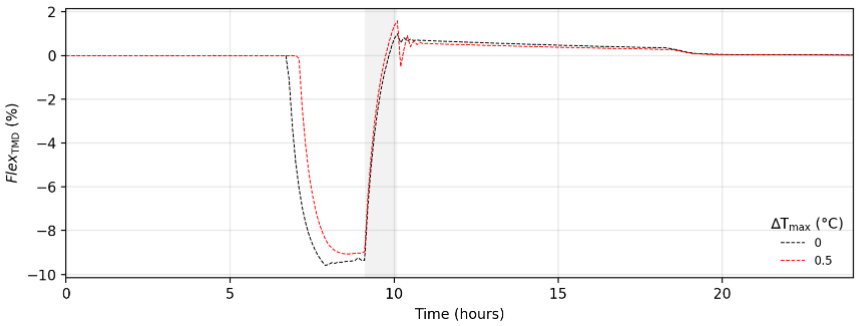

(c)

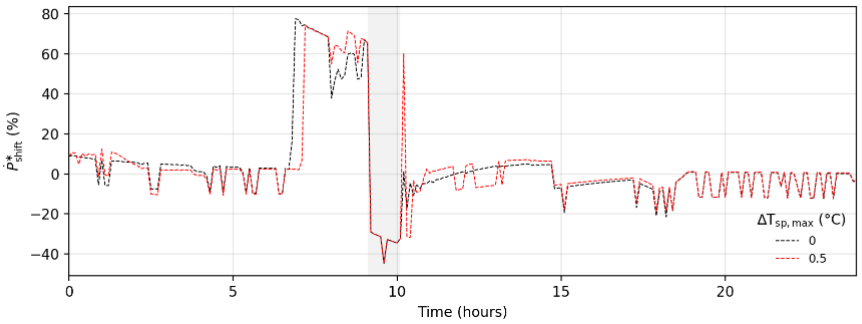

(d)

Figure 6.16. Flexibility evaluation curves for ceiling panels (f_{PSS} equal to 0, Δk_{DR} equal to 1 hour, ΔT_{min} equal to 1 °C, ΔRH_{min} equal to 5 %,ΔRH_{max} equal to 0 % and $k_{start,DR}$ equal to $k_{peak,BL}$): (a) $Flex_{TCL,}$ (b) $Flex_{RH}$, (c) $Flex_{TMD}$ and (d) $\dot{P}^{*}_{shift}$.

Looking at the results obtained, two important aspects can be highlighted. First of all, although with ceiling panels the precooling times are considerably lower than in the previous cases (split and fan coil units), there is no configuration that allows to carry out the event without a precooling strategy, which instead happens in the fan coil with a high exploitation of the flexibility from TCLs (ΔT_{max} equal to 1 °C). Moreover, especially for the more extreme peak reduction (f_{PSS} equal to 0 and 0.25), there is always an increase in electricity consumed before the event ($E_{shift,bDR}$) greater than 80%, while in the case of fan coil it is almost always well below 70% (Table 6.4). In fact, as highlighted even more in the following case (CC), this is an aspect to be taken into consideration when the inertia of the distribution system consists of a passive thermal mass. In this regard, to better introduce this last observation, results about the cooling system with the higher inertia level need to be discussed.

In case of cooling concrete ceiling system, in which the cooling power of the heat pump is removed from a high massive node, the demand response event analyzed for the previous cases (f_{PSS} of 0.5, Δk_{DR} of 1 hour) can be realized almost without using the flexibility from TCLs. In fact, the high storage capability of the roof node allows to keep the fixed set point of 26 ° C during the event at the expense of a small pre-cooling of the thermal mass of the distribution system (Figure 6.17(a)). Although the variation in the temperature of the thermal mass node (T_{ri}) is relatively small (Figure 6.17(a)), the large thermal inertia of the cooling system involves a not negligible increase in the power curve (Figure 6.17(b)). The estimated increase before the demand response event is 29 % for the thermal energy consumption and 53 % for the electricity absorption of the heat pump. As in case of ceiling panels system, also in CC the relative humidity is controlled by the cooling system with a dehumidifier. In Figures 6.18(a), (b) and (c) the results of the latent energy balances are reported.

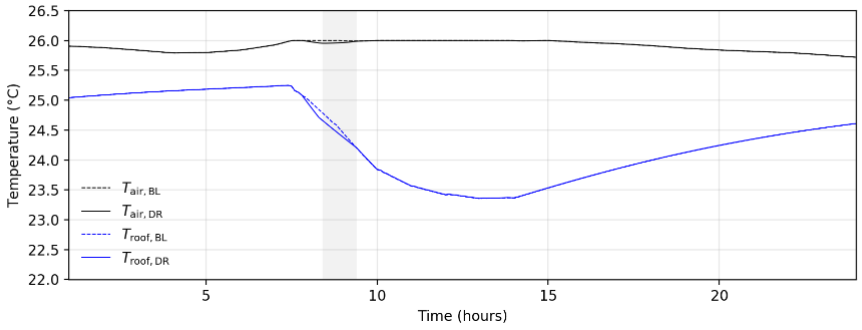

(a)

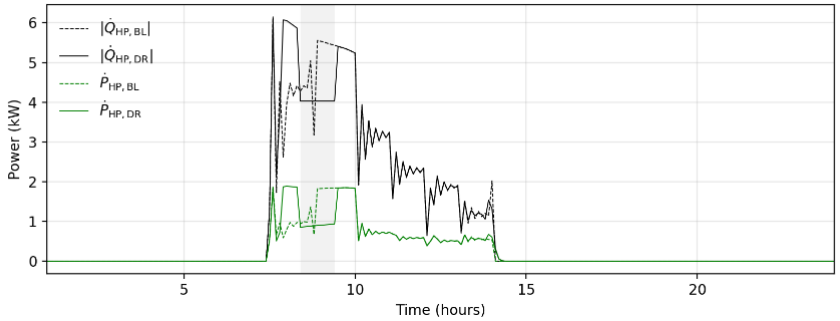

(b)

Figure 6.17. Daily (21 July) comparison between BL and DR event (f_{PSS} equal to 0.50, Δk_{DR} equal to 1 hour, ΔT_{max} equal to 0 °C, ΔT_{min} equal to 1 °C and $k_{start,DR}$ equal to $k_{peak,BL}$) for concrete ceiling with dehumidifier: (a) air and roof temperature and (b) thermal and electrical heat pump power.

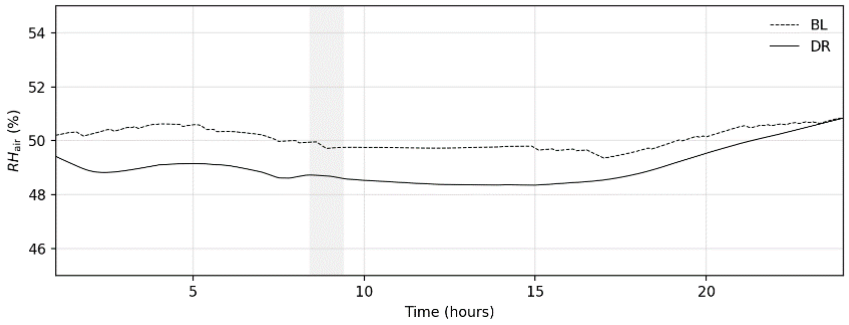

(a)

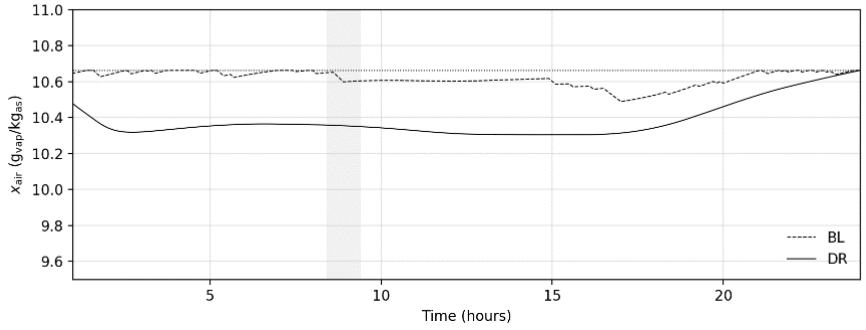

(b)

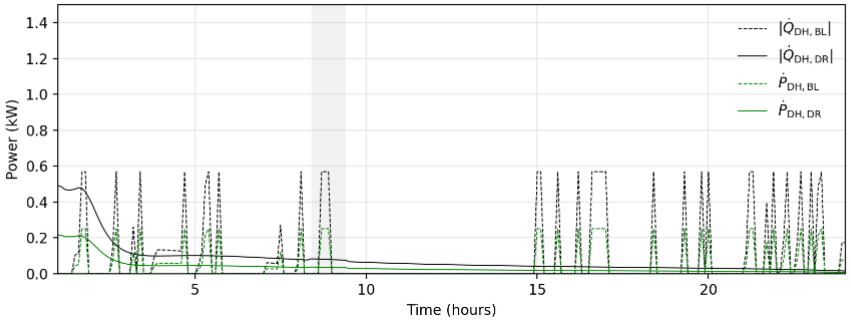

(c)

Figure 6.18. Daily (21 July) comparison between BL and DR event (f_{PSS} equal to 0.50, Δk_{DR} equal to 1 hour, ΔRH_{max} equal to 0 %, ΔRH_{min} equal to 5 % and $k_{start,DR}$ equal to $k_{peak,BL}$) for concrete ceiling and dehumidifier in term of: (a) relative humidity, (b) absolute humidity and (c) thermal and electrical power of the dehumidifier.

It is interesting to notice that, as the thermal inertia level of the node from which the heat is removed increases, all the effects that are observed for the ceiling panels (CP) are extremized and the realization of different DR events is possible with the minimum involvement of the flexibility from TCLs. In particular, it can be noted that the behavior of the concrete ceiling plant in producing a certain peak reduction is quite independent of the DR parameters. This is due to the fact that the storage capacity of the distribution system (TMD) is used almost exclusively. In Figure 6.19 the flexibility curves for a DR event with f_{PSS} equal to 0 are reported (DR parameters: Δk_{DR} of 1 hour, $k_{start,DR}$ equal to $k_{peak,BL}$, ΔT_{mx} of 0.5 °C, ΔT_{min} of 1 °C, ΔRH_{min} of 5 % and ΔRH_{max} of 0 %). Looking at Figure 6.19(a) it can be noted that during the event the upper comfort range (form T_{sp} to $[T_{sp}+ \Delta T_{max}]$) is not exploited and $Flex_{TCL}$ does not reach the value -1 % in the time before the event. On the contrary, considering the large thermal mass of the CC system, the flexibility of the thermal mass of the distribution system it is very much involved ($Flex_{TMD}$ reaches the value of -2.7 %, Figure 6.19(c)). This is also the reason why a higher increase in the electricity power consumption in obtained (Figure 6.19(d)). This behavior is confirmed by results showed in Table 6.6, where the flexibility quantities are calculated for different peak reductions and highlights what is observed for the ceiling panels. Indeed, when unlike a controllable storage system (e.g., the TES of 750 liters), heat is accumulated in a high massive layer of the building envelope (e.g., the roof) different demand response events can be performed limiting the effect perceived by users in terms of temperature to a minimum. On the contrary, large over energy consumption must be predicted, especially before the demand reduction.

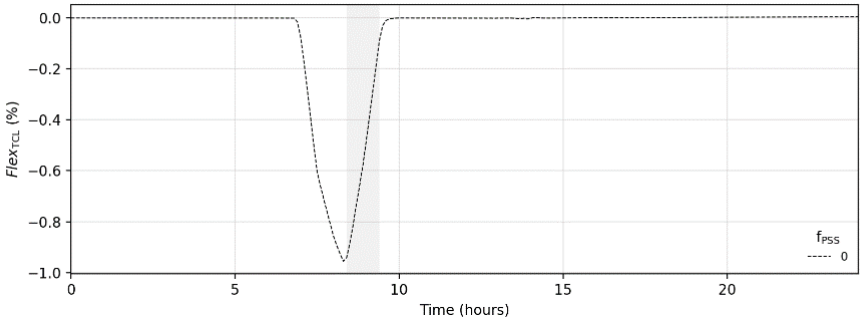
0.0
−0.2
−0.4
−0.6
−0.8
−1.0
$Flex_{TCL}$ (%)
0
5
10
15
20
Time (hours)
f_{PSS}
0

(a)

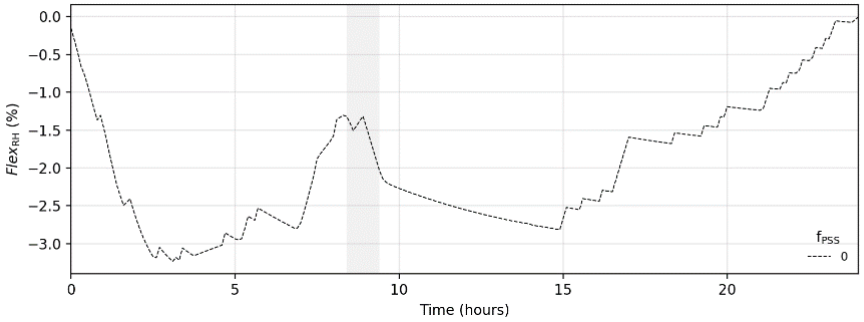
0.0
−0.5
−1.0
−1.5
−2.0
−2.5
−3.0
$Flex_{RH}$ (%)
0
5
10
15
20
Time (hours)
f_{PSS}
0

(b)

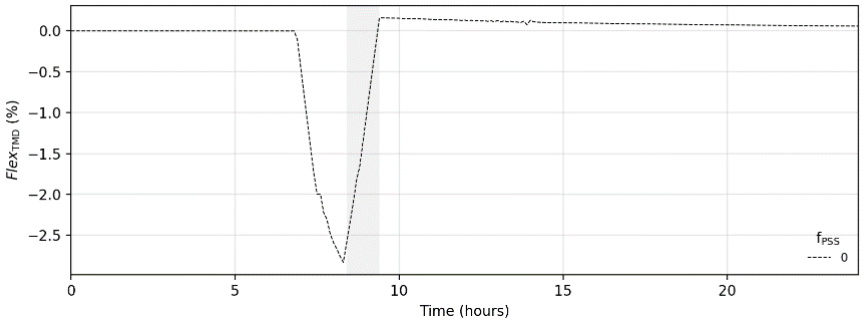
0.0
−0.5
−1.0
−1.5
−2.0
−2.5
$Flex_{TMD}$ (%)
0
5
10
15
20
Time (hours)
f_{PSS}
0

(c)

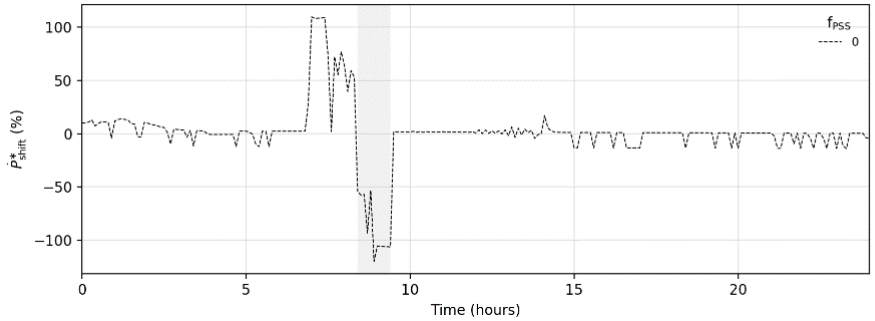

(d).

Figure 6.19. Flexibility evaluation curves for concrete ceiling (f_{PSS} equal to 0, Δk_{DR} equal to 1 hour, ΔT_{max} equal to 0.5 °C, ΔT_{min} equal to 1 °C, ΔRH_{max} equal to 0 %, ΔRH_{min} equal to 5 % and $k_{start,DR}$ equal to $k_{peak,BL}$): (a) $Flex_{TLC}$, (b) $Flex_{RH}$, (c) $Flex_{TMD}$ and (d) $\dot{P}^*_{shift}$.

Table 6.6. Flexibility evaluation quantities as the DR parameters varies (Δk_{DR} equal to 1 hour, $k_{start,DR}$ equal to $k_{peak,BL}$, ΔRH_{max} equal to 0 %, ΔRH_{min} equal to 5 %, ΔT_{max} equal to 0 °C and ΔT_{min} equal to 1 °C). Concrete ceiling with dehumidifier.

f_{PSS}	Optimization	E_{shift} (Wh_{el})	Δk_{prc} (hours)	$\Delta k_{prc,TMD}$ (hours)	$E_{shift,bDR}$ (%)	$E_{shift,aDR}$ (%)
0.00	*feasible*	1488	1.3	1.4	197.6	-6.7
0.25	*feasible*	879	1.0	1.1	146.5	-7.5
0.50	*feasible*	557	0.3	0.5	69.1	-6.9
0.75	*feasible*	162	0.0	0.1	38.6	-8.9

Based on the presented results about the energy flexibility potential of different space cooling technologies a different behavior in the operative scenario can be observed if compared to the design evaluation (sub-section 6.1). Although, the analyzed space cooling technologies differs from the point of view of the heat pump model (i.e., for the FPI calculation it is modelled with an ON/OFF regulation for all the cases, while for the operative evaluation it is modelled as variable load heat pump for all the cases except for the split system) and of the buildings typology (i.e., in sub-section 6.1 apartments are considered, while in the operative evaluation single family houses), which could affect the performance comparison, some consideration can be made.

For instance, while the design evaluation of the flexibility performance produces similar results in term of FPI, the operative evaluation allows to highlight some important differences in behaviors. In this sense, the main conclusions can be summarized by the following three points: (i) The split system with ON/OFF regulation shows rather inflexible behaviors during peak shaving events. Only peak annulment is possible but it's difficult for an hypothetical supervisor (e.g., aggregator) to predict how planning the strategy. For all the other plants (with a variable load heat pump and fan coil, radiant ceiling panels or a radiant cooling concrete ceiling as distribution system), it easier a prediction of the user response in relation to its characteristics. (ii) Fan coil units coupled with a variable load heat pump is a more flexible system if the energy flexibility from thermostatically controlled loads (TCLs) can be activated. To avoid great payback loads, it is advisable to allow the internal air temperature to rise during the event. However, the addition of a thermal energy storage (e.g., a cold water tank) to the distribution system allows to realize short term peak shaving strategies (lasting also 1 hour) without compromising the indoor air temperature with low, drawback effects in terms of anticipated electricity overconsumptions (payback loads increase). (iii) As concern ceiling cooling systems, the passive storage capability of the distribution system allows the realization of different peak reductions events with a combined exploitation of the energy flexibility derived by thermostatically controlled load (TCLs) and by its thermal mass. Results show that, as the thermal mass of the system increases (e.g., cooling concrete ceiling in comparison to ceiling panels) the flexibility of the thermostat is less and less exploited. However, increasing anticipated overconsumption due to pre-cooling of the thermal mass of the system must be expected.

Therefore, the analysis shows that the type of emission system used to satisfy the cooling demand of a residential building has considerable impact on the on how a peak shaving event is handled. Thus, taking this aspect into consideration can be of paramount importance to improve the realization of a large-scale strategy (e.g., cluster load shifting).

Chapter 7

Energy flexibility from aggregate demand

As mentioned in sub-section 2.1.2, evaluating the energy flexibility reserve of a single building is essential from a resource planning perspective. However, the energy quantities involved (except for large industrial or commercial buildings) are not interesting from a market point of view. Therefore, the extension of the energy flexibility analysis at the aggregate level (i.e., clusters of buildings) has a paramount role.
In this section a preliminary evaluation of the energy flexibility potential of clusters of buildings is provided. Firstly, the discussion introduce in sub-section 2.1.2 is extended in sub-section 7.1, where the most whispered clustering techniques adopted to evaluate the energy flexibility potential in buildings are examined. Then, retracing the evaluations proposed in Papers 10 and 11, with the introduction of simple case studies, the objective is to highlight how the careful planning of the cluster allows to realize different demand side management events (e.g., demand response) minimizing the appearance of drawback effects (e.g., payback loads) in the aggregated power demand. In other words, the analysis aims at showing that aggregated energy flexibility, which can be activated by the programmed involvement of different users, allows multiple degrees of freedom to apply demand response events in residential building clusters. In particular, in sub section 7.2.1, the impact of different cooling systems is evaluated. This case study is proposed in Paper 10 and it is based on the space cooling technologies introduced in Chapter 6 (sub-section 6.1). Then, in sub-section 7.2.2, the impact of different occupancy patterns is discussed (analysis presented in Paper 11).

7.1 Focus on the techniques to model the cluster under DSM

As mentioned in sub-section 2.1.2, according to the definition provided by Vigna et al. [28] a building cluster identifies a group of buildings interconnected to the same energy infrastructure, such that the change of behavior/energy performance of each building affects both the energy infrastructure and the other buildings of the whole cluster. The

interconnection of the building is not necessarily physical, but it can be also market related (e.g., different buildings belonging to the same owner).
However, in order to evaluate the energy flexibility potential of a cluster of buildings, it is necessary to select a specific methodology to model the cluster. As introduced, a detailed literature analysis about how to model the energy dynamic of a group of buildings is provided by Goy and Finn [29]. According to them, large-scale building modelling can be divided into two approaches: top-down and bottom-up. The first category (i.e., the top-down) does not distinguish the contribution of the single building. Therefore, the analysis considers the whole residential sector energy consumption. On the other hand, the bottom-up approaches are based on knowledge of the energy behavior of each single building [121]. As also highlighted by Buttitta et. al. [121], when the objective of the cluster analysis is the evaluation of the demand side management strategies, the model must be able to trace the behavior of the individual. Therefore, the adoption of the bottom-up approach is fundamental.
Both statistical and engineering techniques can be adopted [122]. The difference between the two lies in the fact that, for the first (i.e., statistical techniques) data relating to the consumption of the aggregate are required while for the engineering technique they are not needed. Between the available engineering techniques, the most whispered for the residential sector seems to be the archetype methodology [121].
Archetypal buildings are typically reference buildings that are statistical composites of the features found within a category of buildings in the stock [123] derived from available data of the national building stock [30]. Usually, each archetype is defined by specific geometrical, thermal and technical characteristics [124]. Analyzing some works available in literature, for instance, Mata et al. [30] differentiated the archetypes by: type of buildings (e.g., residential or not residential), construction year, climate region and the main fuel source for heating purposes. Famuyibo et al. [31] distinguished the archetypes by means of characteristics that are significant in establishing how energy use might change according to the building regulations (e.g., wall U-value, roof U-value, window U-values, floor U-value, air change rate, floor area, heating system efficiency, dwelling type and domestic hot water cylinder insulation thickness) and construction details or construction types (e.g., wall construction types, roof insulation types, floor construction types and window insulation types). It therefore appears clear that, in this sense, the Tabula Project [64] can be an important starting point to establish the main features of national archetypes of buildings.
A further aspect that must be considered involves the modelling of the users' occupancy profiles. Indeed, as highlighted by Hu and Xiao [32], the uncertainty in the forecast of space occupation by users can compromise the reliability of the energy flexibility estimation. In particularly, they evaluated how, by increasing the cluster size, the energy flexibility estimation is more and more reliable than the case of a single building

(aggregated energy flexibility exponentially decreased from 19.12% for 8 households to 0.74% for 5120 households).
To model the effect of the users' occupancy profile two approaches can be used. The generation of random profiles for each user or the definition of reference profiles (i.e., archetypes). For the first approach, the open web tool StROBe (Stochastic Residential Occupancy Behaviour), developed by the KU Leuven Building Physics Section could be used [125]. Indeed, StROBe is built to generate missing boundary conditions in integrated district energy assessment simulations related to human behavior, (i.e., the use of appliances and lighting, space heating settings and domestic hot water redrawers) [126]. On the other hand, archetypes of occupancy patters can be introduced. They can be evaluated with different approaches. A first technique can be adopted with the analysis of available data for a group of users (e.g., with monitoring or surveys). An example is provided by Buttitta et al. [121]. By means of clustering techniques based on available data, they developed a method to generate realistic occupancy patterns that can be representative of large numbers of households. Another way could be the statistical approach or model based on the experience. For instance, Yao and Steemers [127], on the basis of their experience, defined five fixed common occupancy profiles for UK households, with the aim of characterizing the archetypes in the operational area. However, the definition of the user occupancy patters is a crucial aspect for the effectiveness of the cluster model.

7.2 Importance of differentiating users

From a resource planning perspective, the knowledge of the various degrees of freedom that can be counted on when involving different users in a DSM scenario is fundamental. In the following sub-sections, the effect of users with different cooling systems (sub-section 7.2.1) and different occupancy patterns (sub-section 7.2.1) is discussed with simple case studies. The objective is to present a preliminary assessment to provide food for thought about the increasingly discussed topic of the aggregated energy flexibility.

7.2.1 Role of the HVAC

In order to provide a preliminary evaluation on the effect of the combination of users which differ from each other for their cooling system on the overall operating energy flexibility, the four case studies introduced in sub-section 6.1 are aggregated in a small cluster (analysis presented also in Paper 10). In particular, the effect of different combinations of cooling systems in a demand side management scenario is presented.

A demand response event is modelled. It is a peak shaving strategy starting at 12.00 pm in the same reference day founded for the FPI calculation (see sub-section 6.1). In particular, at 12.00 pm the cooling system is switched off until the internal comfort bound is reached. Two different requests for energy flexibility are modelled for each single user:

(i) High flexibility demand (HFD).
(ii) Low flexibility demand (LFD).

Retracing the demand response event tested for the FPI calculation, the evaluation is focused on thermostatically controlled loads. Therefore, the HFD (i) exploits the overall comfort range available (internal set-point starting from 24°C and 60% of relative humidity can reach 26°C and/or 70% of relative humidity). LFD (ii), instead, consists in requesting a smallest comfort variation (maximum temperature and humidity achievable: 25°C end/or 65% of relative humidity).

The HFD and LFD strategies are applied in several configurations to the space cooling systems in order to achieve different goals, as instantaneous peak reduction, minimum user involvement or peak reduction for long periods (all or some of them are involved or are called to attend the demand response event one after the other).

Figure 7.1 shows the overall electricity demand for the four apartments building without any demand response event and its breakdown in the different space cooling contributions in a time period of 1 hour (from 12.00 to 1.00 pm). Four electric power levels can be distinguished:

(i) A base load of 5 kW.
(ii) An intermediate load of 7 kW.
(iii) A first power peak of 10 kW.
(iv) The higher peak of about 12.5 kW.

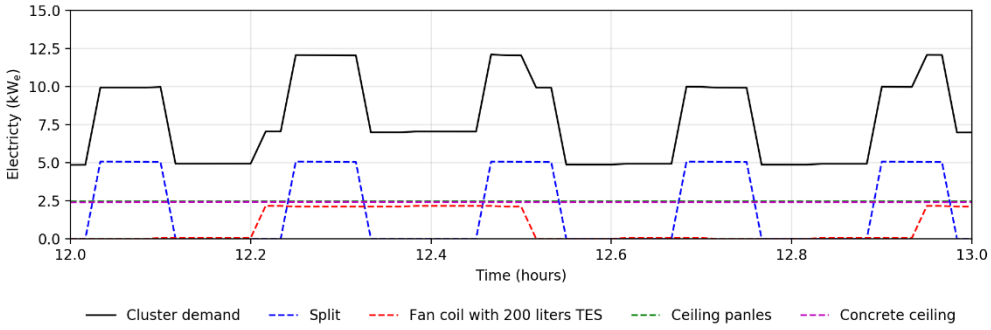

Figure 7.1. Electricity aggregated demand. Total and single contributions.

Since the indoor comfort is still guaranteed for more than 1 hours (Table 6.2), if a high flexibility demand (HFD) strategy is applied independently at each cooling system, the aggregated demand becomes zero for the whole hour as showed in Figure 7.2. A different situation can be noted if, instead, a low flexibility demand (LFD) strategy is applied. Looking at the blue dotted line in Figure 7.2., a power demand of about 5 kW is requested after 0.1 hours. This is due to the shorter response time that the systems present in case of restricted comforts limits. Especially, the apartment with split system reaches the indoor temperature of 25 °C in 0.13 hours. In the same way, the fan coil system response period is 0.78 hours, while 0.47 and 0.60 hours are respectively the values of the duration for the time in which the heat pump is off. for ceiling panels and concrete ceiling radiant cooling. However, if a LFD strategy is applied to all the considered space cooling systems together, the electricity consumption is also zero, even if for a limited time (about 8 minutes). This effect cannot be obtained if only a few space cooling systems are involved with a LFD strategy.

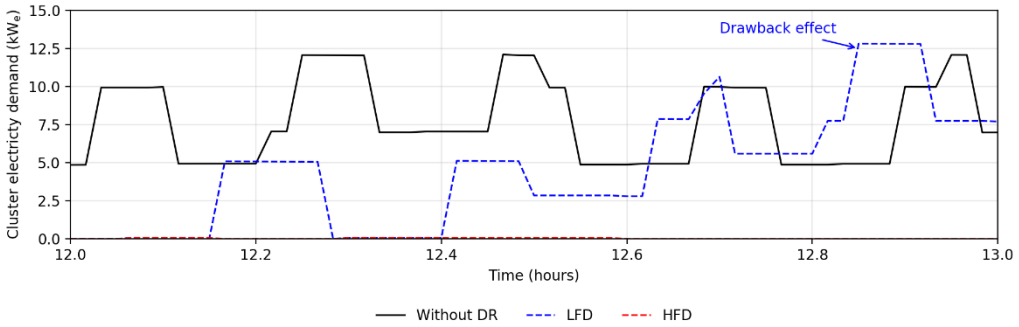

Figure 7.2. Electricity aggregated demand. High flexibility demand (HFD) and low flexibility demand (LFD) activated together for all user.

Table 7.1 reports the percentage of time (in the considered hour between 12.00 pm and 1.00 pm when the network requires flexibility) in which the aggregated demand remains below the power threshold levels described above (7, 10 and 12.5 kW). Since the split system electric load is the highest contribution in the aggregated demand (it accounts for about 42% of the demanded power when all the cooling systems are on), a possible demand response strategy could be the HFD configuration applied only to it (red dotted curve in Figure 7.3). In this way for the whole considered hour, the aggregated electricity demand stays always below 10 kW. Furthermore, the total power is reduced to the base load for about 13.2 minutes (22% of the considered hour), as showed in Table 7.1.

Since the split system power demand is of the same order of magnitude of the aggregated demand of the other three cooling systems (fan coil, concrete ceiling and ceiling panels), in Figure 7.3 the latter strategy is compared to a possible LFD configuration applied to them. In this last case a flattening of the highest peaks is not obtained for the whole considered hour (Table 7.1) but, the base load is maintained for about 50% of the time.

Table 7.1. Percentage of time (in the 12.00-1.00 pm hour) in which the aggregated demand remains below the considered thresholds.

Strategy	Below 7 kW	Below 10 kW	Below 12.5 kW
LFD to all systems	63%	70%	85%
HFD to split system	22%	100%	100%
LFD to split system	17%	17%	22%
LFD to fan coil, concrete ceiling, and ceiling panels	50%	70%	90%
Sequence LFD (Split then fan coil)	12%	17%	100%
Sequence LFD (Split then ceiling panels)	17%	22%	100%

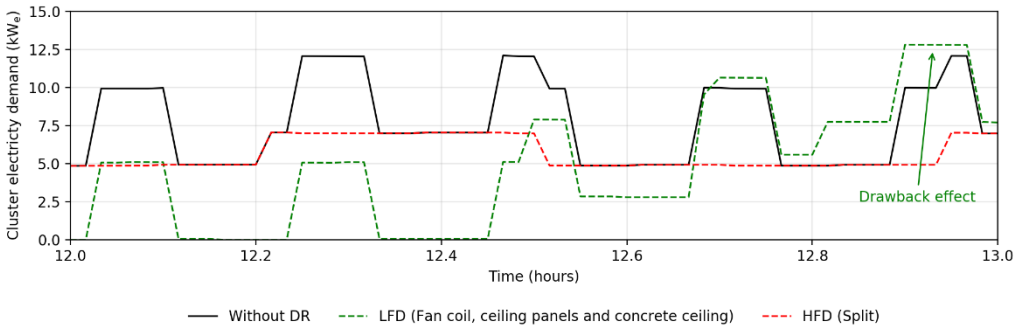

Figure 7.3. Electricity aggregated demand. High flexibility demand (HFD) to split system only and low flexibility demand (LFD) to all the others: fan coil with 200 liters tank, ceiling panels and concrete ceiling.

In order to request a smaller variation of the temperature comfort bound to the final users, the effect of a LFD configuration with subsequent calls of the four cooling systems is investigated. The demand response operator, in order to minimize the involvement of the individual user, which must be economically incentivized, could evaluate to call them one by one in this manner: once the first user has reached its restricted comfort limit, another one is called and so on. Figure 7.4 reports the aggregated power in case in which fan coil or ceiling panels systems are called after the split system. Split system is chosen as first call since its power is high, but its response period is very low (Table 7.1).

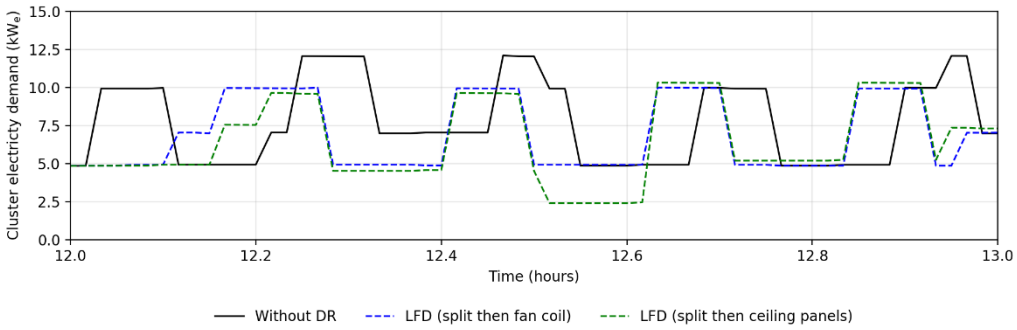

Figure 7.4. Electricity aggregated demand. Low flexibility demand (LFD) in sequence. Comparison between fan coil unit with 200 liters tank after split system and ceiling panels after split system.

In both cases, as shown in Table 7.1, the base load is maintained for a short time (12% and 17% of the flexibility hour respectively for split then fan coil and for split then ceiling panels). While, for both cases, the aggregated electricity demand always remains lower than the maximum power peak threshold (12.5 kW).
Concluding, the results show that if the aggregated electricity power wants to be maintained below the base power threshold for a longer time, the demand response strategy should involve all the users with a LFD configuration in order to get a compromise among load redaction, comfort variation and duration of the aggregated response period. As alternative a LFD configuration with subsequent calls guarantees that the power demand on average is higher, but always lower than the maximum threshold. Instead a HFD strategy only applied to the most energy demanding space cooling system (i.e., split system) allows a peak power reduction more important (always below 10 kW).
However, it is important to notice how differentiating the users involved in the peak shaving event (i.e., type and order), different behaviors in term of aggregated electric demand trend during and after the event can be noted. Indeed, looking at Figures 7.2 and 7.3, a late peak (i.e., drawback effect) power larger than the highest in normal operation (black line in Figures 7.2 and 7.3) can be observed. Looking instead at the case showed in Figures 7.2 (HFD, line red) and 7.4, no drawback effects in the aggregated electric power are observed by 1.00 pm.

7.2.2 Role of the occupancy pattern

Replacing the analysis presented in Paper 11, in this sub-section is discussed the role of the occupancy pattern in the energy flexibility performance on differentiated clusters of buildings. By simulating residential buildings with RC-networks in Python, users with different occupancy behaviour (i.e., archetypes of pattern) are modelled. To use the energy flexibility derived by thermostatically controlled loads, the setpoints are managed to activate the thermal mass of the buildings. Also, in this case, a peak shaving event in tested. However, thanks to the RC-network representation of the building, not just power resets are produced as for the analysis of the previous sub-section (7.1.1), but different percentage variations of the peak power can be tested (as for the operative energy flexibility evaluation in sub-section 6.2).
Going into detail, the single building is modelled as third order RC-network (Figure 5.3). To identify the parameters of the models, a white box approach is adopted (as explained in Section 5.1.1). A single-family house of 100 m^2, located in Milan, Italy (45°27' N, 9°11' E) is considered as case study. Its thermal properties are extrapolated from Tabula Project [64] for the most updated buildings (Table 4.1). As for the cases introduced in Chapter 5, to validate the RC-network, its simulation results are compared to a building with the same features modelled with Type 56 in TRNSYS (*RMSE* equal to 0.31 °C). However, Paper 11 reports details about the RC-network model with also the numerical values of the parameters of the model.
As concern the occupancy pattern archetypes, three kinds of behavior are considered: user U_1 with a fixed set point of 20 °C (reference scenario), user U_2 with a setpoint of 20 °C from 8.00 am 9.00 am, from 12.00 pm to 2.00 pm and from 7.00 pm to 9.00 pm and U_3 with the setpoint equal to 20 °C from 8.00 am 9.00 am and from 7.00 pm to 9.00 pm (in the remaining hours the setpoint is lowered to 18 °C both for U_2 and U_3). In Figure 7.5 the daily users' profiles are showed.

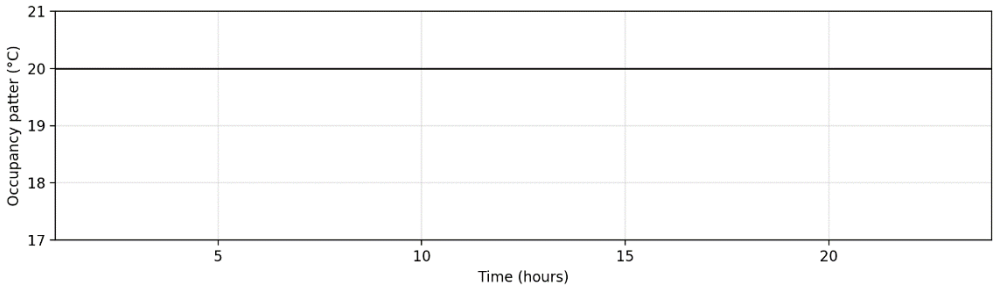

(a)

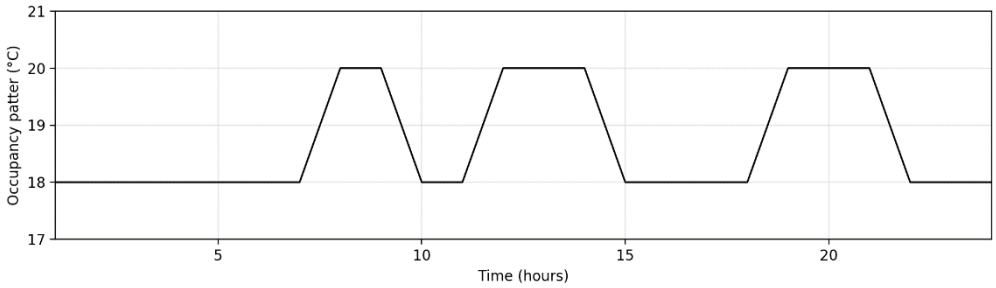

(b)

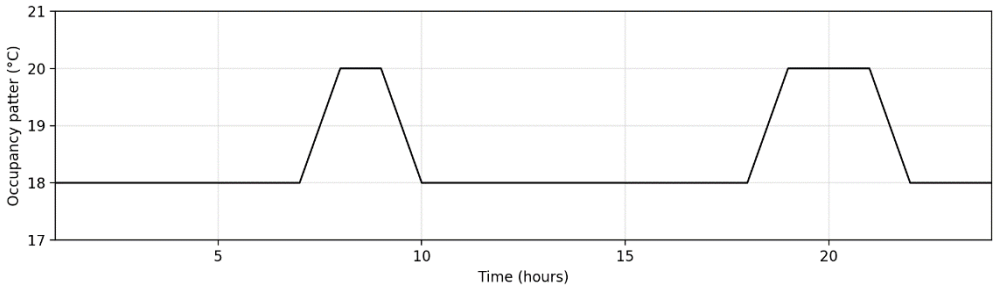

(c)

Figure 7.5. Users occupancy patterns archetypes: (a) U_1, (b) U_2 and (c) U_3**.**

To model the heating system, the contribution of the heating system ($\dot{Q}$) is directly applied to the indoor air node (T_{air}), imposing f_{iq} equal to 0 in Figure 5.3. In this way, no thermal inertia is assigned to it. An air source heat pump is modelled in order to obtain the electricity demand to be managed. In particular, the performance of a commercial heat pump is extrapolated by a manufacture catalogue [65]. Since the detailed representation of the distribution system is not considered, the *COP* depends only on the outdoor air temperature (T_{amb}).

For the state space formulation (Equations (11)), the heating power ($\dot{Q}$) has to be provided as an input for the building model. However, to test demand side management strategies strategy (e.g., demand response), it is necessary that the electricity demand ($\dot{P}$) derived by thermostatically controlled loads becomes an adjustable variable. For this reason, an optimization problem is introduced. The optimization has the objective to minimize the thermal requirements of the building while comfort conditions are maintained. The minimization problem can be written as:

$$\min \sum_{t=1}^{\text{duration}} \dot{Q}(t) \cdot \Delta t \qquad \text{Eq. (48)}$$

subject to the same constraints introduced in Equation (14) and (15). Therefore, the energy behaviour of the building is added to the optimization problem as a set of constrains, one for each time step *t* (Equation (14)). On the contrary, the heating demand, $\dot{Q}(t)$, becomes the decision variable of the problem and, through the *COP*, it can be connected to the electricity demand of the user ($\dot{P}$), which represents the TCLs to be managed during the DR event.

$$\dot{P}(t) = \frac{\dot{Q}(t)}{COP(t)} \qquad \text{Eq. (49)}$$

As in this case, for its linear characteristics, the optimization problem can be solved for the duration of the simulation as a typical linear programming problem.
The introduced demand response event consists of a peak-shaving strategy to produce a controlled hourly reduction of the electricity demand of a group of users. As comparison term, a reference scenario is introduced to reveal the time location of the peak. It is obtained in case of fixed set-point temperature (referring to Equation (14): T_{min} equal to T_{max} equal to 20 ° C) for all the users involved in the cluster. Then, in the form of an additional constraint for the optimization problem, the aggregated electricity demand is forced to an established percentage reduction in the reference case peak-hour. The additional constraint is formulated in Equation (50) where N is the number of users composing the cluster, f_r is the peak electricity power ($\dot{P}_{max}$) reduction factor.

$$\forall\, u\text{:}\;\; 0 \leq \sum_{u}^{N} \dot{P}\,(t) \leq f_r \cdot \dot{P}_{max} \qquad \text{Eq. (50)}$$

Since the energy flexibility has to be activated when the DR event is realized, a tolerance of 2 °C is allowed for the comfort constraints in the optimization problem (T_{min} is lowered by 1°C and T_{max} is increased of 1°C with reference to the occupancy patterns showed in Figure 7.5).
Taking into account a reference winter day (14 January), Figure 7.6 shows the application of the DR event to a single building (occupancy profile U_1 in Figure 7.5). Looking at the black dotted curve in Figure 7.6(b), an electricity peak can be observed at 10.00 am. Therefore, the demand response event imposes a power reduction from 10.00 am to 11.00, allowing an enhanced exploitation of the comfort band. In particular

a half reduction of the power is enforced (f_r equal to 50 % in Equation (50)) in the case showed in Figure 7.6.
In order to maintain the comfort a pre-heating strategy is necessary to reduce the power consumption during peak time (black continuous line in Figure 7.6(a)). As a consequence, an anticipated electricity peak occurs at 9.00 am with even a greater value in amplitude to account for thermal losses. The peak value passes, in fact, from 0.97 kW in reference operation to 1.33 kW with the demand response event (increase of + 37 %). It seems clear that, despite the objective of the event is achieved, a drawback effect connected to it occurs in the previous hours.

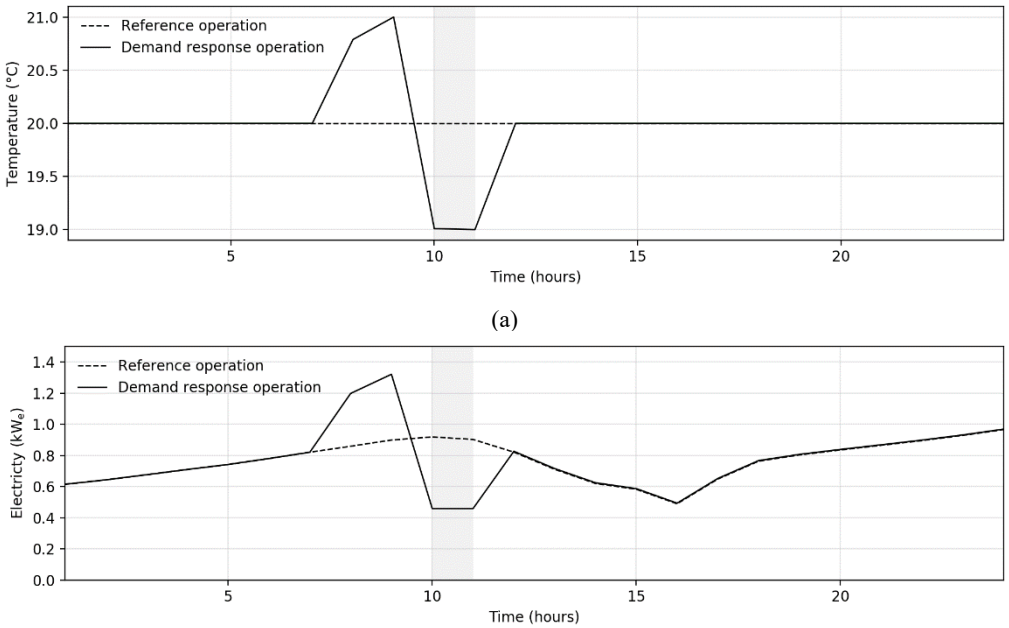

Figure 7.6. Comparison between reference operation and demand response event for a single user (U_1): (a) indoor air temperature and (b) electricity power demand.

When multiple users are aggregated in a cluster, a careful planning of users' participation can allow the event to take place without unexpected load peaks. No improvement compared to case showed in Figure 7.6 can be observed if users with the same behaviour are involved, but the electricity demand of the cluster is only scaled compared to the number of users participating. Therefore, a great contribution can be made by the engagement of users with different occupancy behaviours. In Figure 7.7 a small cluster

composed of three users is subject to the peak-shaving event in the same day. Two of the three users have the reference scenario occupancy profile (U_1), while the third acts as U_2 (Figure 7.5). In this case the anticipated peak no longer appears, while another one appears postponed at 12.00 pm. There is, however, no amplification of the peak value, which remains of the same order of magnitude as the reference case (2.76 kW in reference scenario and 2.86 kW in case of demand response event). Another increase in consumption is also recorded in the evening hours (from 7.00 pm to 9.00 pm). Anyway, it is not related to the demand response event but to the setpoint temperature of user U_2 rising.

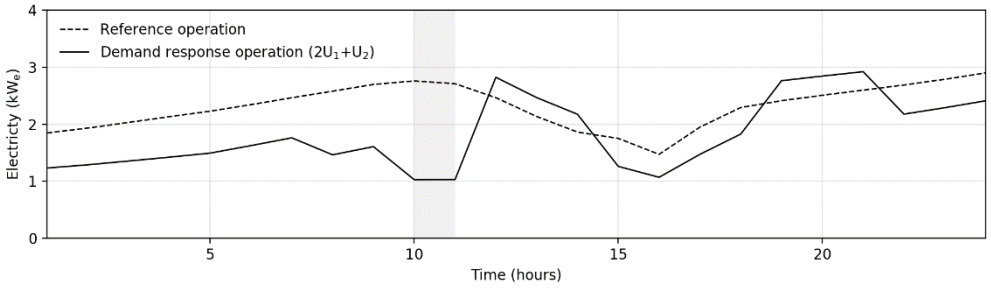

Figure 7.7. Comparison between reference operation and demand response event: cluster of three users: 2 users U_1 and 1 user U_2.

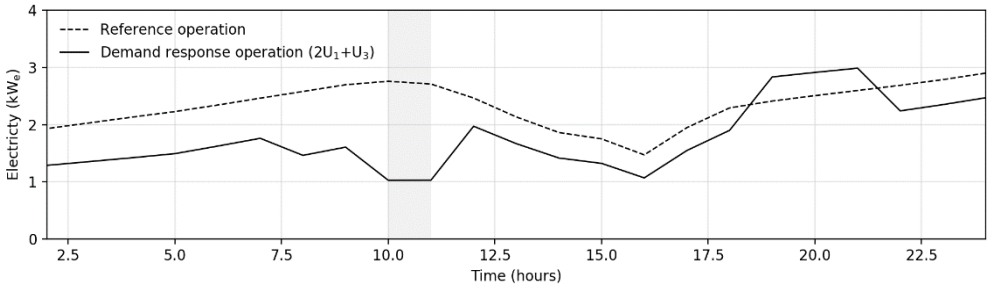

Figure 7.8. Comparison between reference operation and demand response event: cluster of three users: 2 users U_1 and 1 user U_3.

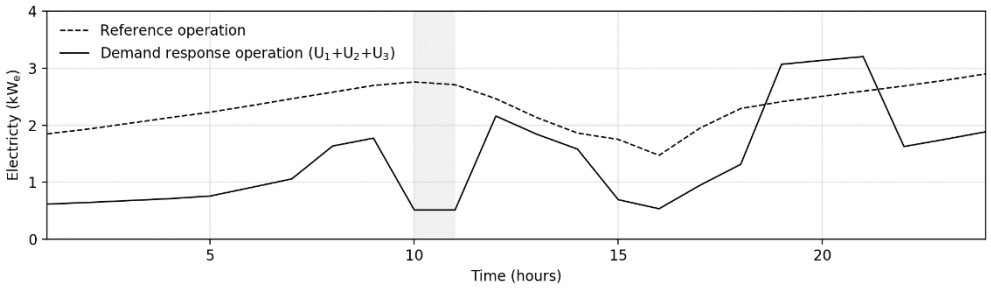

Figure 7.9. Comparison between reference operation and demand response event: cluster of three users: 1 user U_1,1 user U_2 and 1 user U_3.

Further improvements can be observed when also user U_3 is involved in the cluster. Figures 7.8 and 7.9 show this behaviour. Figure 7.8 presents the same case represented in Figure 7.7 in which the user U_2 is replaced by U_3, while in Figure 7.9 all the users (U_1 U_2 and U_3) are involved. Both the clusters tested (Figures 7.8 and 7.9) allow to cut the peak avoiding drawback effects both in the hours before and after the demand response event. Due to the change of the occupancy profile between 7.00 pm to 9.00 pm, also in this case an increase in the electricity consumption respect to the reference operation is observed.

Focussing only on the hours before and after the event, the presence of a user U_3 appears fundamental to avoid new power peaks keeping the demand curve below the reference scenario. This behaviour is also confirmed if larger clusters are tested. In this case, it is possible to connect the minimum number of users U_3 to be involved to avoid such unexpected peaks. In particular, when a peak halving is required (f_r equal to 50 % in Equation (50)), the 8 % of the users should have an occupancy profile as U_3.

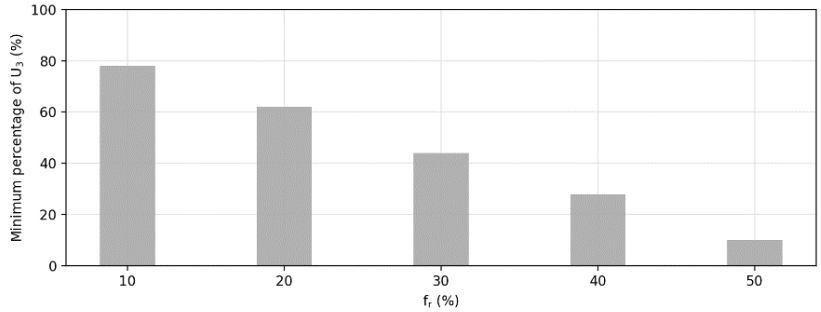

Figure 7.10. Percentage of the minimum number of users U_3 to be involved in a peak-shaving event to produce different peak reduction (f_r) avoiding drawback effects connected to it in the hours before and after the event.

Figure 7.10 shows the percentage of user U_3 involvement in case of different peak power reductions (f_r) required by the demand response event. A high participation (minimum 78 %) is necessary if the peak wants to be reduced by up to 10 %, then the percentage decreases as f_r increases. From this last consideration it is evidenced even more the role of a differentiated cluster of users when the energy flexibility wants to be used for load shifting strategies. Thanks to the differentiation of behaviour, the energy flexibility acquires more degrees of freedom, allowing to perform demand response events by minimizing the presence of undesirable effects connected to it.

Chapter 8

Conclusions and future research

The objective of this thesis is to provide an evaluation and a quantitative analysis of the energy flexibility reserve contained in residential buildings. Introducing novel methodologies of quantification and different case studies, this work aims at evaluating the different aspects that characterize the energy flexibility obtainable from the management of thermal loads in residential buildings equipped with heat pumps.
All the results reported are extrapolated from a series of papers that have been published in scientific journals (see the list at sub-section 1.3). The evaluation starts from the single building level and then gradually the analysis is widened to the aggregate level. Furthermore, the assessment is firstly referred to a design evaluation to provide a rating of the building itself and, secondly, to an operational scenario with a real time use of the flexibility. Table 8.1 summarizes all the case studied.

Table 8.1. Summary of the case studies and the methodologies used divided by type of analysis

Size of the evaluation	Working scenario	Objective of the analysis	Case studies	Methodology and highlighted aspects
Single residential building	Design level	Quantify the building energy capability to produce flexibility services in relation to its intrinsic features (e.g., thermal and geometrical characteristics and HVAC system.)	Simulation-based buildings differentiated for the Italian scenario: (i) Age of construction (i.e., insulation level and HVAC system). (ii) Location. (iii) Heaviness and composition of building envelope. (iv) Season (i.e., heating and cooling season). (v) Refurbishment interventions of the building envelope.	Classification of the buildings in flexibility classes through the calculation of a single indicator: the Flexibility Performance Indicator (FPI).

Single residential building	Design level	Investigate the potential of district cooling networks (DC) to be an external source of energy flexibility in a context of fuel switching.	Simulation-based district cooling residential network, case simulated: (i) Simple 14 users residential DC network. (ii) A residential 14 DC users network feed with wasted cold energy derived from the vaporizer of a L-CNG refueling station.	The methodology and the highlighted aspects concerning the two case studies are: (i) Flexibility additional services provided by DC network. Two quantification indicators are introduced: the wasted cold energy and the overheating time. (ii) Electricity saving in relation to the adoption of traditional cooling systems.
Single residential building	Operative level	Role of advanced control (model predictive control, MPC) to unlock energy flexibility.	Real-time MPC implemented in a simulation environment. Case study tested: (i) Simple MPC realized to unlock flexibility provided by thermostatically controlled loads (TCLs) with a data driven and a physical based building model. (ii) Operative MPC (realized with both data driven and a physical based building model) to manage a multi energy source (MES) in a building with DC.	The performance of the MPC are calculated in relation to a ruled based control (RBC) in terms of energy performance according to the tested objective function and operative *RMSE* (i.e., comparison between the actual and the predicted indoor temperature). The aspects that the two case studies aim to highlight are: (i) The role of the building model in an operative MPC to activate the flexibility derived by TCLs. (ii) Demonstrate the importance of flexibility provided by TCLs to manage a MES building.

Single residential building	Design and operative level	Show the comparison between the design and the operative flexibility evaluation	Simulation-based buildings with different space cooling technologies: (i) Split system. (ii) Fan coil units coupled with air to water heat pump (with and without a thermal energy storage). (iii) Ceiling panels coupled with air to water heat pump and air dehumidifier. (iv) Cooling concrete ceiling coupled with air to water heat pump and air dehumidifier.	For the design evaluation the FPI is calculated while, for the operative evaluation the capability of each system to produce different demand response events is investigated with the evaluation of: energy shifted during the demand response event, the use of the energy flexibility of the thermal mass of the distribution system (time and amount of energy stored), the use of the energy flexibility from TCLs (time and temperature variation) and the presence of payback loads in the electricity power curve.
Cluster of residential buildings	Preliminary operative level	Show the importance of differentiating users in a cluster subjected to a demand response event (DR).	With simulated case studies, two aspects are taken into account: (i) The role of the HVAC system (focus on the cooling season). (ii) The role of the occupancy patterns.	The evaluation is realized applying the same DR event to different clusters (i.e., differentiated for composition of involvement of the users) and highlighting the configurations in which the event is realized with or without drawback effects (i.e., payback loads).

According to Table 8.1, given the diversification of the analyzes and the various case studies introduced, the main topics evaluated in this thesis and the related conclusions are provided grouped in the following points:

- **Quantification of the energy flexibility reserve contained in buildings**.
  As showed in Table 8.1, firstly, the design operation is taken into account with the proposal of a method to quantify the energy flexibility reserve of single buildings according to their intrinsic characteristics (i.e. thermal and geometrical properties of the envelope and features of the heating/cooling system). This methodology consists in the calculation of a single indicator: the Flexibility Performance Indicator (FPI)

which summarizes four flexibility parameters (response time, committed power, recovery time and actual energy variation). As for the energy efficiency labelling already defined in the energy performance certificate of the building, the FPI allows the identification of flexibility classes to label buildings according to their energy flexibility potential. Given the dependency of the flexibility quantification on the boundary conditions (i.e., the specific demand response event, the outdoor and the indoor conditions), a dynamic simulation tool has to be used and standard boundary conditions (e.g., the demand response event, the representative day and comfort constraints) has to be defined in a unique way for the application of the proposed methodology. In order to prove the reliability of the FPI and highlight the main aspects with a bigger influence on buildings flexibility behavior, the methodology is tested on different case studies for the Italian scenario (Table 8.1) whit the aim of highlights the effects of the following aspects:

- The role of the construction age of the buildings (i.e., thermal losses and heating and/or cooling system). In this case, results show that the **FPI is able to distinguish newer buildings from older ones, labelling them in different flexibility classes**. In particular, **a great influence of the distribution system in the evaluation of the flexibility indicators, especially in the heating case** (the radiant floor distribution system has a good level of thermal energy storage and can maintain for long periods the comfort) **is observed**.
- The role of geographical position and the thermal inertia introduced by both the buildings envelope (construction materials or wall composition) and HVAC system. As expected, in this context results show a **great influence of external weather conditions on the flexibility performance evaluated with the FPI**: in cold winter periods, the flexibility performance drops as well as in hot summer periods. Moreover, the importance of the thermal inertia of the thermal distribution system is confirmed. Indeed, high thermal inertia emission systems (i.e. underfloor heating and ceiling cooling) are helpful in achieving good energy flexibility, in particular in presence of low building structure inertia (i.e. internal insulation). Also, the envelope thermal inertia has an important role for buildings flexibility performance (external insulation is recommended), especially in heating case while, with the same thermal insulation position, the FPI does not differ in relation to different heaviness of the construction materials. On the other hand, **in cooling season**, the analysis led to the conclusion that **increasing the building or the heating/cooling emission system thermal inertia increases the flexibility performance but not with the same entity as in heating case**.
- the effectiveness of different refurbishment strategies on buildings energy demand management ability (focus on the heating season). Starting from a

reference old not insulated building, the energy flexibility improvement due to different energy efficiency interventions is quantified. In particular the insulation thickness of the building envelope (floor, roof, external walls) and the windows features are varied, and the heating system size is modified in compliance with the reduction of thermal energy demand and with commercial systems specifications available. From the results of this analysis, it is possible to see a consistent reduction of thermal energy demand by increasing the insulation level of the building envelope. However, the same behavior is not observed for the energy flexibility according to the FPI calculation. Therefore, **taking into account refurbishment strategies on the building envelope, the positive effect on flexibility due to building thermal mass is evident only if the thermal insulation is applied at the same time in the external walls, floor and roof**. If there is even only one surface with high heat losses, the building is not able to maintain in an acceptable band the internal comfort and the flexibility performance is low.

However, testing different case studies, the Flexibility Performance Indicator seems to quantify well the building energy flexibility during a demand response event highlighting how both the aspect of the thermal inertia and the insulation level are fundamental to decouple demand and supply and therefore to design high-flexible buildings.

- **Modeling and performance analysis of innovative solutions for district space cooling.**

  To enlarge the evaluation context, before moving on to the operational flexibility assessment, a focus on the possible sources of energy flexibility outside the building is presented (Table 8.1). In particular the additional energy flexibility reserve of district cooling systems is assessed. With a simulation-based case study, the effect of the different thermal inertia levels available in district cooling network as flexibility providers are qualitatively analyzed. They are (i) the network with the fluid contained in the pipes, (ii) the thermal inertia of the buildings and (iii) the addition of a dedicated devices as thermal energy storage. By calculating two indicators, i.e., the wasted cold energy and the overheating time, results shows that **in district cooling network the pipelines provide a very small contribution** (the cooling demand can be satisfied for less than 1 hour, when there is no cooling power availability)**, the activation** (assuming it is possible to control the inside temperature set points of the users with appropriate predictive control strategies) **of the thermal inertia of the buildings**, pre-cooling the buildings' thermal mass when the cooling supply is expected to be wasted, **seems to have a great flexibility potential**, comparable to the installation of a thermal energy storage **and the addition of a**

dedicated thermal inertia device is confirmed as the best means to decouple and manage in real-time energy supply and demand in the simplest way. Moreover, with the aim of introducing a potential energy sources to activate the energy flexibility derived by the fuel switching in the context of multi energy carriers, a novel application to feed a residential district cooling network recovering wasted energy from the vaporizers of Liquid to Compressed Natural Gas (L-CNG) refueling stations is introduced. By simulating a case study, results show that a **district cooling designed to recovery cold energy from a L-CNG refueling station, is able to provide high electricity saving levels in comparison with the adoption standard cooling systems installed in every building**. Regardless of the supply cooling power profile, electricity consumption reductions greater than 50 % are obtained (even if it is necessary to highlight that these percentages are strongly dependent on the assumptions made to design the network).
However, it is important to underline that the results obtained, and the considerations made proved to be dependent on the hypothesis formulated (design choices such as sizing and methods for estimating the energy availability of the network).

- **Study of advanced controls (model predictive control, MPC) to activate the flexibility reserve in buildings.**
  Once the context of the flexibility reserves of buildings is investigated and the role of external means (i.e., district cooling networks) to activate it is addressed, the operational scenario is taken into account. First of all, the role of advanced controls is analyzed with a focus on the effectiveness of the model-based predictive control (MPC) in comparison to traditional rule-based control (i.e., thermostat controls). As MPC requires a model of the system to be controlled, a focus on the role of different building modelling techniques are compered in an energy flexibility activation scenario. In particular, a data-driven model implemented with an artificial neural network (ANN) and a physical-based model realized with a RC-network are compared in an operative model predictive control. In this first analysis (Table 8.1) an MPC designed to minimize the total energy cost for the thermal demand satisfaction it modelled. For the control has also been provided the possibility of unlocking the energy flexibility provided by thermostatically controlled loads. The results show that **similar cost performances are obtained in the two cases** (a 16 % reduction in the weekly cost respect to the reference case) **for the data driven and the physical base building model**. However, **although the data-driven model shows a good performance in replicating the building thermal power profile, this trend is not confirmed when it works operatively in the controller**. This is due to the difficulty in identify the useful data to train the ANN to predict thermal demand and at the same time to unlock the energy flexibility of thermostatically

controlled loads. Moreover, unlike the RC-network that allows a linear formulation of the optimization problem, the non-linear nature of the data-driven models requires more efforts in formulating the optimization problem in the MPC logic.

- **Application of MPC controls on buildings with availability of different energy carriers (multi-energy systems, MESs) including the connection to a district cooling (DC) network.**
  In order to test the activation of the energy flexibility reserves both inside (i.e., thermostatically controlled loads) and outside (i.e., fuel switching) the building, an MPC (with both a data driven and a physical based building model) is implemented and operatively applied to a simulation-based case study (Table 8.1). The case study consists of a residential building whose cooling demand can be satisfied with a connection to a district cooling network feed with wasted cold energy (i.e. from the vaporizer of a L-CNG refueling station), electricity produced by on-site photovoltaic modules or supplied by the power grid. Moreover, by allowing a certain tolerance to the comfort conditions, the energy flexibility contained in thermostatically controlled loads (TCLs) can be used as additional virtual reserve by the MPC.
  As mentioned, this case study is evaluated both with a ANN-based and with a RC-network based MPC. **Also in the operative scenario of a MES building**, although similar energy performance are obtained, **the physical based** (i.e., RC-network) **formulation seems to allow an easier formulation of the control even if it requires a greater effort in the construction of the model** (i.e., the identification of the parameters). **However, in both the cases, the analysis carried out underline the importance of the activation of the building energy flexibility as additional energy source in MES. Indeed, its exploitation appears fundamental to allow the control to maximize the energy performance**.

- **Comparison between design and operative flexibility evaluation with a focus on the residential space cooling (SC) sector.**
  In the last part of the thesis, before moving to the analysis of aggregate of buildings (i.e., clusters), a comparison between a design flexibility evaluation (i.e., with the FPI calculation) and an operative scenario is discussed (Table 8.1). In particular, the analysis is applied to the space cooling sector, given its increasing share in the whole energy demand. **Introducing simulation-based cases studies to model different space cooling technologies** (i.e., split systems, fan coils, radiant ceiling panels with air dehumidifier and cooling concrete ceiling with air dehumidifier), **the analysis highlights that, even if the FPIs quantify medium flexibility performance** (i.e., all the buildings are labelled in class C or B), **the operative evaluation allows to**

highlights some important differences in behavior due to the intrinsic features of the cooling systems (i.e., thermal inertia of the distribution system and rapidity in speed in meeting the building demand). **For instance, the operative evaluation allows that as the thermal inertia of the distribution system increase, the involvement of the users in term of variation of their comfort conditions decrees**. **However, attention must be paid in avoiding high drawback effects (i.e., payback loads) in the power curve**.

- **Analysis of flexibility at the aggregate level (cluster of buildings).**
  Once the size of the single building has been analyzed in detail, at the end of the thesis, a preliminary evaluation on the additional energy flexibility that can be obtain in an aggerated scenario is discussed by means of simulated case studies (Table 8.1). In particular, the role of the differentiation of the users is discussed in a resource planning scenario. Both the role of the HVAC systems (focusing on the cooling systems) and the occupancy patterns are assessed imposing simple demand response strategies (i.e., peak shaving). The results of this analysis show that **evaluating the flexibility at a cluster level, often drawback effects (anticipated or participated peaks) occur when no thermal inertia is provided by the distribution system and the peak shaving strategy is achieved with a pre-heating or pre-cooling strategy**. **However, a careful planning of the residential clusters can have positive effects in this regard.** The case analyzed highlights that combined flexibility allows multiple degrees of freedom to apply demand response events in residential building cluster, showing the potential of a planned composition of users to be involved to avoid drawback effects (i.e., payback loads) in the demand curve.

The results discussed in this last part of the thesis, although with preliminary evaluations, lay the foundations for continuing to investigate the potential at cluster level. For example, taking into account the application of the MPC to manage a MES building it could be interesting to analyze the effects of the optimization of the single users when some energy resources are shared with other users (as for the district cooling). Indeed, it is not taken for granted that individual user optimization also entails an optimal configuration at the aggregate level. Therefore, it would be interesting to extend the analysis to this aspect as well.
Then, as anticipated, more work should be done on the optimal planning of the cluster to produce different demand side management strategies optimizing the performance. Indeed, assuming that the potential reserve of flexibility of the individual has been established, scaling the evaluation from single buildings to clusters may be fundamental to involve high quantities of energy and/or power minimizing the involvement of the

individual. Therefore, it would be interesting to deepen this aspect to provide instruments to easily plan the exploitation of the energy flexibility of buildings.
To conclude, the analyses and evaluations showed in this thesis allow to confirm the great potential of residential buildings in providing energy flexibility services. However, it is emerged a great influence of the intrinsic features of the building (i.e., its thermal properties and the thermal inertia of its distribution system) on its design flexibility reserve, more in heating than in cooling season. In order to unlock the flexibility, it is necessary to implement advanced control (with all the issues discussed). Besides that, the building can also optimally exploit external flexibility sources represented by the connection to district heating or cooling network or by the fuel switching. Another important aspect is related to the involvement of the users (both in case of single and clusters) to limit drawback effects connected to the demand side management events. The latter aspect can be seen as a reaffirmation of the great potential that, with careful management, residential buildings have to produce energy flexibility services.

List of Symbols

Δk	Timestep (hours)
Δk_{DR}	Duration of the demand response event (hours)
Δk_{prc}	Duration of the pre-cooling phase (hours)
$\Delta k_{prc,TMD}$	Duration of the pre-cooling phase referred to thermal mass of distribution system (hours)
ΔRH_{max}	Upper relative humidity tolerance (%)
ΔRH_{min}	Lower relative humidity tolerance (%)
ΔT_{max}	Upper setpoint tolerance (°C)
ΔT_{min}	Lower setpoint tolerance (°C)
$\Delta T_{TMD,max}$	Upper thermal mass tolerance (°C)
$\Delta T_{TMD,min}$	Lower thermal mass tolerance (°C)
A	Flexibility class
A	Coefficient matrices related to state vector in state space formulation
A+	Flexibility class
A1	Flexibility class
A2	Flexibility class
A3	Flexibility class
ACH	Air changes per hour (h^{-1})
ANN	Artificial neural network
ARX	Linear auto regressive model with exogenous inputs
B	Flexibility class
B	Coefficient matrices related to input vector in state space formulation
$\hat{b}$	Bias vector of the hidden layer in artificial neural network formulation
BAT	Best available technology
BL	Baseline

C	Flexibility class
C	Thermal capacitance (J K^{-1})
c	Energy cost (Eur kWh^{-1})
C	Set of constraints of the optimization problem
C_{air}	Air node thermal capacitance (J K^{-1})
C_e	Envelope thermal mass thermal capacitance (J K^{-1})
$c_{el,G}$	Energy grid cost (EUR kWh^{-1})
$c_{el,PV}$	Energy from photovoltaic cost (EUR kWh^{-1})
C_{fe}	Thermal capacitance related to external floor layers (J K^{-1})
C_{fi}	Thermal capacitance related to internal floor layers (J K^{-1})
C_{fin}	Thermal capacitance related to thermal insulation layer in floor (J K^{-1})
C_i	Thermal capacitance of internal mass (J K^{-1})
C_{re}	Thermal capacitance related to external roof layers (J K^{-1})
C_{ri}	Thermal capacitance related to internal roof layers (J K^{-1})
C_{rin}	Thermal capacitance related to thermal insulation layer in roof (J K^{-1})
C_{TES}	Thermal capacitance of thermal energy storage node (J K^{-1})
$c_{th,DC}$	Energy from district cooling cost (EUR kWh^{-1})
C_{we}	Thermal capacitance related to external layers of vertical walls (J K^{-1})
C_{wi}	Thermal capacitance related to internal layers of vertical walls (J K^{-1})
C_{win}	Thermal capacitance related to thermal insulation layer in vertical walls (J K^{-1})
CC	Cooling concrete ceiling
CF_{DC}	Conversion factor for district cooling source
CF_e	Conversion factor for source e acting as uncontrolled inputs
CF_G	Conversion factor for withdrawals from grid
CF_{PV}	Conversion factor for photovoltaic source
CHP	Combined heat and power
CNG	Compressed natural gas
COP	Coefficient of performance

$\overline{COP}$	Average coefficient of performance
COP_{exp}	Expected coefficient of performance
CP	Concrete ceiling panels
$CTRL_{DC}$	Boolean control for district cooling
$CTRL_{HP}$	Boolean control for photovoltaic modules
$CTRL_{S}$	Boolean control for split system
D	Flexibility class
d	Number of inputs in artificial neural network formulation
D	Mathematical domain of the variables in the optimization problem
D.M.	Ministerial decree
DC	District cooling
DH	Dehumidifier
DR	Demand response
DSM	Demand side management
e	Index for energy sources
$\dot{E}_e$	Availability profile of source e acting as uncontrolled inputs (W)
$\dot{E}_G$	Power from grid, general term (W)
E_{BL}	Electricity in baseline (Wh)
E_{DR}	Actual energy variation
E_{DR}	Electricity in demand response scenario (Wh)
E_G	Electricity from the power grid (Wh)
E_{shift}	Energy shifted during the demand response (Wh)
$E_{shift,aDR}$	Energy shifted after the demand response (Wh)
$E_{shift,bDR}$	Energy shifted before the demand response (Wh)
EBC	Energy in buildings and communities
EPC	Energy performance certificate
EPDB	Energy performance of buildings directive
ES	Number of usable energy sources acting as uncontrolled inputs
EU	European Union
f_{air}	Scalar factor for total gains related to air node temperature
f_i	Scalar factor for total gains related to internal mass node temperature

f_{PSS}	Reduction power factor during peak shaving strategy
f_r	Reduction factor for cluster power
FCU	Fan coil units
$Flex_{RH}$	Use of the energy flexibility of latent loads (%)
$Flex_{TCL}$	Use of the energy flexibility from thermostatically controlled loads (%)
$Flex_{TMD}$	Use of the energy flexibility of the thermal mass (%)
FPI	Flexibility performance indicator
FPI_{limit}	Limit flexibility performance indicator
g	Nonlinear activation function in artificial neural network
G	Power grid
$\dot{G}$	Total gains (solar and internal) (W)
$\dot{G}_{internal}$	Internal gains (W)
$\dot{G}_{s,r}$	Solar gains thought roof (W)
$\dot{G}_{s,w}$	Solar gains thought wall (W)
$\dot{G}_{s,wind}$	Solar gains thought windows (W)
$\dot{G}_{solar}$	Solar gains (W)
h_v	Heat of evaporation of water (J kg_{vap}^{-1})
HFD	High flexibility demand
HP	Heat pump
HVAC	Heating, ventilation and air conditioning
i	Index
IEA	International Energy Agency
j	Index
k	Time (hours)
k_{end}	End time (hours)
k_{end_DR}	End time demand response event (hours)
K_l	Loss coefficient factor of TES (W m^{-2} K^{-1})
k_{start}	Starting time (hours)
k_{start_DR}	Starting time demand response event (hours)
L-CNG	Liquid to compressed natural gas

LFD	Low flexibility demand
LNG	liquefied natural gas
LP	Linear programming
m	Number of neurons in the hidden layer in artificial neural network formulation
$\dot{m}_{dc}$	Flow rate in district cooling network (kg s^{-1})
$\dot{m}_{vent}$	Natural ventilation flowrate (kg s^{-1})
$\dot{m}_{water}$	Water flow rate (kg s^{-1})
M_{air}	Mass of the internal air (kg)
MES	Multiple energy systems
MILP	Mixed integer linear programming
MPC	Model predictive control
N	Number of users
OF_C	Objective function aimed at minimizing cost
OF_G	Objective function aimed at minimizing electricity from grid
OF_P	Objective function aimed at minimizing primary energy
p	Penalty signal
$\dot{P}^*_{res}$	Dimensionless committed power
$\dot{P}^*_{shift}$	Shifted power in relation to baseline (%)
$\dot{P}_{BL}$	Electricity power during baseline (W)
$\dot{P}_{DR}$	Electricity power in case of demand response event (W)
$\dot{P}_G$	Electricity from the power grid (W)
$\dot{P}_{HP,BL}$	Electricity consumption heat pump in baseline (W)
$\dot{P}_{HP,DR}$	Electricity consumption heat pump in demand response scenario (W)
$\dot{P}_{max}$	Maximum electricity power of the cluster (W)
$\dot{P}_{max,BL}$	Maximum value of electricity in baseline (W)
$\dot{P}_{PV}$	Electricity producible by the photovoltaic modules (W)
$\dot{P}_{rated}$	Rated electricity power (W)
$\dot{P}_{REF}$	Electricity power in reference condition (i.e., without demand response events)
$\dot{P}_{res}$	Committed power (W)

$\dot{P}_{SC}$	Electricity power of the space cooling system (W)
p_1	Average weight of t^*_{res}
p_2	Average weight of $\dot{P}^*_{res}$
p_3	Average weight of t^*_{rec}
p_4	Average weight of η_{DR}
P1	Cooling power recovery profile from L-CNG
P2	Cooling power recovery profile from L-CNG
P3	Cooling power recovery profile from L-CNG
PCM	Phase change materials
PF	Penalty factor for an energy source
PF_{DC}	Penalty factor for district cooling source
pf_{DC}	Primary energy conversion factor for district cooling
PF_e	Penalty factor for source e acting as uncontrolled inputs
PF_G	Penalty factor for withdrawals from grid
PF_{PV}	Penalty factor for photovoltaic source
pf_{PV}	Primary energy conversion factor for photovoltaic
PH	Prediction horizon (hours)
PID	Proportional–integral–derivative controller
PSS	Peak shaving strategy
PV	Photovoltaic modules
$\dot{Q}$	Thermal power provided by HVAC (W)
$\dot{Q}_{building}$	Cooling power removed in the building (W)
$\dot{Q}_{DC}$	Cold thermal energy provided by district cooling (W)
$\dot{Q}_{DH}$	Latent cooling power removed by dehumidifier (W)
$\dot{Q}_{max}$	Maximum power provided by HVAC (W)
$\dot{Q}_{SC}$	Cooling power removed by space cooling system (W)
R	Thermal resistance (K W^{-1})
R_{ee}	Thermal resistance between external environment and envelope thermal node (K W^{-1})
R_{ei}	Thermal resistance between envelope thermal node and air node temperature (K W^{-1})

R_{fe}	Thermal resistance between external environment and external floor thermal node (K W^{-1})
R_{fi}	Thermal resistance between air node and internal floor thermal node (K W^{-1})
R_{fin}	Thermal resistance of thermal insulation of floor layer (K W^{-1})
R_{i}	Thermal resistance air node temperature and internal mass node (K W^{-1})
R_{re}	Thermal resistance between external environment and external roof thermal node (K W^{-1})
R_{ri}	Thermal resistance between air node and internal roof thermal node (K W^{-1})
R_{rin}	Thermal resistance of thermal insulation of roof layer (K W^{-1})
R_{w}	Thermal resistance due to windows and natural ventilation (K W^{-1})
R_{wi}	Thermal resistance between air node and internal layers of vertical walls node (K W^{-1})
R_{we}	Thermal resistance between external environment and internal layers of vertical walls node (K W^{-1})
R_{win}	Thermal resistance between of thermal insulation of vertical walls (K W^{-1})
RBC	Rule based control
RC	Resistances and capacitances
RES	Renewable energy resources
RH	Relative humidity (%)
RH_{BL}	Relative humidity in baseline (%)
RH_{DR}	Relative humidity in demand response scenario (%)
$RH_{lower,comfortlimit}$	Minimum relative humidity comfort limit (%)
$RH_{upper,comfortlimit}$	Maximum relative humidity comfort limit (%)
RMSE	Root Mean Square Error
RSE	Root Square Error
SC	Space cooling
SETIS	Strategic energy technologies information system
SFH	Single family house
SRI	Smartness readiness indicator
S	Split system

SSM	State space model
StROBe	Stochastic residential occupancy behavior
t	Time (hours)
t^*_{rec}	Dimensionless recovery time
t^*_{res}	Dimensionless response time
T_{air}	Indoor air node temperature (°C)
$T_{air,BL}$	Air temperature in baseline (°C)
$T_{air,DR}$	Air temperature in demand response scenario (°C)
T_{amb}	External temperature (°C)
T_{data}	Temperature available by measurement data (°C)
t_{DR}	Demand response duration (hours)
T_e	Envelope thermal mass node temperature (°C)
T_{env}	Environment temperature (related to TES) (°C)
T_{fe}	Temperature related to external floor layers (from external to insulation layer) (°C)
T_{fi}	Temperature related to internal floor layers (from internal to insulation layer) (°C)
T_g	Ground temperature (°C)
T_i	Internal mass node temperature (°C)
$T_{lower,\ comfortlimit}$	Minimum temperature comfort limit (°C)
T_{max}	Maximum temperature (°C)
T_{min}	Minimum temperature (°C)
T_{model}	Temperature predicted by the building model (°C)
T_{re}	Temperature related to external roof layers (from external to insulation layer) (°C)
t_{rec}	Recovery time (hours)
t_{res}	Response time (hours)
T_{ri}	Temperature related to internal roof layers (from internal to insulation layer) (°C)
$T_{ri,cp}$	Temperature of internal roof layers (ceiling panels) (°C)
$T_{roof,BL}$	Temperature of the roof layer (coinciding with TMD) in baseline (°C)

$T_{\text{roof,DR}}$	Temperature of the roof layer (coinciding with TMD) in demand response scenario (°C)
T_{sp}	Setpoint temperature (°C)
$T_{\text{sp,minimization}}$	Setpoint temperature calculated by minimization (°C)
T_{sup}	Supply temperature heat pump (°C)
T_{TES}	Temperature of thermal energy storage node (°C)
T_{TMD}	Thermal mass temperature (°C)
$T_{\text{TMD,BL}}$	Thermal mass temperature in baseline (°C)
$T_{\text{TMD,DR}}$	Thermal mass temperature in demand response scenario(°C)
$T_{upper,comfortlimit}$	Maximum temperature comfort limit (°C)
T_{we}	Temperature related to external layers of vertical walls (from external to insulation layer) (°C)
T_{wi}	Temperature related to internal layers of vertical walls (from internal to insulation layer) (°C)
TCL	Thermostatically controlled loads
TCM	Thermo chemical materials
TES	Thermal energy storage
TMD	Thermal mass of distribution system
U	Thermal transmittance (W $m^{-2}K^{-1}$)
U	Input vector in state space formulation
u	Index for users
U_1	Occupancy pattern 1 (archetype)
U_2	Occupancy pattern 2 (archetype)
U_3	Occupancy pattern 3 (archetype)
UF	Utilization factor for energy source
UF_e	Utilization factor for source e acting as uncontrolled inputs
UK	United Kingdom
$\widehat{w}_j$	Weights matrix of the hidden layer in artificial neural network formulation
w_{ji}	Weights matrix of the inputs in artificial neural network formulation
X	State vector in state space formulation
x	Input in artificial neural network formulation

X	Set of variables of the optimization problem
x_{air}	Absolute humidity of internal air ($kg_{vap}\ kg_{as}^{-1}$)
x_{amb}	Absolute humidity of external air ($kg_{vap}\ kg_{as}^{-1}$)
x_{max}	Maximum absolute humidity ($kg_{vap}\ kg_{as}^{-1}$)
x_{min}	Minimum absolute humidity ($kg_{vap}\ kg_{as}^{-1}$)
y	Output artificial in artificial neural network formulation
η_{DR}	Demand response efficiency
μ_c	Cost signal mean value (Eur kWh^{-1})
σ_c	Standard deviation (Eur kWh^{-1})

References

[1] Enerdata. Global Energy Statistical Yearbook 2020.

[2] Commission E. Renewable Energy – Recast to 2030 (RED II) n.d.

[3] Eurostat. Renewable energy statistics. n.d.

[4] Gelazanskas L, Gamage KAA. Demand side management in smart grid: A review and proposals for future direction. Sustain Cities Soc 2014. https://doi.org/10.1016/j.scs.2013.11.001.

[5] Gellings CW. The Concept of Demand-Side Management for Electric Utilities. Proc IEEE 1985. https://doi.org/10.1109/PROC.1985.13318.

[6] Gellings CW. The smart grid. Enabling energy efficiency and demand response. 2009.

[7] Commission E. Energy performance of buildings directive n.d.

[8] Parliament E. Directive (EU) 2018/844 of the European Parliament and of the Council of 30 May 2018 amending Directive 2010/31/EU on the energy performance of buildings and Directive 2012/27/EU on energy efficiency (Text with EEA relevance). Off J Eur Union 2018;156/75:75–91.

[9] Jensen SØ, Marszal-Pomianowska A, Lollini R, Pasut W, Knotzer A, Engelmann P, et al. IEA EBC Annex 67 Energy Flexible Buildings. Energy Build 2017. https://doi.org/10.1016/j.enbuild.2017.08.044.

[10] Statista. Energy & Environment: Environmental Technology & Greentech: Number of heat pumps in operation in the European Union (EU) 2013-2019 n.d.

[11] (IEA) IEA. Heat Pumps n.d.

[12] Annex 67 n.d.

[13] Arteconi A, Hewitt NJ, Polonara F. State of the art of thermal storage for demand-side management. Appl Energy 2012. https://doi.org/10.1016/j.apenergy.2011.12.045.

[14] Reynders G, Diriken J, Saelens D. Generic characterization method for energy flexibility: Applied to structural thermal storage in residential buildings. Appl Energy 2017. https://doi.org/10.1016/j.apenergy.2017.04.061.

[15] Arteconi A, Hewitt NJ, Polonara F. Domestic demand-side management (DSM): Role of heat pumps and thermal energy storage (TES) systems. Appl Therm Eng 2013. https://doi.org/10.1016/j.applthermaleng.2012.09.023.

[16] Gholamibozanjani G, Farid M. Application of an active PCM storage system into a

building for heating/cooling load reduction. Energy 2020. https://doi.org/10.1016/j.energy.2020.118572.

[17] Clark RJ, Mehrabadi A, Farid M. State of the art on salt hydrate thermochemical energy storage systems for use in building applications. J Energy Storage 2020. https://doi.org/10.1016/j.est.2019.101145.

[18] Wei C, Xu J, Liao S, Sun Y, Jiang Y, Ke D, et al. A bi-level scheduling model for virtual power plants with aggregated thermostatically controlled loads and renewable energy. Appl Energy 2018. https://doi.org/10.1016/j.apenergy.2018.05.032.

[19] Klein K, Herkel S, Henning HM, Felsmann C. Load shifting using the heating and cooling system of an office building: Quantitative potential evaluation for different flexibility and storage options. Appl Energy 2017. https://doi.org/10.1016/j.apenergy.2017.06.073.

[20] Treado S, Yan Chen YC. Saving building energy through advanced control strategies. Energies 2013;6:4769–85. https://doi.org/10.3390/en6094769.

[21] Commission E. Directive (EU) 2018/844 of the European Parliament and of the Council of 30 May 2018 amending Directive 2010/31/EU on the energy performance of buildings and Directive 2012/27/EU on energy efficiency 2018;PE/4/2018/.

[22] Commission E. Directive 2010/31/EU of the European Parliament and of the Council of 19 May 2010 on the energy performance of buildings. 2010.

[23] Reynders G, Amaral Lopes R, Marszal-Pomianowska A, Aelenei D, Martins J, Saelens D. Energy flexible buildings: An evaluation of definitions and quantification methodologies applied to thermal storage. Energy Build 2018. https://doi.org/10.1016/j.enbuild.2018.02.040.

[24] Curtis M, Torriti J, Smith ST. A comparative analysis of building energy estimation methods in the context of demand response. Energy Build 2018. https://doi.org/10.1016/j.enbuild.2018.06.004.

[25] Stinner S, Huchtemann K, Müller D. Quantifying the operational flexibility of building energy systems with thermal energy storages. Appl Energy 2016. https://doi.org/10.1016/j.apenergy.2016.08.055.

[26] Le Dréau J, Heiselberg P. Energy flexibility of residential buildings using short term heat storage in the thermal mass. Energy 2016. https://doi.org/10.1016/j.energy.2016.05.076.

[27] Finck C, Li R, Kramer R, Zeiler W. Quantifying demand flexibility of power-to-heat and thermal energy storage in the control of building heating systems. Appl Energy 2018. https://doi.org/10.1016/j.apenergy.2017.11.036.

[28] Vigna I, Pernetti R, Pasut W, Lollini R. New domain for promoting energy efficiency:

Energy Flexible Building Cluster. Sustain Cities Soc 2018. https://doi.org/10.1016/j.scs.2018.01.038.

[29] Goy S, Finn D. Estimating demand response potential in building clusters. Energy Procedia, 2015. https://doi.org/10.1016/j.egypro.2015.11.756.

[30] Mata É, Sasic Kalagasidis A, Johnsson F. Building-stock aggregation through archetype buildings: France, Germany, Spain and the UK. Build Environ 2014. https://doi.org/10.1016/j.buildenv.2014.06.013.

[31] Famuyibo AA, Duffy A, Strachan P. Developing archetypes for domestic dwellings - An Irish case study. Energy Build 2012. https://doi.org/10.1016/j.enbuild.2012.03.033.

[32] Hu M, Xiao F. Quantifying uncertainty in the aggregate energy flexibility of high-rise residential building clusters considering stochastic occupancy and occupant behavior. Energy 2020. https://doi.org/10.1016/j.energy.2019.116838.

[33] Mancarella P. MES (multi-energy systems): An overview of concepts and evaluation models. Energy 2014. https://doi.org/10.1016/j.energy.2013.10.041.

[34] Lo Cascio E, De Schutter B, Schenone C. Flexible energy harvesting from natural gas distribution networks through line-bagging. Appl Energy 2018. https://doi.org/10.1016/j.apenergy.2018.07.105.

[35] Vandermeulen A, van der Heijde B, Helsen L. Controlling district heating and cooling networks to unlock flexibility: A review. Energy 2018. https://doi.org/10.1016/j.energy.2018.03.034.

[36] Zong Y, Su W, Wang J, Rodek JK, Jiang C, Christensen MH, et al. Model predictive control for smart buildings to provide the demand side flexibility in the multi-carrier energy context: Current status, pros and cons, feasibility and barriers. Energy Procedia, 2019. https://doi.org/10.1016/j.egypro.2019.01.981.

[37] IEA. Heat pumps in district heating and cooling systems n.d.

[38] Persson U, Werner S. Heat distribution and the future competitiveness of district heating. Appl Energy 2011. https://doi.org/10.1016/j.apenergy.2010.09.020.

[39] Li Y, Rezgui Y, Zhu H. District heating and cooling optimization and enhancement – Towards integration of renewables, storage and smart grid. Renew Sustain Energy Rev 2017. https://doi.org/10.1016/j.rser.2017.01.061.

[40] Gholamzadehmir M, Del Pero C, Buffa S, Fedrizzi R, Aste N. Adaptive-predictive control strategy for HVAC systems in smart buildings – A review. Sustain Cities Soc 2020. https://doi.org/10.1016/j.scs.2020.102480.

[41] Afram A, Janabi-Sharifi F. Theory and applications of HVAC control systems - A review of model predictive control (MPC). Build Environ 2014. https://doi.org/10.1016/j.buildenv.2013.11.016.

[42] Thieblemont H, Haghighat F, Ooka R, Moreau A. Predictive control strategies based on weather forecast in buildings with energy storage system: A review of the state-of-the art. Energy Build 2017. https://doi.org/10.1016/j.enbuild.2017.08.010.

[43] Serale G, Fiorentini M, Capozzoli A, Bernardini D, Bemporad A. Model Predictive Control (MPC) for enhancing building and HVAC system energy efficiency: Problem formulation, applications and opportunities. Energies 2018. https://doi.org/10.3390/en11030631.

[44] Drgoňa J, Arroyo J, Cupeiro Figueroa I, Blum D, Arendt K, Kim D, et al. All you need to know about model predictive control for buildings. Annu Rev Control 2020. https://doi.org/10.1016/j.arcontrol.2020.09.001.

[45] Oldewurtel F, Parisio A, Jones CN, Gyalistras D, Gwerder M, Stauch V, et al. Use of model predictive control and weather forecasts for energy efficient building climate control. Energy Build 2012. https://doi.org/10.1016/j.enbuild.2011.09.022.

[46] Sturzenegger D, Gyalistras D, Morari M, Smith RS. Model Predictive Climate Control of a Swiss Office Building: Implementation, Results, and Cost-Benefit Analysis. IEEE Trans Control Syst Technol 2016. https://doi.org/10.1109/TCST.2015.2415411.

[47] Bianchini G, Casini M, Vicino A, Zarrilli D. Demand-response in building heating systems: A Model Predictive Control approach. Appl Energy 2016. https://doi.org/10.1016/j.apenergy.2016.01.088.

[48] Mayne DQ, Rawlings JB, Rao C V., Scokaert POM. Constrained model predictive control: Stability and optimality. Automatica 2000. https://doi.org/10.1016/S0005-1098(99)00214-9.

[49] Prívara S, Cigler J, Váňa Z, Oldewurtel F, Sagerschnig C, Žáčeková E. Building modeling as a crucial part for building predictive control. Energy Build 2013. https://doi.org/10.1016/j.enbuild.2012.10.024.

[50] Foucquier A, Robert S, Suard F, Stéphan L, Jay A. State of the art in building modelling and energy performances prediction: A review. Renew Sustain Energy Rev 2013. https://doi.org/10.1016/j.rser.2013.03.004.

[51] Li X, Wen J. Review of building energy modeling for control and operation. Renew Sustain Energy Rev 2014. https://doi.org/10.1016/j.rser.2014.05.056.

[52] Harish VSKV, Kumar A. A review on modeling and simulation of building energy systems. Renew Sustain Energy Rev 2016. https://doi.org/10.1016/j.rser.2015.12.040.

[53] Wei Y, Zhang X, Shi Y, Xia L, Pan S, Wu J, et al. A review of data-driven approaches for prediction and classification of building energy consumption. Renew Sustain Energy Rev 2018. https://doi.org/10.1016/j.rser.2017.09.108.

[54] Brastein OM, Perera DWU, Pfeifer C, Skeie NO. Parameter estimation for grey-box

models of building thermal behaviour. Energy Build 2018. https://doi.org/10.1016/j.enbuild.2018.03.057.

[55] Ferracuti F, Fonti A, Ciabattoni L, Pizzuti S, Arteconi A, Helsen L, et al. Data-driven models for short-term thermal behaviour prediction in real buildings. Appl Energy 2017. https://doi.org/10.1016/j.apenergy.2017.05.015.

[56] Touretzky CR, Patil R. Building-level power demand forecasting framework using building specific inputs: Development and applications. Appl Energy 2015. https://doi.org/10.1016/j.apenergy.2015.03.025.

[57] Drgoňa J, Picard D, Helsen L. Cloud-based implementation of white-box model predictive control for a GEOTABS office building: A field test demonstration. J Process Control 2020. https://doi.org/10.1016/j.jprocont.2020.02.007.

[58] Ferreira PM, Ruano AE, Silva S, Conceição EZE. Neural networks based predictive control for thermal comfort and energy savings in public buildings. Energy Build 2012. https://doi.org/10.1016/j.enbuild.2012.08.002.

[59] Joe J, Karava P. A model predictive control strategy to optimize the performance of radiant floor heating and cooling systems in office buildings. Appl Energy 2019. https://doi.org/10.1016/j.apenergy.2019.03.209.

[60] UNI 10349-1. Riscaldamento e raffrescamento degli edifici - Dati climatici -Parte 1: Medie mensili per la valutazione della prestazione termo-energetica dell'edificio e metodi per ripartire l'irradianza solare nella frazione diretta e diffusa e per calcolare l'irradia 2016.

[61] Terna n.d.

[62] Thermal comfort: Analysis and applications in environmental engineering. Appl Ergon 1972. https://doi.org/10.1016/s0003-6870(72)80074-7.

[63] TRNSYS. TRNSYS 17 Documentation. Univ Wisconsin-Madison 2012.

[64] Corrado V, Ballarini I, Corgnati SP. Typology Approach for Building Stock: D6.2 National scientific report on the TABULA activities in Italy. 2012.

[65] Viessmann. VITOCAL 200-S AWB/AWB-AC 201.B04/ .B07/ .B10 / .B13 /.B16. Commercial datasheet catalogue. 2017.

[66] UNI/TR. 10349-2. Heating and cooling of buildings - Climatic data - Part 2: Data for design load. 2016.

[67] Klein K, Huchtemann K, Müller D. Numerical study on hybrid heat pump systems in existing buildings. Energy Build 2014. https://doi.org/10.1016/j.enbuild.2013.10.032.

[68] MINISTERO DELLO SVILUPPO ECONOMICO. DECRETO MINISTERIALE 11 marzo 2008. Gazz Uff Della Repubb Ital n.d.;2008.

[69] I CARICHI TERMICI n.d.

[70] Development. IM of E. Decree 26 giugno 2015. General criteria and requirements for the energy performance of buildings. Annex 1. Gazz Uff Della Repubb Ital 2015:1–25.

[71] Viessmann. VITOCAL 200-S. Commer Cat n.d.

[72] Wetter M. GenOpt - A Generic Optimization Program. Seventh Int IBPSA Conf 2001.

[73] IEA. Cooling. IEA, Paris 2020. https://www.iea.org/reports/cooling.

[74] Werner S. District heating and cooling in Sweden. Energy 2017. https://doi.org/10.1016/j.energy.2017.03.052.

[75] Passerini F, Sterling R, Keane M, Klobut K, Costa A. Energy efficiency facets: Innovative district cooling systems. Entrep Sustain Issues 2017. https://doi.org/10.9770/jesi.2017.4.3S(6).

[76] Dominković DF, Bin Abdul Rashid KA, Romagnoli A, Pedersen AS, Leong KC, Krajačić G, et al. Potential of district cooling in hot and humid climates. Appl Energy 2017. https://doi.org/10.1016/j.apenergy.2017.09.052.

[77] Commission E. Directive 2012/27/EU of the European Parliament and of the Council of 25 October 2012 on energy efficiency, amending Directives 2009/125/EC and 2010/30/EU and repealing Directives 2004/8/EC and 2006/32/EC Text with EEA relevance 2020;Chapter 12.

[78] Strategic Energy Technologies Information System n.d.

[79] CELSIUS SAS, Manufacturer P industry equipment. Thermal fluid characteristics (Glycol Water) n.d. https://www.celsius-process.com/_it/strumenti.php.

[80] Werner S. International review of district heating and cooling. Energy 2017. https://doi.org/10.1016/j.energy.2017.04.045.

[81] He T, Chong ZR, Zheng J, Ju Y, Linga P. LNG cold energy utilization: Prospects and challenges. Energy 2019. https://doi.org/10.1016/j.energy.2018.12.170.

[82] He T, Karimi IA, Ju Y. Review on the design and optimization of natural gas liquefaction processes for onshore and offshore applications. Chem Eng Res Des 2018. https://doi.org/10.1016/j.cherd.2018.01.002.

[83] Franco A, Casarosa C. Thermodynamic and heat transfer analysis of LNG energy recovery for power production. J. Phys. Conf. Ser., 2014. https://doi.org/10.1088/1742-6596/547/1/012012.

[84] Arteconi A, Polonara F. LNG as vehicle fuel and the problem of supply: The Italian case study. Energy Policy 2013. https://doi.org/10.1016/j.enpol.2013.08.016.

[85] Heisch P. Liquefied to Compressed Natural Gas Opportunities and Strategies. Proc

GasShow Exhib Conf n.d.

[86] FederMetano. EVENTI E NEWS / STAZIONI DI SERVIZIO n.d.

[87] Franci T. Le prospettive del mercato italiano degli usi finali del GNL in Italia Distribuzione primaria del GNL in Italia 2017.

[88] Farzaneh-Gord M, Saadat-Targhi M, Khadem J. Selecting optimal volume ratio of reservoir tanks in CNG refueling station with multi-line storage system. Int J Hydrogen Energy 2016. https://doi.org/10.1016/j.ijhydene.2016.10.050.

[89] Rawlings J., Manye DQ. Model Predictive Control: Theory and Design. 2012. https://doi.org/10.1109/TBME.2009.2039571.

[90] D'Oca S, Hong T, Langevin J. The human dimensions of energy use in buildings: A review. Renew Sustain Energy Rev 2018. https://doi.org/10.1016/j.rser.2017.08.019.

[91] Yoshino H, Hong T, Nord N. IEA EBC annex 53: Total energy use in buildings—Analysis and evaluation methods. Energy Build 2017. https://doi.org/10.1016/j.enbuild.2017.07.038.

[92] Li Q, Meng Q, Cai J, Yoshino H, Mochida A. Predicting hourly cooling load in the building: A comparison of support vector machine and different artificial neural networks. Energy Convers Manag 2009. https://doi.org/10.1016/j.enconman.2008.08.033.

[93] Guo Y, Nazarian E, Ko J, Rajurkar K. Hourly cooling load forecasting using time-indexed ARX models with two-stage weighted least squares regression. Energy Convers Manag 2014. https://doi.org/10.1016/j.enconman.2013.12.060.

[94] Khosravani HR, Castilla MDM, Berenguel M, Ruano AE, Ferreira PM. A comparison of energy consumption prediction models based on neural networks of a bioclimatic building. Energies 2016;9:57.

[95] Hietaharju P, Ruusunen M, Leivisk K. A dynamic model for indoor temperature prediction in buildings. Energies 2018. https://doi.org/10.3390/en11061477.

[96] Walker S, Khan W, Katic K, Maassen W, Zeiler W. Accuracy of different machine learning algorithms and added-value of predicting aggregated-level energy performance of commercial buildings. Energy Build 2020. https://doi.org/10.1016/j.enbuild.2019.109705.

[97] Bagheri A, Feldheim V, Ioakimidis CS. On the evolution and application of the thermal network method for energy assessments in buildings. Energies 2018. https://doi.org/10.3390/en11040890.

[98] Reynders G, Diriken J, Saelens D. Quality of grey-box models and identified parameters as function of the accuracy of input and observation signals. Energy Build 2014. https://doi.org/10.1016/j.enbuild.2014.07.025.

[99] ISO UnE. EN ISO 13790. Energy performance of buildings Calculation of energy use for space heating and cooling 2008:1–24.

[100] Bishop CM. Neural networks and their applications. Rev Sci Instrum 1994;65:1803–32.

[101] Documentation M. Matlab documentation. Matlab 2012.

[102] Manager I energy services. GSE (Gestore Servizi Energetici) n.d.

[103] ISO E. ISO 7730:2005. Ergonomics of the thermal environment — Analytical determination and interpretation of thermal comfort using calculation of the PMV and PPD indices and local thermal comfort criteria. 2005.

[104] Meteotest. Meteonorm Software n.d.

[105] EN. EN 14825. Air conditioners, liquid chilling packages and heat pumps, with electrically driven compressors, for space heating and cooling - Testing and rating at part load conditions and calculation of seasonal performance. 2019.

[106] EN. EN 14511. Air conditioners, liquid chilling packages and heat pumps for space heating and cooling and process chillers, with electrically driven compressors. 2018.

[107] GmbH HQC. Q.PRO-G3 250-265. Photovoltaic module in polycrystalline silicon. Commercial datasheet catalogue 2013.

[108] Rossi F, van Beek P, Walsh T. Handbook of Constraint Programming Introduction. 2006.

[109] Russell S, Norvig P. Artificial Intelligence A Modern Approach Third Edition. 2010. https://doi.org/10.1017/S0269888900007724.

[110] 2015. K. ENEA. n.d.

[111] Verhelst C, Logist F, Van Impe J, Helsen L. Study of the optimal control problem formulation for modulating air-to-water heat pumps connected to a residential floor heating system. Energy Build 2012. https://doi.org/10.1016/j.enbuild.2011.10.015.

[112] Eurostat. Electricity prices statistics 2020. https://ec.europa.eu/eurostat/statistics-explained/index.php/Electricity_price_statistics.

[113] IEA. Cooling. More efforts needed. Track Rep 2020. iea.org/reports/cooling.

[114] Lutz M. Learning Python. 2007. https://doi.org/10.1016/0019-1035(89)90077-8.

[115] Pedersen CO, Fisher DE SJ. ASHRAE. Cooling and heating load calculation principles. 1998.

[116] Ogunsola OT, Song L. Review and evaluation of using R-C thermal modeling of cooling load prediction for hvac system control purpose. ASME Int. Mech. Eng. Congr. Expo. Proc., 2012. https://doi.org/10.1115/IMECE2012-86988.

[117] Group R. ECOdry CN+. Dehumidifier for radiant cooling. n.d.

[118] UNI. Heating and cooling of buildings - Climatic data - UNI 10349-1:2016. Part 1: Monthly averages for the evaluation of the thermo-energy performance of the building and methods for distributing the solar irradiance in the direct and diffuse fraction and for 2016.

[119] Cui W, Ding Y, Hui H, Li M. Two-stage payback model for the assessment of curtailment services provided by air conditioners. Energy Procedia, 2017. https://doi.org/10.1016/j.egypro.2017.12.409.

[120] Viessmann. VITOCELL 100-E/-W. Commer Cat n.d.

[121] Buttitta G, Turner W, Finn D. Clustering of Household Occupancy Profiles for Archetype Building Models. Energy Procedia, 2017. https://doi.org/10.1016/j.egypro.2017.03.018.

[122] Swan LG, Ugursal VI. Modeling of end-use energy consumption in the residential sector: A review of modeling techniques. Renew Sustain Energy Rev 2009. https://doi.org/10.1016/j.rser.2008.09.033.

[123] Moffatt S. Methods for Evaluating the Environmental Performance of Building Stocks. 2004.

[124] Corgnati SP, Fabrizio E, Filippi M, Monetti V. Reference buildings for cost optimal analysis: Method of definition and application. Appl Energy 2013. https://doi.org/10.1016/j.apenergy.2012.06.001.

[125] Baetens R, Saelens D. Modelling uncertainty in district energy simulations by stochastic residential occupant behaviour. J Build Perform Simul 2016. https://doi.org/10.1080/19401493.2015.1070203.

[126] Baetens, R and Saelens D. StROBe website 2020.

[127] Yao R, Steemers K. A method of formulating energy load profile for domestic buildings in the UK. Energy Build 2005. https://doi.org/10.1016/j.enbuild.2004.09.007.

[128] UNI/TR 11552. Opaque envelope components of buildings Thermo-physical parameters 2014:1–44.

[129] UNI/TS 11300-1. Energy performance of buildings Part 1: Evaluation of energy need for space heating and cooling 2014.